Ph.D. Dissertation of Engineering

A Study on the Nonlinear Structure–Soil Interaction Model of Jack–up in Soft over Stiff clay

잭업의 비선형 구조–지반 연성 모델에 대한 연구 : 상부 연약한 점토–하부 단단한 점토 조건

August 2020

Graduate School of Engineering

Seoul National University

Naval Architecture & Ocean Engineering

Junhwan Choi

A Study on the Nonlinear Structure-Soil Interaction Model of Jack-up in Soft over Stiff clay

잭업의 비선형 구조-지반 연성 모델에 대한 연구 : 상부 연약한 점토-하부 단단한 점토 조건

지도교수 장 범 선

이 논문을 공학박사 학위논문으로 제출함

2020년 7월

서울대학교 대학원

조선해양공학과

최 준 환

최준환의 공학박사 학위논문을 인준함

2020년 7월

위 원 장 노 명일 (인)

부위원장 장 범선 (인)

위 원 추 연욱 (인)

위 원 원 종화 (인)

위 원 최 정인 (인)

Abstract

Offshore structures with jack-up systems can be operated at depths up to 150 meters and are used not only as drilling rigs and production rigs but also as support and accommodation units. The jack-up operation is carried out under environmental loads such as wind and wave, for which it is essential to understand jack-up behavior and structural response. As the boundary condition, the foundation model of offshore structures affects the vibration mode of the structure, and consequently, the behavioral and structural analysis results as well. Typical simple foundation models such as pinned and linear spring do not reflect a structure-soil interaction in the jack-up analysis. As an alternative, the International Organization for Standardization (ISO) guideline has suggested this structure-soil interaction model considering soil plasticity, from a simple secant model to a yield interaction model and a time-consuming but accurate soil continuum model. In this study, a structural analysis of jack-up has been conducted, focusing on the yield interaction model and the soil continuum model as a structure-soil interaction model. Jack-up structural analysis is performed for dynamic loads in consideration of the structure-soil interaction, and an appropriate interaction model for soft over stiff clay is presented in this study. A yield envelope study as yield criteria of the combined loads has been performed on soft over stiff clay. Studies on soft over stiff clay tend to be less studied because a squeezing effect ensures

sufficient vertical bearing capacity. Tensile vertical capacity is independent of the lower stiff clay, and a corresponding best-fit equation of yield envelope and the ultimate capacity ratio are presented about soft over stiff clay. The yield interaction model, the model B for clay, derived for consideration of the nonlinear behavior of soil, has been studied continuously improved until recently. The existing model generally assumes a linear load-displacement relationship in the elastic region. However, this linear relationship may overestimate the load as the plastic occurs gradually in soil behavior in practice. In this study, the Hyperbolic model B is proposed, and the horizontal and rotational load-displacement curves in the elastic region are assumed to have a hyperbolic relationship. The regression equation for the initial stiffness accompanying the model is presented. A fully coupled structure-soil interaction analysis with a soil continuum model has been performed to validate the yield interaction model. Large deformation of the soil accompanied by the deep penetration is considered simultaneously in the structural analysis of jack-up. The proposed yield interaction model uses yield envelope and ultimate capacities that are well suited to soft over stiff clay, and a hyperbolic nonlinear load-displacement relationship is assumed before the yield. As a result, inside the yield envelope, the existing model overestimates the moment acting on the soil, thereby underestimating the bending moment at the hull-leg joint. The model proposed in this study has predicted the soil response and bending moment distribution of the leg well, and these results are validated with the those of the soil continuum model. Wave

load analysis has been performed using the proposed yield interaction model and the soil continuum model. The dynamic effects that should be considered compared to the monotonic load analysis have been investigated, and it has been validated that the proposed yield interaction model can predict the response of the wave load analysis in the elastic region well.

Keyword : jack-up, spudcan, yield interaction model, soil LDFE, structure-soil interaction (SSI)

Student Number : 2014-21827

List of Contents

List of Figures

List of Tables

NOMENCLATURE

a : depth coefficient (yield envelope in ISO)

B : diameter of spudcan

e : eccentricity in yield envelope

D : diameter of spudcan (in Chapter 2)

E : elastic modulus of soil

E/s_u : rigidity index

f : yield envelope

$\boldsymbol{F}$: Combined loads vector $(V, H, M)^{\mathrm{T}}$

$\boldsymbol{F}_{trial}$: Trial load vector (in Chapter 5)

G : shear modulus of soil

G_H : shear modulus of soil at boundary $(w = H)$

H_{o} : horizontal capacity of soil

H : horizontal reaction force on spudcan

H_2 : horizontal reaction force component (x) in 3D

H_3 : horizontal reaction force component (y) in 3D

h_{o} : horizontal capacity ratio, H_{o}/V_{ult}

$H_{V=0}$: intercept value of horizontal axis

H_{nor} : normalized horizontal force, H/H_o

H_{trial} : horizontal component of trial load vector $\boldsymbol{F}_{trial}$

H_{env} : environmental load (in Chapter 5, 6)

H_{max} : design wave height (in Chapter 6)

$\boldsymbol{K}_{el}$: elastic stiffness matrix in yield interaction model

$\boldsymbol{K}_{tangent}$: tangent stiffness matrix

$\boldsymbol{K}_{ep}$: elasto-plastic stiffness matrix in model B

K_v : vertical stiffness

k_v : normalized vertical stiffness coefficient

K_h : horizontal stiffness

k_h : normalized horizontal stiffness coefficient

K_m : rotational stiffness

k_m : normalized rotational stiffness coefficient

$K_{m,r}$: reduced rotational stiffness in secant model (secant stiffness)

k : depth gradient of undrained shear strength

M : reaction moment on spudcan

M_2 : reaction moment component (y) in 3D

M_3 : reaction moment component (x) in 3D

M_{o} : rotational capacity of soil

m_{o} : rotational capacity ratio, M_{o}/V_{ult}

M_{nor} : normalized horizontal force, M/M_o

$M_{V=0}$: intercept value of rotational axis

M_{yield} : reaction moment at yield

M_{trial} : rotational component of trial load vector $\boldsymbol{F}_{trial}$

$M_{Jackup,\,wave}$: moment on spudcan of jack-up structural analysis with wave load (in Chapter 6)

$M_{Jackup,\,qs}$: moment on spudcan of jack-up structural analysis with quasi-static load (in Chapter 6)

$M_{spud.,\,dyn}$: moment on spudcan of single spudcan analysis with fast rotation motion equivalent to wave load (in Chapter 6)

$M_{spud.,\,qs}$: moment on spudcan of single spudcan analysis with slow rotation motion equivalent to quasi-static load (in Chapter 6)

R : radius of spudcan

s_u : undrained shear strength

s_{um} : undrained shear strength at seabed ($w = 0$)

$s_{u,H}$: undrained shear strength at boundary ($w = H$)

$s_{u,stiff}$: undrained shear strength of lower stiff clay

S_t : sensitivity of soil

T_n : natural period of jack-up

T_p : peak period of wave

u : horizontal displacement of spudcan

$\boldsymbol{u}$: displacement vector, $(w, u, \theta)^{\mathrm{T}}$

$\Delta\boldsymbol{u}$: displacement increment vector

V : vertical compressive reaction force on spudcan

V_{o} : vertical capacity of soil

V_{ult} : vertical capacity of soil ($=V_{\mathrm{o}}$)

V_{ten} : vertical tensile reaction force on spudcan

V_{nor} : normalized vertical force

w : vertical displacement of spudcan

z : coordinates in depth direction

$\alpha_{friction}$: friction coefficient of soil

γ' : effective unit weight of soil

δ_{rem} : strength ratio of the soil

θ : rotation of spudcan

θ_e : elastic component of rotation

θ_p : plastic component of rotation

μ : rate parameter

$\dot{\xi}$: maximum shear strain rate

$\dot{\xi}_{ref}$: reference strain rate

ξ : accumulated absolute plastic strain

ξ_{95} : accumulated absolute plastic strain required for 95% remolding

ν : Poisson's ratio of soil

χ : tensile capacity ratio, V_{ten}/V_{ult}

Chapter 1. Introduction

1.1. Research background

An offshore fixed platform is an offshore structure that installs structures on the seabed to withstand environmental loads such as waves and wind. Unlike floating platforms, it is relatively easy to install as it supports structures on the seabed. However, it is important to accurately consider this fixed state because the installed depth is limited and the behavior varies greatly depending on the seabed soil (Wilson, 2002). In the structural analysis of the fixed platform, these seabed soils act as boundary conditions. The boundary condition of the structure generally governs the global vibration mode and the local stress of the structure (Zhang et al., 2017). In the preliminary design of the fixed platform, a simple support model or a linear spring is used as a simplified foundation model (Baglioni et al., 1982; Williams et al., 1998). This simple foundation model is still limited in use to date and is known to exhibit high accuracy only when the deformation of the soil is very small. However, when designing offshore structures, it is required to calculate the response of structures under severe environmental conditions, and in this situation with large deformation of the soil, simple foundation models, such as simple support conditions and linear springs cannot accurately simulate the actual soil (Houlsby et al., 1992; Williams et al., 1998). Inaccurate boundary conditions

possibly misestimate not only the structural response at a specific site, but also the entire vibration mode of the structure. So how the accuracy of the foundation model is an essential factor in the structure design. Significant deformation of the soil occurs by the structure, which leads to a change in boundary conditions and affects the structure behavior again. It is known that it is more challenging to simulate the exact behavior and structural response of the structure due to structure–soil interaction (SSI).

A fixed platform generally refers to a jacket or a concrete caisson–structured platform supported by piles. In the case of piled structure, the pile–soil interaction (PSI) is considered and the soil is modeled through a linear spring for each depth of the pile penetrated deeply (API, 2002; Mao et al., 2015; Shi et al., 2015). A jack–up is a special platform that has both the characteristics of fixed and floating platforms. During operation, legs penetrated into soil behave like a fixed platform but can move like a floating platform before and after operation. Jack–up, called self–elevating unit, is equipped with a jacking system to lower and lift legs, and 3~6 legs are put on the seabed to support the hull from environmental loads (Young et al., 1984; Williams et al., 1999). The operation process of this jack–up is divided mainly into four stages: (1) transit, (2) installation, (3) operation, (4) retrieval (Le Tirant and Pérol, 1993). (1) The first stage is a transit process that moves to the target area while lifting the leg. In the case of a rig that does not have the self–movability, it moves through a tug boat. Second, after reaching the target area, through (2) the preloading process, the leg is penetrated

and the jack-up platform is installed. In this process, the leg is penetrated into the seabed through the hull weight, ballast water, and jacking power. It is easy to secure stability during this penetration process and subsequent work through the spudcan, an inverted conical steel structure under the leg. Legs must be penetrated deeply until sufficient resistance is obtained, and this process should involve a large deformation of the soil and changes in soil properties. (3) The third stage is an operation stage in which the work is carried out with the hull lifted after the installation is completed. This is the process in which the structure is affected by the environmental loads during the operation period. In this process, the jack-up behaves like a fixed platform, and an appropriate foundation model must be used for structural and global behavior analysis. (4) The last step is the retrieval process of lifting the leg after the work is done. Unlike jackets, repeated preloading and retrieval processes are essential for jack-up that require a relatively short-term operation and move to a different location. In this process, suction force due to adhesion of the clay soil must be considered.

In the preloading phase for the installation of the jack-up, the leg is penetrated into the seabed until their sufficient bearing capacity is obtained. A spudcan at the bottom of the leg has various shapes depending on applications but generally an inverted cone shape with a sharp spigot which help to facilitate penetration into the seabed, while allowing sufficient resistance through a large bearing area (Hossain et al., 2015). Leg penetration analysis calculates the

vertical bearing capacity curve of its corresponding spudcan shape through penetration and is necessary to determine the preloading load and leg penetration depth during design (Endley et al., 1981; Hossain and Randolph, 2010; Houlsby and Martin, 2003; Kee and Ims, 1984; Teh et al., 2008). The penetration process inevitably involves a large deformation of the ground, such as the backflow phenomenon where the spudcan is pushed directly under the ground and the surrounding ground moves. In particular, in the case of the North Sea, mainly consists of sand layer, sufficient resistance is secured even if the depth of penetration is not deep. However, in the case of the Gulf of Mexico (GoM), the South China Sea in the Southeast Asian region, and the southwest coast of Korea, the soft ground mainly composed of clay (Ahn et al., 2017; Menzies and Roper, 2008; Nancy et al., 2014). Spudcan must be deeply penetrated in this area, so the ground deformation behavior must be considered to perform the penetration analysis accurately. In order to calculate the bearing capacity of the spudcan by depth, analytical methods according to the existing bearing capacity theory have been verified and used, and the results of penetration analysis through the centrifugal model test have also been used in the design (Randolph and Gourvenec, 2017). In addition, recently, finite element analysis techniques using Arbitrary Lagrangian Eulerian (ALE) techniques or Coupled Eulerian–Lagrangian (CEL) techniques, which can simulate large deformation behavior, have been used for numerical simulation for this penetration behavior of a spudcan (Hu and Randolph, 1998; Qiu et al., 2009; Tho et al.,

2010). Large Deformation Finite Element (LDFE) analysis technique can simulate not only the penetration analysis of jack-up leg but also various situations in which large soil deformation can occur. It can be more useful when designing offshore structures considering the seabed soil.

In the operation stage, which is supported by the seabed soil and withstands environmental loads, the foundation model mentioned above affects the global behavior of the structure, and the structure-soil interaction in which boundary conditions change due to the soil is affected by the response (Martin, 1994; Schotman, 1989; Vlahos et al., 2005). In addition, the large deformation of the seabed soil that occurs during the preloading process before the operation phase also affects the properties and corresponding foundation model after spudcan penetration (Zhang et al., 2014). There are a number of failure modes that can occur during jack-up operation (Fig. 1). Representatively, the failure modes can be 'overturning' where the windward leg lifted up, sudden leeward leg penetration such as 'punch-through' (Fig. 2), and especially 'seabed slides' in which the leg is pushed without being able to penetrate stiff soil (Martin, 1994). In addition, a sudden collapse can be accompanied by structural failures at weak points such as spudcan-leg connections or leg-hull connections. In order to prevent risks, the failure should be predicted in the design phase through the calculation of the bearing capacity and the combined loads analysis, but few studies have been conducted to solve this problem.

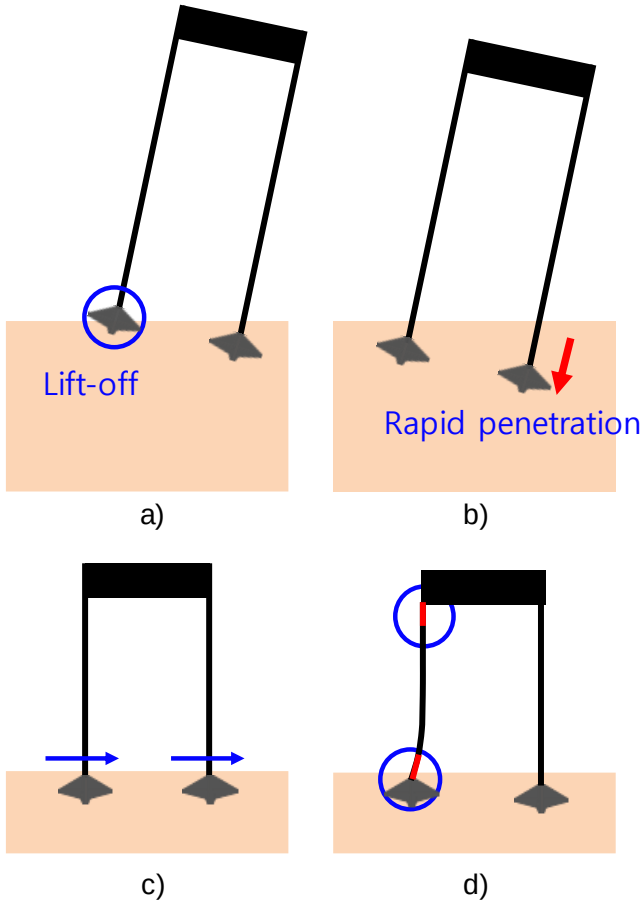

Fig. 1 Failure modes in jack-up operation; a) overturning; b) punch-through; c) seabed sliding; d) Critical point of leg

Fig. 2 Maersk Victory : punch-through failure (Aust, 1997)

In this way, the foundation model used in the operation of jack-up cannot be simplified as a simple boundary condition such as simple support or a linear spring because its complex behavior. Several foundation models have been proposed by ISO (2012). They are pinned model, linear spring, secant model, yield interaction model and soil continuum model as listed in Fig. 3. The secant model that uses arbitrarily reduced stiffness in the rotation direction. The yield interaction model that calculates plastic displacement using nonlinear stiffness. The secant model and yield interaction model are classified as simple foundation model. The soil continuum model that performs numerical analysis using soil continuum are representative foundation models that incorporate the interaction of structures and soil. From the pinned model to the soil continuum model, more accurate analysis is possible, and in the ISO, a more complicated model has been used when performing a high level of acceptance check (Table 1).

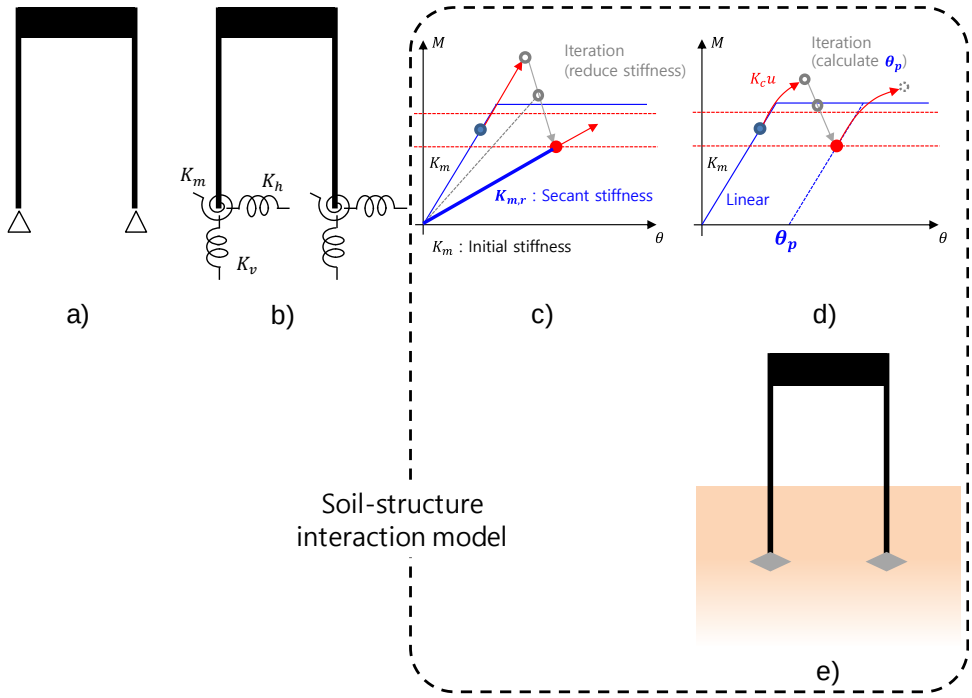

Fig. 3 Foundation models suggested in ISO (2012);
a) Pinned model; b) Linear spring model; c) Secant model;
d) Yield interaction model; e) Soil continuum model

Table 1 Acceptance check in ISO (2012)

Check level	**Step 1**		**Step 2**			**Step 3**	
	Step 1a	Step 1b	Step 2a	Step 2b	Step 2c	Step 3a	Step 3b
Foundation model	Pinned			Secant model	**Yield interaction model (Model B)**	Step 2 foundation model	**Continuum**
Check point	Preload (leeward leg)	Preload (windward leg)	Foundation capacity, Sliding (all leg)	Foundation capacity, Sliding (all leg)	Foundation capacity	Displacement (Additional penetration, sliding)	
Coverage	V	V	V, H	V, H	V, H, M	V, H (,M)	V, H, M

Before briefly explaining the existing foundation model, the load–displacement curve assumed for numerical analysis has been briefly described (Fig. 4). The elasto–perfectly plastic curve, which is assumed to be the simplest material property, has a linear relationship in the elastic section and the slope of the plastic section after yield is zero. Therefore, after yield, the element cannot have stiffness. Another commonly used model is elasto–plastic with strain hardening. It is the same as elasto–plastic in that it has a linear relationship in the elastic region, but differs in that hardening occurs in the plastic region after yield. Hardening relationships are modeled linearly, logarithmic, and hyperbolic, depending on the properties. And the model that best describes the behavior of the actual material is the nonlinear elastic–plastic model. Even in the elastic region before yield, a nonlinear relationship is shown, and accordingly, a hysteresis curve is drawn according to loading and unloading.

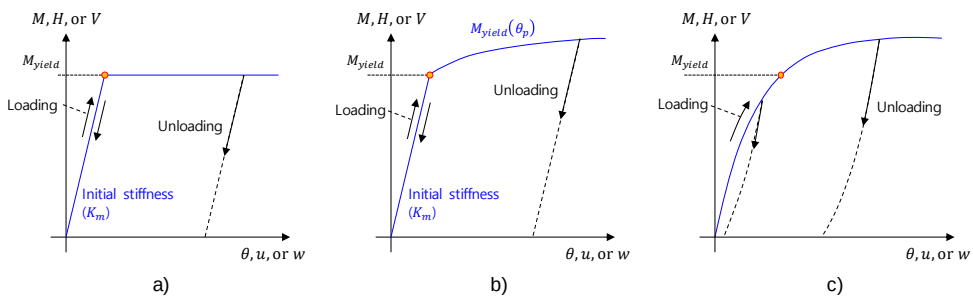

Fig. 4 Load–displacement curve in numerical analysis;
a) Elasto–perfectly plastic; b) Elasto–plastic;
c) Nonlinear elastic–plastic

The yield strength that determines yield is generally a material property. When a material is subjected to a 1-dof load, it appears as a single value, but when loads in multiple directions are applied, the combination of loads is a condition of yield. The yield envelope is a set of these yield points, and in general, the yield envelope in the n-dimensional load space is an n-1 dimensional figure (Simo and Hughes, 2006). In the spudcan study, the soil is assumed to follow a force-resultant yield envelope (Cheng and Cassidy, 2016b). It is mainly represented by a two-dimensional surface for vertical, horizontal, and rotational forces applied on the soil. In ISO(2012), the equations of yield surfaces for vertical, horizontal, and rotational loads are presented in Eq.(1), and cigar-shaped yield surfaces for clay and sand are also presented in Fig. 5 (Martin, 1994; Cassidy, 1999). If a combination of loads applied to the soil after the structure-soil analysis is inside the yield curve, it is considered to be in the elastic region. It is considered to be in the elasto-plastic if it is on the yield surface. If the combination of loads is outside the yield curve, it is assumed to plastic, and various foundation models try to explain their behavior in the plastic region.

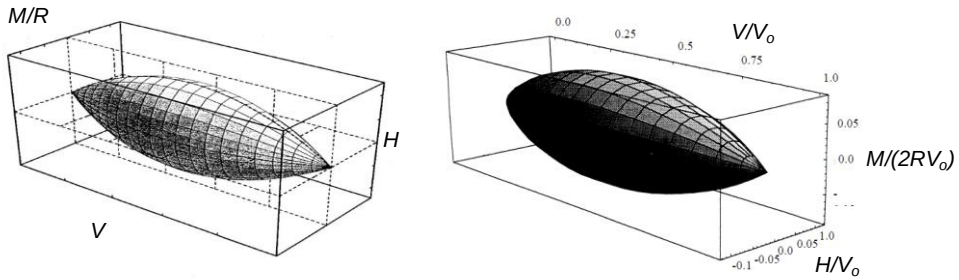

Fig. 5 Cigar-shaped yield surface in jack-up research;
a) Model B, clay (Martin, 1994); b) Model C, sand (Cassidy, 1999)

$$f = \left[\frac{H}{H_o}\right]^2 + \left[\frac{M}{M_o}\right]^2 - 16(1-a)\left[\frac{V}{V_o}\right]^2\left[1-\frac{V}{V_o}\right]^2 - 4a\left[\frac{V}{V_o}\right]\left[1-\frac{V}{V_o}\right] \quad (1)$$

where V_o, H_o, M_o is the maximum capacity of foundation in V, H, M direction, and V, H, M is the reaction forces applied on the spudcan in V, H, M direction. a is the coefficient about penetration depth.

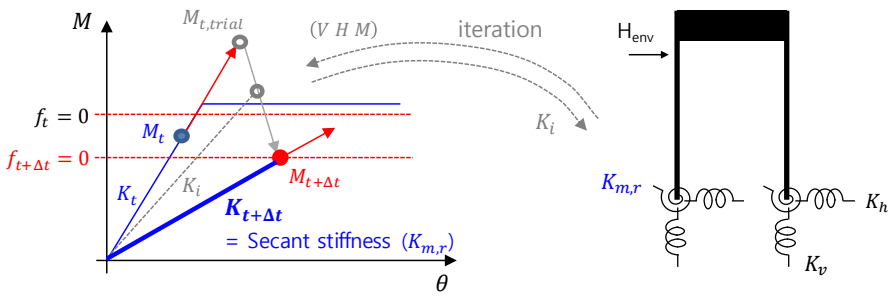

Fig. 6 Foundation model : Secant model in M- θ graph

ISO (2012) proposes a secant model as a simple foundation model that considers structure–soil interaction. The secant model in Fig. 6 uses secant stiffness in the rotational direction with linear vertical and horizontal stiffnesses (Purwana et al., 2012; Wong et al., 2012). In general, in numerical analysis, the behavior at the next increment is determined by considering the time increment (or load increment) and corresponding tangent stiffness of the load–displacement curve. However, secant stiffness refers to the stiffness that connects from the starting point to the design point when all of the load or displacement is applied (Sullivan et al., 2004). In this secant stiffness concept, the load–displacement at the design point coincides, but an incorrect load–displacement relation occurs at different locations. Although the secant stiffness that fits only at a certain point has limitations, it also has the advantage of being a foundation model that can be modeled simply in the form of a linear spring in the structure in consideration of the plasticity of the soil. In the ISO, when the load combination is in the plastic region, structural analysis is repeatedly performed by arbitrarily reducing the rotational stiffness, and the iterative calculation ends when the load combination is placed on the yield envelope. In this process, the rotational stiffness decreases, and this reduced stiffness is used for structural analysis as secant stiffness.

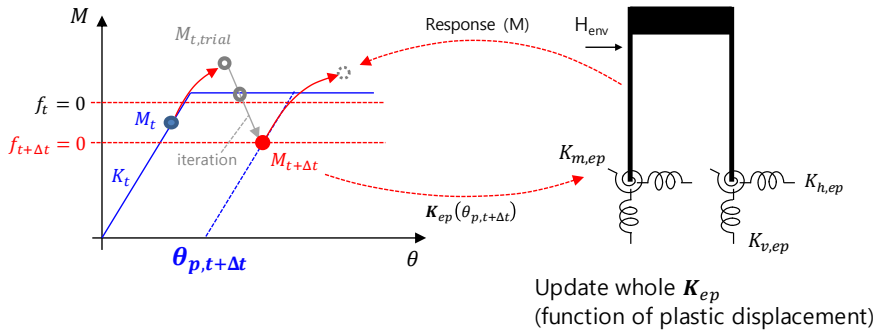

Fig. 7 Foundation model : modified model B in M− θ graph

The yield interaction model, which calculates moment failure through the calculation of plastic displacement, is called model B for clay soil. ISO has suggested this model as a more complex and accurate model than the secant model and recommends using it at a high acceptance check level. The model B was proposed by Martin in 1994 and introduced the Elasto−plasticity framework to predict the behavior when the load combination is in the plastic region. Elasticity, yield envelope, flow rule for plastic behavior, hardening law for additional vertical penetration are all formulated in an iterative procedure. As a result, plastic displacement corresponding to the time increment (or load increment) is calculated. When the plastic displacement converges, the tangent stiffness calculated together and the load state derived from the elastic displacement are updated and used for the calculation of the next increment. Such a framework is still in use today, and a modified model B of Zhang et al. (2014) has been presented an improved model (Fig. 7). In the model B, the effect of horizontal and rotational coupling behavior occurring in the actual soil is considered, and also in modified model

B, the tensile capacity due to spudcan extraction is implemented in yield envelope. This model has the advantage that it can express the elasto-plastic behavior of the soil relatively accurately and requires less time for analysis than the soil continuum model. Especially when the soil is in the plastic region and in a specific situation, there is an advantage that the accuracy of the model can be easily increased by improving the relational expression for it. However, by assuming a linear relationship other than the coupling in the horizontal-rotation direction in the elastic region, a vulnerability can be found in the case of repeated loads in the elastic area.

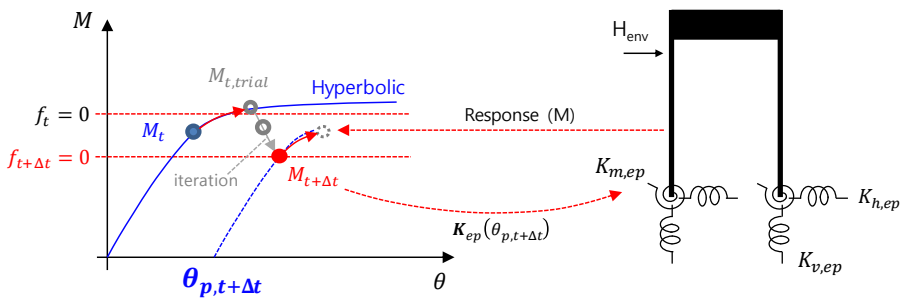

Fig. 8 Foundation model : Hyperbolic model B in M- θ graph

For this loading and unloading situation, Vlahos et al. (2006) has formulated the elasticity of the model B framework by introducing a hyperbolic backbone curve in the direction of rotation. In Vlahos et al. (2006), the hyperbolic backbone curve has been implemented through spring-slider element using hyperplasticity framework based on the thermomechanical energy potential. In this study, the hyperbolic relationship of load-displacement has been implemented

to follow in the elastic region, which was extended in the horizontal direction and introduced into the model B framework along with the coupling behavior in horizontal–rotational direction (Fig. 8). The behavior of the elastic region has been improved while maintaining the advantages of the model B plasticity framework for calculating the plastic displacement, and the hysteresis curve could be expressed in the elastic region.

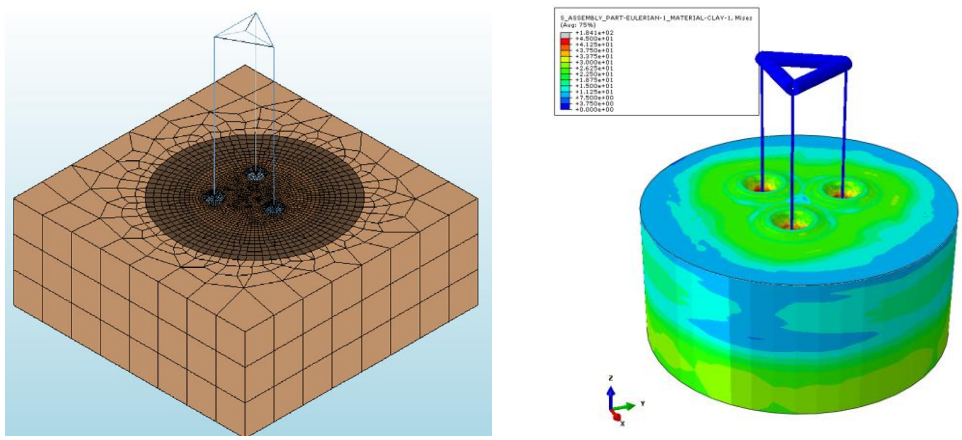

a) b)

Fig. 9 Foundation model : soil continuum model; a) Modified Mohr–Coulomb model for sand at shallow embedment (Pisanò et al., 2019); b) Jack–up structural analysis with soil LDFE technique

The soil continuum model is the most reliable and accurate method in the numerical method to consider the structure–soil interaction (Fig. 9). The load transferred from the structure is applied to the ground simultaneously, and the influence of the structure due to the corresponding behavior of the soil is considered as two–way. Even if this accuracy, the computational cost makes

the method difficult to use widely, especially for time series analysis. In the jack-up problem, the soil continuum model has been considered by using a basic mohr-coulomb model for sands with relatively small deformation (Pisanò et al., 2019). However, for clays accompanied by large deformations, the fully coupled structure-soil interaction analysis is not widely performed due to the excessively high cost to simulate the large deformations and the resulting changes in soil properties.

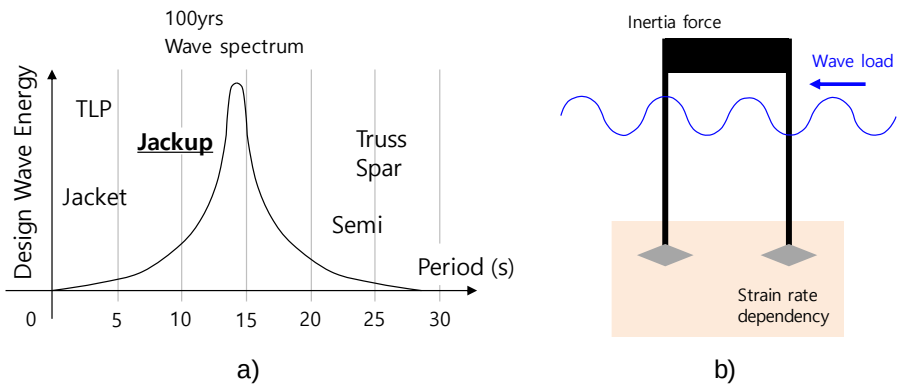

Fig. 10 Dynamic effects of wave load analysis in jack-up;
a) Natural period of offshore platform;
b) Jack-up structural analysis with dynamic load

In particular, when the structure-soil interaction analysis is performed using the above-described soil continuum model, dynamic effects occur in the results more (Fig. 10). The dynamic effects of structural aspects are 'phase shift' due to inertia force and 'Dynamic Amplification Factor (DAF)', which is a resonance effect according to the natural period of the structure. In a typical jack-up

structure, a natural period is in the range of 5 and 15 seconds, which makes dynamic effects in wave load analysis unavoidable (ABS, 2014). Meanwhile, wave load analysis in the soil continuum model also causes the dynamic effects of the soil. Clay is a representative rate-dependent material, and it is known that hardening occurs according to the strain rate (Abelev and Valent, 2009; Nanda et al., 2017; Robinson and Brown, 2013). In numerical analysis, quasi-static analysis is generally performed to remove dynamic effects. However, in the wave load analysis, in which a wave of about 10 seconds acts as environmental loads, quasi-static analysis can decrease the accuracy.

1.2. Research objective and scope

The objective of this study is to propose an accurate method of dynamic wave analysis for jack-up by improving the structure-soil interaction model. For this objective, the yield envelope for soft over stiff clay and hyperbolic model B is proposed and implemented as boundary condition of jack-up structural analysis. Fully coupled structure-soil interaction analysis using soil LDFE technique is performed and compared with proposed model. Accompanying dynamic effects of jack-up wave analysis has also been presented and investigated.

The southwest sea of South Korea is mainly deposited with clay, especially with a soil profile of stiff-soft-stiff clay. To operate a jack-up type "wind turbine installation vessel (WTIV)" to create an offshore wind farm, its legs should be penetrated until sitting on a stiff layer. In this case, penetrated spudcan are placed in transition zone that is affected by both the lower stiff and upper soft layers. To model this transition zone, the target soil has been simplified to soft over stiff clay. A nonlinear soil model for a general single clay soil has been studied by improving the accuracy of yield envelope and plastic potential from the model B, which considered the coupled effect of the combined loads. In addition, recently, studies on the nonlinear soil models for multi-layered soils, especially sand over clay, where punch-through can occur, have been conducted. On the other hand, studies have not been performed on soft over stiff clay where squeezing of the upper clay occurs. In the aspect of the

spudcan for installation, the squeezing phenomenon, in which the weak ground is squeezed due to the lower stiff soil and the bearing capacity increases, is very advantageous to secure sufficient bearing capacity. However, if a spudcan is placed between two clay soils during the operation phase of the jack-up, the spudcan is simultaneously affected by both upper soft clay and lower stiff clay, so the model on a single clay cannot be applied as it is.

In this study, a nonlinear foundation model that interacts with the structural response of jack-up in real time is presented. Combined loads, transferred to the soil through the jack-up structure from the environmental loads, change the foundation model and soil properties. The changed foundation model becomes a boundary condition and affects the structural behavior of jack-up in real time. This structure-soil interaction should be considered for simulating accurate jack-up behavior. This study has been conducted through numerical analysis considering the large deformation effect of the soil due to the spudcan penetration. For this, soil Large Deformation Finite Element (LDFE) analysis technique is implemented in Abaqus/Explicit commercial program, and validated (Chapter 2). Combined loads analyses on soft over stiff clay have been performed using the developed soil LDFE numerical model. Ultimate capacities in the vertical, horizontal, and rotational directions have been calculated and analyzed, and the effect of lower stiff clay on the capacities have been investigated. In addition, a best-fit yield envelope expression has been proposed (Chapter 3). The model B, the yield interaction model of clay, consists of elasticity, yield

envelope, flow rule, and hardening law. Unlike the actual soil in which gradual plasticity occurs, linear load-displacement relationship of the foundation model can overestimate the load acting on the soil. To improve this, a hyperbolic relationship has been applied to the elastic region, and a hysteresis curve in elasticity has been implemented. In addition, a regression model of initial stiffness is presented for the proposed hyperbolic model B (Chapter 4). The soil continuum model is the most accurate method to numerically simulate the structure-soil interaction. It was mainly used for small strain problems such as shallow embedment of sand due to computational cost. To validate the proposed hyperbolic model B, a fully coupled structure-soil interaction analysis using soil continuum has been performed. The interaction between the jack-up and the soil was considered simultaneously in this model. Using the LDFE technique in Chapter 2, large deformation of clay is simulated and reflected in combined loads analysis. It has been confirmed that the proposed model follows the LDFE results well before the yield, and it has also been shown that the moment distribution of the leg can be accurately predicted compared to the existing linear relationship model (Chapter 5). Wave load analysis of jack-up has been performed using the proposed yield interaction model in soft over stiff clay and the soil continuum model using the LDFE technique. Comparative analysis has been conducted on the involved dynamic effects of the structure and soil behavior. As a result of the analysis, it has been confirmed that the proposed model and the continuum model have similar results for the repetitive wave

load in the elastic region. This will allow the proposed model to be used when performing the fatigue strength assessment of jack-up (Chapter 6).

Chapter 2. Soil LDFE analysis technique

2.1. Introduction

The jack-up system uses a pinion and guide to raise and lower legs of the hull. This system is installed in a jack-up rig and a jack-up type Wind Turbine Installation Vessel (WTIV). When the jack-up system stands on legs, a spudcan directly touches the seabed underneath the leg to support the load of the entire structure of platform. Since the jack-up type offshore structure can be installed in various soil environment, precise assessment of the structure during installation and operation phase is required. Especially in the installation process of the jack-up, it is accompanied by large deformation of the soil due to penetration of spudcan. Therefore, it is necessary at the design stage to accurately predict the large deformation behavior and bearing capacity of the soil.

Table 2 Conventional researches of soil LDFE analysis

	Centrifuge	LDFE (RITSS)	LDFE (CEL)
Description	• Model test which simulate the realistic stress field through centrifugal force • Widely used in geotechnical problem	• Remeshing and Interpolation Technique with Small Strain (RITSS) • Based on Arbitrary Lagrangian and Eulerian (ALE)	• Coupled Eulerian-Lagrangian (CEL) method • Supported by Abaqus commercial program
First suggestion in geotechnical problem	• From 1960~1970 • Mikasa in Osaka univ. • Schofield in Cambridge univ.	• Hu (1998) – Large deformation problems in soil – Cavity Strip footing Spudcan	• Qiu (2009) – Large deformation problems in soil – Strip footing Pile jacking Ship grounding
Usage in Spudcan penetration issue	• Yu (2018), Lattice leg effect • Kim (2018), sloped seabed • Hossain (2017), Footprint	• Hossain (2009), Spudcan penetration prediction • Zhang (2018), Spudcan angle • Jun (2018), Spudcan shape	
Multi-layered soil	• Sand over clay – Hu (2014), Analytic expression of bearing capacity for sand over clay – Hu (2018), Post-peak behavior of spudcan in sand over clay – Li (2018), Bayesian approach of spudcan behavior in sand over clay • Multi-layered clay – Hossain (2010), Bearing capacity of spudcan in stiff-over-soft clay – Zheng (2018), Spudcan behavior in stiff-soft-stiff clay		

In general, three methods have been used to calculate the bearing capacity of the Spudcan. There are a method using a formula combining theoretical and empirical equations recommended by a guideline or rule (SNAME, 2008; ISO, 2012), a finite element method simulating the penetration behavior of the spudcan (Hossain and Randolph, 2010b; Hu et al., 2015; Zheng et al., 2017), and a centrifuge test method (Hossain and Randolph, 2010a; Hu and Cassidy, 2017; Teh et al., 2010). Various case studies have been conducted using numerical analysis methods. The remeshing and interpolation technique with small strain (RITSS) method developed by Hu and Randolph (1998) has been used for numerical analysis of large deformation problem based on ALE. In addition, Qiu (2009) has simulated the soil behavior using the CEL method provided in

the Abaqus/Explicit commercial program, and since then, the method has been used for the large deformation problem of soil.

In this paper, the large deformation behavior of the soil is simulated using the finite element method. Since the mesh distortion occurs due to the large deformation, the penetration behavior of the spudcan cannot be analyzed by general finite element method. Analysis technique for large deformation is adopted in the soil problem, and verification about the various case is performed. Simple structure is verified first, and then the spudcan penetration on clay and sand is verified, too. The soil model and the details of verification case is introduced. As a result, it is confirmed that the developed Large Deformation Finite Element (LDFE) method shows similar results to the centrifuge model test results and the existing LDFE analysis results.

2.2. Numerical methodology

Generally, the Lagrangian description is used for structural analysis problems, and the Eulerian description is used for fluid problems. In Lagrangian description, the detailed history of material deformation is represented by the movement of mesh. Lagrangian elements are always 100% full of single material, so it is easy to divide the material boundary. On the contrary, in Eulerian description, the mesh is fixed and the materials pass through the mesh. The material is allowed to move independently of the finite

elements, so the Eulerian elements may not always be 100% full of material. The CEL technique has been developed combining the Lagrangian description with advantages for boundary and contact problems and the Eulerian description, which are less affected by mesh distortion (Simulia, 2013). Remesh and advection process simulate large deformation of the soil.

Tresca model incorporating strain softening and rate dependency is used for the numerical modeling of clay soil. The undrained shear strength is determined using the following strain / strain rate dependent equation proposed by Einav and Randolph (2005) (Eq. (2)).

$$s_u = \left[1 + \mu \log\left(\frac{\mathrm{Max}\left(|\dot{\xi}|, \dot{\xi}_{ref}\right)}{\dot{\xi}_{ref}}\right)\right] \left[\delta_{rem} + (1 - \delta_{rem}) e^{-3\xi/\xi_{95}}\right][s_{um} + kz] \quad (2)$$

where, s_u is the undrained shear strength at the depth z considering strain softening and rate hardening. μ is a rate parameter and has a value of 0.05 to 0.2 in marine clay typically. $\dot{\xi}$ means the maximum shear strain rate. $\dot{\xi}_{ref}$ is the reference strain rate and is 1 to 4%/h in the triaxial test and 20%/h in the direct simple shear test. δ_{rem} is the inverse of the sensitivity as the strength ratio of the soil. In general, the sensitivity of marine clay is 2 ~ 5. ξ stands for accumulated absolute plastic strain and has the definition of the following equation. ξ_{95} is the value of ξ when 95% remolding is performed after the soil is disturbed. Generally, it has a value of 10

to 25 (Hossain and Randolph, 2009). s_{um} is the undrained shear strength at the top surface of the clay layer. The k value is a strength depth gradient. Using these two parameters, undrained shear strength at the corresponding depth, z, is obtained.

2.3. Analysis model

Using the CEL method provided by the Abaqus commercial program, the large deformation of soil caused by the penetration of the spudcan is simulated. As mentioned above, spudcan is modeled by using Lagrangian element, and soil by Eulerian element. Lagrangian element comprises both 6-noded linear triangular prism element(C3D6) and 8-noded linear brick element with reduced integration(C3D8R) is used for spudcan structure. Eulerian element comprises 8-noded linear brick element with reduced integration (EC3D8R) is used for the soil (Qiu and Grabe, 2012; Tho et al., 2010). Mesh size is determined by considering the diameter D of the spudcan, D, and mesh size of 0.025D ~ 0.05D is used. In the spudcan penetration simulation, the rate of penetration is also important. It should be slow enough to avoid the inertia effect. Penetration rate is also determined considering the D, and the speed of 0.005D ~ 0.01D/s is mainly used. This means a penetration rate of 0.05 ~ 0.1m/s assuming D of about 10m. The following figure is an example of the spudcan penetration model, which consists of spudcan structure and soil layer (Fig. 11).

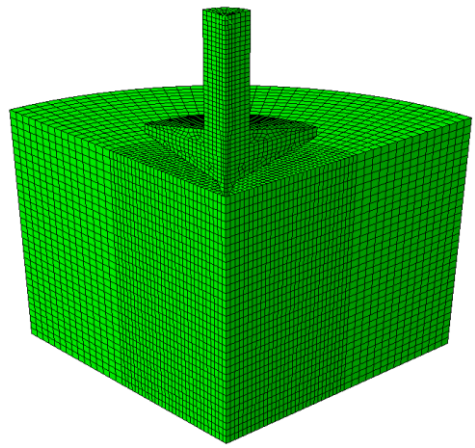

Fig. 11 Numerical analysis model about penetration of spudcan in clay

2.4. Verification results

2.4.1. Penetration of pipe in clay

Wang et al. (2010) is referred for the simulation about penetration of pipe in clay. In this referred paper, The LDFE approach has been verified by comparison with a centrifuge test of pipe-soil interaction in Kaolin clay, so the result of pipe penetration is used for this verification. Unit length (=1 m) is used to simulate 2D in 3D domain, and diameter of pipe, D, is 0.8m. Pipe structure is assumed to rigid body, because the deformation of pipe is too small to neglect.

Clay soil is modeled as the elasto-perfectly plastic material obeying a Tresca yield criterion. Effective unit weight of clay is 6.5kN/m^3. Undrained shear strength is 2.3 kPa at the top surface of

clay layer and increases to 3.6 kPa/m with depth. A rigidity index, the ratio between the Young's modulus to the undrained shear strength (E/s_u), is used as 500, the general value of marine clay. There are several factors that should be selected for nonlinear model of undrained shear strength. In the strain softening term, 0.3125 is used as strength ratio, δ_{rem}, and 10 of ξ_{95} is used for the value of ξ required for the soil to undergo 95% remolding. For the strain rate hardening term, 0.1 of rate parameter value μ is used, and 1.5%/h is used as reference shear strain rate, $\dot{\xi}_{ref}$.

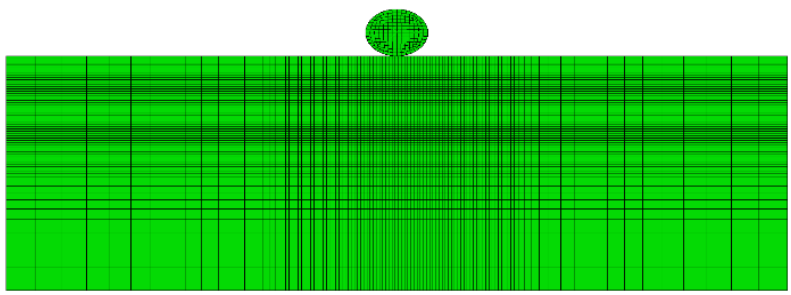

Fig. 12 Numerical analysis model about penetration of unit pipe

Numerical model of pipe penetration is introduced in Fig. 12. Pipe structure is modeled using Lagrangian element, and soil is modeled as Eulerian element. Mesh size is 0.04m, which is same with 0.05D, and penetration rate is 0.005m/s of 0.00625D.

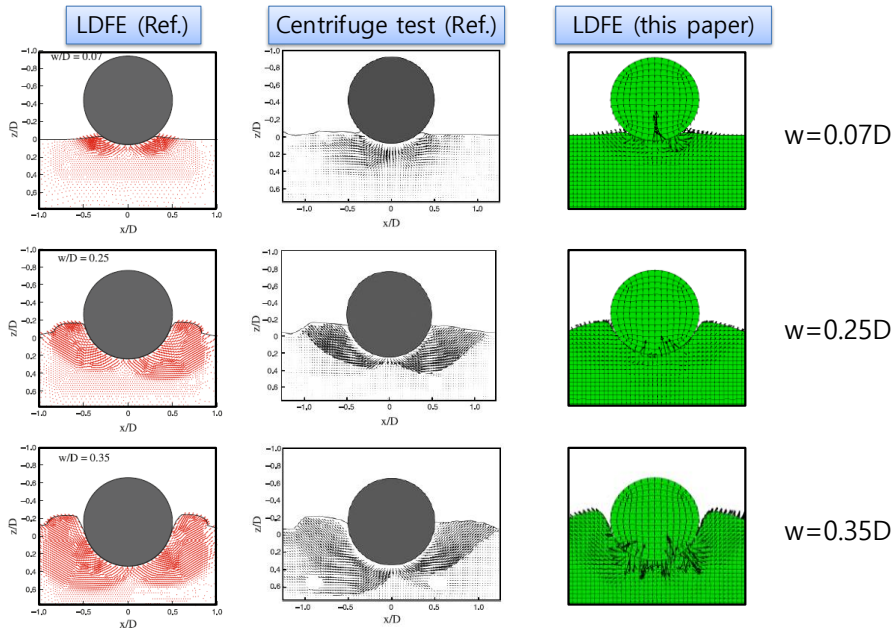

Fig. 13 Cross-sectional view of deformed shape of soil

(Ref. = Wang et al., 2010)

Fig. 13 shows the deformed shape of soil when the penetration depth is 0.07D, 0.25D, and 0.35D. At each depth, it can be seen that the deformed shape of soil is similar to the results of centrifuge tests and referred LDFE. The movement of the soil during penetration and the shape of soil berm could be compared and confirmed similar.

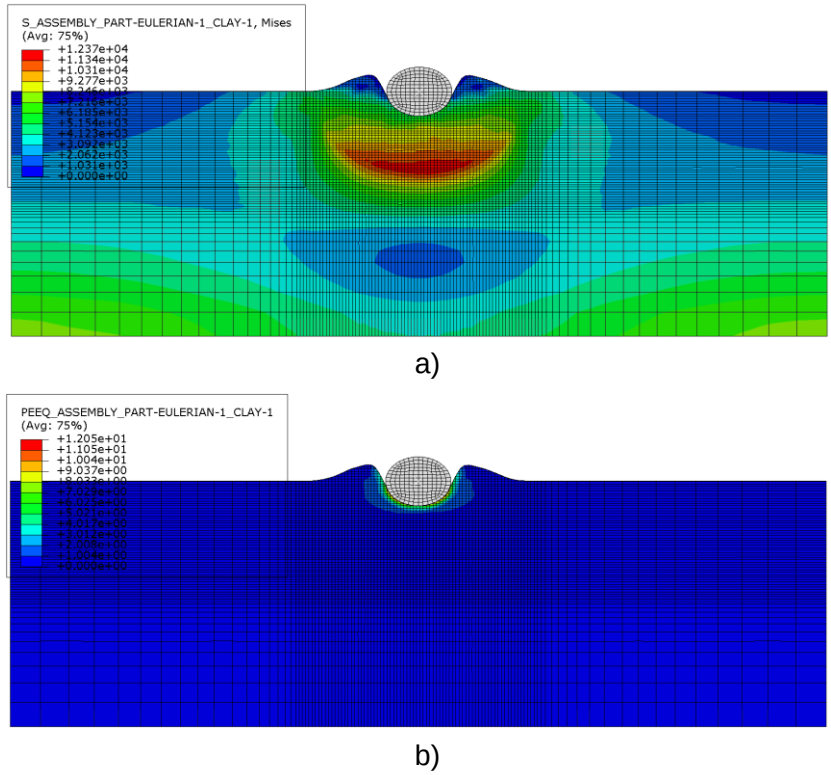

Fig. 14 Soil response in clay (unit pipe); a) Mises stress; b) Equivalent plastic strain

Soil stress and plastic strain after the penetration of pipe are presented at Fig. 14. High stress is observed under the pipe after the penetration. This high stress is dominantly affected by the elastic behavior of the soil, so the little plastic strain occurs in that region. Unlike elastic strain, plastic strain occurs right under the structure where force is applied directely.

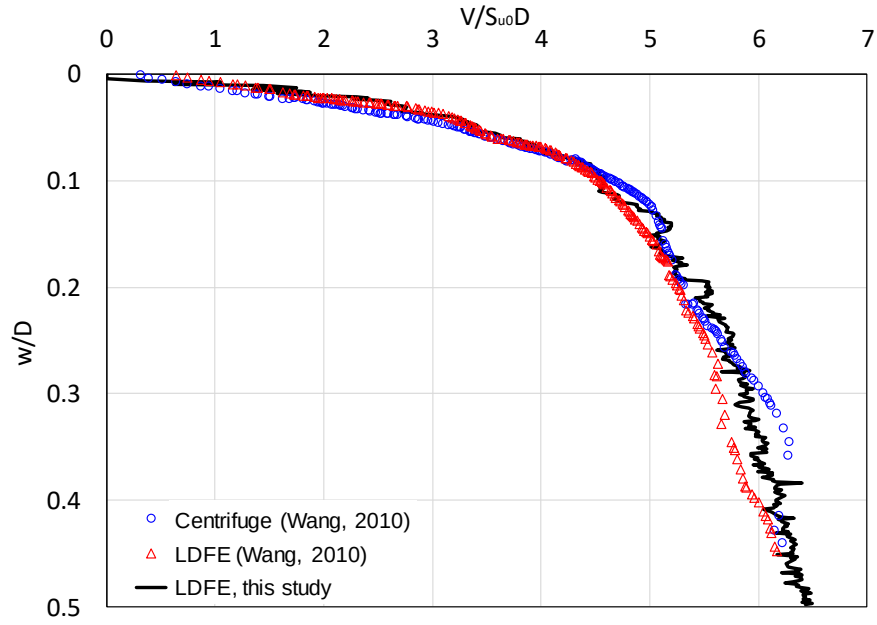

Fig. 15 Bearing capacity curve of unit pipe in clay

As a result of the penetration behavior simulation, the bearing capacity curve is shown in the Fig. 15. The penetration of 0.5D is simulated, and the non-dimensionlized results are compared with centrifuge model tests and LDFE results. Simulation results are similar to those of the two references.

2.4.2. Penetration of spudcan in single clay

In Hossain et al. (2015), the bearing capacity about penetration of various shape of spudcan in clay has been studied. Penetration and extraction resistance has been researched using a series of centrifuge tests and LDFE analyses. Three different base geometries used in the real field is treaed in this paper, so a

representative shape of spudcan is selected for this verification. The penetration behavior of the spudcan is simulated, and the maximum bearing area of the spudcan has 6m of diameter. Spudcan structure is assumed to rigid body, same as the case of pipe, because the deformation of pipe is small enough. Detailed configuration of spudcan is shown in Fig. 16.

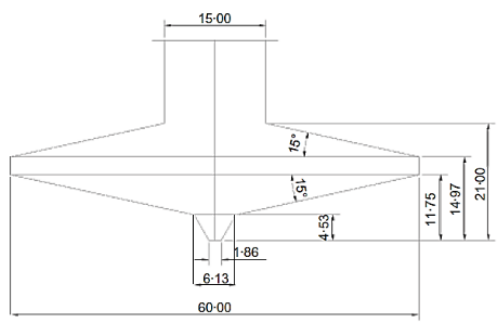

Fig. 16 Spudcan used in validation (Hossain et al., 2015)

Clay modeling is the same as the previous case of unit pipe. However, the properties are applied diffrenetly as used in Hossain et al. (2015). Soil layer is modeled as the elasto-perfectly plastic material obeying a Tresca yield criterion. Effective unit weight of clay is 7.5kN/m3. Undrained shear strength is 0.9kPa at the top surface of clay layer and increases to 1.95kPa/m as depth increases. The rigidity index is used as 500, the same as clay model used in unit pipe case. Several factors for nonlinear model of undrained shear strength is used in this clay model. In the strain softening term, 0.3436 is used as strength ratio, δ_{rem}, and 15 of ξ_{95} is used. For the strain rate hardening term, 0.1 of rate parameter value is used, and

1.5%/h is used as reference shear strain rate $\dot{\xi}_{ref}$. Numerical analysis model about this verification case is shown in Fig. 11. spudcan structure is modeled using Lagrangian element, and soil is modeled as Eulerian element. Mesh size is 0.3m, which is same with 0.025D, and penetration rate is 0.1m/s of 0.0083D, which is also used in the reference paper.

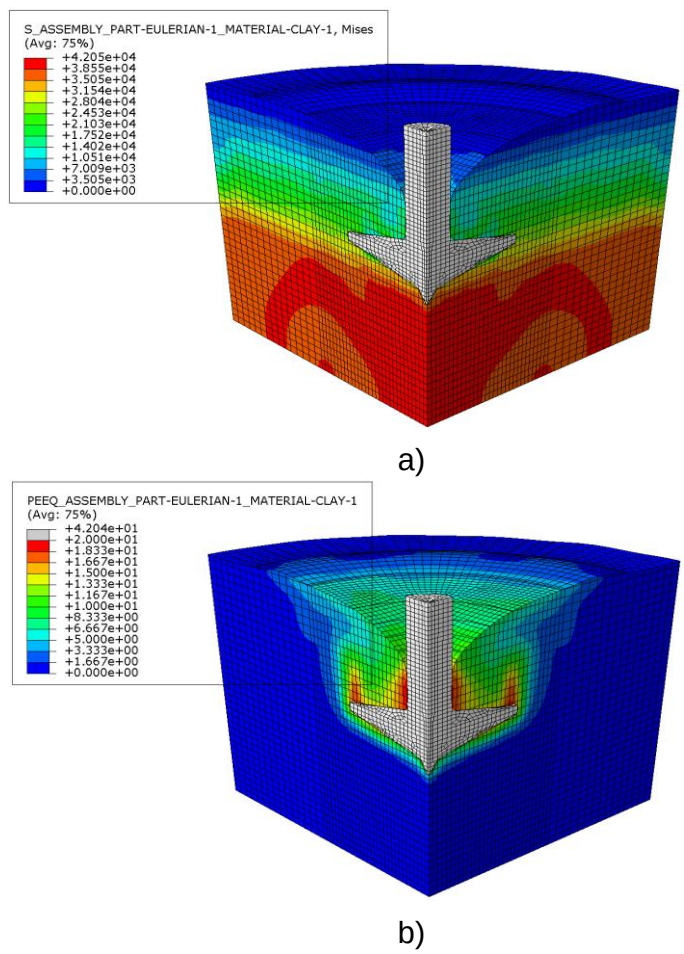

Fig. 17 Soil response at spudcan penetration; a) Mises stress; b) Equivalent plastic strain

Soil stress and plastic strain after penetration are presented at Figure. High stress is observed under the pipe after penetration. This high stress is caused by the elastic behavior of the soil, which can be confirmed from the plastic strain results. Unlike elastic strain, plastic strain usually occurs right under the structure where force is applied directely, shear deformed region by spudcan edge, and upper part of the spudcan where large deformation occurs due to backflow.

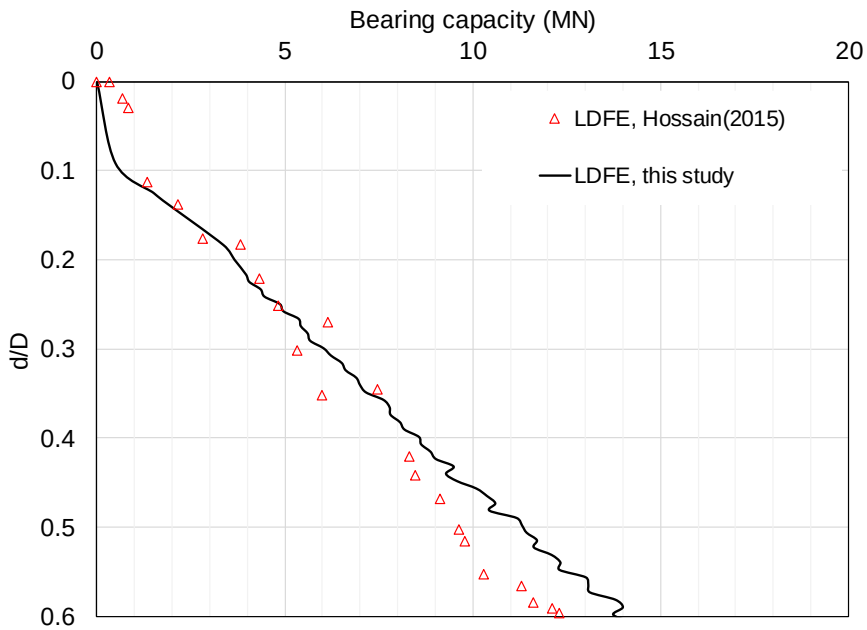

Fig. 18 Bearing capacity curve for numerical model validation

The bearing capacity curve of spudcan penetration is shown in Fig. 18. The penetration is simulated unitil 0.6D depth. Simulation results are similar to a reference, however, the value is larger as the penetration depth is deeper. Since the size of the domain is small

in the depth direction, it is considered that the boundary effect is generated. Therefore, the greater the depth, the greater the bearing capacity. These results are expected to improve when the size of domain is large enough.

2.4.3. Penetration of spudcan in multi-layered clay

Before carrying out the present numerical analysis, the soil LDFE analysis technique needs to be validated. The results of the penetration analysis of the multi-layered clay soils are compared with those of the centrifuge model test and the existing numerical LDFE analysis. Hossain et al. (2011) performed the centrifuge model test on multi-layered clay soils and analyzed the occurred punch-through and squeezing phenomena. Notably, squeezing was observed in their T8 test due to the lowest stiff layer, and this case was also simulated by LDFE analysis in Zheng et al. (2018).

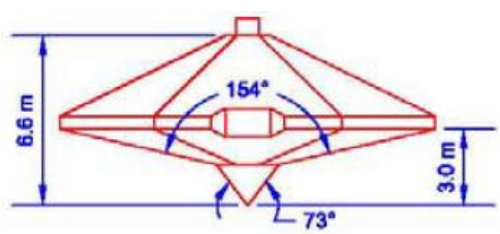

Fig. 19 Spudcan used in validation (Menzies and Roper, 2008)

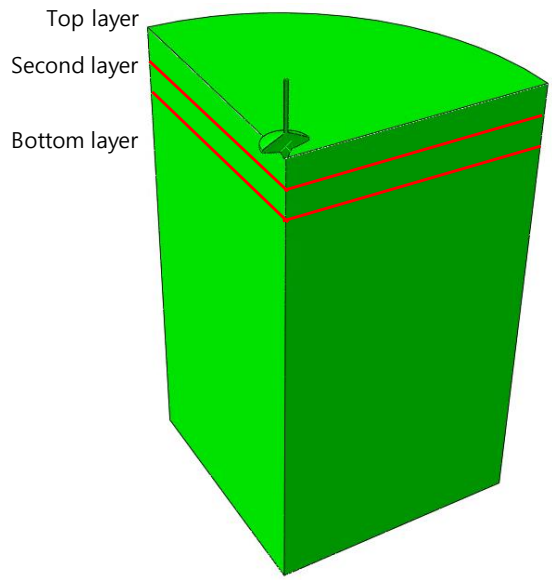

Fig. 20 FE model in multi-layered clay validation

Since squeezing is an important phenomenon in soft-over-stiff clay, which is the target soil of the present study, this case is selected for validation of this LDFE analysis. The T8 test covered three-layered clay with interbedded soft clay. The undrained shear strengths of each layer in Zheng et al. (2018) were, in order, 21 kPa, 8.5 kPa, and 35.5 kPa for the first, second, and third layers. With these undrained shear strengths, 200 rigidity index (E/s_u), rough condition of spudcan-soil interface, unit weights of 7.5 kN/m^3 (top layer) and 7.3 kN/m^3 (lower layers) in Zheng et al. (2014) are referred for the validation. The strain-softening and rate-hardening parameters in this validation also are the same values as in Zheng et al. (2018) (i.e., μ=0.1, $\dot{\xi}_{ref}$=1.5%/h, δ_{rem}=0.36, ξ_{95}=12).

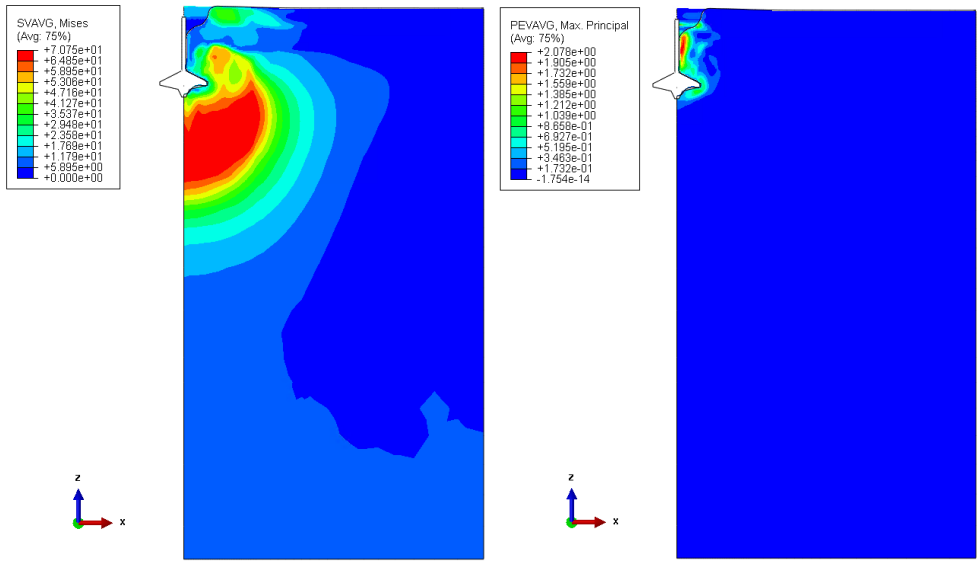

Fig. 21 Soil response in multi-layered clay validation;

a) Mises stress in penetration analysis;

b) Maximum principal plastic strain

Fig. 21 shows the total equivalent mises stress and plastic strain of the soil due to the spudcan penetration behavior in stiff-soft-stiff clay. In the strain rate dependent term in Eq. (2), total stress is used to calculate the total strain. Although not exactly the same, the range of mises stress plot is similar to the range affected by rate hardening. Likewise, although not exactly the same, the range that the maximum principal plastic strain plot affects is similar to that of strain-softening and has a large plastic strain around the disturbed soil.

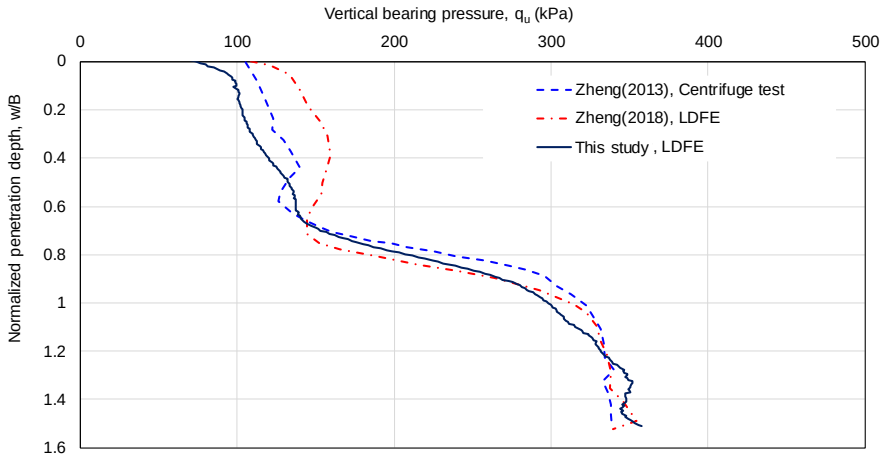

Fig. 22 Bearing capacity results of multi-layered clay

The centrifuge test data, existing LDFE analysis result, and numerical analysis results of the present study well shows the squeezing effect at the interface of the second soft layer and third stiff layer (w=0.92B). Although a small difference in bearing capacity curve can be caused by application of a different modeling technique in numerical analysis, it is thought that reasonable results have been obtained by using this LDFE analysis technique. Verification of the multi-layered clay soil has been performed, and it has been confirmed that the vertical capacity value obtained results similar to those of the existing results.

In this chapter, verification has been performed on the clay soil. For single clay and multi-layer clay soils, the results of the soil LDFE analysis developed in this study have been verified using the centrifugal model tests and LDFE results provided in the existing researches. As a result, it has been confirmed that the vertical

capacity value is well predicted according to the spudcan penetration behavior. This numerical analysis technique has been used to study the nonlinear soil model in the following chapters.

Chapter 3. Yield envelope in soft over stiff clay

3.1. Introduction

A fixed platform is an offshore structure that is fixed to the seabed in order to withstand wave, current, and wind loads. Whereas fixed platforms have long been used owing to their convenient installation, the operatable water depth is significantly limited. jack-up platforms, in-service mainly at depths within 150m, behave like fixed platforms by penetrating their legs into the seabed, but transport in float before and after operation. A jack-up platform consists of a superstructure, hull, and three-to-six independent lattice legs, each with an underlying footing called a spudcan. The Legs need to be embedded until achieving sufficient bearing capacity. Especially in clay seabed such as in the Southwest Sea of South Korea, spudcans can penetrate up to three times their diameter or until meeting stiff soil (Menzies and Roper, 2008). In the operation phase after penetration, a jack-up platform is subjected to environmental loads in addition to the load of its own weight, applying combined loads to the spudcan. Combined loads applied to the spudcan can be simplified in their classification as vertical (V), horizontal (H) loads, and rotational moment (M).

Strength assessment of a jack-up system subject to environmental loads is dynamically sensitive to the stiffness of the spudcan foundation due to the limited number of supporting

legs(Cheng and Cassidy, 2016a). Simple support and linear soil springs have been often used as the simplest stiffness models, and recently, a force–resultant model based on a plasticity framework has been formulated as an alternative foundation model. Models that described the combined foundation capacity and the empirical yield envelope expressed in terms of allowable combinations of V, H, M loads were pioneered and developed by Butterfield and Ticof (1979), Roscoe and Schofield (1956), and Schotman (1989). In the intervening years, significant improvements have been achieved in terms of clay and sand, as represented in the model B and model C, respectively (Cassidy, 1999; Cassidy et al., 2004; Martin, 1994; Martin and Houlsby, 2001). These models for both clay and sand have been the basis for plasticity framework models as well as modified models (Cheng and Cassidy, 2016b; Zhang et al., 2014a). In particular, for single clays, extensive research has been conducted into strength non–homogeneity, cyclic loading, soil plugs, and consolidation (Gourvenec and Randolph, 2003; Ragni et al., 2017; Vlahos et al., 2006; Vulpe, 2015). Vlahos et al. (2008a) demonstrated the concept of tensile capacity using a centrifuge model test, and Zhang et al. (2014b) formulated a modified model B by combining improvements such as tensile capacity, non–associated plastic potential, and others. Centrifuge model tests have mainly been used in the development of foundation models, while additionally, numerical studies have been performed by Templeton (2009); Templeton et al. (2005); Zhang et al. (2011b). However, most of the conventional studies in this vein have used numerical

analysis that has assumed an embedded position of spudcans as wished-in-space, with no consideration of soil disturbance caused by spudcan penetration (Zhang et al., 2014b). Meanwhile, studies on multi-layered soil considering actual soil profiles also have been carried out. The relevant previous studies have mainly investigated conditions wherein a strong layer overlies a soft layer with a possibility of punch-through failure (Abyaneh et al., 2018; Hu et al., 2017; Ko et al., 2017; Rao et al., 2015; Yin and Dong, 2019); that is to say, there has been no detailed investigation into a foundation model in soft-over-stiff layered soil such as clay-over-sand or soft-over-stiff clay, wherein the squeezing effect is operative (Wang et al., 2018).

The present study aims to derive yield envelope for soft-over-stiff clay, a condition that is mainly prevalent in the Southwest Sea of Korea. Large deformation finite element (LDFE) analysis using the Coupled Eulerian-Lagrangian (CEL) technique is adopted to simulate spudcan penetration and to perform a subsequent combined loads analysis to determine the disturbed soil properties owing to penetration and obtain, thereby, the yield envelope. Prior to the case of soft-over-stiff clay, the yield envelope data for single clay with a deep-embedded spudcan is accounted for. It is found that the conventional yield envelope equation is well matched for single clay, even at deep embedment more than 1.5 times the spudcan diameter. Subsequently, the effect of the lower stiff clay on the yield envelope is examined in two aspects: ultimate capacity and normalized shape. The underlying stiff clay enlarges the yield envelope directly in the

vertical direction due to the squeezing effect, which in turn affects the horizontal and rotational directions. As mentioned above, the squeezing effect refers to the phenomenon where the upper soft soil is squeezed due to the lower stiff soil. With this effect, the vertical bearing capacity of the foundation increases significantly, and the yield envelope changes accordingly. Furthermore, the shape of the resulting yield envelope cannot be represented by a simple quadratic surface. Consequently, it is found that the conventional equation for single clay has a limitation in its utility to express results for soft-over-stiff clay. Accordingly, based on the form of the conventional formulation of the yield envelope for single clay, this paper proposes a modified equation that is applicable to soft-over-stiff clay.

3.2. Numerical methodology

3.2.1. Soil conditions and spudcan specifications

Offshore wind farms have been established in the Southwest Sea of South Korea, in which location a common soil profile is soft-over-stiff clay (Ahn et al., 2017; Jin et al., 2019). A wind turbine installation vessel (WTIV) of the jack-up type that is operated in this region needs to penetrate its legs into the stiff soil layer to ensure sufficient bearing capacity.

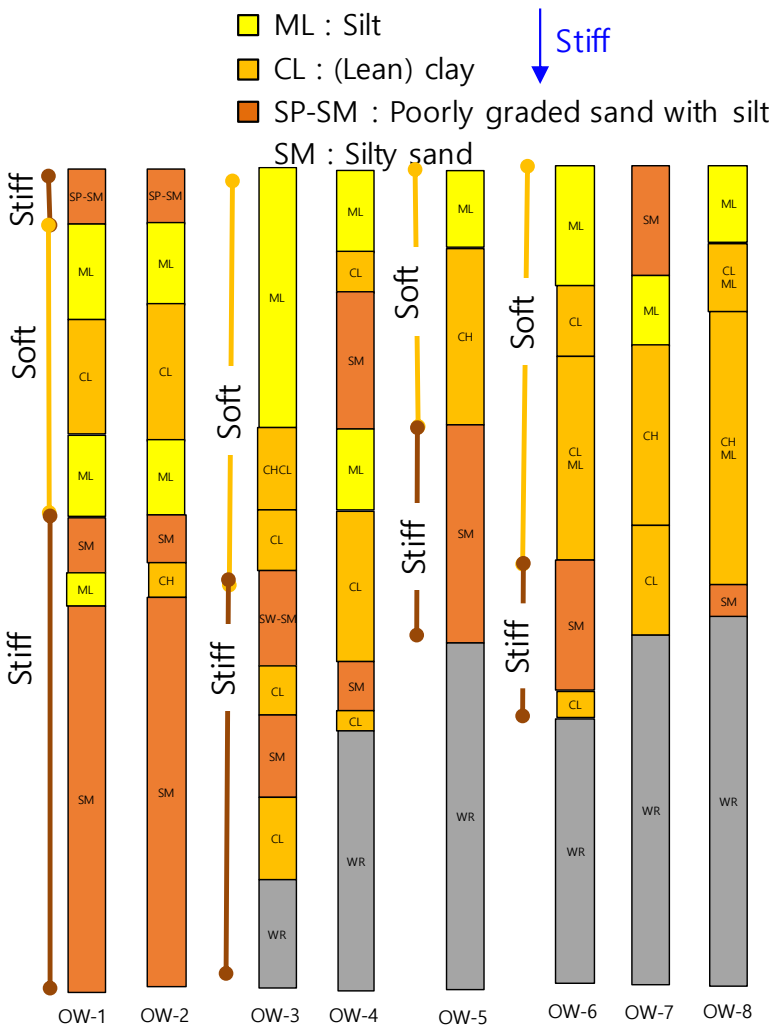

Fig. 23 Soil profiles of 8 boreholes in Southwest sea

Eight boreholes were drilled to investigate the soil properties of the southwest sea of South Korea (Fig. 23). The result is a soil profile consisting mainly of stiff−soft−stiff clay layer or soft over stiff clay layer. In the jack−up design, stiff clay near the seabed is not enough to obtain sufficient bearing capacity. That is why the jack−up leg should penetrate deeply until meeting the stiff soil.

When encountering such stiff soil, the spudcan is placed in the

transition area affected by both the upper soil clay and the lower stiff clay. However, the foundation model affected by both layers has not yet been established. In this study, soft over stiff clay is assumed as target soil of this study for simplicity.

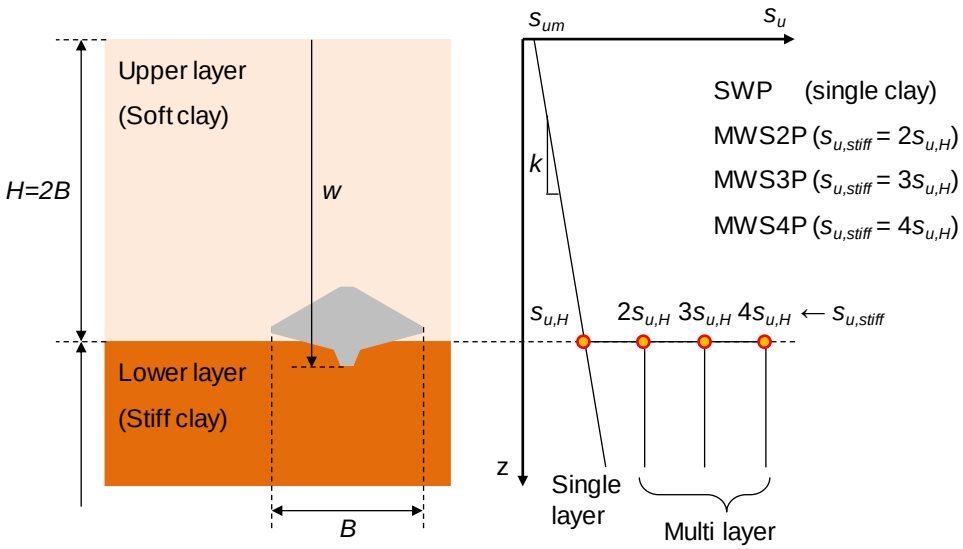

Fig. 24 Shear strength profiles of soft-over-stiff clay

Assuming this general soil condition of soft-over-stiff clay, the present study adopts representative soft marine clay properties for the upper layer. Menzies and Roper (2008) obtained Gulf of Mexico (GoM) jack-up data for spudcan specifications, soil properties and the corresponding observed vertical bearing capacity. Among these data sets, the spudcan specifications and clay properties for their site 1 are used in the present study to represent the upper soft clay layer. Also, an intact undrained shear strength of 2.4 kPa and an increasing slope of 1.35 kPa/m with depth are applied (s_u =

2.4+1.35z kPa). An averaged value of unit weight (γ = 5.36 kN/m^3) is assigned to the upper layer, and the general rigidity index and the Poisson ratio value of marine clay are used in the numerical analysis (E/s_u = 500, ν = 0.49). The height of the upper layer is modeled as 2.0B for the deep embedment necessary to achieve sufficient bearing capacity in soft clay.

In the case of the lower stiff clay layer, homogeneous undrained shear strength is assumed for the purposes of a simplified case study on soil stiffness. The stiff clay layer in multi-layered seabeds has often been assumed as homogeneous in literatures (Hossain and Randolph, 2010; Zheng et al., 2015; Zheng et al., 2016), and so accordingly, the lower stiff layer in the present study is also assumed to have uniform properties. The undrained shear strength is set as two, three, and four times the value at the interface of the upper layer, which cases are named MWS2P, MWS3P, and MWS4P, respectively. In fact, the realistic profile of soil has the continuous increase of s_u in the boundary of multi-layered soil. However, there is no exact information about soil profile in this transition zone. This detailed soil profile can affect the soil capacities like horizontal capacity, so the specific discontinuous soil profile has been used to clarify the lower clay effect. A comparative study on the effect of the lower stiff layer is performed using these three cases along with a single clay case (SWP). These cases and the corresponding shear strength profiles are illustrated in Fig. 24.

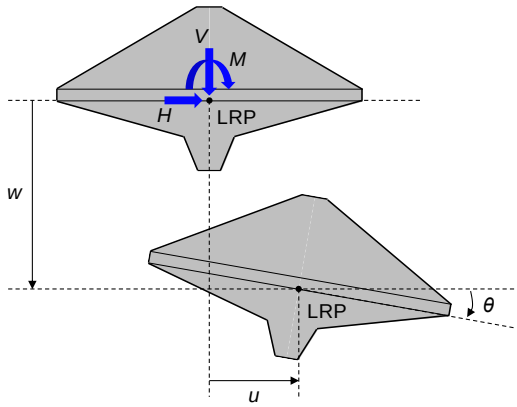

Fig. 25 Combined loads applied to spudcan (Zhang et al., 2014)

As noted earlier, a spudcan used in a real GoM field (Marathon LeTourneau Design, Class 166-C) is used as the basis for the simplified spudcan applied in the present study (Menzies and Roper, 2008). The simplified spudcan has a circular cross-sectional shape with same maximum bearing area. The slope of the lower conical geometry and the overall volume are maintained, but the sharp edge is smoothed out for numerical stability and cost efficiency. Therefore, the simplified spudcan has an equivalent diameter of 13.52m, a maximum bearing area of 143.6m^2, and a volume of 275m^3. Vertical, horizontal and rotational motions are loaded to the load reference point (LRP), the center of the lowest cross-section with the maximum bearing area. Displacements w, u, θ and reaction forces V, H, M in the vertical, horizontal, and rotational directions at the LRP, respectively, are given in Fig. 25.

3.2.2. Finite element model

A soil LDFE analysis based on the CEL technique and using the Abaqus/Explicit commercial program is performed to simulate soil behavior. Eulerian description is generally used to simulate the behavior of fluid, and so, in this description, the movement of the continuum is taken as a function of its instantaneous position and time. By comparison, Lagrangian description is mainly used for structural analysis with small deformation, and this description describes the movement of the continuum as a function of its initial coordinates and time (Qiu et al., 2009). Especially in large soil behavior problems such as spudcan penetration, Lagrangian description can incur mesh distortion. Eulerian description can solve this mesh distortion problem; however, it remains difficult to define an interface between structure and soil. Because the CEL technique overcomes each difficulty by taking advantage of both descriptions, spudcan penetration behavior has been simulated through this technique (Qiu and Grabe, 2012).

Soil properties change sensitively according to significant environmental disturbances. These clay properties are known to be dependent on both strain and strain rate (Einav and Randolph, 2005). In order to simulate the disturbed properties of clay, elasto-perfectly plastic material obeying a Tresca yield criterion incorporating strain softening and rate dependency is used. Einav and Randolph (2005) proposed the following equation of undrained shear strength as a function of strain softening and rate hardening

and this nonlinear model is presented in Eq.(2).

In the case of the upper soft layer, s_{um} is 2.4 kPa and k has the value of 1.35 kPa/m, as mentioned above. For general marine clay, the typical values of the parameters in Eq.(2) are provided below. The parameters in this study for the penetration and combined loads analysis (δ_{rem}=0.35, ξ_{95}=15, μ=0.1, $\dot{\xi}_{ref}$=1.0%/h) are adopted appropriately from within the following ranges:

- δ_{rem} (strength ratio) : 0.2 ~ 0.5
  (inverse of sensitivity S_t, 2 ~ 5)
- ξ_{95} (value of ξ for 95% remolding) : 10 ~ 25
- μ (rate parameter) : 0.05 ~ 0.20
- $\dot{\xi}_{ref}$ (reference strain rate) : 1 ~ 4%/h in triaxial sehar test, 20%/h in direct simple shear test.

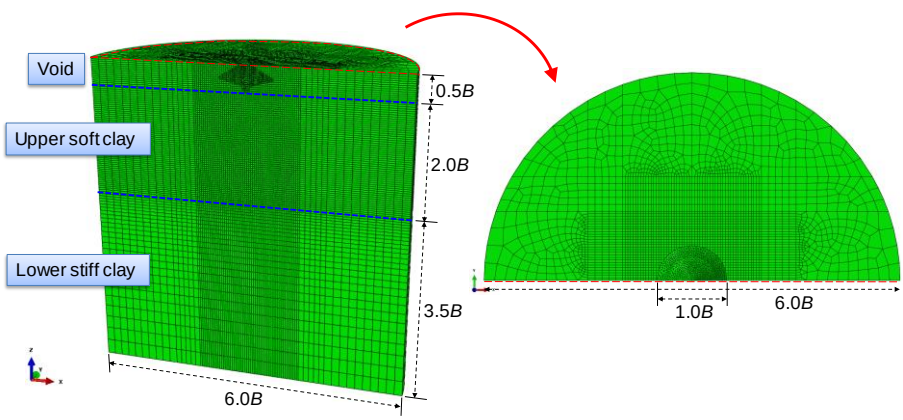

Fig. 26 Finite element model for constant V test and swipe test

The numerical analysis is performed using the CEL technique and the nonlinear undrained shear strength model. The geometry of the spudcan is face symmetric, and the vertical, horizontal, and

rotational motions also have symmetricity. Therefore, the half model and corresponding soil domain are modeled in this simulation (Fig. 26). The Eulerian element comprises 8-node linear brick elements with reduced integration (EC3D8R) for the soil domain, and the Lagrangian element comprises both a 6-node linear triangular prism element (C3D6) and an 8-node linear brick element with reduced integration (C3D8R) for the Spudcan structure. To avoid the boundary effect, a sufficiently large soil domain should be selected. Considering several previous numerical analyses such as penetration and combined loads analyses, 6.0B (=81.12m) of diameter and 6.0B of depth have been determined and validated through parametric study (Bienen et al., 2012; Ragni et al., 2017; Zhang et al., 2014b).

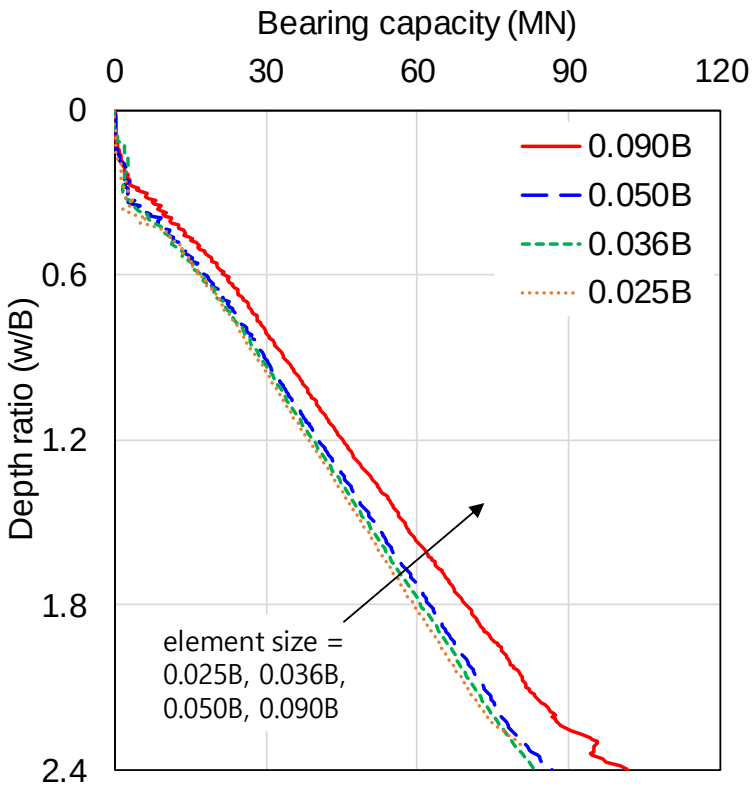

Fig. 27 Mesh convergence test in single spudcan analysis

A mesh convergence test has been carried out (Fig. 27), based on which, the spudcan and its surrounding mesh size used in this study are adopted as 0.05B (=0.676m). This fine mesh zone is modeled in the 3.0B range, with larger mesh sizes being used outside the region for computational efficiency. In the penetration analysis and subsequent combined loads analysis in this study, the coefficient of friction between the spudcan structure and the soil is assumed to be 0.1.

3.3. Penetration analysis to simulate soil disturbance

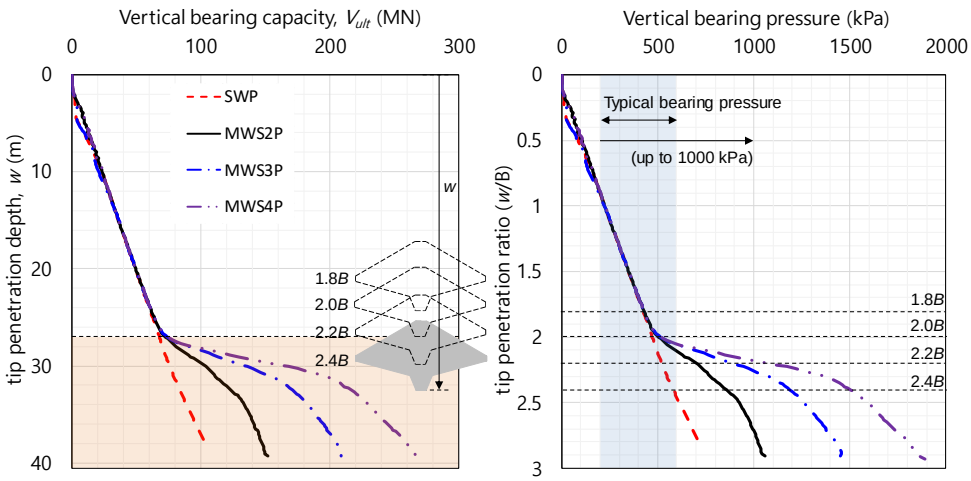

a) b)

Fig. 28 Penetration curve for soft-over-stiff clay;

a) Bearing capacity curve;

b) Bearing pressure curve and typical bearing pressure of jack-up

Penetration analysis, performed for consideration of disturbed soil properties due to large deformation, is completed prior to the combined loads analysis for the yield envelope calculation. The vertical bearing capacities for the soft-over-stiff clay cases (MWS2P, MWS3P, and MWS4P) as well as the single clay case (SWP) are shown in Fig. 28(b).

The effects of lower layer stiffness on the vertical bearing capacity can be checked in this penetration curve. As the spudcan tip passes to the boundary of the two layers, w = 27.04 m (= 2.0B), the squeezing effect starts to occur. The stiffer the clay is in place below, the larger the squeezing effect and the greater the increase

of vertical bearing capacity. On the basis of the depth at the boundary, 1.8B, 2.0B, 2.2B, and 2.4B are selected as the spudcan embedment for the yield envelope research. 1.8B shows a slight squeezing effect, which starts from the depth of 2.0B (the upper layer height). This squeezing effect becomes large at 2.2B, and the 2.4B embedment represents a situation wherein the maximum bearing area of the spudcan has passed to the boundary between the two layers. The calculated bearing capacity results for these penetration depths are shown in Table 3. There is little difference in these results according to the lower clay property at 1.8B, and the bearing capacity starts to vary at 2.0B. From the embedment of 2.2B, the bearing capacity has a larger value as the lower clay property becomes stiff. Typical spudcan bearing pressure is known to be in the range of 200 ~ 600 kPa, and a few cases have shown higher bearing pressures up to 1000 kPa (Hu & Cassidy, 2017). The penetration depths between 2.0B and 2.2B are calculated for the soft-over-stiff clay cases based on 600 kPa, which is generally the maximum bearing pressure. The stiffer cases, MWS3P and MWS4P, are also able to cover the specific case of 1000 kPa before 2.4B (Fig. 28(b)). Therefore, it can be thought that the selections of upper layer height and clay properties are appropriate in that the typical spudcan bearing pressure can be covered.

Table 3 Penetration results for single clay and several cases of soft-over-stiff clay

Bearing capacity (MN)				
w/B	SWP	MWS2P	MWS3P	MWS4P
1.8	60.70	61.86	61.83	61.97
2.0	68.15	72.56	74.41	74.82
2.2	75.00	99.53	127.44	153.64
2.4	83.25	123.27	170.84	216.44
Bearing pressure (kPa)				
w/B	SWP	MWS2P	MWS3P	MWS4P
1.8	422.78	430.87	430.71	431.64
2.0	474.70	505.45	518.29	521.16
2.2	522.41	693.29	887.71	1070.21
2.4	579.92	858.61	1190.01	1507.60

3.4. Combined loads analysis for single clay

3.4.1. Applied load sequence and load cases

Combined loads (V, H, M) analysis is conducted for the calculation of the yield envelope following the penetration analysis. This analysis is divided into two types of test, the swipe test and the constant V test. A commonly used swipe test has been

performed to outline the overall shape of the yield envelope. Both the compressive swipe test, which is the horizontal/rotational motion or combined motion after spudcan penetration, and the tensile swipe test, which is the motion after a small extent of extraction, are carried out. In addition, a constant V test is used to calculate the horizontal and rotational capacities at a specific constant vertical load. The obtainable results from the swipe test and constant V test are illustrated conceptually in Fig. 29. As shown in the figure, the overall shape of the yield envelope can be calculated through two swipe tests (blue line). Then, the maximum values of the horizontal/rotational directions are calculated through the constant V test (red line).

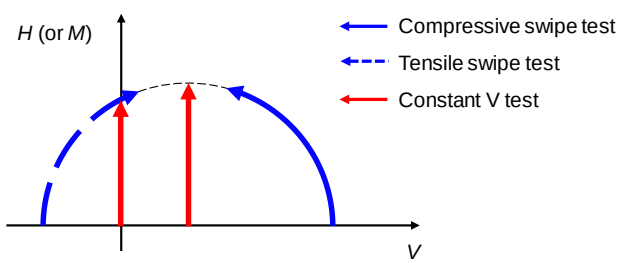

Fig. 29 Conceptualization of swipe test and constant V test

Through the swipe test, the combined critical state can be calculated from the load path after spudcan penetration and subsequent achievement of the critical state of the soil. Since it was adopted from the yield envelope studies by Tan (1990), the swipe test has often been used to calculate the yield envelope in conventional studies (Cassidy et al., 2004; Cheng and Cassidy, 2016;

Gourvenec and Randolph, 2003; Martin and Houlsby, 2000; Zhang et al., 2014a). The swipe test first moves the spudcan in a vertical direction by displacement control until the vertical capacity converges. The critical state is then maintained when the spudcan moves in the horizontal or rotational direction while fixing the vertical displacement. The critical load combination is calculated during the displacement controlled motion, and consequently, the load path tracks the yield envelope (Gourvenec and Randolph, 2003). The test is divided into the compressive and tensile swipe test, according to whether the vertical motion is penetration or extraction, respectively. In the present study, the approximate shape of the yield envelope is calculated using these swipe tests.

The constant V test has been used mainly in conventional studies to calculate the plastic behavior of soil. However, calculating the reaction force through the displacement-controlled motion occurring in a specific environment is the most common way to calculate the capacity. In this study, the specific point in the yield envelope is calculated by this test, especially a capacity at $V = 0$ and the maximum capacity in the horizontal or rotational direction (red line). Existing studies have indicated that the maximum value of horizontal/rotational capacity is reached at the median of the compressive and tensile vertical capacities (Vlahos et al., 2008; Zhang et al., 2013), and this is also shown in the numerical analysis of the present study. After calculating the compressive and tensile vertical capacities from the penetration and extraction motion, the median value is loaded vertically. While the vertical load is kept

constant, the horizontal/rotational movement is given. The converged reaction force in each direction is defined as the horizontal and rotational maximum capacity, respectively.

At the various spudcan embedments (1.8B, 2.0B, 2.2B, and 2.4B), capacity calculations and combined loads analyses for the yield envelope are carried out for both the single clay and soft-over-stiff clay cases. Prior to the multi-layered clay cases, a numerical analysis for single clay is conducted with the different embedments. The results for above the 1.4B embedment are recorded and validated against the existing theories suggested for single clay at a shallow depth. The capacities at 1.4B are additionally calculated for comparison. Then, the capacities in the three directions and the yield envelopes are calculated for the soft-over-stiff clay cases. Owing to the lower stiff clay, spudcan embedment and soil stiffness can affect the capacities and yield envelopes. The representative soft-over-stiff clay case (MWS2P) is selected for the case study with various embedments. Also, for the same penetration depth (w = 2.2B), the calculated yield envelope results are analyzed by changing the stiffness of the lower clay (MWS2P, MWS3P, MWS4P). The results from the softest case (SWP) to the stiffest case (MWS4P) for the effect of the lower stiff clay on the yield envelope are analyzed according to spudcan embedment and the soil properties.

3.4.2. Maximum capacity analysis for single clay

As mentioned earlier, the maximum capacities are calculated by constant V test. Fig. 30 shows the load−displacement ($H-u$) curve in the horizontal direction and the moment−rotation ($M-\theta$) curve in the rotational direction. The displacement−controlled motion is applied in the horizontal and rotational directions under the vertical median load between the compressive and tensile vertical capacities. Consequently, as in the experiments with plastic materials, the linear $H-u$ ($M-\theta$) relationship is shown until the yield point and then gradually converged in the plastic region. The converged values of H and M are defined as the horizontal and rotational maximum capacities (H_o and M_o), respectively. At this time, the location of the convergence point can have a significant effect on the calculation of the capacity. Based on the yield point, which is the end of the linear relationship, the convergence load becomes too small. If the displacement is applied until load convergence, it is difficult to determine the end, because the load and moment continue to increase little by little due to the characteristics of the nonlinear material. For this reason, a clear criterion is needed to determine the convergence. In previous research, the maximum capacity was defined based on a displacement of 0.5% diameter in the horizontal direction (Martin and Houlsby, 2000). Vlahos et al. (2008a) presented the horizontal load−displacement relationship until $0.035B$, and Cassidy et al. (2006) and Zhang et al. (2013) described the displacement up to $0.15B$ and $0.083B$ for clay and sand,

respectively. Taken together, it can be confirmed that the convergence is sufficiently satisfied if the horizontal displacement of $0.1B$ is considered as the criterion. In the present study, convergence loads corresponding to 4, 7, and 10% diameters (u = $0.04B$, $0.07B$, $0.1B$) are defined as the horizontal maximum capacity. The rotation multiplied by the diameter ($B\theta$) is also used on the same basis as the horizontal displacement (u), so the moment at the $B\theta$ of $0.04B$, $0.07B$ and $0.1B$ are calculated as the rotational maximum capacity. As such, since the convergence point can affect the capacity results, the equations of yield envelope are proposed with three different criteria. No matter which criterion is adopted, reasonable conclusions can be drawn if the capacity is calculated on a consistent basis for convergence.

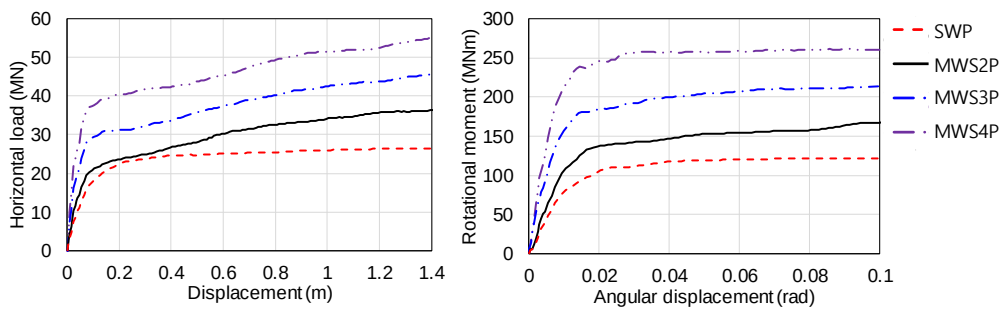

a) b)

Fig. 30 Load(Moment)−displacement(rotation) curve;
a) in horizontal direction; b) in rotational direction

$$h_o = \frac{H_o}{V_{ult}} \tag{3}$$

$$m_o = \frac{M_o}{V_{ult}} \tag{4}$$

The horizontal and rotational maximum capacities of single clay are calculated, and the results are shown in Fig. 31. h_o and m_o are the maximum capacity ratio and the mean of the horizontal maximum capacity and rotational maximum capacity divided by the vertical ultimate capacity, respectively (Eq. (3), (4)). These ratio values are used to compare the maximum capacities on the same basis as in the conventional studies. First, as mentioned above, the maximum capacities are calculated by using the constant V test. This test can calculate the horizontal/rotational capacity for the specific vertical load under which other factors are not taken into account. However, conventional studies such as that of Zhang et al. (2014c) have calculated the maximum capacities by regression of the peak from the swipe test results. Conventional studies suggested that the yield envelope from numerical analysis accords the ellipsoid, and that the yield envelope from the centrifuge test follows the paraboloid. In consideration of this, in the present study, both the elliptic and parabola shapes are fitted to the swipe test results of each VH, VM plane. The regressed peak values of the two shapes are illustrated with the results of conventional studies in Fig. 31.

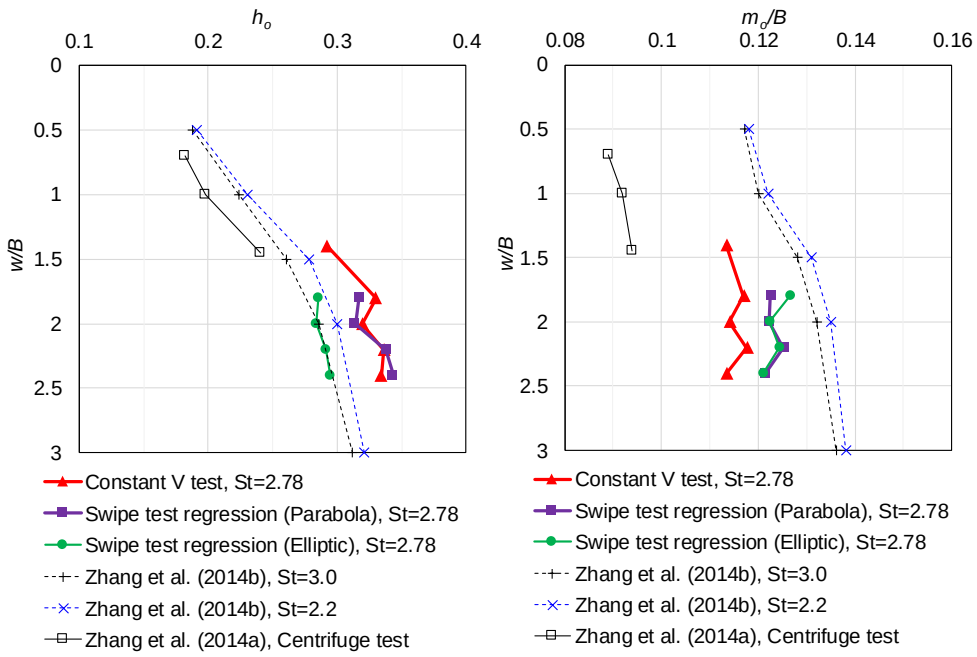

a) b)

Fig. 31 Comparison of maximum capacity ratio;
a) horizontal direction; b) rotational direction

In Fig. 31(a), the calculated horizontal maximum capacity ratio (h_o) is compared with the results from the centrifuge tests and numerical analyses of conventional studies (Zhang et al., 2013; Zhang et al., 2014b). The two numerical analysis cases that can cover the sensitivity of 2.78 used in the present study are presented (S_t = 2.0, 3.0), and the regression results for the elliptic shapes exist between those cases. The results of the constant V test and the regression with the parabola have a larger value of about 0.33. In the numerical results of the previous study, the slope of the h_o value decreased as the embedment increased, which is the same as the result of the present study. For 1.4B, the h_o value is smaller

than 0.3, but approaches to a larger value for $1.8B$ and above. The results of the centrifuge test exist only below $1.45B$ of embedment, and the ratio value also increases as the depth increases in that range. In summary, it is found that h_o increases linearly with embedment up to a specific depth (about $1.5B$). After that depth, the rate of increase decreases and h_o finally comes close to a certain value, about 0.33.

The ratio values of rotational maximum capacity (m_o/B) are shown in Fig. 31(b) in the same way as in the horizontal direction. The m_o/B values of this study are found to exist between the numerical analysis and the centrifuge test results of conventional studies. In the previous study, the slope in the rotational direction was smaller than that in the horizontal direction, and the same result is shown in this figure. The m_o/B values from the constant V test at embedments from $1.4B$ to $2.4B$ have a similar value of about 0.115, and the regression results also converge near 0.12. Unlike the horizontal direction, the maximum capacity in the rotational direction can be considered to show a relatively similar trend to that of the vertical ultimate capacity, due to the converged capacity ratio.

3.4.3. Yield envelope in single clay

Fig. 32(a) summarizes the calculated yield envelope results for the vertical–horizontal (VH) plane, vertical–rotational (VM) plane, and horizontal–rotational (HM) plane in the case of single clay. Combined loads analyses are carried out for the embedments of 1.8B, 2.0B, 2.2B and 2.4B, respectively. The size of the yield envelope increases regularly as the embedment deepens. The uniform spacing of the graphs means that the shapes of the yield envelope are similar, which phenomenon can also be seen in the normalized yield envelope (Fig. 32(b)). The graphs in Fig. 32(a) are normalized using the vertical ultimate capacity (V_{ult}) in the vertical direction, and the capacities at $V = 0$ in the horizontal/rotational directions ($H_{V=0}$, $M_{V=0}$), respectively. These values represent the vertical positive intercept, the horizontal intercept, and the rotation. In the single clay, the normalized yield envelopes all have a similar shape in the VH, VM, and HM plane, regardless of the embedment. Since the normalization process divides the influence of the two factors of the yield envelope, the size and shape are analyzed separately.

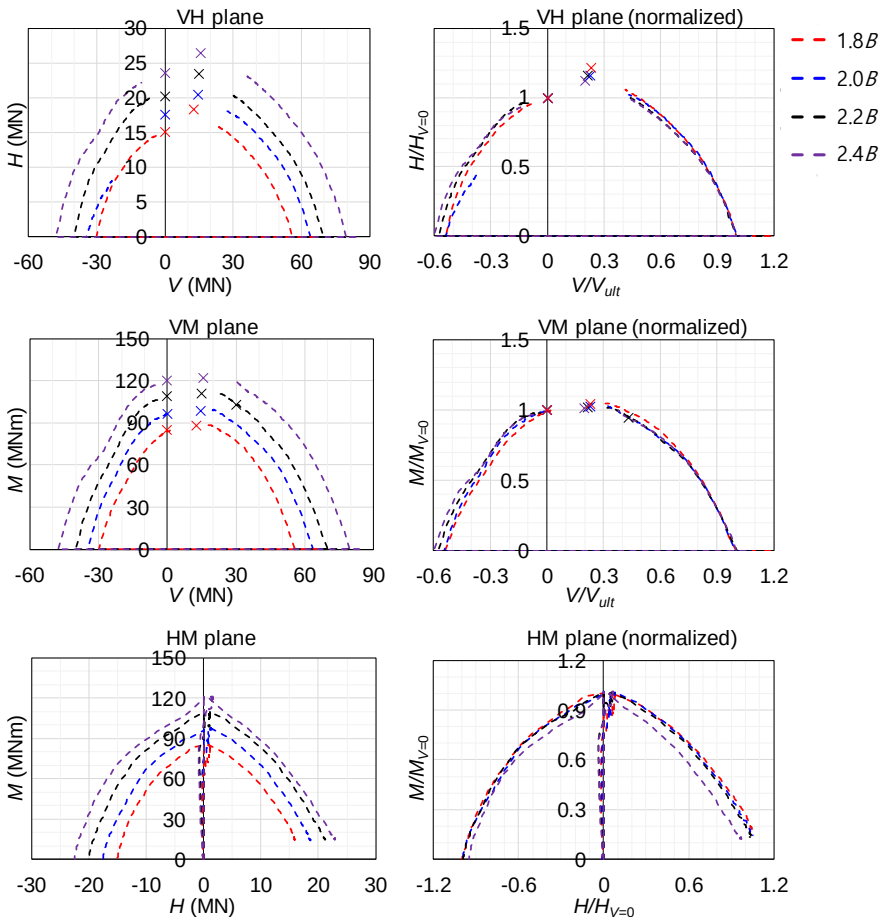

a) b)

Fig. 32 Numerical analysis results of SWP; a) Load path; b) Normalized shape with each intercept

In the VH, VM planes, the shape has a vertex defined as the maximum horizontal/rotational capacities at the median between the compressive and tensile vertical capacities. This load path is shaped like a quadratic curve, which is consistent with the results of Vlahos et al. (2008a) and Zhang et al. (2013) considering the tensile capacity. Backfill soil has a significant impact on the calculation of tensile capacity, which has already been considered in this study.

However, time effects such as consolidation and suction effects have not considered in this study. The calculated tensile capacity ratio is similar to the value in the existing centrifuge model test, and it is used as it is. However, it is considered that a more accurate yield envelope can be calculated by using the tensile capacity reflecting these effects.

The yield envelope at deep embedments above $1.5B$ through numerical analysis is calculated in the present study, unlike the existing studies which used relatively shallow embedment. The normalized yield envelope illustrates that the embedment does not affect the yield envelope shape, and so the conventional analytic equation for shallow depth can also be applied to the deeper case. This conventional equation is fitted to the single clay results at deep embedments in the present study, and the regression results are reported in Table 4.

Table 4 Parameters fitted with conventional equation of single clay

	W	h_o	m_o	e	χ
Centrifuge test (Zhang et al., 2014a)	0.7D	0.182	0.089	0.380	0.6
	1.0D	0.198	0.092	0.244	0.6
	1.45D	0.242	0.094	0.150	0.6
Numerical analysis (present study)	1.8B	0.317	0.123	0.140	0.54
	2.0B	0.314	0.122	0.118	0.54
	2.2B	0.338	0.125	0.079	0.58
	2.4B	0.344	0.122	0.053	0.60

The h_o and m_o values of Table 4 are also presented in Fig. 31 above, where the conventional centrifuge test data is the black line with empty square points, and the numerical analysis result is the purple line with filled square points. The trend in the centrifuge test that appears as the embedment increases is also continued in the numerical analysis. The eccentricity continues to decrease, so that the yield curve approaches symmetry, and the tensile capacity ratio (χ) has a similar value of 0.6. This slight eccentricity is presented in the HM plane. Zhang et al. (2011a), who performed a small-strain finite element (SSFE) analysis below the $1.4B$ depth, documented that the deeper the embedment, the more minor the eccentricity. The embedment covers in the present study ranged from $1.8B$ to $2.4B$, and the earlier study noted above also has determined that the eccentricity is not significantly revealed at these depths. The normalized shapes of the HM plane are grouped as one regardless of embedment, like those of the VH, VM planes. This shows that, in the formulation of the yield envelope, size and shape can be considered separately through the normalization process.

3.4.4. Soil flow mechanism in combined loads analysis

Combined loads analyses are subsequently performed on the soft-over-stiff clay, which is the target soil of the present study. Fig. 33 shows the soil behavior of each motion when the tip of the spudcan has touched the boundary. As can be seen in Fig. 33(a), when the spudcan penetrates vertically, the soil below is first

pressed. At the same time, the soil on both sides moves upward, and so the soil below flows round and rises up. This flow of soil is called backflow, and ISO (2012) suggests an analytic equation for this. As such, the lower soil has a great influence on the vertical behavior of the spudcan. On the other hand, the horizontal behavior of the spudcan causes movement of the lateral and upper soil (Fig. 33(b)). When the spudcan rotates, the around soil rotates in the same direction (Fig. 33(c)). The right-side soil of the spudcan moves downward and the left-side soil moves upward, and so both the soil below and above affect the rotational behavior of the spudcan. The main concern for soft-over-stiff clay is the existence of lower stiff clay. Penetration behavior is predicted to be strongly influenced by the underlying soil, whereas horizontal behavior is predicted to be relatively independent. Rotational behavior, meanwhile, is expected to be affected by both the upper and lower soils, depending on the side of the spudcan.

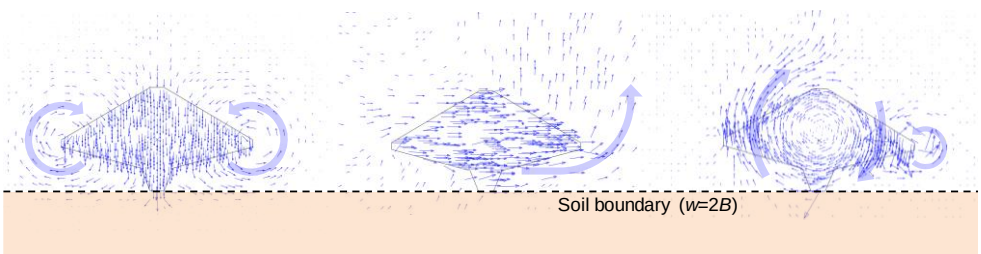

a) b) c)

Fig. 33 Soil flow in combined loads analysis; a) vertical direction; b) horizontal direction; c) rotational direction

3.5. Combined loads analysis for soft-over-stiff clay

3.5.1. Maximum capacity for soft-over-stiff clay respecting embedment

Fig. 34 shows the horizontal and rotational maximum capacities in a soft−over−stiff clay case (MWS2P), under the vertical median load between the compressive and tensile vertical capacities. The calculated results from the constant V test are plotted according to the embedment and the lower soil properties. The penetration results for soft−over−stiff clay and single clay show very little difference until the spudcan tip reaches 2.0B, the soil boundary (Fig. 34). The maximum capacity calculation of the embedment from 1.8B to 2.4B is performed to cover the range with and without influence from the lower stiff soil. The maximum capacity is greater with deeper embedment, due to stiffness, pressure, and so on. This tendency is presented not only in the vertical capacity, but also in the horizontal/rotational capacity in Fig. 34(a). The single clay results (the red dashed line) increase nearly linearly with increasing depth, whereas the soft−over−stiff clay shows a sharp increase in capacity values near 2.2B. When the spudcan tip penetrates more than 2.0B, the squeezing effect begins to occur, and 2.2B is the depth affected by the lower stiff clay, while 2.4B is the point where the maximum bearing area of the spudcan penetrates into the lower stiff clay, thus resulting in increased capacity.

Fig. 34(b) shows the ratio of the maximum capacity in the

horizontal/rotational directions to the vertical ultimate capacity. In the case of the horizontal direction, the ratio of the maximum capacity decreases at the depth of 2.2B. According to the soil flow mechanism and Wang et al. (2018) and Wang et al. (2019), the horizontal behavior of the spudcan is affected by the lateral soil. The laterally projected area of the spudcan is not overlapped with the lower stiff clay, and so the horizontal behavior is less affected by the lower stiff clay than is the vertical capacity. As the horizontal capacity increases less than the rapidly increasing vertical capacity, the ratio value starts to decrease at 2.2B. However, at 2.4B, where most of the spudcan has penetrated the soil, the laterally projected area overlaps much with the lower clay. This causes the horizontal capacity to be much larger, and the ratio value increases compared to the 2.2B depth. Regardless of the underlying soil stiffness and embedment, it is found that the ratio value in the stiff clay region becomes smaller than that of single clay, due to the squeezing effect.

The ratio value in the rotation direction shows a difference from the horizontal direction. The slightly reduced ratio value at 2.2B starts to decrease significantly at 2.4B. As shown in Fig. 33(c), the rotational behavior of the spudcan causes movement of the surrounding soil, and so both the soil below and above affects the capacity. Unlike the horizontal direction, a side of the maximum bearing area of the spudcan is pressed against the lower stiff layer at 2.2B (Fig. 33(c), right). As the squeezing effect occurs in that area, the rotational capacity also increases significantly. The capacity ratio decreases due to the left side, which is less affected

by the lower stiff clay, but the difference is small. However, as the spudcan penetrates, no further squeezing effect occurs, and the movement of the opposite side raises the upper soft clay. As a result, the rotational capacity does not increase much compared with the vertical capacity, which is affected directly by the lower stiff clay, and consequently, the capacity ratio decreases at 2.4B.

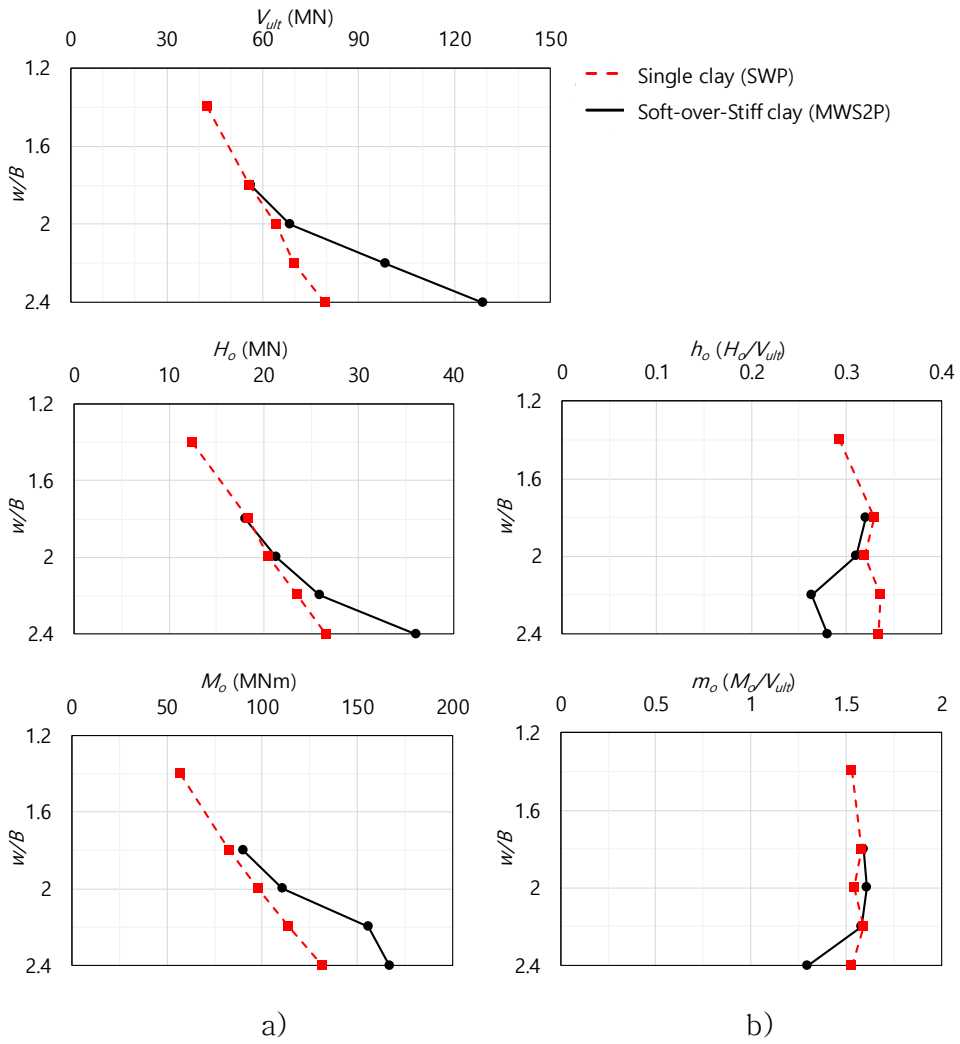

Fig. 34 Constant V test results for depth; a) maximum capacity; b) maximum capacity ratio

3.5.2. Maximum capacity in soft-over-stiff clay for lower clay properties

Fig. 35 shows the trend of the maximum capacity according to the stiffness of the lower clay. The results of the combined loads analysis in the $1.8B$ case, which show little difference between single clay and soft-over-stiff clay, are presented first. And then, the maximum capacities and the capacity ratios at the $2.2B$ and $2.4B$ depths represent the region affected by the lower stiff clay. At $1.8B$, where the spudcan tip does not reach the soil boundary, the soft-over-stiff clay has similar vertical, horizontal and rotational capacities to those of the single clay (Fig. 35(a)). This result is also consistent with the capacity results respecting embedment. In the regions where there is no effect from the lower stiff clay, the single clay and soft-over-stiff clay shows the same results.

At the graph about the maximum capacities of $2.2B$, the effects of the lower stiff clay are presented in Fig. 35(b). As the undrained shear strength of the lower clay becomes two, three, and four times stiffer than that of the upper soft clay, the maximum capacities in the horizontal/rotation direction all increase. Large capacities relative to single clay reflects a large effect of the lower layer, which has also been demonstrated by the tendency according to which stiffer lower clay properties mean greater maximum capacity values. In comparison, the maximum capacity ratio for the vertical ultimate capacity decreases as the lower clay properties become stiffer. The horizontal capacity is greatly reduced, and the rotational capacity is

small but also tends to decrease. As mentioned above, the horizontal behavior has been affected by the lateral soil, not the underlying soil, and so the horizontal capacity in the soft-over-stiff clay does not increase as much as the vertical capacity does. As a result, the horizontal maximum capacity ratio is greatly reduced. However, the rotational behavior is found to be related to the lower stiff soil, as it is influenced by both the soil below and above, and accordingly, the maximum capacity increases significantly according to the stiffness of the lower clay. Since this increase rate is smaller than that of the vertical capacity due to the squeezing effect, the capacity ratio decreases slightly as a result.

The maximum bearing area of the spudcan crosses the soil boundary at $2.4B$ of spudcan tip penetration, and so the squeezing effect is stronger and the trend mentioned in the previous paragraph becomes more pronounced (Fig. 35(c)). As shown in Fig. 34(a), the horizontal capacity starts to be affected by the lower clay at $2.4B$ because the spudcan laterally significantly overlaps the lower ground, and thus too, the capacity value is slightly increased. Nevertheless, the rate of increase in vertical capacity is the greatest, and the capacity rate decreases accordingly. The same phenomenon happens in the rotation direction. The value of maximum capacity increases due to the lower stiff clay; however, the capacity ratio for the vertical capacity decreases as the lower clay becomes stiffer.

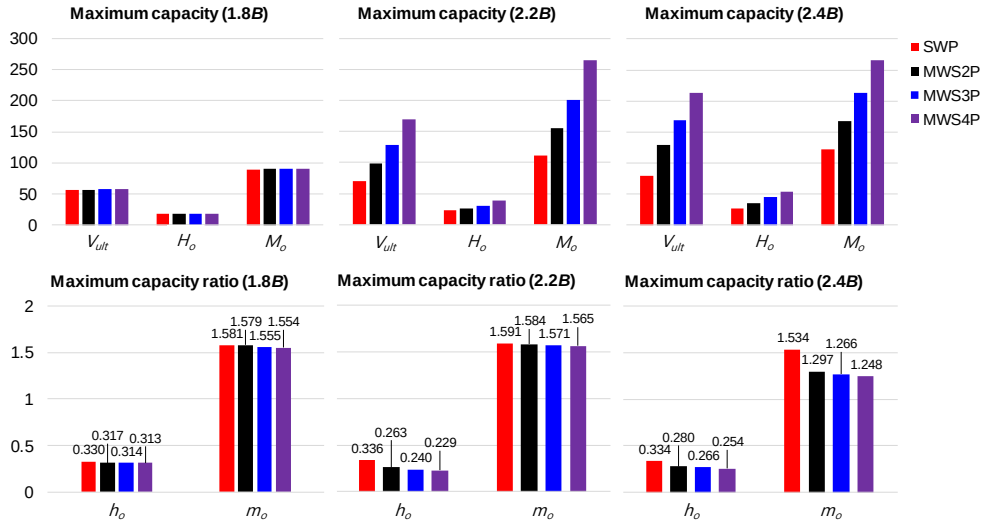

a) b) c)

Fig. 35 Constant V test results for lower clay properties;

a) w=1.8B; b) w=2.2B; c) w=2.4B

3.5.3. Yield envelope in soft-over-stiff clay respecting embedment

Fig. 36 shows the results of the yield envelope calculation for different depths of soft-over-stiff clay, the target soil of this study. The MWS2P case, where the undrained shear strength of the lower clay is twice the boundary value of the upper clay, is selected as the representative case. As with the case of single clay, the yield envelopes are shown for the VH, VM, and HM planes.

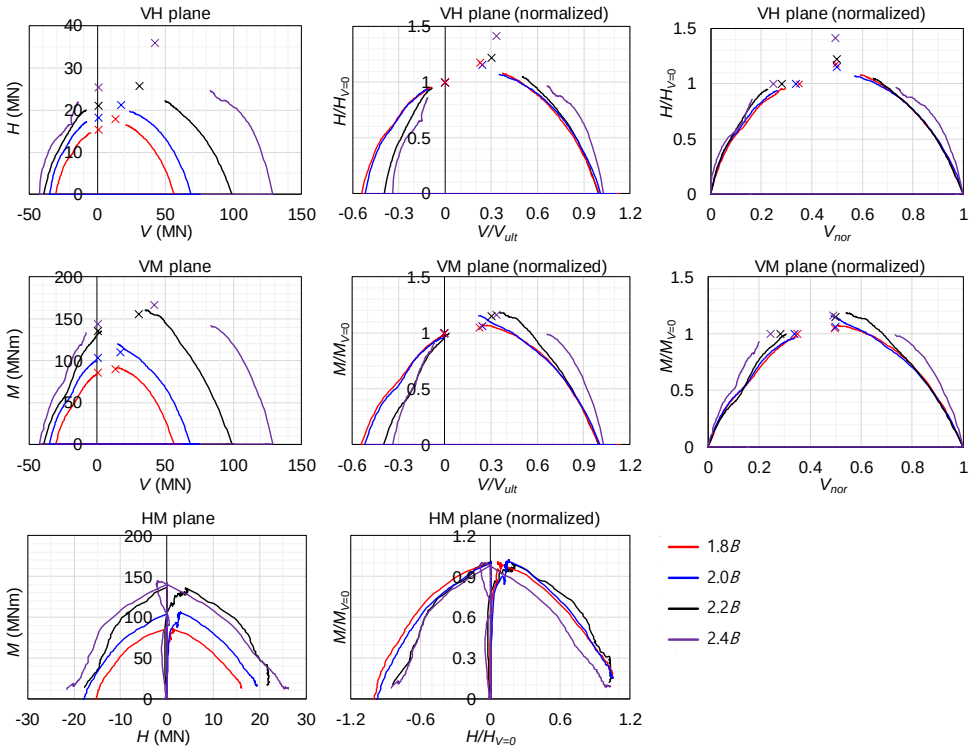

a) b) c)

Fig. 36 Numerical analysis results for MWS2P respecting depth; a) Load path; b) Normalized shape with each intercept; c) Normalized shape considering vertical tensile capacity

The increase in the compressive maximum vertical capacity can be seen in the yield envelopes of the VH, VM planes (Fig. 36(a)). This trend is also shown in the results for the penetration curve in Fig. 28. As the spudcan approaches the lower stiff clay, the deeper the depth, the greater the vertical capacity due to the squeezing effect becomes. In comparison, the tensile maximum vertical capacity does not increase significantly. The tensile capacity is calculated from the extraction of the spudcan, which is mainly influenced by the soft clay of the upper part. This change in vertical

capacity causes the center of the yield envelope to move to the right. The maximum capacity in the horizontal and rotational directions is calculated at this center point by moving along the vertical direction. As with the trend of maximum capacity, the yield envelope results from the swipe test consistently show increasing capacity. The deeper the embedment, the larger is the yield envelope in all directions.

Fig. 36(b) shows the yield envelope normalized to the compressive maximum vertical capacity, horizontal capacity at $V = 0$, and rotational capacity at $V = 0$, respectively. For the VH, VM planes, the yield envelope of $2.0B$ depth is similar to that of $1.8B$. There is little effect of the lower stiff clay at the embedment of $2.0B$, so that the shape is consistent as in the case for the single clays. However, the shape starts to change from $2.2B$, when the effect of the lower stiff clay begins to be not negligible. It is found that the tensile capacity does not increase relative to the compressive maximum vertical capacity, which increases due to the squeezing effect, and thus the normalized shape narrows in the tensile part. The tensile capacity is normalized as the tensile capacity ratio (χ), and it is found that χ gradually decreases from the typical value of single clay, about 0.6. This trend is further exacerbated at $2.4B$, where the effects of the lower stiff clay are greater.

Narrowed shape in the vertical direction makes the effect in the horizontal/rotational direction less obvious. The normalization method is changed in the vertical direction as depicted in Fig. 36(c),

so the maximum capacities at the different embedments gathers at a line. In Fig. 36(c), the yield envelope is normalized to have a value between 0 and 1 in the vertical direction. It is first horizontally shifted first by the tensile capacity and then is divided by the sum of the tensile and compressive capacities. The tensile capacity is defined as χV_o using the definition of the tensile capacity ratio used in the existing equation, and the equation summarized using this is shown in Eq. (5).

$$V \quad \rightarrow \quad V_{nor} = \frac{V + \chi V_o}{(1+\chi)V_o} \tag{5}$$

where V: Vertical reaction force in load path, V_o: Vertical ultimate capacity (compressive capacity), χ: Tensile capacity ratio.

Fig. 36(c) shows that deep embedment makes the ratio of the maximum capacity ratio large. As in the vertical direction, the shapes rise in the horizontal/rotational direction from the embedment of $2.2B$, and the maximum capacity ratio also increases. The ratios of the maximum capacity and intersection point at V=0 are constant in the case of single clay, so that the peak matches; however, lower stiff clay ensures that the horizontal/rotational capacities do not increase at a constant rate with respect to other vertical loads. This effect should be considered at the yield envelope of soft-over-stiff clay.

The yield envelope in the HM plane shows a different trend from the VH and VM planes. As indicated in Fig. 36(a), the deeper the

embedment, the larger the yield envelope. However, if the calculated yield envelope is normalized to the horizontal and rotational capacities at $V = 0$, the shape becomes similar regardless of the embedment. It is noted earlier that the tensile part is calculated from the extraction behavior of the spudcan and is affected by the upper soft soil. The point $V = 0$ is close to the tensile maximum vertical capacity, and so its cross-section, the yield envelope in the HM plane, is more affected by the upper soft soil. For this reason, it can be determined that the yield envelope in the HM plane is less affected by the lower stiff clay than in the VH and VM planes.

3.5.4. Yield envelope in soft-over-stiff clay for lower clay properties

In order to analyze the effect of lower stiff clay in detail, the yield envelope is plotted for varying undrained shear strengths of the lower layer (Fig. 37). It is noted above that the characteristics of single clay and soft-over-stiff clay diverge from $2.2B$ of embedment. Accordingly, with the $2.2B$ embedment fixed, the swipe test are performed when the undrained shear strength of the lower clay is two, three, and four times the boundary value of the upper clay, and those results are showed in Fig. 37. Those cases are named MWS2P, MWS3P, and MWS4P, and are plotted with the single clay case (SWP) for comparison.

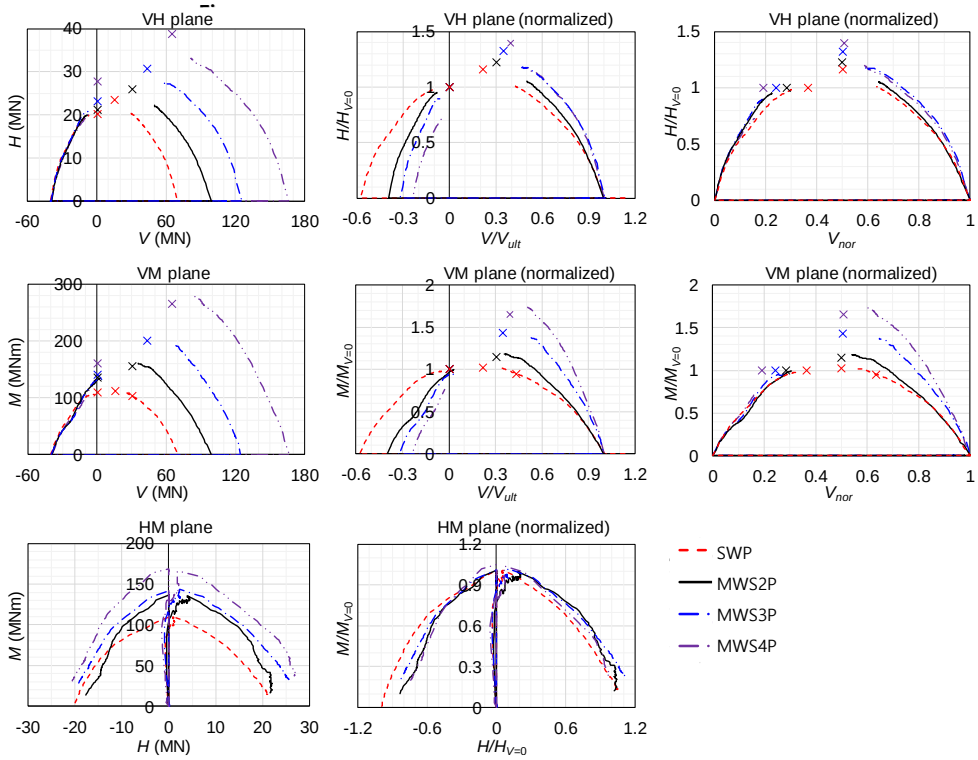

a) b) c)

Fig. 37 Numerical analysis results for lower clay properties at w=2.2B; a) Load path; b) Normalized shape with each intercept; c) Normalized shape considering vertical tensile capacity

Fig. 37(a) shows the calculated yield envelope according to the lower clay properties. There is a larger vertical capacity in the stiffer lower clay in the penetration curve, which is also presented in the compressive maximum vertical capacity of the yield envelope. On the other hand, it is apparent that the tensile capacity has a constant value regardless of the stiffness of the lower clay. From the results for embedment, it has already been concluded that the tensile capacity is less affected by the underlying soil. These results

according to the stiffness of the lower clay clearly indicate that the tensile capacity is little related to the lower stiff clay. These effects make the tensile part fixed and enlarge the yield envelope in the compressive direction. It can also be found that the maximum capacity increases in the horizontal and rotational directions as the lower clay stiffens. Just as the deeper embedment makes the effect of the lower clay increase, the stiffness of the lower clay also increases this effect.

The normalized shapes in Fig. 37(b) show the effect of the lower stiff clay, which increases with stiffness. As in the Fig. 36(b), the calculated yield envelopes are normalized using the intercept value of each axis. The width of the yield envelope is narrowed due to the decreasing tensile capacity ratio (χ). The ratio decreases due to the increasing compressive capacity relative to the constant tensile capacity. Fig. 37(c) shows the modified normalization in the vertical direction as in Eq. (5) considering the tensile capacity. According to the stiffness of the lower clay, the shape and the maximum capacity ratio are increased in the horizontal/rotational direction. All of these trends are identical to those observed at the embedments of $2.2B$ and $2.4B$, and so they can be considered to be characteristic of the shape of the yield envelope due to the lower stiff clay.

In the HM plane of Fig. 37, similar results are found between single clay and soft-over-stiff clay. The calculated yield envelopes are larger when the lower clay becomes stiffer, but similar when normalized. As with the results in Fig. 36, it is found that stiff clay affects the VH and VM plane sections of the yield envelope, but the

HM plane section less so. In this study, the effects of lower stiff clay in the VH and VM planes are quantified into an analytic expression. For the HM plane, since the soft-over-stiff clay has a shape similar to that of the single clay, the existing formula of the single clay is used as is.

3.6. Yield envelope equation proposed for soft-over-stiff clay

3.6.1. Derivation of the quadratic curve in the VH, VM plane

Keeping the form of the single clay equation suggested in the previous studies, an analytic equation that can express the yield envelope for soft-over-stiff clay is proposed. The equation for the yield envelope of single clay has been sought after in various studies. ISO (2012) has suggested a yield envelope equation with interpolating paraboloid and ellipsoid using a depth coefficient. In addition, spudcan-soil adhesion can be considered to provide additional horizontal and rotational capacity. Recently, a yield envelope in the form of a paraboloid in consideration of the tensile capacity was presented in Zhang et al. (2013) via a centrifuge model test. With reference to these equations, this paper intends to present an analytical equation that can represent soft-over-stiff clay in consideration of its tensile capacity.

Before presenting the analytic expression, the normalization

method is modified in order to express the result of the swipe test as a representative shape. In the vertical direction, the yield envelope is normalized to have a value between 0 and 1 (Eq. (5)). In the horizontal and rotational directions, the calculated load path is normalized using the maximum capacity in each direction (Eq. (6), (7)). The maximum capacity value is obtained using the constant V test at the specific vertical load, and the swipe test results are divided by this value. All normalized values should be between 0 and 1 in theory. However, in Fig. 38, there are some graphs that are expected to exceed 1 at the vertex. This is due to the fact that, because of the calculation procedure of the constant V test, a slight difference can exist between the calculated maximum capacity from the constant V test and that from the swipe test. In numerical analysis, instability occurs when horizontal or rotational motion has been given immediately after penetration behavior. In order to prevent this, a small downward displacement is applied along with the vertical load prior to loading of the horizontal or rotational motion. Especially in the cases of the $2.2B$ and $2.4B$ embedments, where squeezing occurs, the vertical capacity is sensitively increased even with a slight downward movement, which is considered to affect the maximum horizontal and rotational capacity. However, these effects are not significant, and so analysis stability is given priority in the present study.

$$H \quad \rightarrow \quad H_{nor} = \frac{H}{H_o} \tag{6}$$

$$M \quad \rightarrow \quad M_{nor} = \frac{M}{M_o} \tag{7}$$

where H, M: Horizontal reaction force and Rotational reaction moment in load path, H_o, M_o: Horizontal and Rotational maximum capacity

Through this normalization process, the load path becomes a curve that passes through (0,0), (1,0) and has vertices of (0.5, 1) in the VH and VM planes. Before presenting the new expression of this curve, a quadratic curve is derived. First, a parabola is assumed, one of the representative quadratic curves (blue dashed line). Assuming that the cross-section in VH (VM) plane is a parabola, the yield envelope becomes paraboloid. The parabola about the VH plane is summarized through the procedure of Eq. (8). Since the form of the equation is the same in the VM plane, it is omitted.

$$\begin{aligned} H_{nor} &= 4 \cdot V_{nor} \cdot (1 - V_{nor}) \\ &= 4 \cdot \frac{V + \chi V_o}{(1+\chi)V_o} \cdot \left(\frac{V_o + \chi V_o}{(1+\chi)V_o} - \frac{V + \chi V_o}{(1+\chi)V_o} \right) \\ &= \frac{4}{(1+\chi)} \cdot \left(\frac{V}{V_o} + \chi \right) \cdot \left(1 - \frac{V}{V_o} \right) \end{aligned} \tag{8}$$

As in Eq. (8), the exponent of V in three-dimensional paraboloid has two times that of H (or M). Regardless of the consideration of tensile capacity, this form of paraboloid has been used as the yield envelope by Martin (1994); Martin and Houlsby (2000); Vlahos et al. (2008a); Zhang et al. (2014b). ISO (2012) also has

recommended a paraboloid formula for shallow depths (w=0). If the tensile capacity is not taken into account, the ratio of V to V_o is used as the value of V_{nor} (V/V_o).

Second, the equation is derived by assuming the normalized shape as an elliptic, another form of quadratic curve (blue dotted line). The cross-section of the ellipsoid becomes an ellipse, and so this elliptic equation is derived as Eq. (9) by formulating it with respect to the VH plane. Also, the result for the VM plane is the same as that for the VH plane.

$$\frac{(V_{nor}-0.5)^2}{0.5^2}+ {H_{nor}}^2 = 1$$

$$\begin{aligned} {H_{nor}}^2 &= 4 \cdot V_{nor} \cdot (1 - V_{nor}) \\ &= \frac{4}{(1+\chi)^2} \cdot \left(\frac{V}{V_o}+\chi\right) \cdot \left(1-\frac{V}{V_o}\right) \end{aligned} \tag{9}$$

In the form of the last expression, the right side is the same as the parabolic equation in Eq. (8), but the exponent of H_{nor} on the left side is square. This type of equation has been used as the yield envelope for the case of deep penetration ($w > 2.5B$) in ISO (2012).

Through this derivation procedure, it is found that the existing equations of the yield envelope have used parabolic and elliptic quadratic equations. The expression of the normalized shape is adjusted in this study while maintaining the form of the existing equation.

3.6.2. Modified equation of soft-over-stiff clay

As noted above in the case of ISO (2012), linear interpolation between paraboloid and ellipsoid has been used in the equation for single clay. In the present study, the shape of the curve is controlled by exponent fitting rather than linear interpolation. A different form of expression from the quadratic curve can effectively represent the results of the swipe test, and this exponent-fitting process was carried out by Vulpe (2015). Fig. 38 shows the newly normalized shapes of all of the load paths calculated by the swipe test, along with the fitted curves to all of those results.

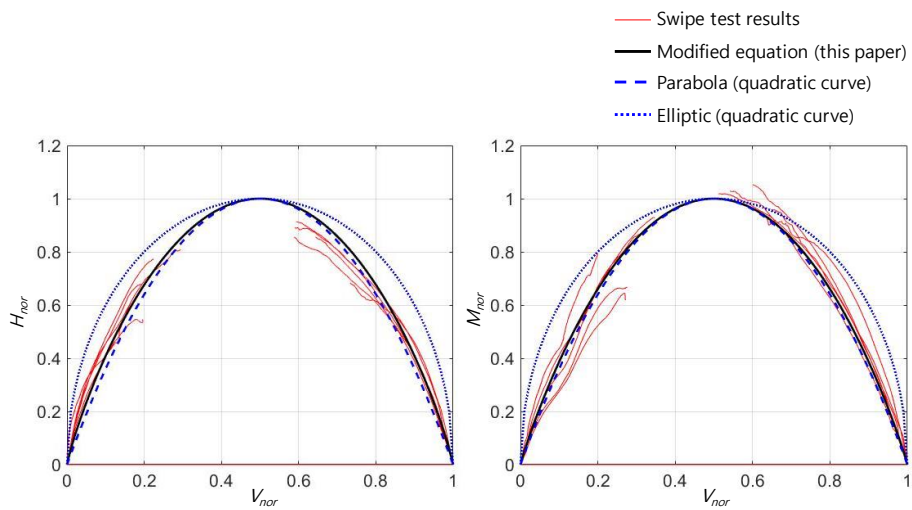

a) b)

Fig. 38 Fitted results to quadratic curves and modified equation; a) VH plane; b) VM plane

Fig. 38(a) shows the fitting results for the VH plane and Fig. 38(b) for the VM plane. The values of the exponent fitted in the two planes are applied to the equation of the yield envelope, respectively. The soft-over-stiff clay shows similar behavior to that of the single clay in the HM plane, and so the related terms are not changed. The fitted equations in the two planes and the final three-dimensional equation of the yield envelope are shown in Eq. (10) to Eq. (11). As formulated above, an exponent of 1 in H_{nor} and M_{nor} term represents the parabolic shape, so that the regressed result approaches to the parabolic. Although somewhat different, Eq. (11) has a similar form compared to that of single clay. This means that the lower stiff clay does not significantly affect the shape of the newly normalized yield envelope. The yield envelope in soft-over-stiff clay is found to be more sensitive to the capacity in each direction than the interaction of V, H, and M.

$$H_{nor}{}^{1.140} = 4 \cdot V_{nor} \cdot (1 - V_{nor}) \tag{10}$$

$$M_{nor}{}^{1.075} = 4 \cdot V_{nor} \cdot (1 - V_{nor}) \tag{11}$$

$$\left(\frac{H}{H_o}\right)^{2.28} + \left(\frac{M}{M_o}\right)^{2.15} - \frac{2HMe}{H_o M_o} - \left(\frac{4}{(1+\chi)^2}\right)^2 \left(\frac{V}{V_o} + \chi\right)^2 \left(1 - \frac{V}{V_o}\right)^2 = 0 \tag{12}$$

Yield envelope expressed as Eq. (11) is represented in three dimensions (Fig. 39). First, in the Fig. 39(a), the yield envelope is

shown along with all swipe test results about soft-over-stiff clay in the normalized space. The results in HM plane when V is zero are shown in several planes, with V_{nor} varying with the compressive and tensile maximum vertical capacities at each case. It is found that the yield envelope obtained from the swipe test results effectively is represented in three dimensions. Fig. 39(b) shows the non-normalized results of MWS2P case, for example. The yield envelope when the spudcan is subjected to upward force ($V < 0$) is revealed. Tensile swipe tests are performed through numerical analysis, and the yield envelope of soft-over-stiff clay including the negative region can be calculated.

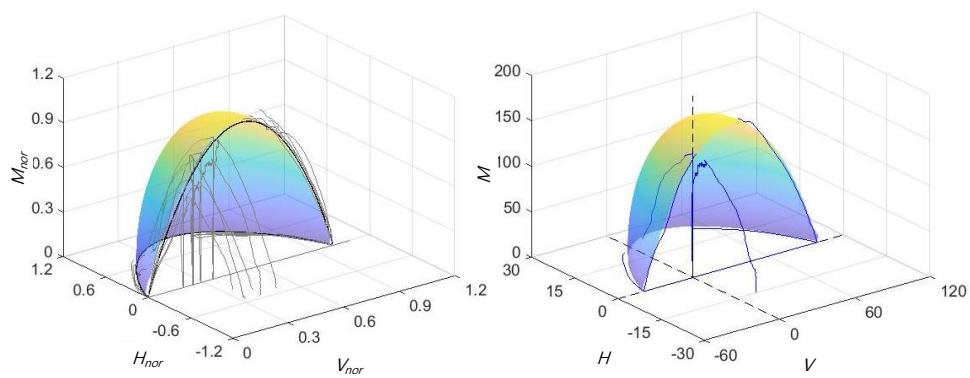

a) b)

Fig. 39 Three-dimensional yield envelope;

a) Yield envelope with the swipe test results in normalized space;

b) MWS2P case results and corresponding yield envelope

3.6.3. Effect of convergence criteria on the yield envelope

The maximum capacity is defined as the converged value of the load–displacement (moment–rotation) curve at the constant V test (Chapter 3.4.2). Convergence criterion is properly decided through the existing studies as $u = B\theta = 0.1B$, however, it is needed to find out how this criterion affects the yield envelope calculation. Maximum capacity is one of the main reasons why the yield envelope of soft–over–stiff clay differs from that of single clay, and convergence criterion can affect this value significantly. This study focuses on how the yield envelope is changed by the maximum capacity values obtained through three different criteria. Table 5 summarizes the estimation results. The maximum capacities increase with the displacement criteria, which results in reduced exponents. As mentioned above, the exponent close to 1 means a parabola, so this means that large convergence criterion makes the normalized shape narrower and closer to the parabola. This tendency is represented in Fig. 40. As the criteria for capacity calculation, small displacement criteria render the yield envelope closer to an ellipsoid, while large criteria to a paraboloid.

Table 5 Regression results for different maximum capacity criteria

Displacement criteria	$H_{nor}{}^{a}$	$M_{nor}{}^{b}$
0.04B	1.508	1.467
0.07B	1.239	1.216
0.10B	1.140	1.075

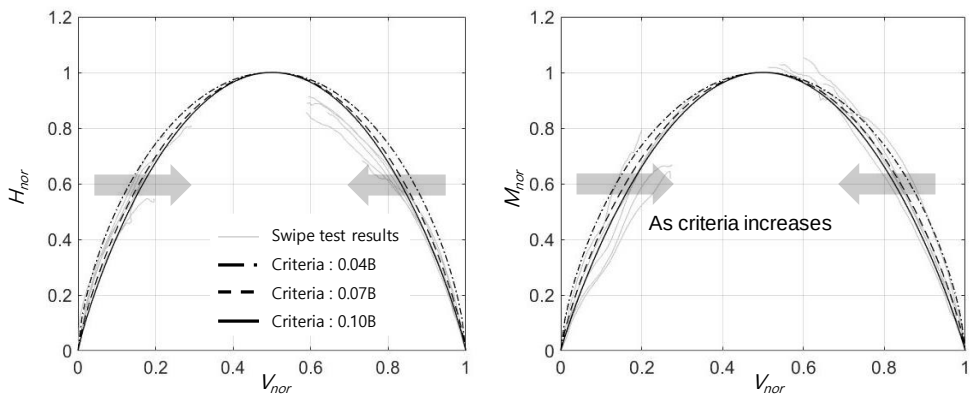

a) b)

Fig. 40 Fitted results according to the convergence criteria; a) VH plane; b) VM plane

Chapter 4. Yield envelope in soft over stiff clay

4.1. Introduction

During the operation phase where the jack-up is designed, the leg penetrates and receives environmental loads under sufficient bearing capacity. Due to the environmental loads, the soil experiences loads in the V, H, and M directions. The study on the yield envelope, which determines the yield for these acting loads, has been conducted in Chapter 3. How the force-resultant yield envelope for V, H, and M in soft over stiff clay is different has been figured out.

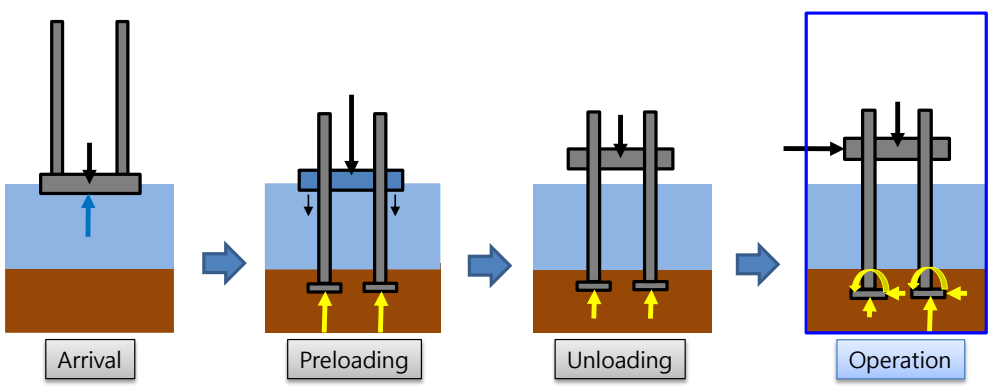

Fig. 41 Jack-up operation in overall procedure

The fitted parameter values and the expression of yield envelope for the soft over stiff clay within the possible range have been presented in Chapter 3. The foundation model, which is a boundary condition for structural analysis, is a ground model that performs

structural–soil interaction analysis through the process of determining the reaction force of the soil by receiving the reaction force in real–time. Model B framework, the foundation model of clay, formulates not only the yield envelope that determines yield, but also the elasticity that defines the behavior before yield, the flow rule that determines the behavior in plasticity, and the hardening law that establishes the additional penetration of spudcan. Plastic displacement is calculated through the formulation of those relations, and this is reflected to simulate the plastic behavior of the soil. In this chapter, a study on elasticity has been conducted to determine the behavior in the elastic range before yield. Hyperbolic relation is suggested as the more realistic elasticity relationship than that of the existing model. Through this, spudcan behavior in the elastic region along with the yield envelope of Chapter 3 has been described. Through the yield envelope that determines the elastic region and the elasticity within the elastic region, it has been intended to accurately represent the behavior within the elastic region in soft over stiff clay.

The existing model B is a work hardening plasticity–based numerical model for spudcan behavior on clay, as briefly described above. This concept of work hardening plasticity–based numerical model was first introduced in jack–up behavior by Schotman(1989) as model A. Afterward, elasticity, yield envelope, flow rule, and hardening law were improved overall by Martin(1994) and presented as model B. The model B presented an empirical yield envelope formula based on the results of the 1g experiment. After a

minor improvement, a yield envelope formula was proposed that included an eccentricity concept in a horizontal–rotation plane as a cigar–shaped shape.

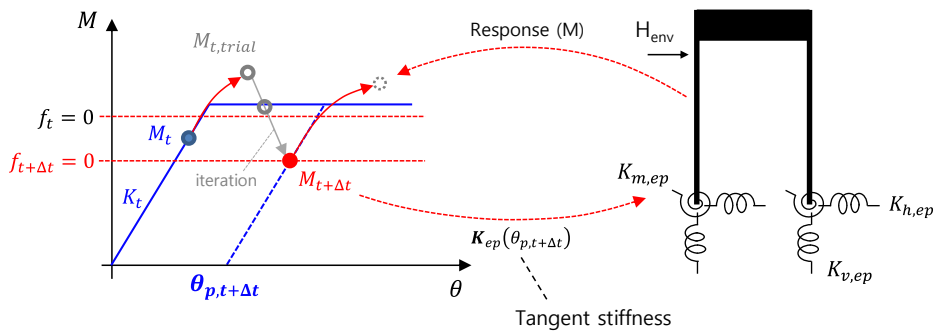

Fig. 42 Schematic diagram of model B in M–θ graph

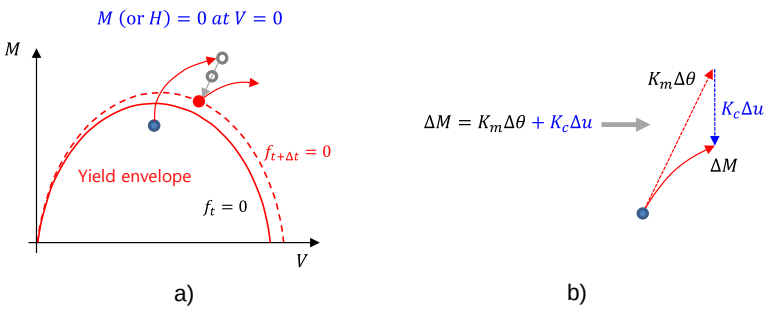

Fig. 43 Schematic diagram of model B; a) Load path in yield envelope; b) Horizontal–rotational interaction term in elasticity

In the elasticity relationship inside the yield envelope, Martin(1994) introduced terms related to interaction with horizontal and rotational directions (Eq. (13)). Through this, despite the linear diagonal term, it shows a characteristic that does not have a perfectly linear relationship in each material curve in the horizontal and rotational directions.

$$K_{el} = \begin{bmatrix} K_v & 0 & 0 \\ 0 & K_h & K_c \\ 0 & K_c & K_m \end{bmatrix} = \begin{bmatrix} k_v GR & 0 & 0 \\ 0 & k_h GR & k_c GR^2 \\ 0 & k_c GR^2 & k_m GR^3 \end{bmatrix} \quad (13)$$

The model B expresses plasticity by calculating the plastic displacement of the soil. First, if displacement is given through global jack-up analysis, it is assumed to be elastic, and response is calculated by using elasticity relation. If the calculated response is in the plastic region outside the yield envelope, an iterative calculation is performed. Elasticity, yield envelope, flow rule, and hardening law are all formulated and used for iterative calculation. Plastic displacement is calculated through iteration, and design point and tangent stiffness are calculated using this value. These calculated values are the result of this step and are used to calculate the next step in the global jack-up analysis. Through this process, model B proposed a plasticity framework reflecting each equation.

Modified model B is the state-of-art yield interaction model for clay that has improved model B. The plasticity framework of the model B was used as it was. Still, the model was improved, considering the backflow and surrounding soil in spudcan behavior. The modified model B is proposed by Zhang et al. (2014b) and is applied not only to single clay but also to various multi-layered soils containing clay in subsequent studies.

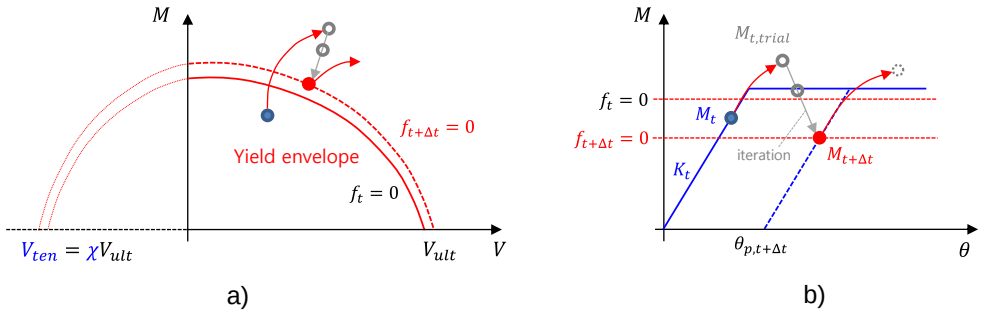

Fig. 44 Schematic diagram of modified model B;
a) Load path in yield envelope; b) Modified model B in M–θ graph

First, Zhang et al. (2014b) proposed a yield envelope equation considering tensile capacity through a centrifuge model test and suggested the coefficients for this expression. In the improved yield envelope, horizontal and rotational capacity remained even when the vertical load is zero due to tensile capacity. In actual single clay, capacity remains even when there is no vertical load due to backflow and adhesion after the penetration, and this phenomenon was reflected. The elastic relationship and plasticity are the same as that of the existing model B of Martin (1994), but the necessary coefficients for the elastic relation were presented for a single clay in various embedments and properties. Accordingly, improvements have been made to simulate the behavior of spudcan more accurately in a single clay.

Vlahos et al. (2006) simulated a non-linear relationship rather than a linear relationship as the elastic behavior within the yield envelope. In the rotational direction, the stiffness decreases as rotation occurs, and the hysteresis curve in the elastic region is

simulated through this (Eq. (14)). To simulate this strength degradation, Vlahos et al. (2006) introduced the hyperplasticity theory to simulate the rotational direction spring, which adopted the thermomechanical principle to formulate soil plasticity. The spring–slider element suggested in the hyperplasticity theory, the non–linear spring in the rotational direction is simulated (E_{N*}^{t}). In contrast, the horizontal and rotational interaction term of the elastic relation is removed for simplicity. Hyper–model B with this nonlinear rotational spring was introduced.

$$K_{el} = \begin{bmatrix} k_v GR & 0 & 0 \\ 0 & k_h GR & 0 \\ 0 & 0 & 8E_{N*}^{t} GR^3 \end{bmatrix} \tag{14}$$

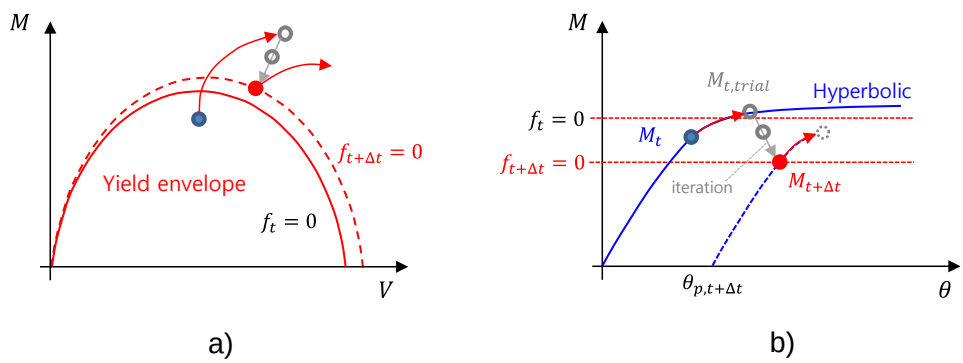

Fig. 45 Schematic diagram of Hyper–model B;
a) Load path in yield envelope; b) Hyper–model B in M–θ graph

Like the previous yield interaction model, Hyper–model B has the same plasticity framework because it is based on existing model B. First, the response is calculated according to elastic relation and

displacement. At this time, the moment of rotation is calculated according to the hyperbolic relationship. At this time, if the response is in the plastic region, iterative calculations are performed as well, and the plastic displacement is calculated. And the reaction force and moment also decrease accordingly. In this process, hyperbolic relations are used.

In this chapter, hyperbolic model B is proposed, which extends the nonlinear hyperbolic relation in the elastic region in the horizontal and rotational directions and presents the coefficients for this. The existing Hyper-model B applied a nonlinear relationship only to the direction of rotation; however, the proposed model has extended it in the horizontal direction and added the interaction terms of horizontal and rotational directions (Eq. (15)). In addition, the state-of-art model for single clay proposed by Zhang et al. (2014b) has been combined and applied.

$$K_{el} = \begin{bmatrix} k_v GR & 0 & 0 \\ 0 & \boldsymbol{f_{K_h}(u)} & f_{K_c}(\theta) \\ 0 & f_{K_c}(\theta) & \boldsymbol{f_{K_m}(\theta)} \end{bmatrix} \tag{15}$$

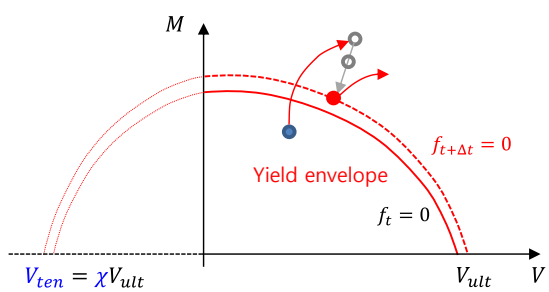

Fig. 46 Schematic load path in Yield envelope

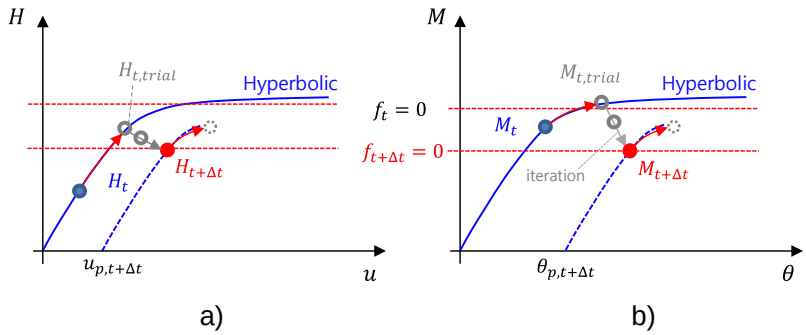

Fig. 47 Hyperbolic model B in a) H–u; b) M–θ graph

The yield envelope for the soft over stiff clay presented in Chapter 3 has been applied. Also, the nonlinear hyperbolic relation can be used not only to the moment–rotation but also to the horizontal force–displacement relation. The interaction terms of the horizontal and rotational direction of the elastic relation of the model B is considered as a function of rotation. In the plastic region, the existing model B plasticity framework is used as it is. So the response is calculated according to the given nonlinear elastic relation within the yield envelope, and the plastic displacement is calculated to simulate the behavior outside the yield envelope. At this time, the nonlinear hyperbolic relation is determined by the initial stiffness and capacity. In particular, the initial stiffness can vary significantly depending on the criteria. Accordingly, a regression model has been proposed to present the initial stiffness for the soft over stiff clay. When using the hyperbolic model B presented in this chapter, the regression model and fitting results are expected to be used for nonlinear hyperbolic relations.

4.2. Model B with hyperbolic elastic curve

Hyperbolic backbone curves have often been used to express ground hysteresis behavior (Vlahos et al., 2006; Huang, 2020). The equation of the hyperbolic curve is as follows in Eq. (16).

$$f_{hyper}(x) = \frac{x}{a + bx} \tag{16}$$

This hyperbolic curve equation has been used to express the strength degradation in the horizontal and rotational directions. In Chapter 3, the combined loads analysis of the single spudcan has been performed. Spudcan penetration has been simulated, and then reaction force and moment have been calculated through a horizontal and rotational motion under a specific vertical force with the maximum capacity. In this chapter, H−u and M− θ relationships are assumed to be hyperbolic, and this relation is fitted to those results of single spudcan analysis. The model B with hyperbolic elastic curve is proposed as Hyperbolic model B.

First, the hyperbolic expression has been formulated using physically meaningful parameters (Eq. (17), (18)).

$$H(u) = \frac{\mathrm{u}}{\left(\frac{1}{K_h} + \frac{1}{H_o} abs(u)\right)} \tag{17}$$

$$M(\theta) = \frac{\theta}{\left(\frac{1}{K_m} + \frac{1}{M_o} abs(\theta)\right)} \tag{18}$$

where, K_h and K_m are initial stiffness, respectively, and mean the slope at u= θ =0. H_o and M_o mean the capacity and converged value at u= θ =∞. Each soil parameter is presented in Fig. 48.

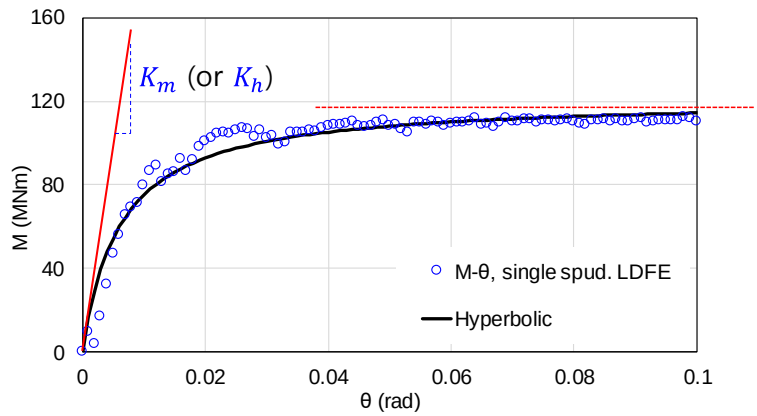

Fig. 48 load-displacement curve from single spud. LDFE

The results of fitting according to the proposed equation are shown in Fig. 49, Fig. 50 and Table 6. In one of several cases, the results of single clay and soft over stiff clay at w=2.2B has been selected.

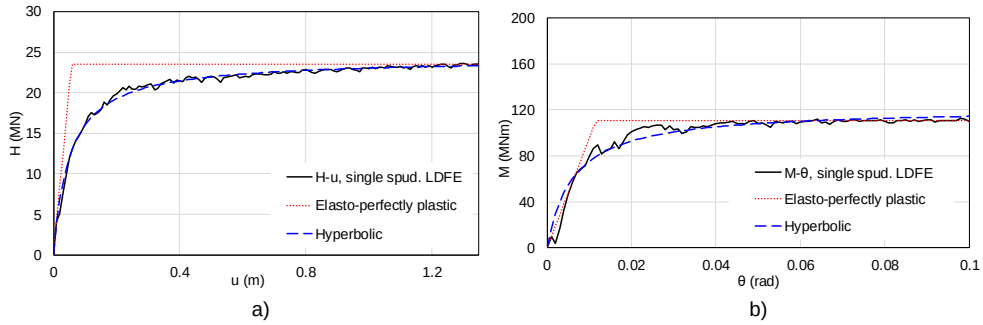

Fig. 49 Fitting results in single clay;

a) horizontal direction; b) rotational direction

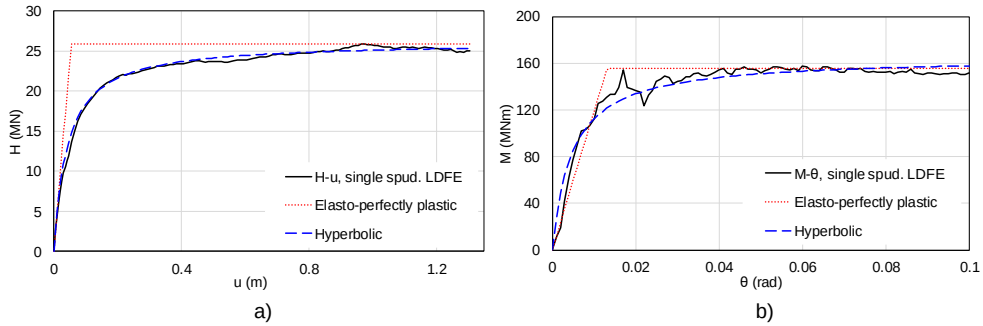

Fig. 50 Fitting results in soft over stiff clay;

a) horizontal direction; b) rotational direction

Table 6 soil parameter of single clay and soft over stiff clay (MWS2P)

	Single clay	Soft over stiff clay
K_h	473.90 MN/m	622.90 MN/m
H_o	24.20 MN	26.16 MN
K_m	19760 MNm/rad	35080 MNm/rad
M_o	121.40 MNm	165.20 MNm

As shown in the Fig. 49 and Fig. 50, the fitted hyperbolic curve (blue dashed line) fits the single spudcan analysis (black line) result. When it is assumed to be elastic−perfectly plastic (red dotted line), the strength degradation is poorly expressed. The effect of lower stiff clay on soil parameters obtained through fitting is well revealed. In Chapter 3, vertical and rotational capacity with downward motion have increased in soft over stiff clay due to squeezing effect. In the case of soil parameters obtained through the fitting, the horizontal capacity does not change much, while the moment capacity increases. Initial stiffness is a parameter that determines the initial part of the material curve. Both the horizontal and rotational stiffness increases due to the influence of the lower stiff clay. In particular, the rotational stiffness affected by the surrounding soil increases significantly. The fitting results for different embedments and properties of lower clay are as follows.

Table 7 Fitted result about horizontal initial stiffness (MN/m)

K_h	SWP	MWS2P	MWS3P	MWS4P
1.8B	415.73	478.01	505.89	522.12
2.0B	444.22	605.58	706.74	759.16
2.2B	455.64	646.88	918.74	1014.40
2.4B	524.81	806.74	1661.17	2502.79

Table 8 Fitted result about rotational initial stiffness (MNm/rad)

K_m	SWP	MWS2P	MWS3P	MWS4P
1.8B	12829	19214	22400	23646
2.0B	17366	27448	36762	41904
2.2B	17581	30432	41698	18796
2.4B	17711	35113	44346	75547

Table 9 Fitted result about horizontal capacity (MN)

H_o	SWP	MWS2P	MWS3P	MWS4P
1.8B	18.73	18.47	18.61	18.65
2.0B	21.32	21.67	21.54	21.50
2.2B	24.62	25.96	28.98	32.77
2.4B	28.03	28.62	35.42	44.42

Table 10 Fitted result about rotational capacity (MNm)

M_o	SWP	MWS2P	MWS3P	MWS4P
1.8B	99.44	97.99	97.28	96.62
2.0B	108.87	117.26	116.85	116.14
2.2B	127.63	174.68	183.34	299.08
2.4B	140.84	175.32	227.13	284.55

4.3. Regression model of initial stiffness

To define the horizontal and rotational hyperbolic relations in Hyperbolic model B, two parameters, initial stiffness and capacity, should be determined. It is not easy that the response reaches the capacity in the jack-up analysis, because combined loads are applied to the soil and the capacity is the yield condition of a single dof. Initial stiffness, dominant factor of the initial phase of the material curve, is very important in this respect. However, the initial stiffness is determined by the response at a small strain, and the value varies greatly depending on the criteria of the displacement causing the small strain.

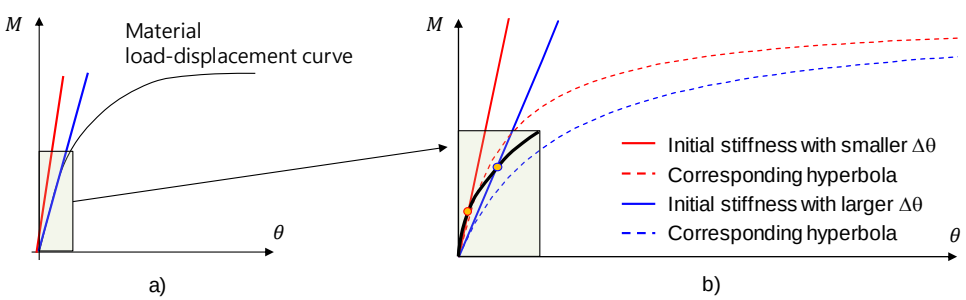

Fig. 51 Difficulties in determination of initial stiffness;
a) initial stiffness of two different criteria; b) enlarged graph

The Fig. 51 shows that the initial stiffness may vary depending on the criteria. The smaller the displacement interval yields the larger the stiffness. It seems that the blue slope at a larger reference reveals the overall shape better in overall shape. In contrast, when

it is enlarged(Fig. 51(b)), it can be confirmed that the red slope is the better representative of the slope at the beginning. This difference in the initial slope also causes a difference in the hyperbolic curve using the corresponding value. Even if the capacity is the same, the difference in the initial slope can cause a large difference in the early stage as shown in the Fig. 51(b). As the displacement increases, it converges to the same capacity, but differences occur in small displacements where jack-up analysis experiences actually, which means that hyperbolic relations can be greatly affected by soil parameters. Although the initial stiffness obtained through centrifuge model tests or other methods is the correct value, if used differently in the hyperbolic model according to the criteria, the results may not be validated. This study has presented a regression model for initial stiffness in soft over clay that can be used in hyperbolic model B. Equations are presented so that the corresponding parameters can be used in the range of the given embedments and the lower clay properties.

Before presenting the regression equation, two variables that can reveal spudcan in soft over stiff clay have been selected. In chapter 3, the impact of the lower stiff clay has been analyzed by dividing it into the properties of lower clay and embedment. In the regression model of this chapter, two variables have been selected, undrained shear strength ratio and depth ratio, for the purpose of clarifying the effects of normalization and lower stiff clay.

$$\text{undrained shear strength ratio} = \frac{s_{u,stiff}}{s_{u,H}} \tag{19}$$

$$\text{depth ratio} = \frac{w}{H} \tag{20}$$

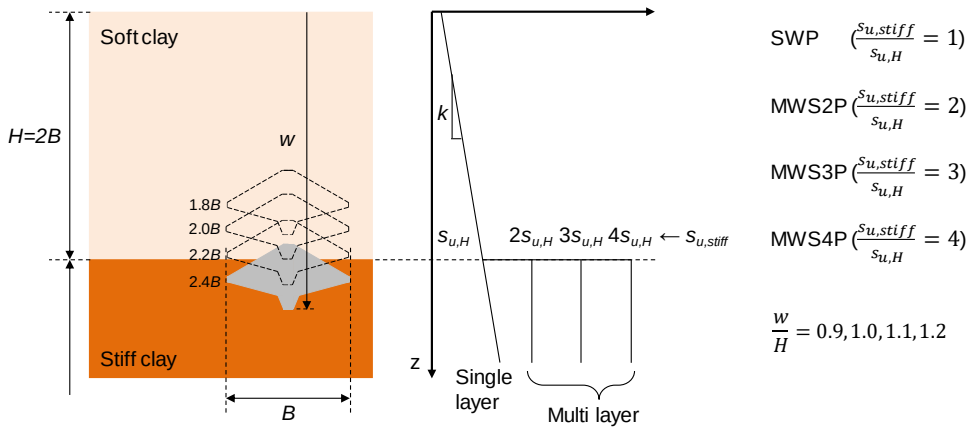

Fig. 52 Two variables in regression model

The undrained shear strength ratio refers to the ratio of the undrained shear strength of the upper soft clay and the lower stiff clay at the boundary (Eq. (19)). The effect of the lower clay can be normalized and expressed using the ratio of undrained strength. A regression model has been proposed for the lower stiff clay, which is 1 to 4 times harder than the upper clay. The depth ratio means the ratio of the depth of penetration to the height of the upper clay (Eq. (20)). Simple penetration depth cannot clearly present the relationship with the lower stiff soil, and for this purpose, the depth ratio has been selected by including the location of the lower stiff clay. A regression model has been proposed for depth ratios from 0.9 to 1.2, and in particular, when looking at the results of chapter 3, it is expected that the depth ratio of 0.9 or less will only affect

the upper soft clay and not the lower clay. This selected range can cover the bearing pressure of a typical jack-up.

For the selected undrained shear strength ratio and depth ratio, fitting has been performed for the combined loads analysis results in the horizontal and rotational directions. The soil parameters obtained through these fittings are listed in the Table 7 ~ Table 10.

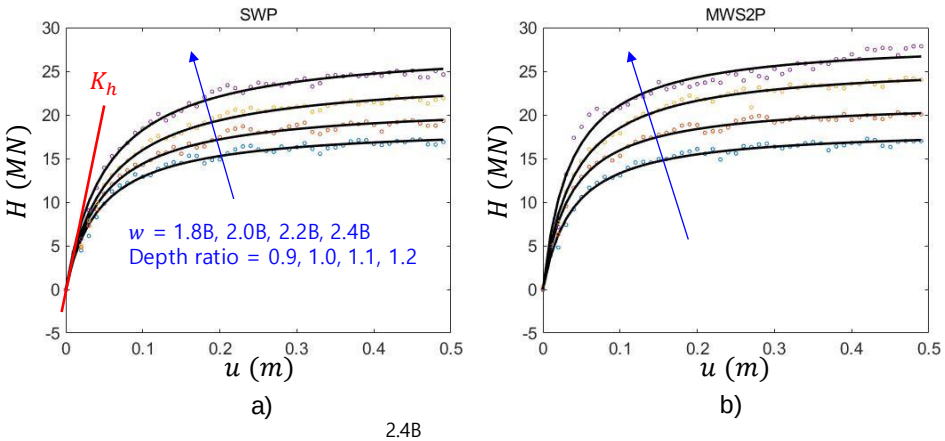

Fig. 53 Horizontal material curve obtained from single spudcan analysis and fitted results; a) SWP; b) MWS2P

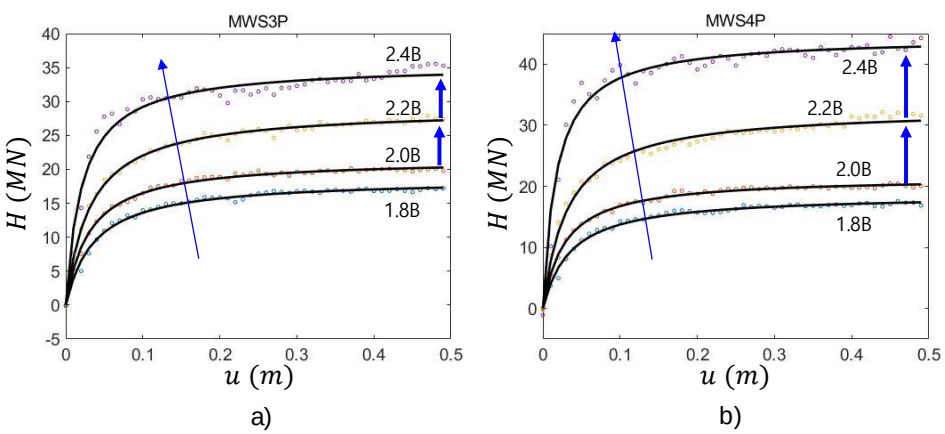

Fig. 54 Horizontal material curve obtained from single spudcan analysis and fitted results; a) MWS3P; b) MWS4P

The result of varying embedment according to the properties of the lower stiff clay has been shown for the H−u curve in the horizontal direction. The fitting result is shown as a solid black line. For all cases of SWP, MWS2P, MWS3P, and MWS4P, it has been confirmed that the deeper the penetration depth, the greater the initial stiffness and the capacity, which are the slope at the origin and the convergence value, respectively. This significant increase occurs in MWS3P and MWS4P, which have a large impact by the lower stiff clay. In addition, it is shown that the increase is large at w=2.2B and 2.4B.

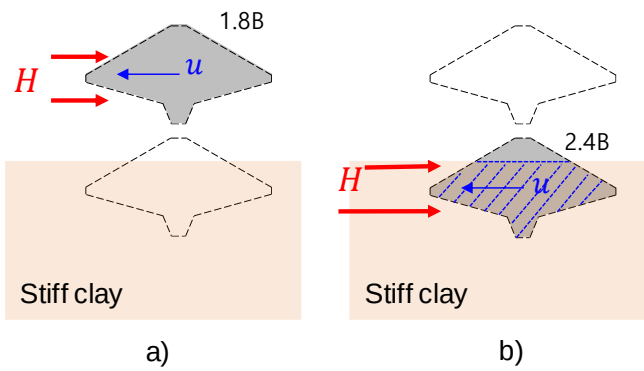

Fig. 55 Schematic diagram of horizontal reaction force acting on the spudcan at; a) w=1.8B; b) w=2.4B

As mentioned in Chapter 3, horizontal capacity is greatly influenced by the overlapped area with lower stiff clay. As shown in the figure, at w=1.8B, spudcan does not meet the lower stiff clay, so the soft clay applies the small reaction force. However, at w=2.4B, spudcan overlaps much with the lower stiff clay, and the

stiff clay applies a corresponding large reaction force. The horizontal capacity increases significantly in 2.2B and 2.4B, where overlapped areas are increased due to the large reaction force from the stiff clay.

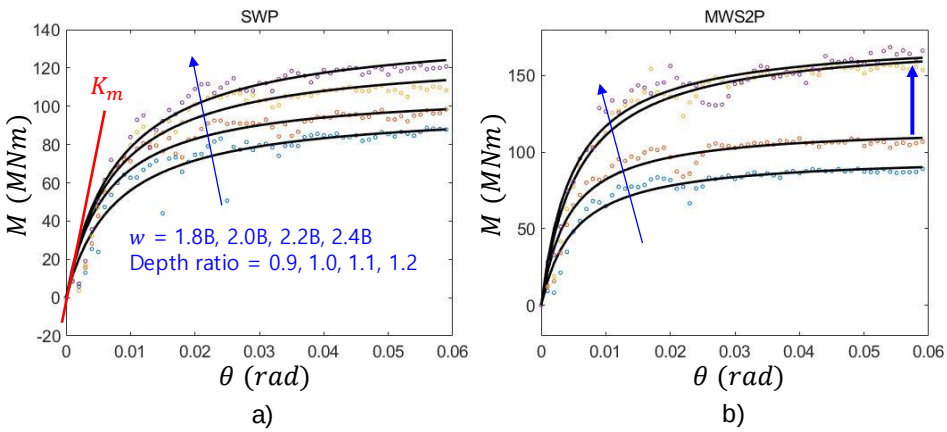

Fig. 56 Rotational material curve obtained from single spudcan analysis and fitted results; a) SWP; b) MWS2P

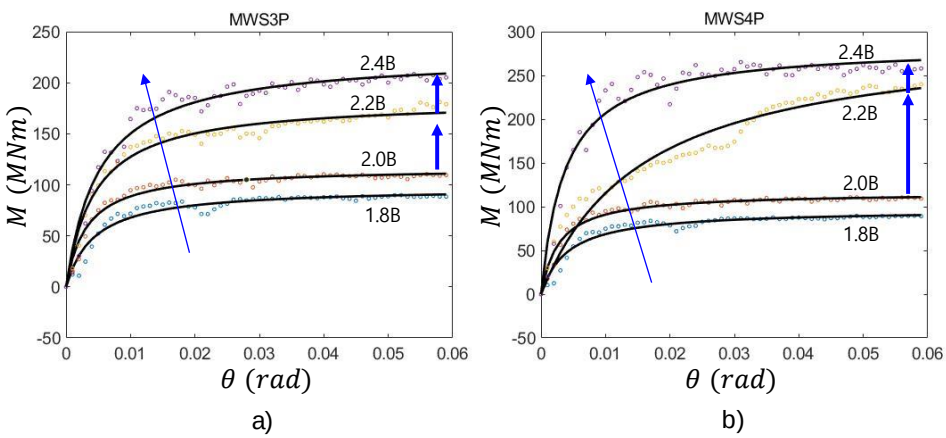

Fig. 57 Rotational material curve obtained from single spudcan analysis and fitted results; a) MWS3P; b) MWS4P

The result of varying the embedment according to each lower stiff soil is shown for the M− θ curve in the rotational direction in Fig. 56 and Fig. 57. The fitting result is shown as a solid black line. As in the horizontal direction, The initial stiffness, which is the slope at the origin, and the capacity, which is the convergence value, increases as the depth of penetration increases for all cases of SWP, MWS2P, MWS3P, and MWS4P.

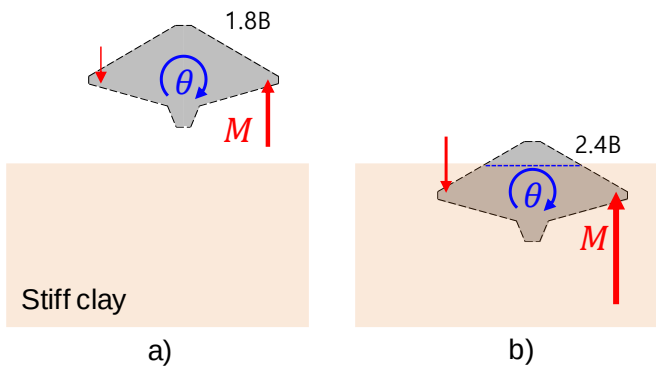

Fig. 58 Schematic diagram of rotational reaction moment acting on the spudcan at; a) w=1.8B; b) w=2.4B

The reaction moment increases more than the horizontal reaction force due to the downward motion of one side to the lower stiff clay. This increase is particularly pronounced in 2.2B and 2.4B, which also depends on the location of the spudcan. When the spudcan is located at 1.8B, the side with downward motion will be affected by squeezing. However, when the spudcan is located at 2.4B, the side with downward motion is only affected by the stiff clay, and the reaction force increases accordingly. On the other hand, the side

with upward motion is affected by soft clay and has little influence. Due to this effect, the stiffness and capacity in the rotational direction also have a more considerable value as the penetration depth increases and the lower clay is stiffer.

Initial stiffness and capacity for hyperbolic relations are calculated by the fitting from the results of single spudcan LDFE analysis. The following regression model is presented for the initial stiffness calculated as above.

$$k_h = 0.15\left(\frac{s_{u,stiff}}{s_{u,H}}\right)^{2.15}\left(\frac{w}{H}\right)^{14.78} + 1.04\left(\frac{s_{u,stiff}}{s_{u,H}}\right) + 9.03 \quad (21)$$

$$k_m = 13.89\left(\frac{s_{u,stiff}}{s_{u,H}}\right)\left(\frac{w}{H} - 0.85\right)^{0.53} + 1.01\left(\frac{s_{u,H}}{s_{u,stiff}} - 2.90\right) + 4.50 \quad (22)$$

The regression model is presented for the stiffness coefficient concept presented by ISO (Eq. (21), (22)). The actual fitting has been performed for K_h and K_m, but an equation for the normalized coefficient is provided to be applied to general properties and spudcan (Eq. (23), (24)). Shear modulus (G) and spudcan radius (R) have been used for normalization. G used at this time has been calculated by using the general relation with E and the relationship with s_u (Eq. (25)). G_H uses the upper soft clay properties at the boundary for the normalization (Eq. (26)). The properties of the lower clay have been considered in the regression model through the undrained shear strength ratio variable. Therefore, when

normalizing using the upper soft clay property, all the properties of soft over stiff clay can be considered.

$$K_h = k_h G_H R \tag{23}$$

$$K_m = k_m G_H R^3 \tag{24}$$

$$G = \frac{E}{2(1+\nu)} = \frac{500}{2(1+\nu)} s_u \tag{25}$$

$$G_H = \frac{500}{2(1+\nu)} s_{u,H} \tag{26}$$

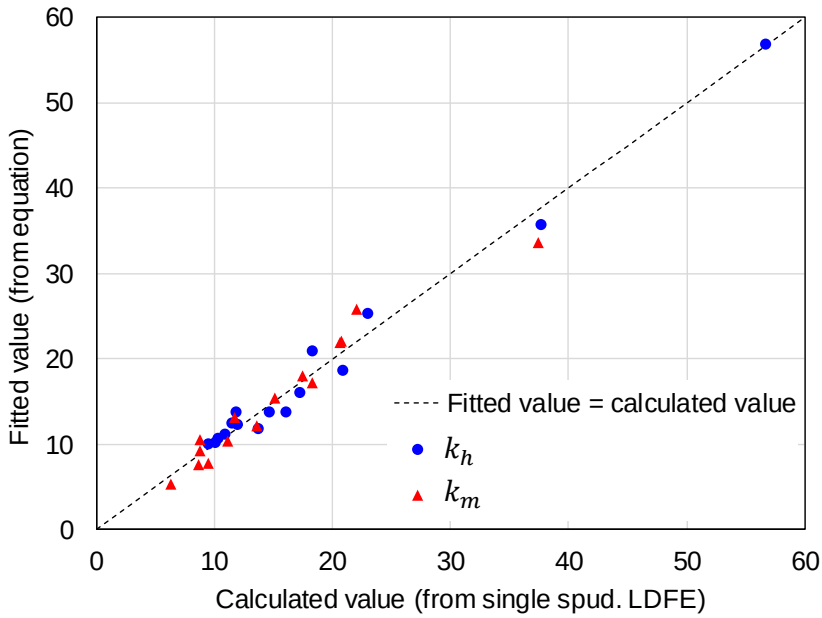

Fig. 59 Accuracy of regression model about initial stiffness

4.4. Hysteresis curve

The results from the LDFE analysis and that from the regression model are shown in the Fig. 59. In the Fig. 59, the x−axis represents the results from LDFE, and the y−axis represents the results from the regression model. The diagonal dotted line is a set of points where both results are the same, that is, the closer to this dotted line, the higher the accuracy of the regression model. Stiffness coefficients in both horizontal and rotational directions are shown. Both results are close to the linear dotted line. This means that the regression model expresses the initial stiffness well within the range (0.9~1.2 of depth ratio, 1~4 of undrained shear strength ratio).

The hyperbolic curve is introduced in the horizontal and rotational directions, and a backbone curve and hysteresis relation can be implemented in the elastic region. Bolisetti(2014) used hyperbolic backbone curves and implemented the hysteresis relation of the soil using the Masing rule (Masing, 1926). Masing rule is about material curves to be followed when loading and unloading and is divided into three rules.

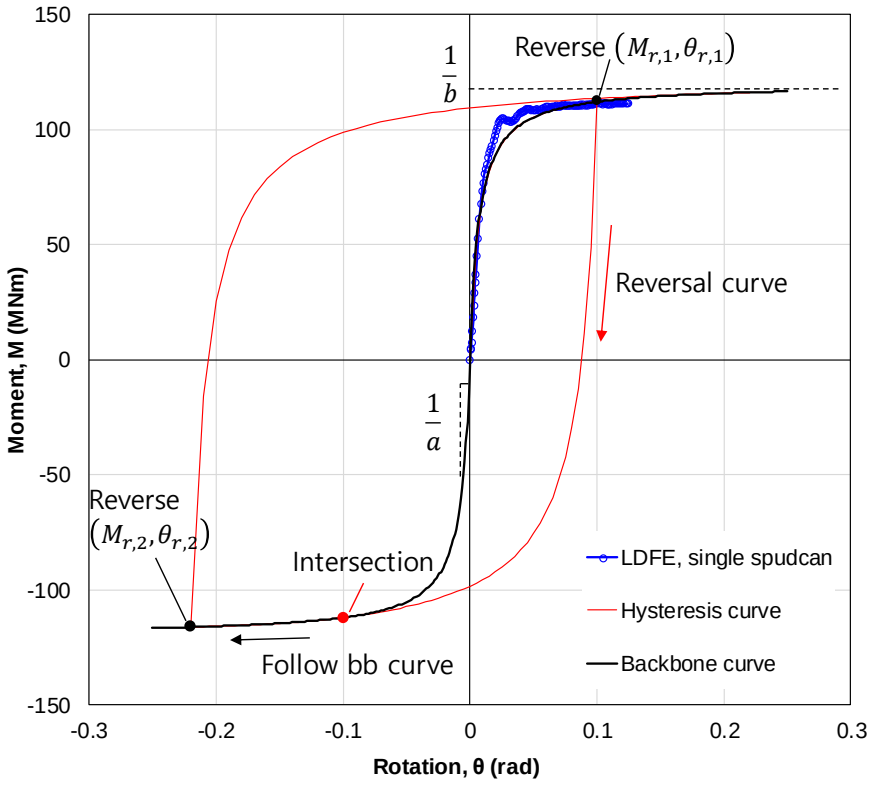

Fig. 60 Masing rule (Masing, 1926) for hysteresis curve

First, the initial loading follows the backbone curve. In this study, since the hyperbolic relation is adopted for the nonlinear material curve, the hyperbolic backbone curve has been used for implementation. The blue LDFE result(Fig. 60) can be seen as the initial loading, and it is shown to follow the hyperbolic backbone curve well. Second, after unloading occurs at a certain point, the material curve follows the reversal curve. The reversal curve is twice the enlarged backbone curve in the opposite direction (Eq. (27)).

$$\frac{M - M_r}{2} = F\left(\frac{\theta - \theta_r}{2}\right) \tag{27}$$

Finally, if unloading continues along this reversal curve, the backbone curve meets again at the origin symmetric point with the point where the unloading started. From this intersection point, the material curve follows the backbone curve again, not the reversal curve. Loading and unloading are repeated accordingly, and the hysteresis curve is made around the backbone curve.

This Masing rule is identical to the ideal hysteresis curve in general materials. The hyperbolic model B has been designed to express the hysteresis curve in the horizontal and rotational direction under repeated loads by implementing the hysteresis curve through the Masing rule. In the case of Modified model B, a linear relationship is used in the elastic region except for the interaction term, so the loading and unloading curves in the elastic region are almost the same. However, jack-up structure is frequently subjected to wave-like repetitive loads, and not only large loads that cause yield but also repetitive loads in the elastic region are important in terms of fatigue strength. In the hyperbolic model B, the nonlinear hyperbolic relationship and the hysteresis curve have been used to accurately simulate the response to repeated loads in the elastic region.

Chapter 5. Validation with structural analysis of jack-up using different foundation models

5.1. Introduction

The structure−ground interaction model among the foundation models of jack−up is the secant model, yield interaction model, and soil continuum model. Chapter 3 has studied the yield envelope of soft over stiff clay which can be used in the secant model and the yield interaction model. The characteristics of the yield envelope in soft over stiff clay have been analyzed and the yield envelope expression and corresponding coefficients have been presented. In Chapter 4, the elastic relationship that determines the behavior in the elastic region has been improved in the yield interaction model. Strength degradation in the elastic region has been implemented through hyperbolic relations, and soil parameters applicable to soft over stiff clay have been introduced in the form of regression model and tables.

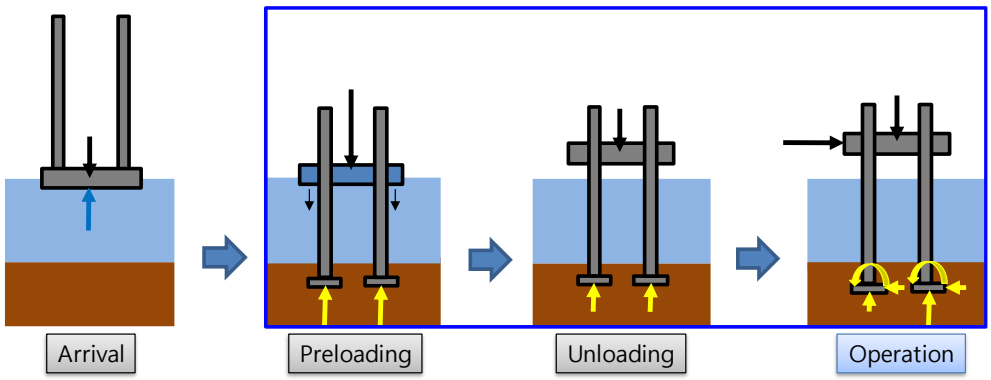

Fig. 61 Jack-up operating phase considered in Chapter 5

In Chapter 5, LDFE has been used to implement the soil continuum model. Structure-soil interaction analysis with soil continuum model has been performed. The yield interaction model in soft over stiff clay presented in Chapters 3 and 4 has been validated with the soil continuum model. The complicated structure-soil interaction model, yield interaction model and soil continuum model, have been presented that it can be applied to single clay and soft over stiff clay. In order to perform the jack-up structural analysis under the environmental loads during the operation phase, the penetration of the jack-up structure should be first simulated. Penetration procedure and corresponding disturbed soil properties are reflected in this chapter (Fig. 61).

5.2. User element (UEL)

5.2.1. Implementation of model B

The elasto-plastic framework of the model B, which is the basis of modified model B and hyperbolic model B, has been implemented first in order to perform structural analysis using the yield interaction model. For the explicit formulation of the model B, Vlahos et al. (2008b) is referred. The macro element reflecting the formulated expression has been implemented using the user element subroutine of Abaqus. UEL subroutine can directly define the constitutive equation of element, and thus the relationship between load and displacement for multiple dof. In particular, the model B, which is the yield interaction model of clay, is effectively implemented through the user element because it is necessary to perform repetitive calculations using displacement and reaction forces, and define elastic and plastic relations, respectively.

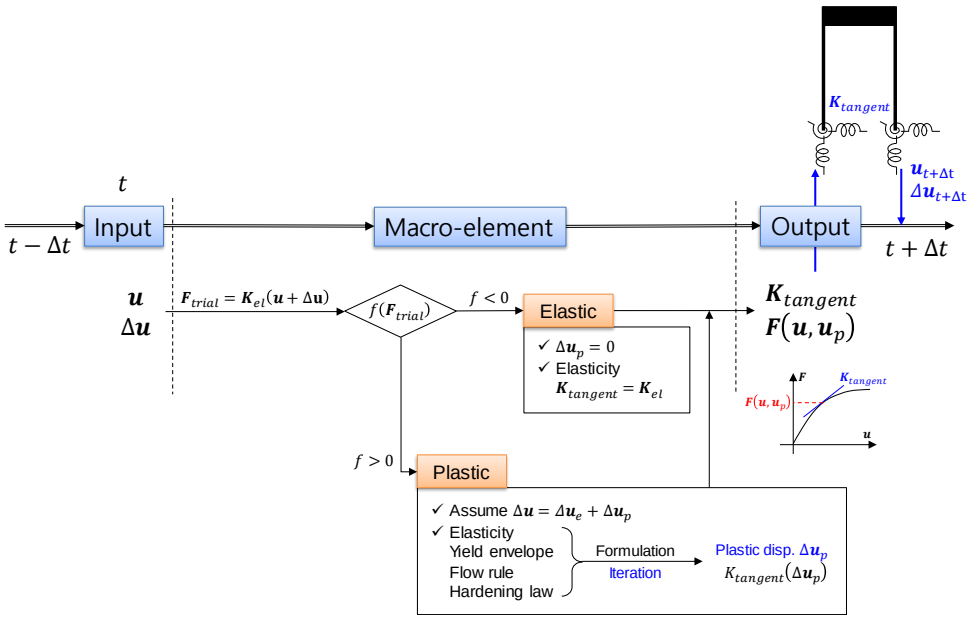

Fig. 62 Iterative procedure in macro element of the model B

First, the displacement of the increment from the global jack-up analysis of Abaqus is inputted. In the corresponding increment, the response is temporarily calculated according to the elastic relationship ($\boldsymbol{K_{el}}$) of the model B using the previously received displacement, and the value is defined as the trial load state ($\boldsymbol{F_{trial}}$). $\boldsymbol{F_{trial}}$ is substituted to the force-resultant yield envelope to determine whether the trial load state is in the elastic region or the plastic region. If the load state is in the yield envelope, it is elastic, so the elastic stiffness of the model B becomes tangent stiffness, and the trial load state becomes the final load state. However, if the trial load state is outside the yield envelope, iteration begins because it is plastic. The purpose of this iteration is to calculate the plastic displacement, so the elasticity, yield envelope, flow rule, and hardening law are considered in the interactive calculation. The

plastic displacement is finally calculated through the iterative calculation, and the total displacement is divided into elastic displacement and plastic displacement. The tangent stiffness is defined as a function of plastic displacement, and the load state is placed on the yield envelope through repeated calculations. This load state at this time is calculated from the elastic displacement. The calculated tangent stiffness and load state (response) become the load-displacement relationship in the corresponding increment. This information is transferred to the global jack-up analysis, where checks the analysis convergence and calculates the displacement of the next increment, and the same process is repeated.

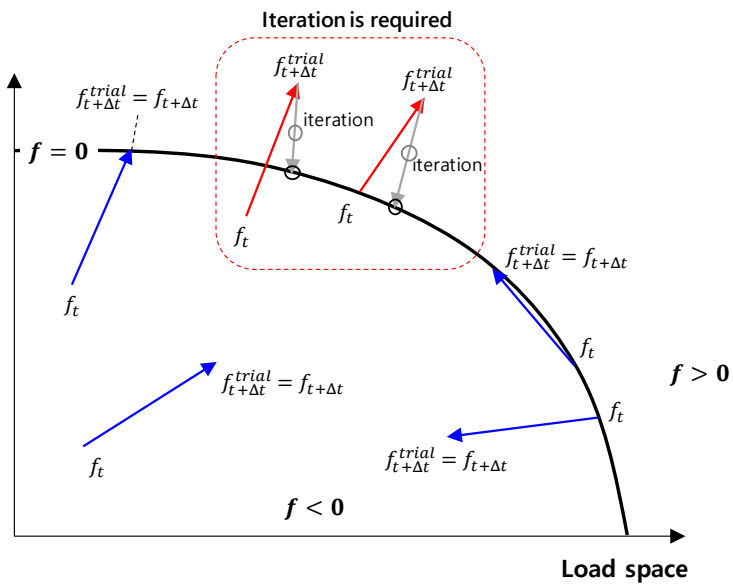

Fig. 63 Schematic diagram of yield envelope check using trial load state ($\boldsymbol{F}_{trial}$)

There are six cases where a trial load state can place on, among which two cases outside the yield envelope need the iteration(Fig. 63). After the plastic displacement is calculated through the iterative calculation, the final load state is placed on the yield envelope. In this procedure, the flow rule determines the direction and speed of approaching the yield envelope. If additional penetration in the vertical direction should be needed during this process, the vertical compression capacity is changed and the yield envelope and accompanying other equations are recalculated in consideration of this. Four plasticity equations, including elasticity which is the elastic relationship that determines the behavior within the elastic region, each play a role in the model B framework.

5.2.2. Validation of macro element

The model B implemented through the UEL in the Abaqus commercial program has been validated. First, the swipe test performed in Chapter 3 has been selected as a verification case as it has been to see if the result calculates well (Fig. 64).

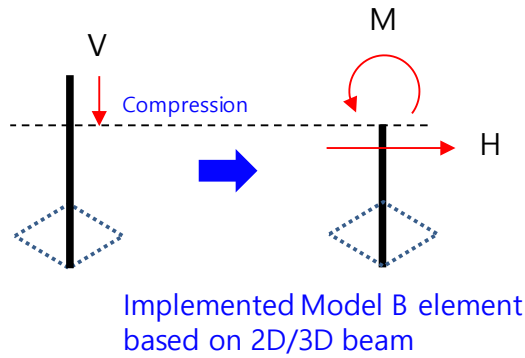

Fig. 64 Loading sequence of the swipe test

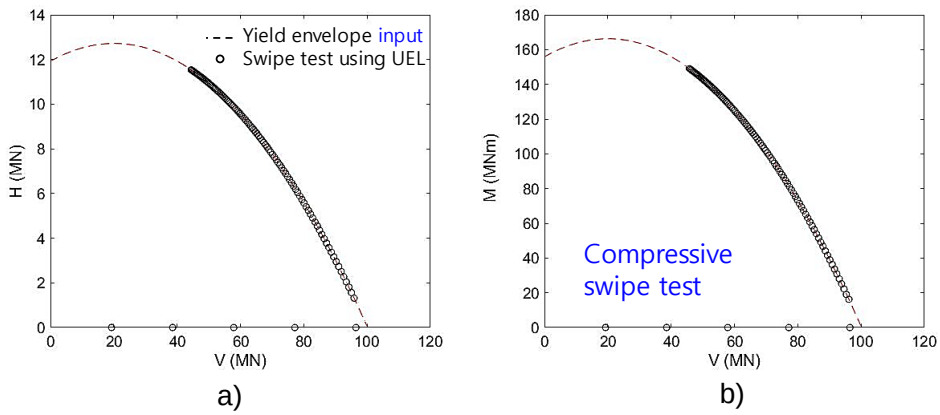

Fig. 65 Swipe test results in a) VH plane; b)VM plane

The vertical, horizontal, and rotational capacity and yield envelope entered in the subroutine are shown in dotted lines in the picture. As a result of the swipe test of the UEL, it has been confirmed that the results (circular point) follow the dotted line well. This well-matched result indicates that the input entered into the UEL is implemented as it is (Fig. 65).

Validation using jack-up structural analysis should be performed on whether the macro element is well implemented. 2D jack-up

analysis in Vlahos et al. (2008b) has been selected as a validation case. Validation on the simplified jack-up is conducted and then expanded into a 3D case to compare the results.

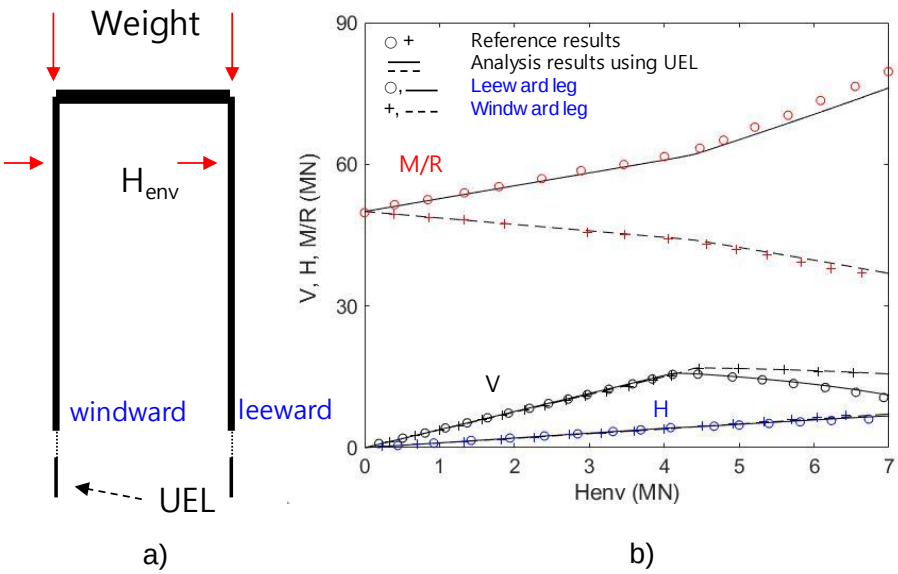

Fig. 66 2D Jack-up validation case;

a) Schematic diagram of validation case;

b) Soil responses of macro element and Vlahos(2008)

The environmental load is 7MN, and the applied vertical load is 50MN in the validation case. The capacity of each direction given in reference has been used as it is. The results of Vlahos et al. (2008b) are shown as a mark (o, +) in the Fig. 66. As a result, yielding at about H_{env}=4MN and moment failure of the leeward leg has been simulated well. In addition, the reaction force in the vertical and horizontal directions of the macro element follows the reference results well.

The same validation case has been used in expanded 3D UEL. 3D yield envelope equation (Eq. (28)) using symmetric conditions has been used (Bienen and Cassidy, 2006).

$$f = \left(\frac{H_2}{H_o}\right)^{\alpha} + \left(\frac{M_3}{M_o}\right)^{\beta} - 2e\frac{H_2}{H_o}\frac{M_3}{M_o} + \left(\frac{H_3}{H_o}\right)^{\alpha} + \left(\frac{M_2}{M_o}\right)^{\beta} + 2e\frac{H_3}{H_o}\frac{M_2}{M_o} + \left(\frac{Q}{Q_o}\right)^2 - \left(\frac{4}{(1+\chi)^2}\right)^2 \left(\frac{V}{V_o} + \chi\right)^2 \left(1 - \frac{V}{V_o}\right)^2 \quad (28)$$

The sign of horizontal and rotational direction is changed according to the sign convention, and a torsion term(Q) is added. As a result of performing the validation case analysis using this equation, the same result of the 2D UEL code result has been obtained. Through this validation process, it has been confirmed that the macro element using UEL subroutine can effectively implement the existing model B. Modified model B (state-of-art model) and hyperbolic model B presented in this study have been implemented based on the existing model B subroutine. These implemented yield interaction models are used in this chapter for the structure-soil interaction analysis.

5.3. Single clay at deep embedment

5.3.1. Jack-up structure

Jack-up, corresponding to the spudcan used in Chapter 3, has been selected for modeling of jack-up structure (Menzies and Roper, 2008). MLT 116C (Fig. 67) is a jack-up oil platform with leg length = 125.08m, leg spacing 39.32m, hull length 74.09m, and breadth 61.11m.

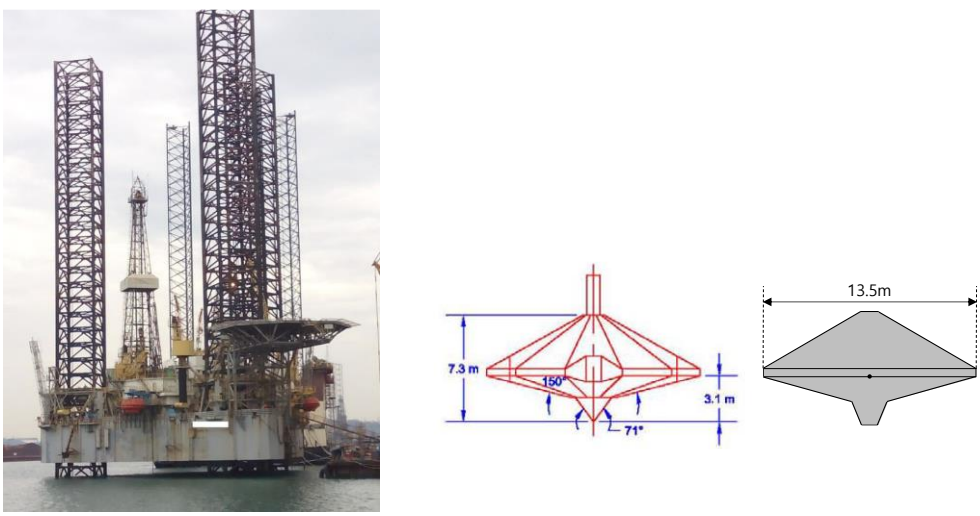

Fig. 67 Jack-up structure used in numerical analysis;
a) Jack-up oil platform (MLT-116C);
b) Simplified spudcan used in Chapter 3

However, it is challenging to know detailed information about this actual jack-up, so the similar-sized jack-up used in the other research has been selected. Zhang et al. (2014a) presented a

detailed specification of the jack-up structure used for verification of modified model B. Given detail has legs with 120m length and 37.87m spacing and spudcans with 14m equivalent diameter. This model closely resembles the leg and spudcan specification of MLT 116C, which is referred in this study. Therefore, corresponding leg section information and stiffness have been used in this study model. The second moment of area of the leg modeled by the equivalent 1D beam in the reference is $7.2m^4$, and this study assumes a rectangular-shaped section of 3.05 m with the same second section moment. In the case of Hull, the reference gives as a 1D beam with a second section moment of $72m^4$, and similarly, in this study, the hull structure is modeled with a rectangular-shaped section of 5.42 m with the same second moment of area. The elastic modulus and shear modulus of the leg use the value of 200 GPa and 80 GPa, respectively, which are common steel values.

5.3.2. FE model used in single clay analysis

The FE model used in structure-soil interaction analysis using the soil continuum model is shown in the figure.

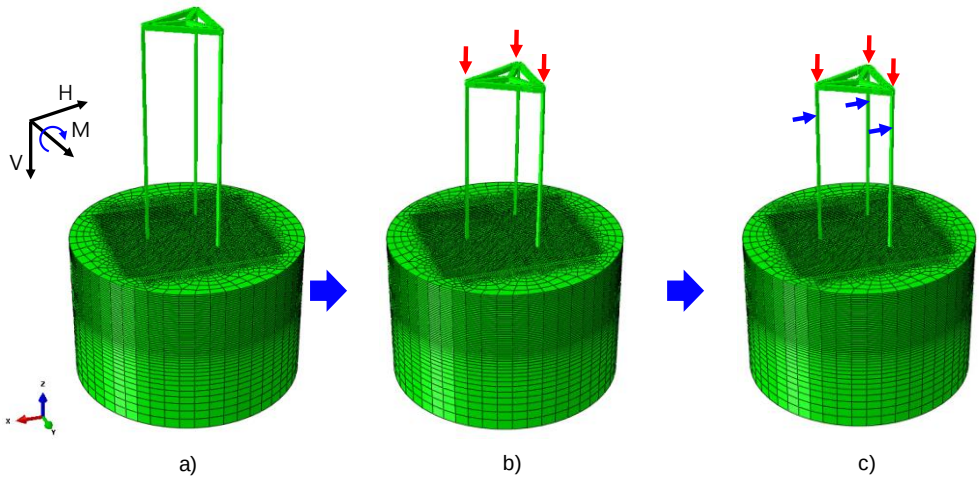

Fig. 68 FE model used in single clay analysis;
a) Starting position; b) Penetration; c) Environmental load analysis

First, jack-up penetrates from the seabed to the target location of 2.2B (Fig. 68(b)). The penetration process simulating the jack-up installation phase has been performed at a 0.2 m/s (=0.015 B/s) of penetration rate. After penetration and positioning at the target position, structure-soil interaction analysis has been performed by applying an environmental load (Fig. 68(c)). The weight of the jack-up structure has been applied to the hull-leg joint as a vertical point load. In the case of environmental loads, a load has been applied to the 105m position (airgap 15m) from the spudcan, assuming the water depth. The environmental load has been applied until the structure failure, so a total of 15MN has been applied by combining the three legs.

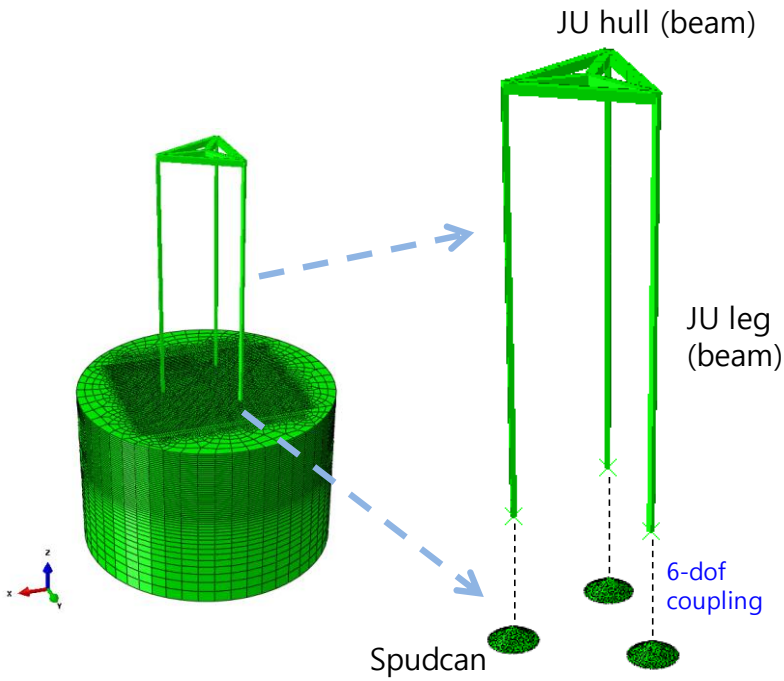

Fig. 69 FE model of jack-up structure

The details of the jack-up structure are as follows (Fig. 69). An equivalent beam model has been used for the jack-up model consisting of leg and hull. This model called stick model has been proposed as one of the leg model types, which can be used for structural analysis in ISO (2012). The stick model can calculate the global response of jack-up, such as base shear and overturning moment, and global leg force such as bending moment, and overturning check and foundation check are also possible because the overall soil reaction response and displacement are calculated. However, since detailed modeling of leg members has not been performed, it is impossible to calculate local response like member forces of legs, hulls, jacking unit, and fixation system. The beams

that make up the legs and hulls are modeled as Timoshenko beams that allow transverse shear deformation (Fig. 70(a)).

Model type	Applicability						
	I	II	III	IV	V	VI	VII
	Base shear and overturning moment	Overturning checks	Foundation checks	Global leg forces	Leg member forces	Jacking/fixation system reactions	Hull element forces
a) Fully detailed leg	Yes	Yes	Yes	Yes	Yes	Yes	See note
b) Equivalent leg (stick model)	Yes	Yes	Yes	Yes	—	—	—
c) Combined equivalent/detailed leg and hull	Yes	Yes	Yes	Yes	Yes	Yes	See note
d) Detailed single leg and leg-to-hull connection model	—	—	—	—	Yes	Yes	—
NOTE Hull stresses are only available from more complex hull models.							

Ref. ISO(2012), Table A.8.2-1

a)

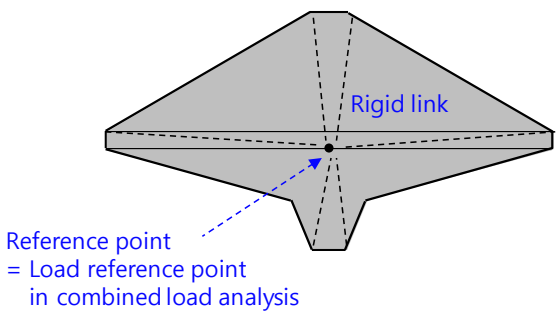

b)

Fig. 70 Analysis condition of jack-up structure;
a) Applicability of leg stick model suggested in ISO(2012);
b) spudcan assumed as rigid body

Spudcan is a steel structure that transfers reaction force and moment by directly performing interaction with the soil. For simulating the structure-soil interaction through the CEL technique, spudcan has been modeled using 3D solid elements. The lagrangian mesh comprises C3D6 and C3D8R elements. The local strength of the spudcan has a minimal effect in terms of overall structural

strength. Therefore, spudcan is assumed to be rigid to clarify the structure−soil interaction without compromising the accuracy of the global analysis. The load reference point(LRP) of spudcan becomes a rigid link (Fig. 70(b)), and this point has been connected to the lower part of the leg through 6−dof coupling.

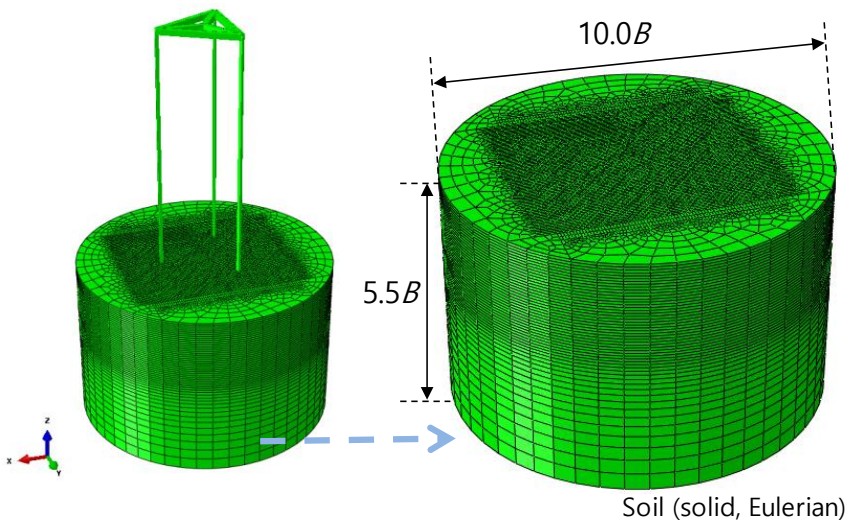

Fig. 71 FE model of soil continuum

The soil continuum has been modeled as 3D soild to perform LDFE analysis through CEL. The eulerian mesh comprises the EC3D8R element. Tresca model incorporating strain softening and rate dependency is used for modeling clay. This nonlinear clay model has been introduced in Chapters 2 and 3. Soil domain has been modeled large enough to avoid boundary effects, width 10 times the spudcan diameter, and height 5.5 times the spudcan diameter (Fig. 71).

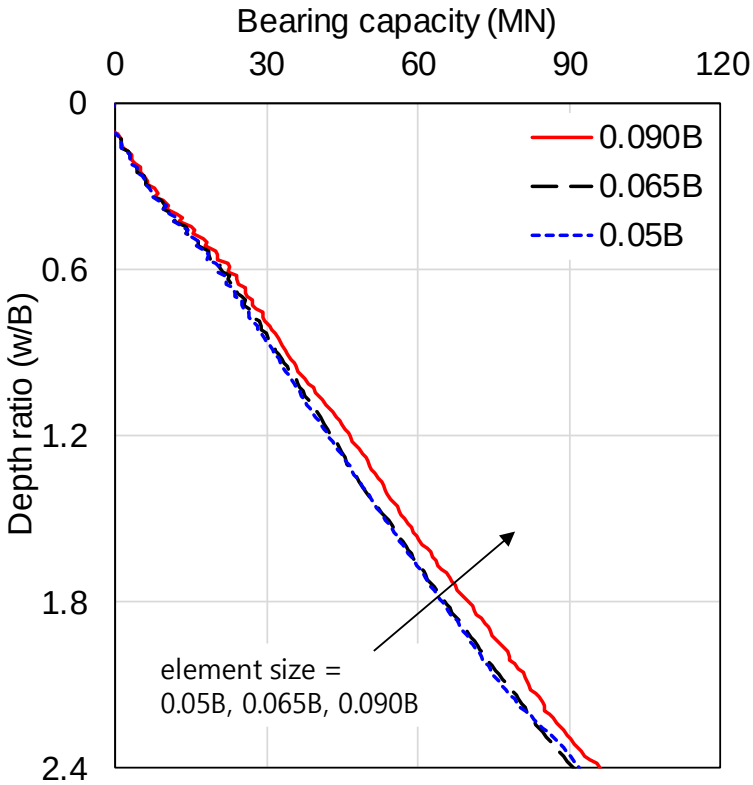

Fig. 72 Mesh convergence test in jack-up analysis

The element size has been determined to be 0.065B considering the computational cost and the accuracy of the analysis. As the element size increases, the analysis time decreases, but the accuracy of the analysis also decreases. Large-sized element typically shows that the bearing capacity value increases (Fig. 72). An element size of 0.065B, which shows similar results compared to 0.05B used in single spudcan analysis, has been adopted.

Table 11 Soil properties used in single clay analysis

	Value	Remarks
γ'	5.36 kN/m^3	Unit weight
s_{um}	2.4 kPa	s_u at mudline
k	1.35 kPa/m	s_u slope with depth
E/s_u	500	Rigidity index
ν	0.49	Poisson's ratio
$\alpha_{friction}$	0.35	Friction coefficient
$S_t\ (=1/\delta_{rem})$	2.86	$\left[\delta_{rem}+(1-\delta_{rem})e^{-3\xi/\xi_{95}}\right]$
ξ_{95}	15	
u	0.1	$\left[1+\mu\log\left(\frac{Max\left(\lvert\dot{\xi}\rvert,\dot{\xi}_{ref}\right)}{\dot{\xi}_{ref}}\right)\right]$
$\dot{\xi}_{ref}$	1%/h	

The soil properties used in single layer modeling are shown in the Table 11. The single clay used in Chapter 3 has been used in the same way. It has been attempted to compare under the same conditions as the yield interaction analysis using soil parameters obtained from the single clay analysis performed in Chapter 3.

5.3.3. Yield interaction model used in single clay analysis

jack-up structural analysis has been performed using the yield interaction model implemented in UEL and compared with the analysis results using the soil continuum model described above. The same model of jack-up structure with the soil continuum model in 5.3.2 has been used. This is for comparison of the differences according to the nonlinear foundation model in the same structure.

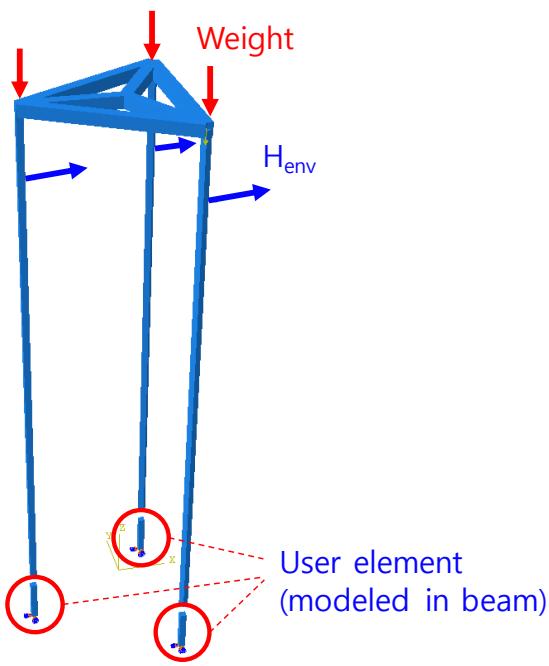

Fig. 73 FE model for structure-soil interaction analysis with yield interaction model (model B)

FE model of jack-up analysis using the yield interaction model is shown. The implemented user element is placed in the lower part of the jack-up leg as a 1D beam. Legs and user elements are

connected by 6-dof coupling like spudcan so that the reaction and displacement calculated from user elements can be transferred. The bottom of the user element is fixed so that only the user element reaction becomes the boundary condition of the jack-up structure.

Two types of yield interaction models have been used to compare each other. First, hyperbolic model B, a proposed model for soft over stiff clay, has been used in this study. Although it is a proposed model for soft over stiff clay, it is thought that the hyperbolic relation in the elastic region will be effective even for single clay. And for comparison, the modified model B (Zhang et al., 2014b), which is a state-of-art model on a single clay, has been used. The difference between the proposed model and the latest model is analyzed in this chapter.

Table 12 Soil parameter used in single clay analysis

Capacity	Value	Stiffness	Value
V_{ult}	69.79 MN	K_v	574.52 MN/m
H_o	24.20 MN	K_h	473.90 MN/m
M_o	121.40 MNm	K_m	19760 MNm/rad
		K_c	-120.27 MN/rad

For comparison in the same criteria, both models use the same soil parameters (stiffness, capacity). Zhang et al. (2012) has suggested stiffness and capacity for single clay. However, if two

models using different parameters are compared, the difference in methodology becomes unclear. To remove the effect of soil parameters on the results, the soil parameters obtained through single spudcan analysis (Table 12) have also been used in modified model B. It has been intended to show the difference of the methodologically proposed model and existing model.

5.3.4. Results

The results of the jack-up analysis considering structure-soil interaction by using a nonlinear foundation model for single clay were compared. The results of the reaction force, moment, and displacement acting on the soil are shown in the figure. The results of the soil continuum model and two yield interaction models, described in 5.3.2 and 5.3.3 respectively, are shown in the figure.

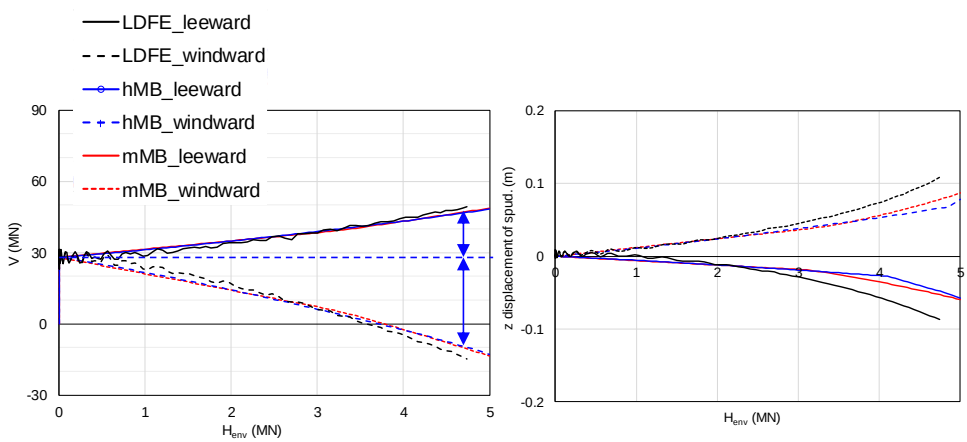

Fig. 74 Soil response in vertical direction of single clay analysis; a) Reaction force; b) Displacement

The Fig. 74 shows the vertical reaction force and displacement of the structure-soil interaction models. When an environmental load is applied, the whole structure rotates in the environmental load direction, so that the leeward leg shows the downward motion and the windward leg shows upward motion. This phenomenon is shown in the Fig. 74 about the vertical load and displacement. The reaction force of Leeward leg increases, and accordingly downward motion is shown in the vertical direction. The windward leg shows upward motion and the corresponding reaction force decreases accordingly. The load applied direction is the direction in which two of the three legs are leeward leg and one is the windward leg. Accordingly, it is shown that the displacement and reaction force of the windward leg are about twice as large as the leeward.

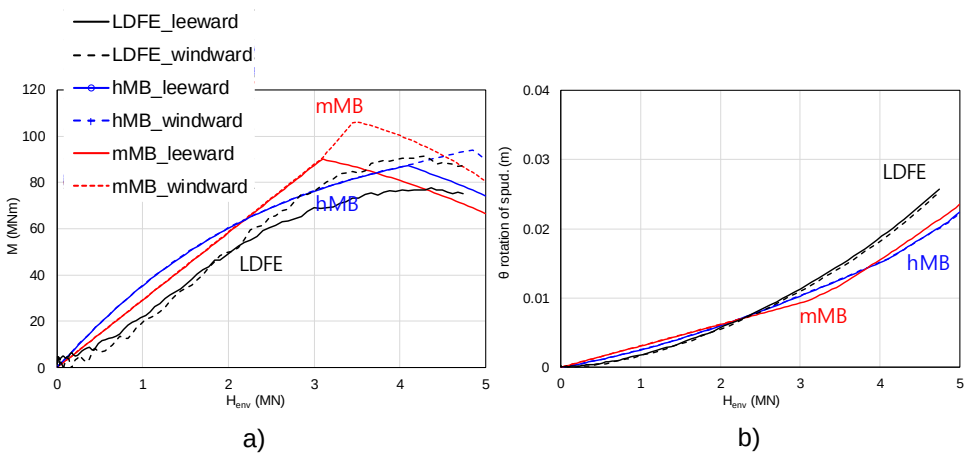

Fig. 75 Soil response in rotational direction of single clay analysis; a) Reaction moment; b) Rotation

The Fig. 75 shows the rotational reaction moment and rotation of the structure-soil interaction models. In general, the soil experiences moment failure first among the other directions during jack-up behavior. That is the reason why the secant model introduced the concept of secant stiffness for moment stiffness. Soil continuum model (LDFE) and yield interaction results have also confirmed that failure occurs first in the rotational direction. When looking at the LDFE results, the increased rate of moment gradually decreases as the environmental load increases and eventually starts to fall near 4 MN. This moment failure occurs gradually, and the displacement also shows increasing the slope progressively. In the case of the yield interaction models, both models well predicted the moment failure. In particular, plasticity occurs in the case of the environmental load 5MN, where the failure of the structure occurs. In the hyperbolic model, strength degradation in the elastic region has been simulated through hyperbolic relation before plasticity occurred. Accordingly, the reaction moment gradually decreased as the environmental load increased, such as LDFE. In contrast, the modified model B shows that the reaction moment increased relatively linearly as the environmental load increased before yield occurs. Thus it has been confirmed that the moment is slightly overestimated at the yield point. In the case of displacement, hyperbolic model B results are gradually increased, but the difference between foundation models is not significant.

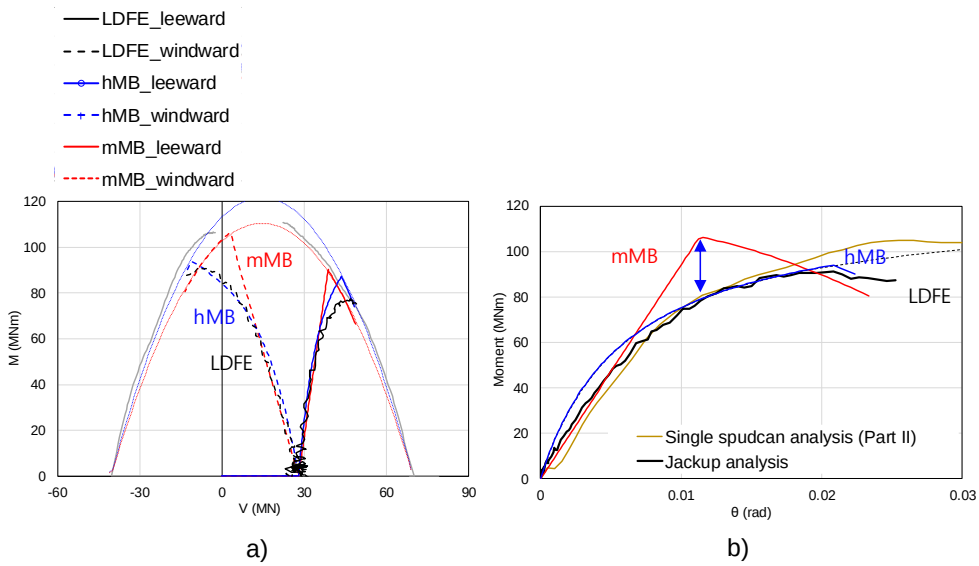

Fig. 76 Soil response of single clay analysis;

a) Load path in VM plane; b) M− θ relationship of analysis

The difference between the two yield interaction models is better shown in the Fig. 76(a). The load path for the vertical reaction force and the rotational reaction moment shows the difference between the two models before the yield point. In the case of Hyperbolic model B, the overall load path, including the gradual moment failure, follows the LDFE results relatively well, especially in the windward leg. In the case of modified model B, the behavior after the yield point is similar to that of the other two models. However, the behavior before yield is somewhat close to linear so that the difference is presented.

Fig. 76(b) shows the moment−rotation material curve in the rotational direction where yield occurs. By using the same soil properties, the material curve obtained from single spudcan analysis

and that from jack-up structural analysis are almost identical. Hyperbolic model B using hyperbolic relation fitted from singe spudcan analysis follows the strength degradation before yield and moment failure after yield. However, the modified model B accurately simulates the plastic behavior after yielding, while the elastic behavior shows a curve close to linearity. Gradual moment failure in LDFE results has not been simulated in modified model B.

5.4. Soft over stiff clay

5.4.1. FE model used in soft over stiff clay analysis

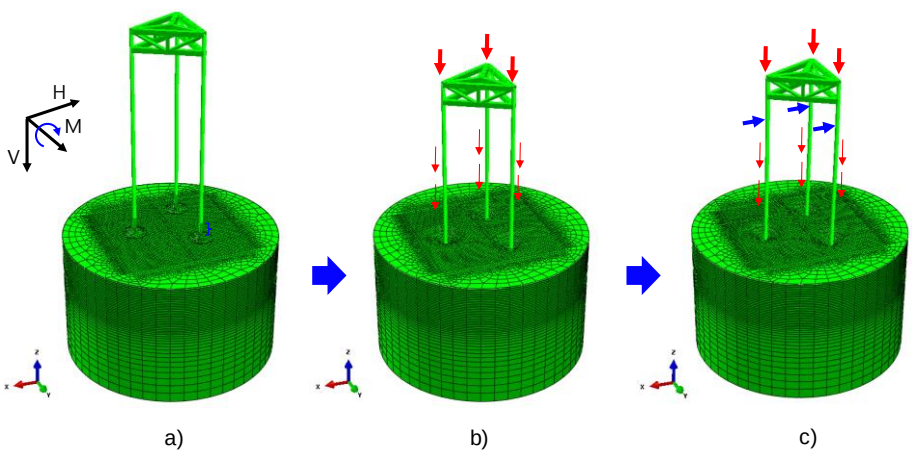

Fig. 77 FE model used in soft over stiff clay analysis; a) Starting position; b) Penetration; c) Environmental load analysis

The FE model used in structure-soil interaction analysis using the soil continuum model is shown in Fig. 77. As a typical soft over stiff clay, the MWS2P case is selected, in which the physical

properties of the lower clay is twice as hard as the upper soft clay. After the penetration of the jack-up structure, the same load sequence with the single clay case is performed to apply the environmental load. The penetrated location of 2.2B and the penetration rate of 0.015B/s have also been the same. In the soft over stiff clay case, the soil profile, which is the main point of the analysis, has been changed, as well as the jack-up structure and the applied load. jack-up structure has been damaged by the impact due to lower stiff clay. To prevent this, the hull leg joint and spudcan-leg joint have been reinforced. First, the hull-leg joint has been reinforced through additional brace structures to increase strength. In addition, the local spudcan-leg joint has been changed from the pipe section to the circular section to increase the strength without changing the outer diameter. Also, in the case of vertical load, the total load is the same, but the leg weight is applied as the distribution load. And as the soil properties changed, the environmental load reaching the failure of the structure has been changed. A total of 19.5MN of the load has been applied to the leg by combining the three legs.

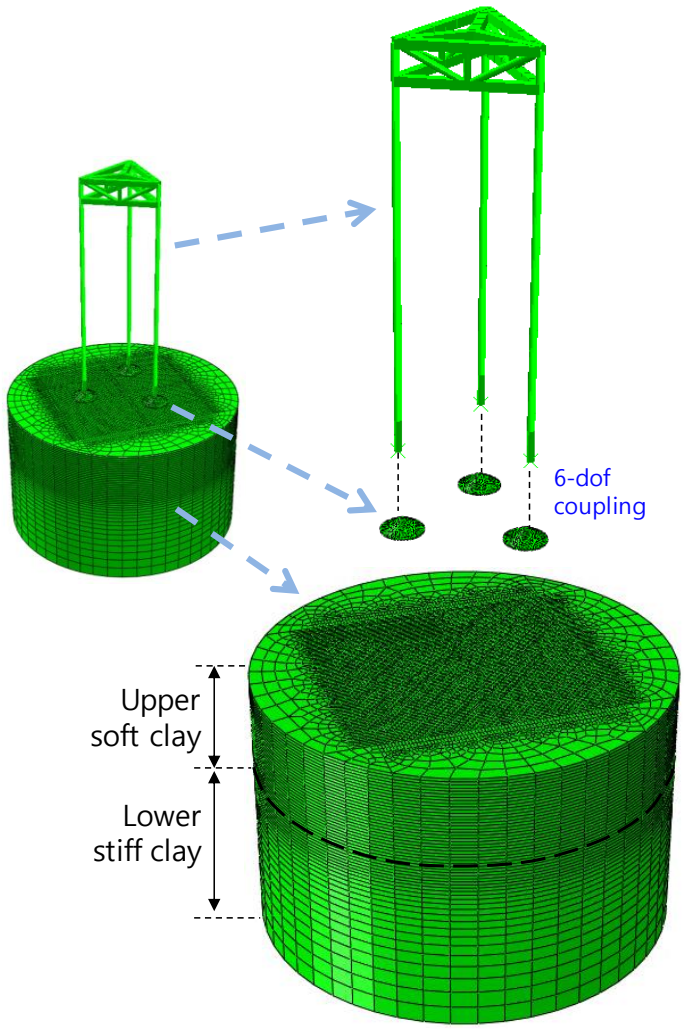

Fig. 78 Detailed FE model used in soft over stiff clay analysis

As described above, the same jack-up structure and spudcan as single clay case are used in soft over stiff clay case. Jack-up modeling has been performed with a stick model using a Timoshenko beam. To use the CEL technique, the spudcan has been modeled as a 3D solid lagrangian model and assumed to be a rigid body for analysis clarity. Jack-up structure and spudcan is connected using 6-dof coupling which transfers the reaction force, moment and

displacement. The whole soil domain has remained the same, and accordingly, the domain size and element size of the eulerian mesh is the same (Fig. 78). However, the soil domain has been divided into two layers to model the upper and lower clays. The upper layer is composed of the same soft clay as the existing single clay, and the lower layer is modeled by applying twice the undrained strength at the boundary of the upper soft clay. This is the same as the MWS2P case of Chapter 3, which is for comparison under conditions such as yield interaction analysis using soil parameters obtained from soft over stiff clay analysis performed in Chapter 3. Details are given in the Table 13.

Table 13 Soil properties used in soft over stiff clay analysis

	Value	Remarks
γ'	7.46 kN/m^3	Unit weight
s_{um}	77.81 kPa	$s_{u,stiff} = s_{u,H}$ Twice the upper clay strength
k	–	Homogeneous soil (assumed)
E/s_u	500	Rigidity index
ν	0.49	Poisson’s ratio
$\alpha_{friction}$	0.35	Friction coefficient

5.4.2. Yield interaction model used in soft over stiff clay analysis

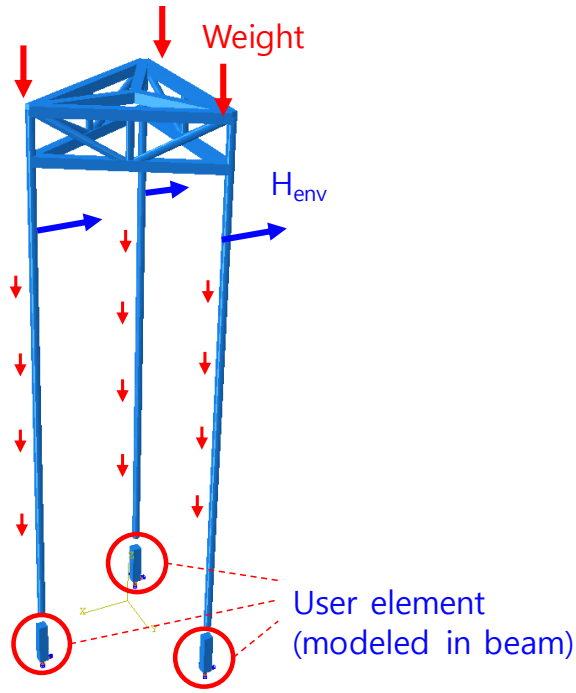

Fig. 79 FE model used in soft over stiff clay cas for structure-soil interaction analysis with yield interaction model (model B)

The jack-up structure changed in 5.4.1 has been used in the yield interaction model for consistency (Fig. 79). The soil continuum model described in 5.4.1 and the jack-up analysis with yield interaction model with the same structure are compared. Like a single clay case, the user element with the yield interaction model is implemented as a 1D beam and placed at the bottom of the leg. UEL and leg is connected by using 6-dof coupling. In the soft over stiff clay case, the hyperbolic model B proposed in this study and the latest modified model B have been used (Zhang, 2014). Modified model B is a model for a single clay, but soil parameters obtained

from soft over stiff clay have been applied for analysis.

Table 14 Soil properties used in soft over stiff clay analysis

Capacity	Value	Stiffness	Value
V_{ult}	110.95 MN	K_v	654.94 MN/m
H_o	26.16 MN	K_h	622.90 MN/m
M_o	165.20 MNm	K_m	35080 MNm/rad
		K_c	−62.62 MN/rad

There is no suggested soil parameter of modified model B for soft over stiff clay. Accordingly, the soil parameter obtained in this study has been applied equally to both models for consistency. The comparison between two yield interaction models in soft over stiff clay is intended to be analyzed by methodology.

5.4.3. Results of soft over stiff clay analysis

Fig. 80 shows the vertical reaction force and displacement of the structure–soil interaction models.

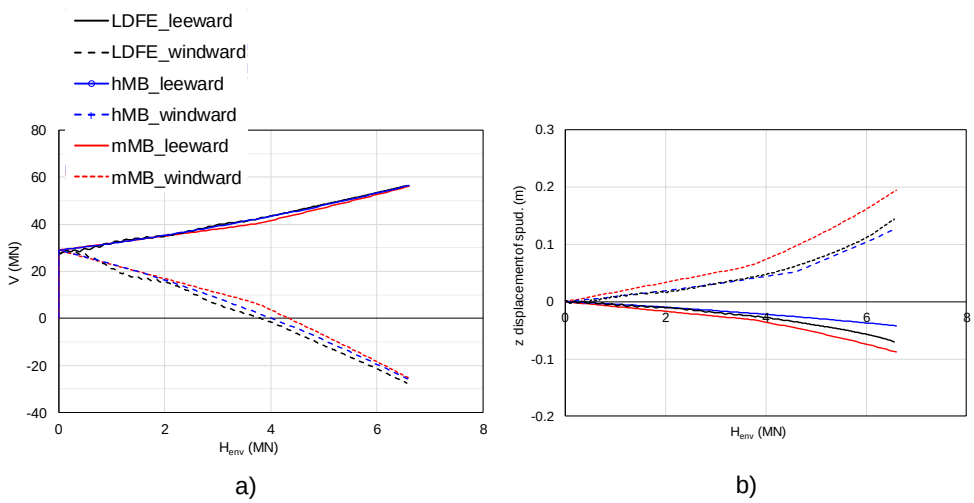

Fig. 80 Soil response in vertical direction of soft over stiff clay analysis; a) Reaction force; b) Displacement

As mentioned in 5.3.4, when an environmental load is applied, the jack–up rotates as a whole in the direction in which the environmental load is applied, so that the leeward leg is downward and the windward leg is subjected to upward forces. This phenomenon also occurs in the soft over stiff clay case. Leeward leg shows downward motion, and at the same time, vertical reaction force increases. In contrast, the windward leg shows upward movement, and the vertical reaction force decreases.

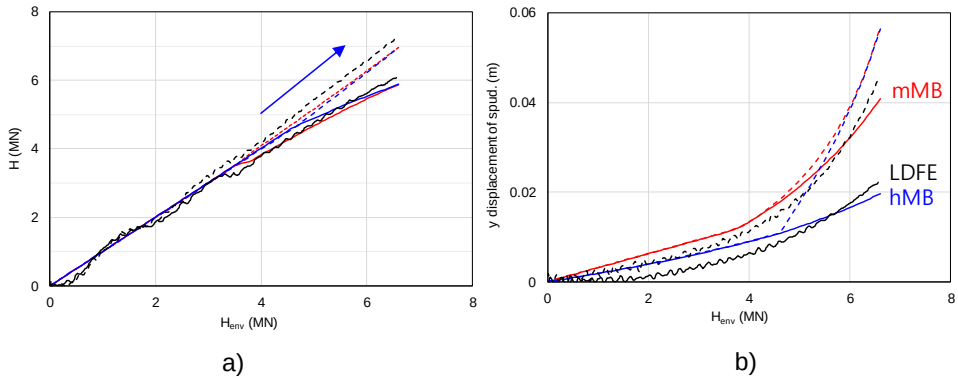

Fig. 81 Soil response in horizontal direction of soft over stiff clay analysis; a) Reaction force; b) Displacement

Fig. 81 shows the horizontal reaction force and displacement. As the environmental load is applied in the horizontal direction, in the elastic region, the horizontal reaction force acting in the opposite direction should be the same value by the principle of action-reaction. Before the yield occurs near H_{env}=4MN, it has been confirmed that the horizontal reaction force of the same magnitude as the environmental load occurs in both the soil continuum model and the two yield interaction models. When yield occurs, moment failure occurs first, and redistribution of force occurs accordingly. The horizontal response of the leeward and windward legs is changed because of their different vertical forces. Typical pushover test using centrifuge also shows an increased H of windward leg. As a result of the structure-soil interaction analysis of this study, it is shown that the response of the two legs becomes different due to the redistribution of the force after yield, and the response of the windward leg is greater.

Displacement results show a difference between the hyperbolic model B and the existing modified model B, in which the hyperbolic relation is implemented in the horizontal direction in the hyperbolic model B (Fig. 81(b)). The soil continuum model by using LDFE analysis results in a gradual increase in displacement, which is also simulated in hyperbolic model B. However, modified model B shows a relatively linear relationship, and accordingly, the yield occurs more quickly. As a result, there is a difference in displacement between two yield interaction models. Hyperbolic model B shows similar results to the soil continuum model, especially in the leeward leg.

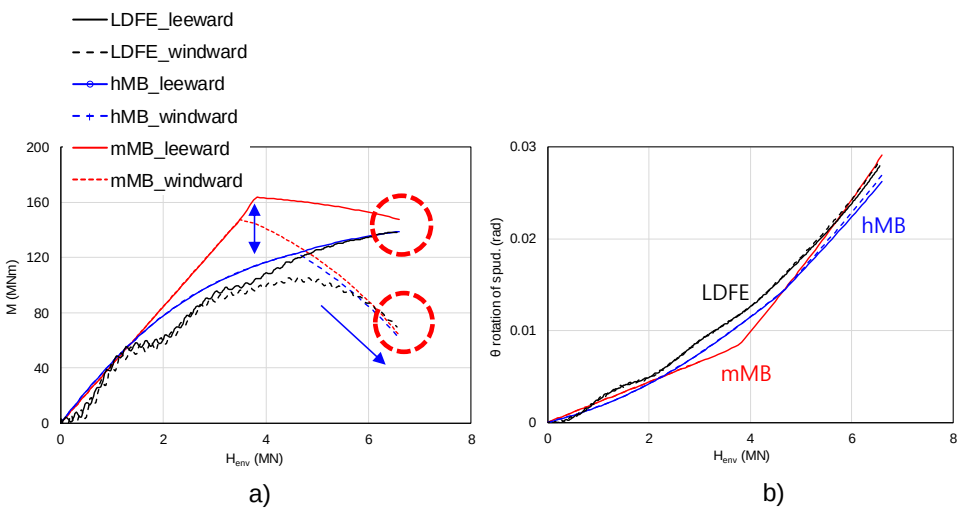

Fig. 82 Soil response in rotational direction of soft over stiff clay analysis; a) Reaction moment; b) Rotation

Fig. 82 shows the rotational reaction moment and rotation according to the environmental load. Soil failure usually occurs first

in the rotational direction, and in this respect, it is important to simulate the reaction moment precisely. In soft over stiff clay cases subjected to larger environmental loads, the gradual moment failure appears well. The moment increases slowly as the environmental load increases in the results of the soil continuum model, and it is shown that the moment values of the windward leg become different due to yield near the environmental load of 4MN. Modified model B predicted the yield point of 4MN well, and it is shown that the moment in the plastic region is close to the LDFE result. In Hyperbolic model B, the yield point is somewhat slower (Henv=4.5MN), but the strength of degradation at the moment is well simulated. With this nonlinear hyperbolic relation in the rotational direction, the moment results about the environmental load approach close to the LDFE result. In the case of modified model B, despite the similar results after yield, the moment is overestimated due to the near-linear moment increase in the elastic region. In the case of rotation of the spudcan(Fig. 82(b)), hyperbolic model B expresses a gradual increase due to hyperbolic relation, but modified model B also shows a good fit with LDFE results due to the changed slope after yield.

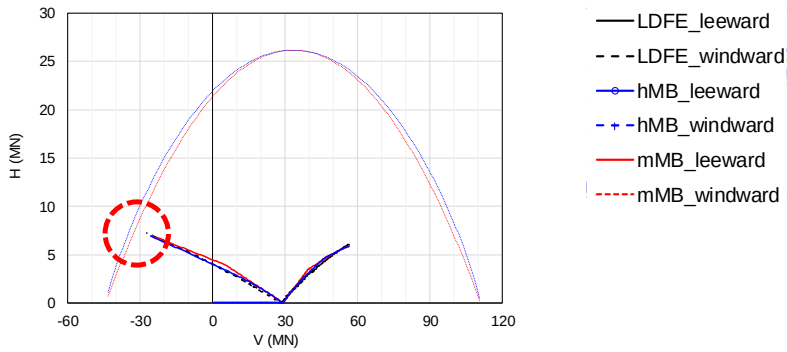

Fig. 83 Load path of soft over stiff clay analysis in VH plane

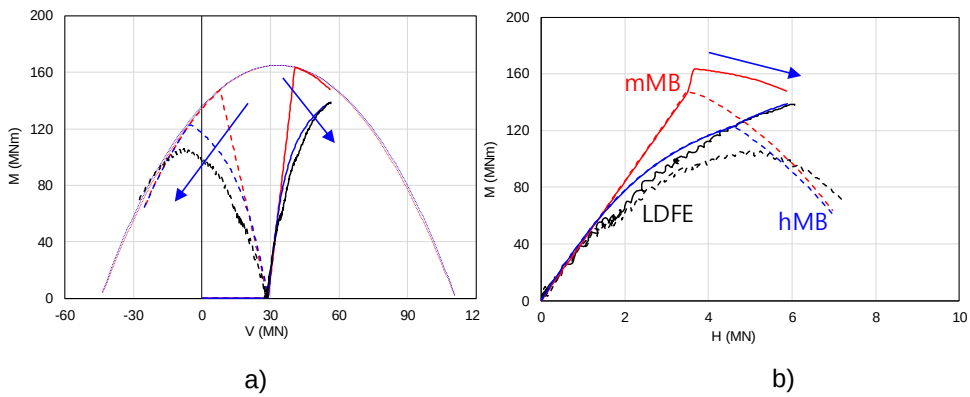

Fig. 84 Load path of soft over stiff clay analysis;

a) in VM plane; b) in HM plane

For the vertical reaction force, horizontal reaction force and rotation reaction moment shown above, the load path is plotted on the plane with each force as the axis (Fig. 83, Fig. 84). First, in the case of the load path in the VH plane (Fig. 83), LDFE, hyperbolic model B, and modified model B results are similar. Compared with the yield envelope used in the yield interaction model, the load path has not yet been reached the yield envelope in a horizontal direction. Therefore, the horizontal reaction force reduction did not occur

because of yield, such as the moment.

The load path in the VM plane and HM plane shows the effect of moment failure (Fig. 84). The load path in the VM plane shows that the results of hyperbolic model B follow the results of LDFE better. Unlike modified model B, which approaches the yield envelope in a direction close to linear at initial stiffness, the slope of hyperbolic model B gradually decreases in the increment of the moment and thus becomes similar to the result of the soil continuum model, where the gradual moment failure occurs. In addition, the modified model B rapidly approaches the yield envelope, and yield occurs in the leeward leg. In contrast, the hyperbolic model B does not reach the yield envelope, and yield does not occur. This indicates that, like the load path in the HM plane, the linear elastic relationship of modified model B can overestimate the moment before yield. On the other hand, hyperbolic model B similarly simulates gradual moment failure due to the implemented nonlinear hyperbolic relations.

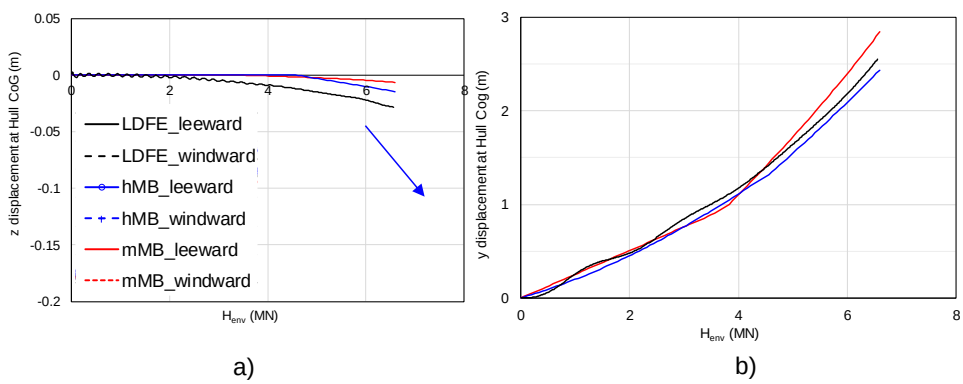

Fig. 85 Hull displacement of soft over stiff clay analysis;
a) Vertical displacement; b) Horizontal displacement

The vertical and horizontal hull displacements are shown in the Fig. 85. As the soil continuum model simulates the gradual plasticity of the soil, the hull gradually moves down and shifts in the horizontal direction. In the yield interaction model, these plastic deformations can be simulated, but due to the characteristics of the elasto-plasticity framework, plastic deformation is not calculated before yield occurs. Accordingly, both yield interaction models have a vertical displacement of 0 in the elastic region, and then plastic deformation increases after yield. The plastic displacement of the hull calculated in the hyperbolic model B approaches the LDFE result faster (Fig. 85(a)). In general, horizontal behavior in the hull is affected by rotation at the spudcan due to the long leg length. Spudcan rotation is similar in the three models, so the horizontal displacement of the hull is also similar (Fig. 85(b)).

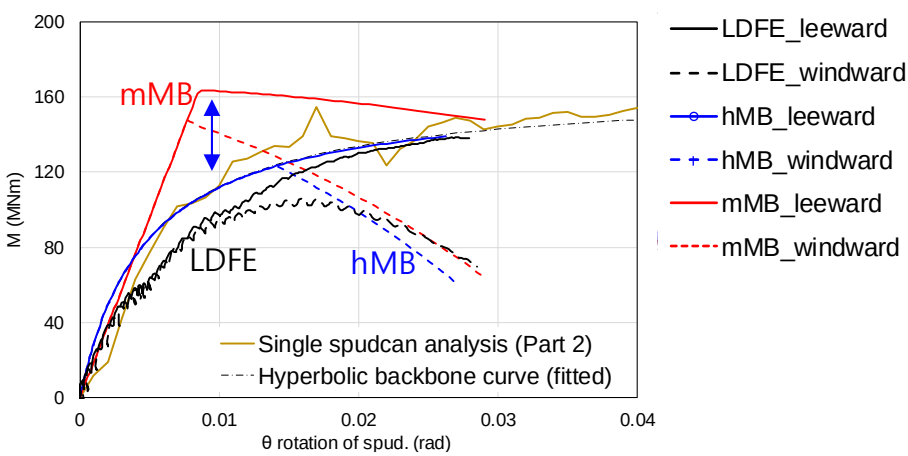

Fig. 86 M-θ material curve of soft over stiff clay analysis

To present the moment failure, the M− θ material curve in single spudcan analysis, jack−up analysis using a soil continuum model, and those of two yield interaction models are shown in Fig. 86. Hyperbolic model B uses a fitted hyperbolic curve from the results of single spudcan analysis and follows the entered curve well. The decreasing moment has also been simulated in the windward leg where yield occurs due to the vertical and horizontal forces. A smaller moment is available under vertical and horizontal reaction force than that under no vertical and horizontal forces in the concept of force−resultant yield envelope. In contrast, in the case of modified model B, the moment overestimates in the elastic region before yield. However, the results approach the LDFE results fast after yield.

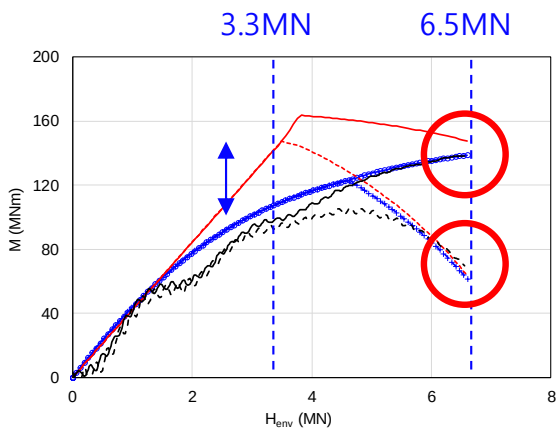

Fig. 87 Two moments for structural response of jack−up (H_{env}=3.3MN for elastic, 6.5MN for plastic)

Two moments are selected to compare the structural response of jack−up. First, the point within the elastic region, where the

moments of the two yield interaction models are different (H_{env}=3.3MN in Fig. 87), and the point within the plastic region, where ground failure and structure failure occur (H_{env}=6.5MN in Fig. 87), are selected.

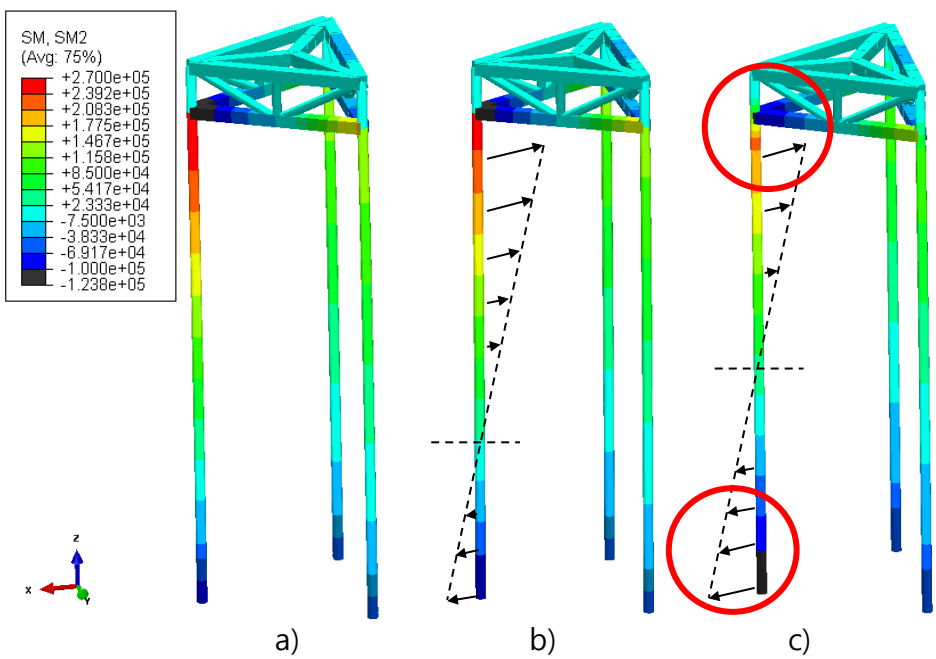

Fig. 88 Bending moment at H_{env}=3.3MN; a) LDFE analysis; b) Hyperbolic model B; c) modified model B

The structural response at the H_{env}=3.3MN, where a difference in soil reaction moment between modified model B and hyperbolic model B occurs, is shown in Fig. 88. The stick model is suitable for viewing the global jack-up response, not local member forces, and thus the distribution of the bending moment of the leg is presented. Hyperbolic model B shows a similar distribution to soil continuum model results using LDFE. On the other hand, modified model B

shows that the reaction moment on the soil is larger than the other two models, and the bending moment of the leg is also different accordingly. The moment acting on the spudcan–leg joint is larger than the other two models like soil response, so the distribution of the moment of the entire leg is shifted. As a result, the bending moment at the hull–leg joint is underestimated due to the shifted distribution. This joint is the critical point of jack–up structural analysis, and the hyperbolic model B shows a more accurate bending moment distribution of leg.

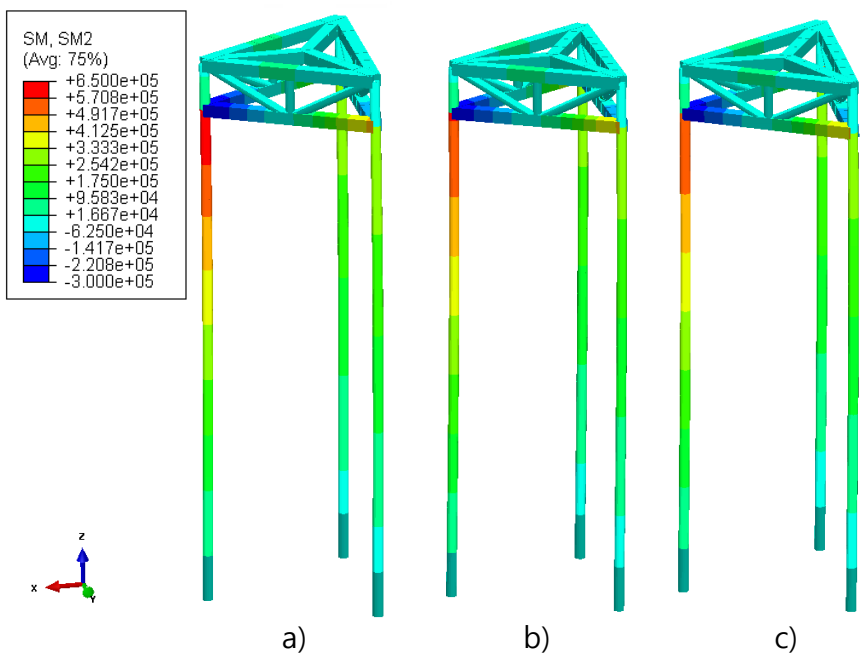

Fig. 89 Bending moment at H_{env}=6.5MN; a) LDFE analysis; b) Hyperbolic model B; c) modified model B

The structure response at H_{env} = 6.5MN, where the plasticity of the soil and the failure of the structure occurs, is shown in Fig. 89.

In this plastic region, the three models show similar values. This is because modified model B simulates a moment in the plastic region well through the plasticity framework after yield. As a result, all three models showed a similar distribution in terms of the bending moment of the leg.

Through the bending moment results, it has been confirmed that the magnitude of the reaction moment acting on the spudcan, which is the same with the applied moment on soil, affects the distribution of the bending moment of the leg. The distribution of bending moments is similar if they show similar soil reaction moments (Fig. 89). However, it is important that the large reaction force on the soil may lead to an underestimation of the bending moment in the hull–leg joint (Fig. 88).

Chapter 6. Dynamic effects of jack-up structural analysis

6.1. Introduction

Jack-up is an offshore structure that is subjected to environmental loads such as wave, current, and wind during operation. Random wave is generally expressed as the sum of regular waves of different periods and heights, and have a great influence on the dynamic response of structures.

Offshore platforms are always designed for the specific field, so the natural period varies depending on the design and characteristics of the individual structures. However, in general, fixed offshore structures have a small natural period (T_n < 5s). In comparison, floating offshore structures typically have a comparatively long natural period (T_n > 20s). Jack-ups typically have a natural period between 5 ~ 15 seconds, depending on their size, which overlaps the maximum wave energy spectrum (ABS, 2014). This means that jack-up is the dynamically sensitive offshore platform in wave analysis (Fig. 90(a)).

To consider these dynamic characteristics, jack-up structural analysis of dynamic loads has been performed using a soil continuum model. In this chapter, the dynamic effects that accompany jack-up dynamic analysis are investigated. These include the effects due to inertia force, resonance with wave, and dynamic characteristics of

the soil (Fig. 90(b)). These effects were investigated and reflected in the yield interaction model and compared with the results of the soil continuum model.

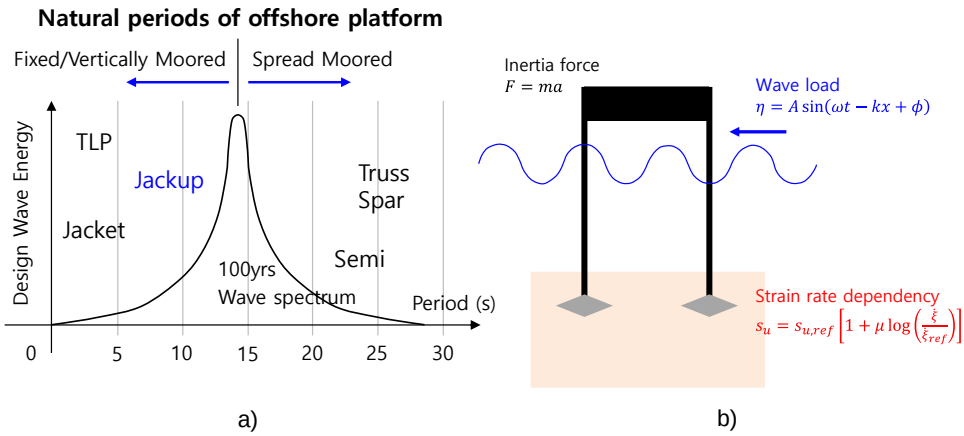

Fig. 90 Dynamic effects of jack-up;

a) Typical natural period of offshore platform;

b) Jackup structural analysis with dynamic load

6.2. Dynamic effects in jack-up structural analysis

6.2.1. Categorization of dynamic effects

Dynamic effects are caused by several factors about time. It has been divided into two categories in this chapter, structural aspect, and geotechnical aspect.

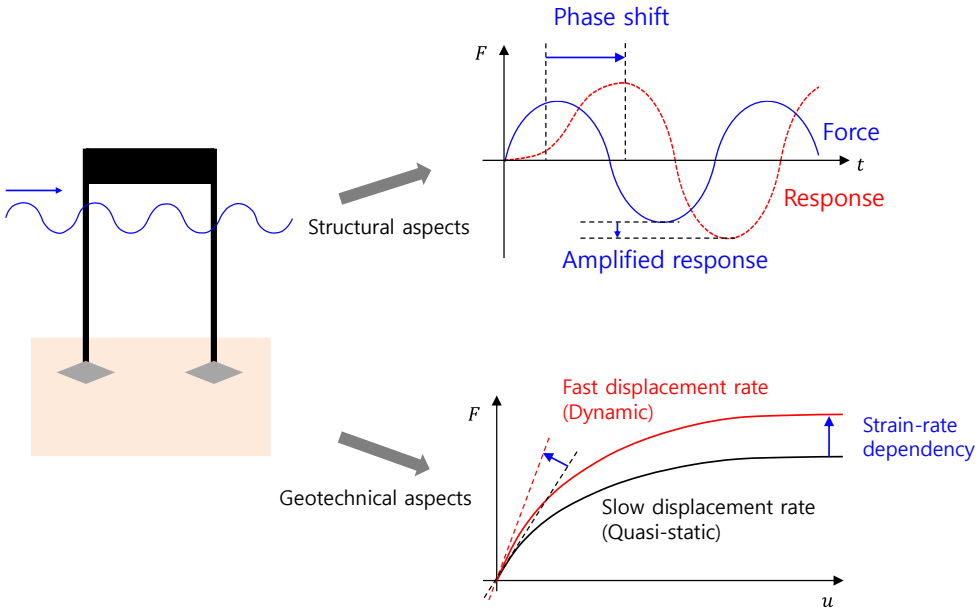

Fig. 91 Schematic figure of dynamic effects

Dynamic effects about clay can be a strain rate dependency of properties, energy dissipated damping, material damping, and so on. Damping is generally considered by observation and calculation of coefficient through experiments, and the material damping has been usually simulated using a viscous material model. Among these dynamic effects, the strain rate dependency has been described in this chapter. In general, as the strain rate increases, the strength increases, and the stiffness and capacity increase accordingly. This effect has been reflected in the numerical analysis with the soil continuum model. Soil parameters considering the rate hardening are entered into the yield interaction model, and the results are compared with those of LDFE analysis.

Structural dynamic effects include amplified response and phase shift, due to inertia force. The amplified response is caused by

several factors, such as resonance with a wave, wave damping, and the effect of soil damping on the boundary condition. In general, when determining the dynamic response of a structure, these various factors are collectively considered as DAF (Spidsøe and Karunakaran, 1996; Yu et al., 2012). Although it is difficult to calculate the exact DAF, this study has assumed the DAF carefully and applied to the yield interaction model. The analysis results are compared with those of the soil continuum model.

6.2.2. Strain rate dependency of clay on jack-up wave analysis

In general, as the strain rate increases, s_u increases in logarithmic scale. This relationship is also introduced in Abelev and Valent (2009) and Nanda et al. (2017). Rate hardening with logarithmic relation is also implemented in nonlinear clay model (Eq. (29)) used in this study.

$$s_{ui} = \left[1 + \mu \log\left(\frac{\mathrm{Max}\left(\left|\dot{\xi}\right|, \dot{\xi}_{ref}\right)}{\dot{\xi}_{ref}}\right)\right] \left[\delta_{rem} + (1 - \delta_{rem}) e^{-3\xi/\xi_{95}}\right] [s_{\mathrm{umi}} + kz_i] \tag{29}$$

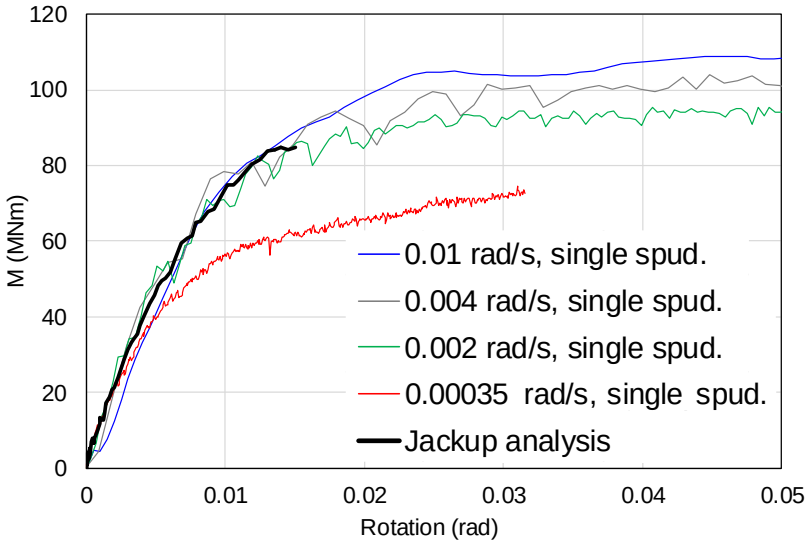

Fig. 92 M− θ curve according to the rotation rate

Fig. 92 shows the effect of rotation rate on material curve (M–θ) in single spudcan analysis. Wave load analysis results of Jackup is also plotted together (black line). Quasi static case has both small stiffness and small capacities (red line), but the rate is far from dynamic wave analysis. M–θ curve in this study (Chapter 3) based on 0.01 rad/s is rather close to wave analysis. When typically calculating soil parameters, the analysis has been performed at a sufficiently slow rate to eliminate the inertia effect. However, quasi−static analysis cannot accurately consider soil properties due to rate dependency. This rate dependency is considered in this study through soil parameter calculation, both stiffness and capacity, and these calculated soil parameters are used in static yield interaction model.

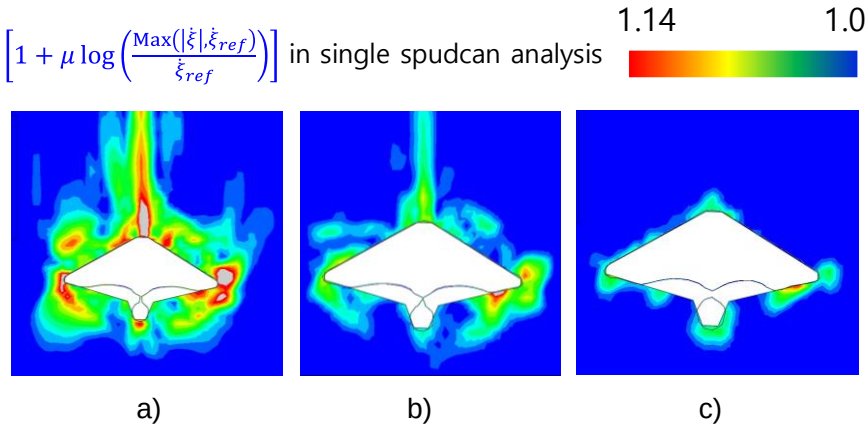

Fig. 93 Contour about rate hardening value in nonlinear clay model; a) 0.01 rad/s; b) 0.002 rad/s; c) 0.00035 rad/s

6.2.3. Phase shift effect

Phase shift is typically caused by inertia force in dynamic analysis. To identify the phase shift in jack-up analysis, mass scaling technique in Abaqus is used. Mass scaling technique increase the mass of the model artificially in numerical simulation. Mass scaling is a technique that forcibly increases the time increment by artificially increasing the mass term because this mass term is proportional to the time step in the explicit analysis. With this increased time increment, explicit analysis that takes longer can be performed more cost-efficiently. In this scaled-mass analysis, inertia effect is amplified through mass scaling, but the rate dependency of material is maintained (Simulia, 2013). This study has focused these features of the technique. In a situation where the response due to the rate dependency did not change, how the

amplified inertia effect by artificially increasing the mass affects the response is examined.

In Fig. 94, phase shift occurs in the case of amplified inertia effect (mass scaling = 4). Immediately after the load is applied, the response is delayed due to the high value of initial acceleration. However, inertia effect is reduced and responses converge as the analysis progresses. Under monotonic load analysis, phase shift due to inertia effect occurs at initial phase but does not affect the response after stabilization. When designing offshore structures, the magnitude of the response is more important than the phase. After sufficient stabilization, it is assumed that the inertia effect does not exist in the response, and the phase shift effect after stabilization is not considered in this study.

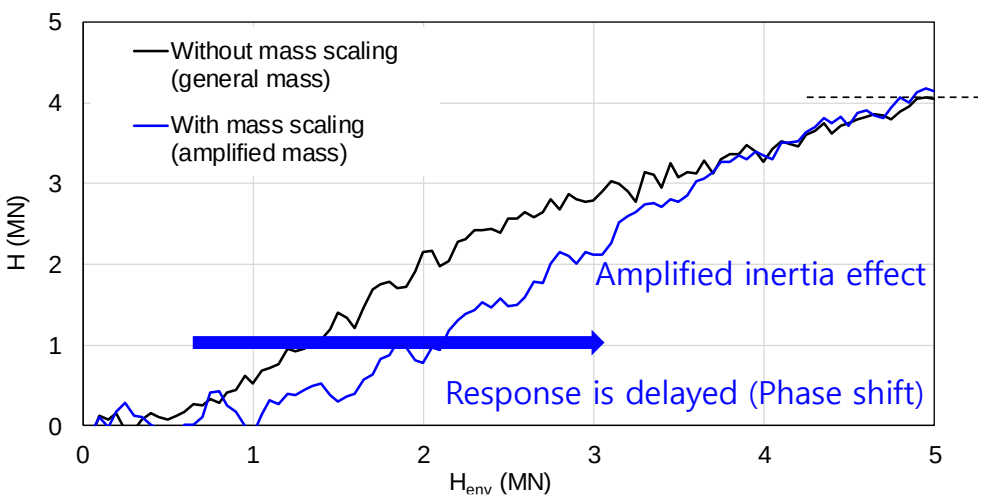

Fig. 94 Inertia effect on Jackup analysis under monotonic load analysis

6.2.4. Dynamic Amplification Factor (DAF)

Natural period is very important factor for calculating DAF in offshore platform. Typical natural period of jack-up is between 5~15s (ABS, 2014). Soil stiffness, as the boundary condition, has great influence on natural period. In the soil continuum model where the strength degradation occurs, it is impossible to accurately calculate the natural period. As an alternative, Fig. 95 shows the result of calculating the natural period using the initial stiffness. Calculated natural period is 7.76s, and 12.03s for pinned condition. Corresponding motion of 1st and 2nd mode are translated motion, which is surge, sway.

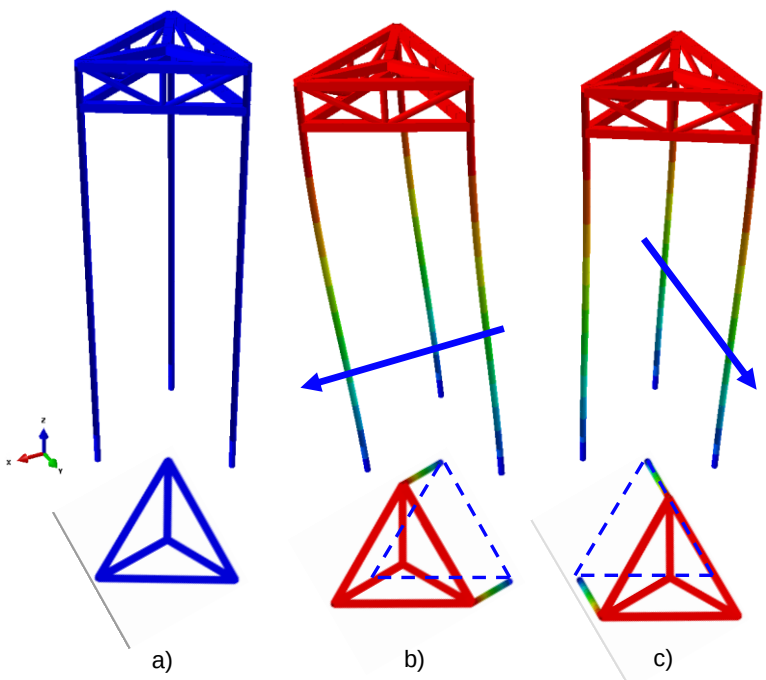

Fig. 95 Mode shape of jack-up; a) original structure; b) 1st mode (surge); c) 2nd mode (sway)

Definition of DAF is the structural response ratio between static and dynamic analysis. Conservative DAF is generally calculated using this definition, and then used in the platform design.

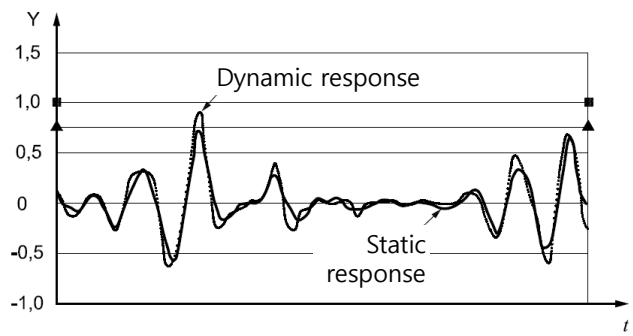

Fig. 96 Example of DAF (ISO, 2012)

For comparison of wave load analysis between static analysis with yield interaction model and dynamic analysis with soil continuum model, DAF should be considered. However, calculating DAF accurately is challenging. DAF calculation using classical single degree of freedom (SDOF) analogy is suggested in guideline (Eq. (30)).

$$DAF = \frac{1}{\sqrt{(1-\Omega^2)^2 + (2\zeta\Omega)^2}} \tag{30}$$

Where Ω is Natural period divided by the wave excitation period (T_n/T), and ζ is damping ratio. Natural period of structure, wave excitation period, wave damping, soil damping should be considered

in this DAF calculation using SDOF analogy, and this is the reason difficult to calculate DAF exactly. And also, this suggestion is conservative equation for design, not proper in calculation of realistic response. In this study, DAF is assumed excluding strain-rate dependency from amplified response (Fig. 97).

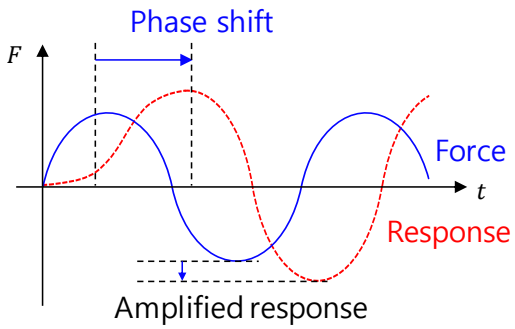

Fig. 97 Effect of DAF on the amplified response

6.3. Application : Jack-up structural analysis under dynamic wave load

6.3.1. Selection of soft over stiff clay

One of the purposes of the application is to validate the soil parameters, including regression model about initial stiffness, presented in Chapter 4. Soft over stiff clay soil has been presented for both depth ratio (w/H) and undrained shear strength ratio ($s_{u,stiff}/s_{u,H}$) variables. Soil parameters have been presented in the range of depth ratio from 0.9 to 1.2 and undrained shear strength ratio from 1 to 4. It is believed that this range can cover typical soft over stiff

clay properties. In this chapter, a middle point, 2.5 times stiffer lower clay and 2.1B of embedment case, has been selected to validate the interpolative capability of the regression model (Fig. 98). This is equivalent to a depth ratio of 1.05 and a undrained shear strength ratio of 2.5. Proposed regression model for initial stiffness and interpolated values of other soil parameters are used for validation.

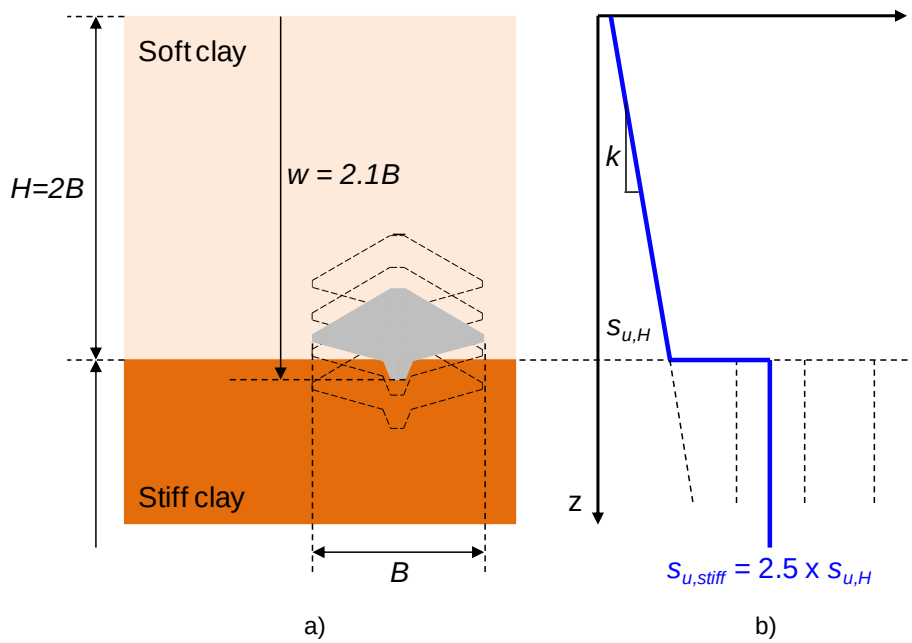

Fig. 98 Soft over stiff clay case used in application;
a) Depth ratio of 1.05; b) Strength ratio of 2.5

6.3.2. Wave environmental load

Wave environmental load is assumed as similar value with field data of reference jack-up (MLT-116C). Detailed information is shown in Table 15.

Table 15 Environmental condition for wave load

	Water depth	Airgap	Height (H)	Period (T)
reference	64~ 80m	15~ 20m	H_s=6.4~ 9.0m	T_p=11.1~ 13.1s
Case 1	65m	25m	H_{max}=8.0m	T_p=8.0s
Case 2	65m	25m	H_{max}=12.0m	T_p=13.0s

Load cases are selected for validation about hyperbolic relation of material in elastic region. Case 1, regular wave with H_{max} = 8m, T = 8s, is selected because the wave period is close to natural period with initial stiffness (7.76s). It has been selected to investigate the dynamic characteristics of the jack-up near the natural period, and the height suitable for wave steepness (0.08) has been calculated. Case 2, regular wave with H_{max} = 12m, T = 13s, is selected according to the concept of design wave selection. Design wave height is decided from the referenced significant wave

height is selected (H_s =6.4m). Corresponding wave period is calculated using proper wave steepness (0.046).

The wave load is calculated using the morison equation (Eq. (31)) depending on the location. This calculated load is especially key load in the cylinder structure like jacket or jack-up.

$$F = \rho C_m V\dot{u} + \frac{1}{2}\rho C_d A u|u| \tag{31}$$

Wave load applied at leg cannot be calculated using stick model, so the drag coefficient and inertia coefficient is modified according to leg design. For computational cost, Abaqus/Aqua analysis is performed in initial stiffness. Drag force and inertia force, including buoyancy, have been calculated and acted on the jack-up leg (Fig. 99). Corresponding nodal force is scanned and applied in 3D soil-jack-up interaction analysis (Fig. 100).

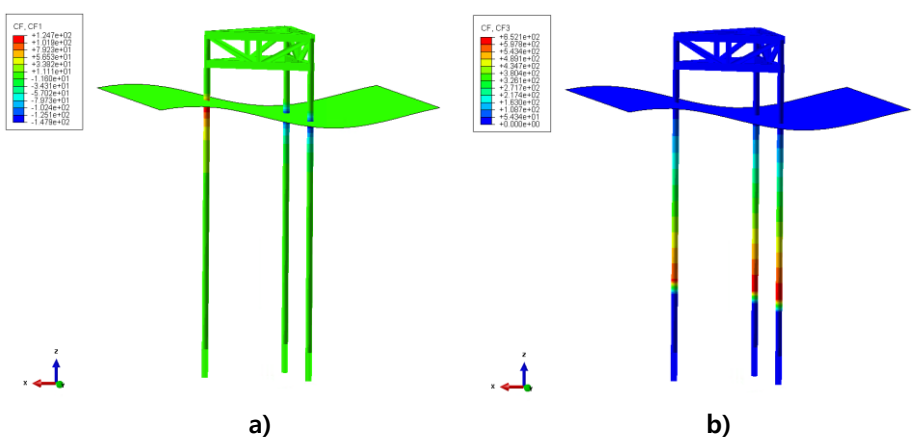

Fig. 99 Abaqus/Aqua analysis results;

a) Vertical force; b) Horizontal force

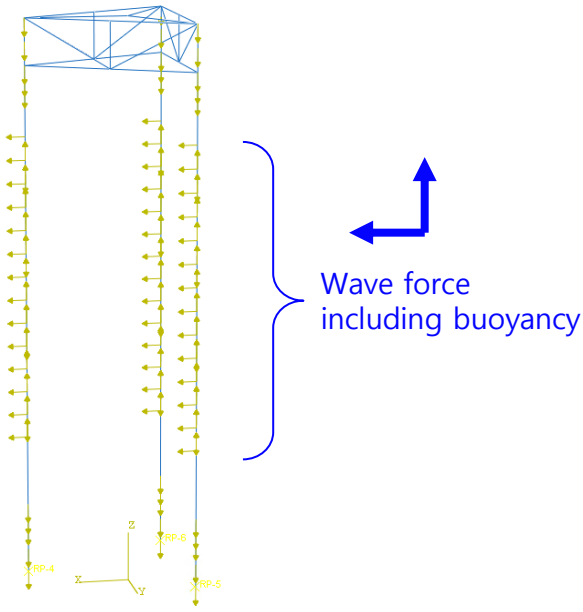

Fig. 100 Applied nodal force in jack-up

6.3.3. FE model for application

Same FE model with soft over stiff clay case, including reinforced jack-up structure, is used for application. Hull-leg joint and spudcan-leg joint have been reinforced so that the structure can withstand the impact due to the stiff soil below. Assuming a different payload, a vertical load of 33MN has been applied, and a repeated regular wave has been applied as an environmental load (Fig. 101(a)).

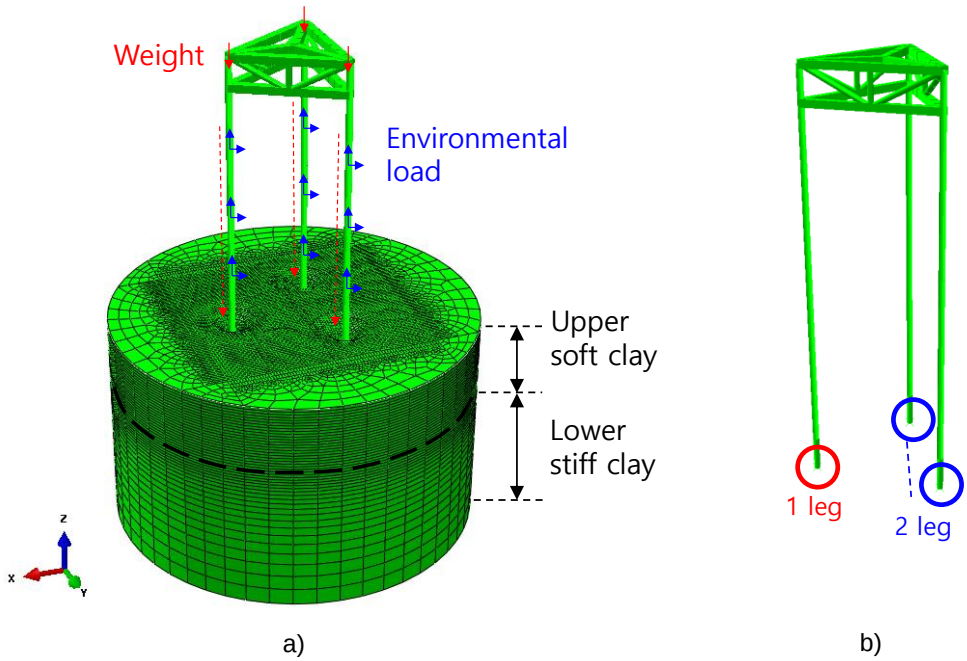

Fig. 101 a) FE model for application; b) Notation of legs

Since the direction of load is changed in regular wave, a specific leg cannot be defined as a leeward or windward leg in the application case. For the purpose of classification, the legs has named as "1-leg" and "2-leg" and the results have been shown accordingly (Fig. 101(b)).

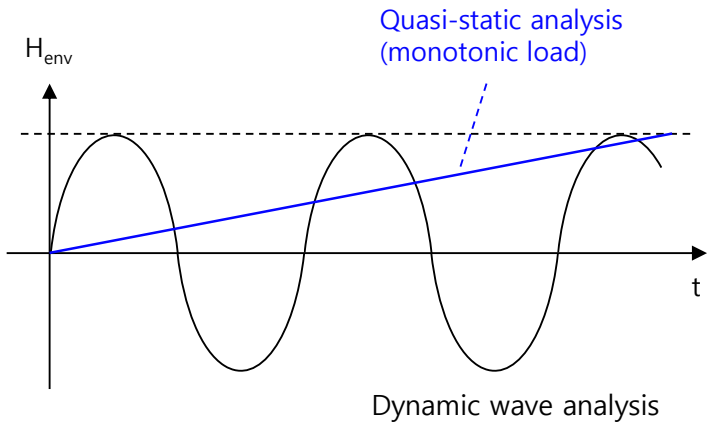

Fig. 102 Schematic figure of applied load

As an environmental load, a sinusoidal load has been assumed and applied using the peak load obtained through scanning like Fig. 100. To calculate DAF, the quasi-static analysis has also been performed in which the peak load of the wave is applied monotonically and slowly (blue line in Fig. 102). This is for using the definition of DAF, the ratio of dynamic response and quasi-static response.

The dynamic analysis has used the environmental load of the two cases mentioned above. Case 1, which is close to the natural period, has been used to investigate the dynamic effect, and case 2 has been used according to the design wave decision.

6.3.4. DAF calculation

As mentioned earlier, it is difficult to calculate the DAF. In the DAF calculation process using SDOF, the natural period of Jack-up, wave excitation period, wave damping, and soil damping should be considered. It is impossible to accurately calculate the natural period of Jack-up because the boundary condition is changed due to the change of the soil properties. Wave damping terms that vary depending on the structure are applied indirectly through the model tests. The soil damping term is divided into material damping and energy dissipation damping, and each influence must be accurately considered. It is not easy to accurately calculate and compare DAF under the influence of many factors.

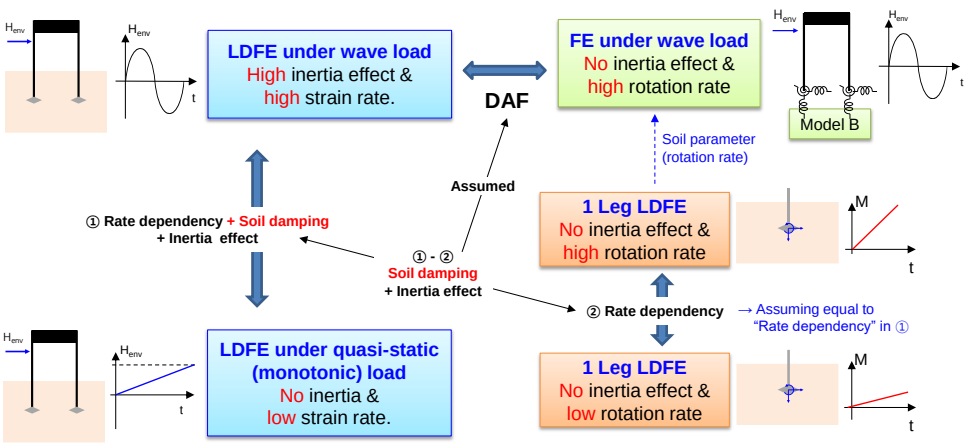

Fig. 103 Simplified diagram of DAF calculation procedure

In this study, since it is difficult to calculate all factors accurately, DAF has been assumed through an appropriate procedure. Using the

definition of DAF, the ratio between the time series analysis result and the quasi-static analysis result has been used, and the rate dependency of the soil strength has been considered separately. Rate dependency term has been calculated using a single spudcan analysis in which amplification of the reaction due to the inertia effect does not occur (Fig. 103).

First, in the Jack-up analysis using the soil continuum model, wave load analysis and quasi-static analysis have been performed (Fig. 102). Wave load analysis has a high inertia effect and a high strain rate, as a time series sinusoidal load has been applied. On the other hand, quasi-static analysis of slowly applying the load corresponding to the peak load has no inertia effect, and the strain rate is also sufficiently low. Therefore, the difference in response between the two analyzes can be divided into the effects of rate dependency, soil damping, and inertia effect. The difference in response between the two calculated analyzes is shown in the Table 16.

Second, the difference in soil strength due to rate dependency is considered. A single spudcan analysis has been used, reflecting only the effects of soil properties according to the rotation rate. The difference between the two responses is defined as a response that is different due to the rate-dependent soil strength by applying rotational motion at high speed and slow speed. The calculated results are also shown in the Table 16.

Table 16 Assumed DAF

	Case 1	Case 2	Remarks
$\frac{M_{Jackup,\,wave}}{M_{Jackup,\,qs}}$	5.50	2.66	① in Fig. 103 DAF + Rate dep.
$\frac{M_{spud.,\,dyn}}{M_{spud.,\,qs}}$	1.35	1.31	② in Fig. 103 Rate dependency
DAF	4.07	2.03	(① − ②) DAF

It has been assumed that the effect of soil strength obtained through single spudcan analysis is the same as the rate dependency term in Jack-up analysis. Finally, DAF to be applied to static analysis has been assumed using the difference in response from Jack-up analysis and the response from single spudcan analysis. The assumed DAF is applied to the static analysis result using the yield interaction model, and this has been compared with the Jackup analysis result using the soil continuum model analyzed in the time domain.

6.3.5. Analysis condition

Jack-up structural analysis with yield interaction model is performed in static analysis. Two yield interaction models are used; Hyperbolic model B, proposed in this study, and modified model B, state-of-art model of clay (Zhang et al., 2014b). According to the corresponding depth ratio of 1.05 and undrained shear strength ratio of 2.5, soil parameter from regression model proposed in Chapter 4 and interpolation with fitting results are used in application case.

Table 17 Soil parameters used in application case

Capacity	Value	Stiffness	Value
V_{ult}	106.32 MN	K_v	613.88 MN/m
H_o	29.34 MN	K_h	610.46 MN/m
M_o	173.65 MNm	K_m	33798 MNm/rad
→ From regression model		K_c	73.68 MN/rad

V_{ult} is obtained from the penetration analysis, and it is thought that this approach can use the V_{ult} in a nonlinear soil model using the bearing capacity obtained in the penetration process in the actual jack-up design. K_h and K_m is calculated from the proposed regression model in Chapter 4. Since the initial stiffness is sensitive to the criteria, the regression equation has been presented. Verification about this equation is attempted through this application.

Other soil parameters is interpolated from fitted results in Chapter 3 and 4 (Table 9, Table 10).

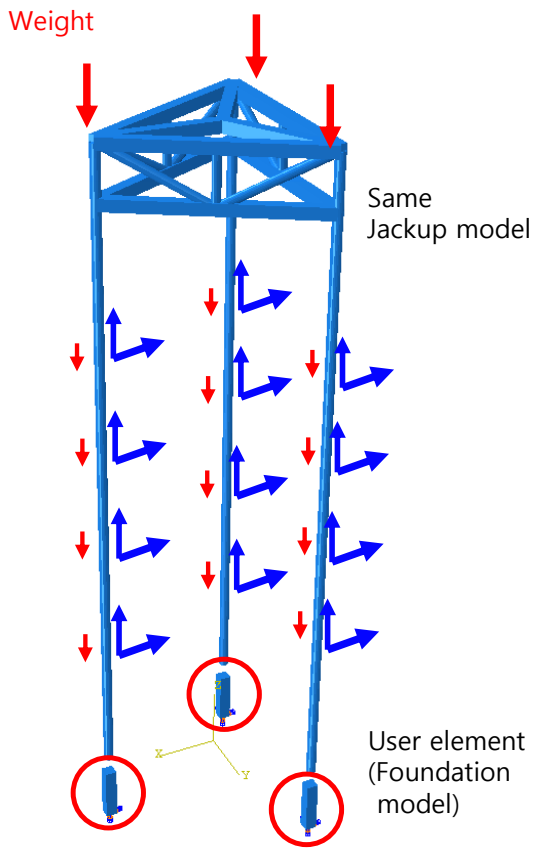

Fig. 104 FE model of jack-up analysis with yield interaction model

Nodal force equivalent to wave load is applied. Assumed DAF is multiplied to static nodal force for considering the dynamic effect on response (Fig. 104). In general, the DAF is multiplied by the response and used to compensate for the difference in response between static and dynamic analysis. However, in this study, since it is a linear analysis in the elastic region, it is an attempt to obtain

the corresponding material curve by multiplying the load by DAF rather than response. Vertical load is applied to reflect the weight and payload of the structure. The load corresponding to the weight has been applied to the leg through the distributed load, and the load corresponding to the hull weight and payload has been applied through the hull-leg joint. User elements which implements the yield interaction model are placed below the leg as the boundary condition of the jack-up analysis. The lower part of the UEL is fixed so that the behavior of UEL can be completely the boundary condition of the entire structure.

6.3.6. Case 1 : Analysis results

DAF is calculated based on the moment and rotation, so the soil response in rotational direction is shown in Fig. 105. DAF in case 1 is 4.07, which is close to the natural period and has a high value. DAF based on moment is applied in static analysis with two yield interaction models.

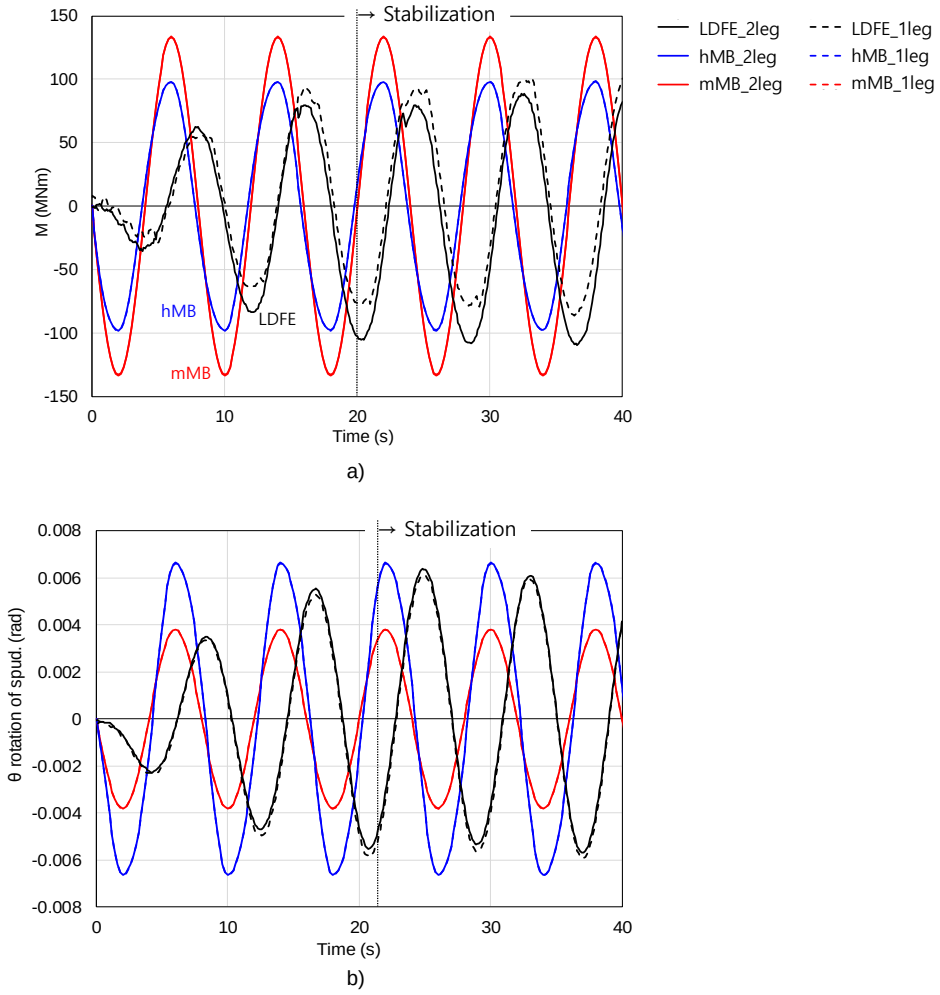

Fig. 105 Soil response in rotational direction;

a) Moment about time; b) Rotation about time

After stabilization, responses of Hyperbolic model B and those of soil continuum model shows similar results. In contrast, the rotation is small while the moment shows a large value in modified model B.

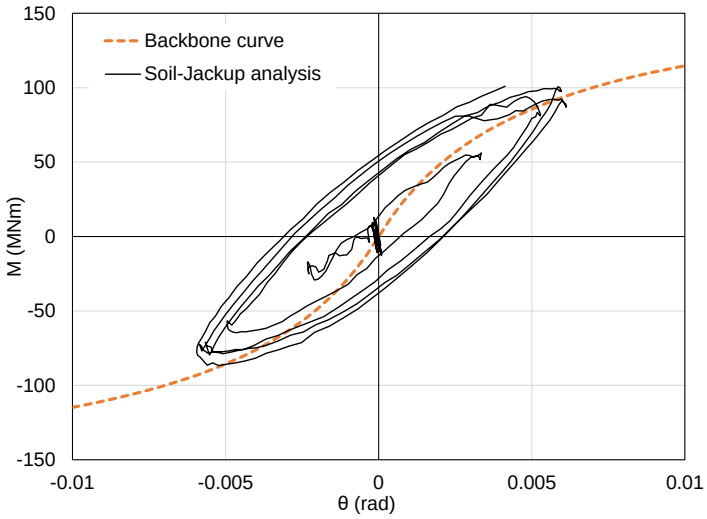

a)

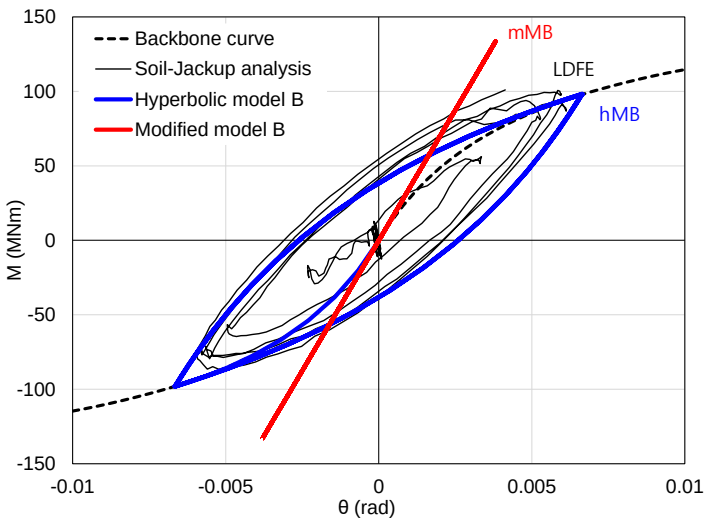

b)

Fig. 106 Soil hysteresis curve; a) Comparison with proposed backbone curve; b) Comparison with yield interaction model

Moment – rotation hysteresis curve occurs in results of soil continuum model (Fig. 106(a)). This hysteresis curve follows the backbone curve of soil parameters from regression model. Through this, regression model proposed in Chapter 4 shows good agreement

with LDFE analysis with dynamic load.

This well-matched backbone curve and hysteresis curve according to Masing rule are implemented in Hyperbolic model B. As a result, hysteresis curve simulated in Hyperbolic model B shows the similar shape with that of soil continuum model. Modified model B uses the almost linear relationship as elasticity relation, so the loading curve and unloading curve is the same as a line.

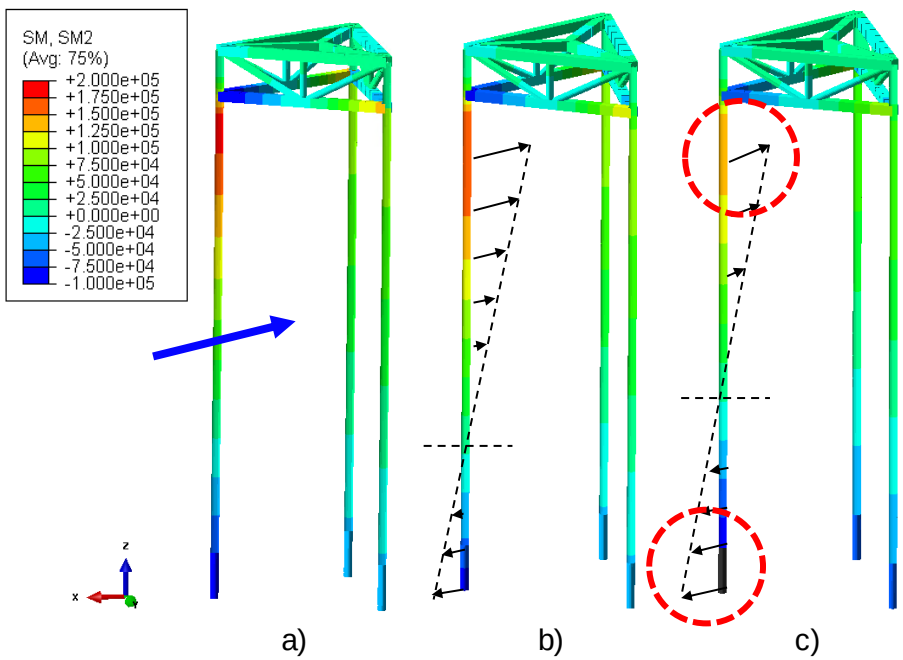

Fig. 107 Structure response : bending moment;

a) LDFE analysis; b) Hyperbolic model B; c) Modified model B

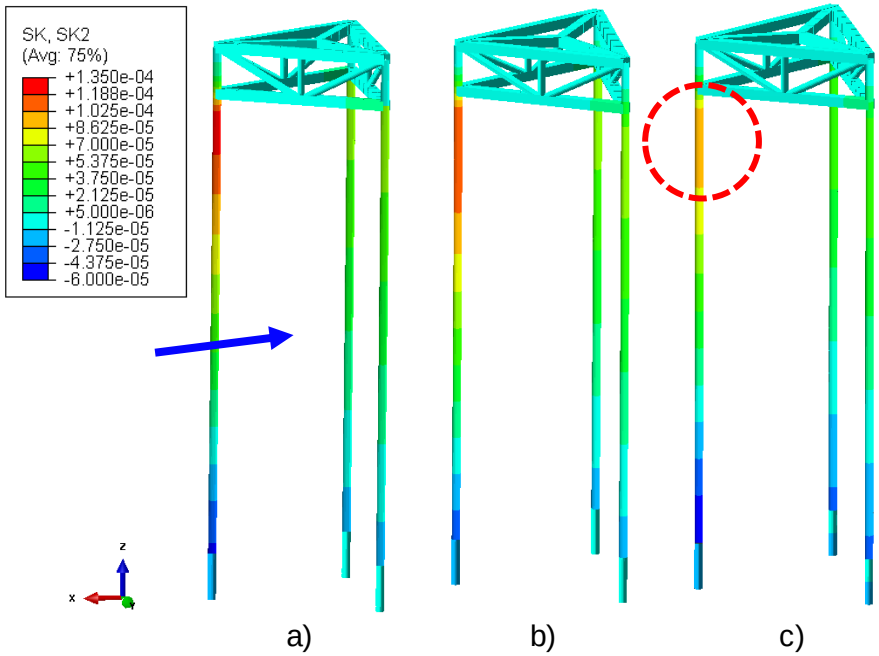

Fig. 108 Structure response : curvature;

a) LDFE analysis; b) Hyperbolic model B; c) Modified model B

Fig. 107 and Fig. 108 show the bending moment and curvature of jack-up leg. Bending moment and curvature show same trend. Because the windward leg is under the tension, large bending moment is applied. Among three structure-soil interaction model, Modified model m shows different moment distribution. Because of the over-estimated moment response of soil, hull-leg joint is under-estimated in bending moment and curvature. Different soil response can result in the different structural response.

6.3.7. Case 2 : Analysis results

DAF is calculated based on the moment and rotation, so the soil response in rotational direction is shown in Fig. 109. DAF in case 2 is 2.03, which is smaller than that of case 1. 13s of period is far from the natural period of jack-up, so the DAF is small value in case 2. Assumed DAF is applied in static analysis with two yield interaction models.

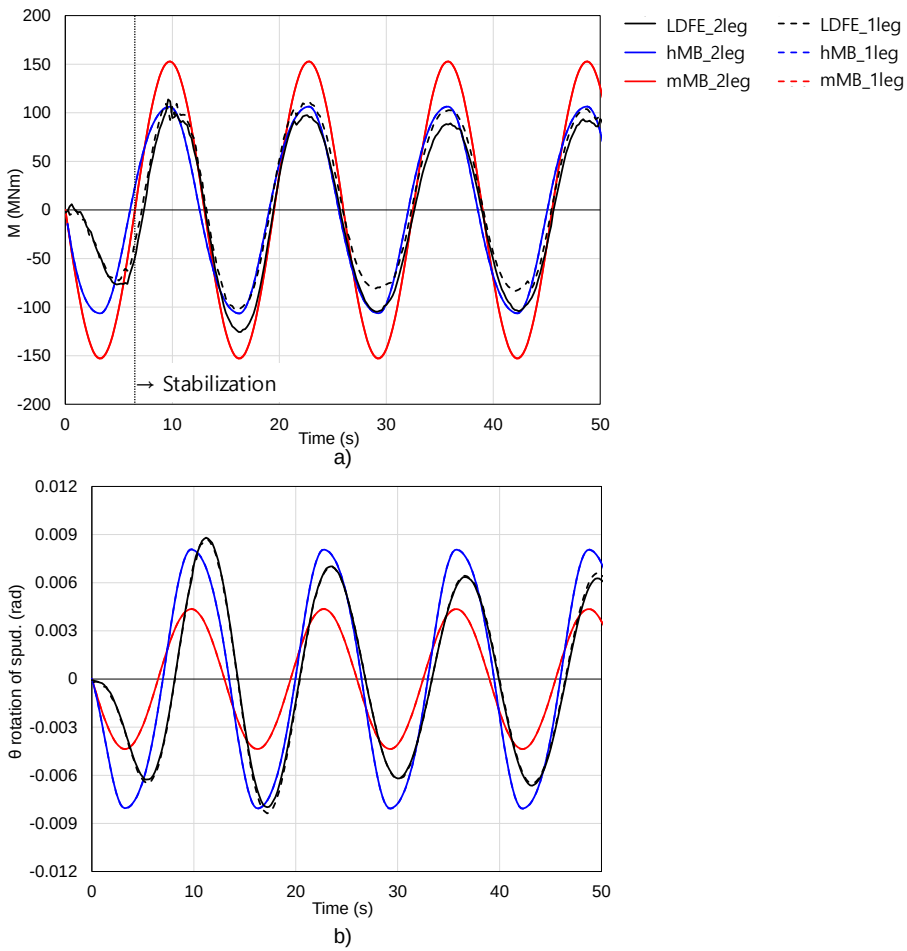

Fig. 109 Soil response in rotational direction;

a) Moment about time; b) rotation about time

After first peak, phase shift rarely occurs because the wave excitation period is far from natural period of jack-up. Compared to the case 1 of the 8s period, the dynamic characteristics are less when far from the natural period. Also in case 2, responses of Hyperbolic model B and structure-soil interaction analysis with soil continuum model are similar and the rotation is small while the moment has large value in modified model B.

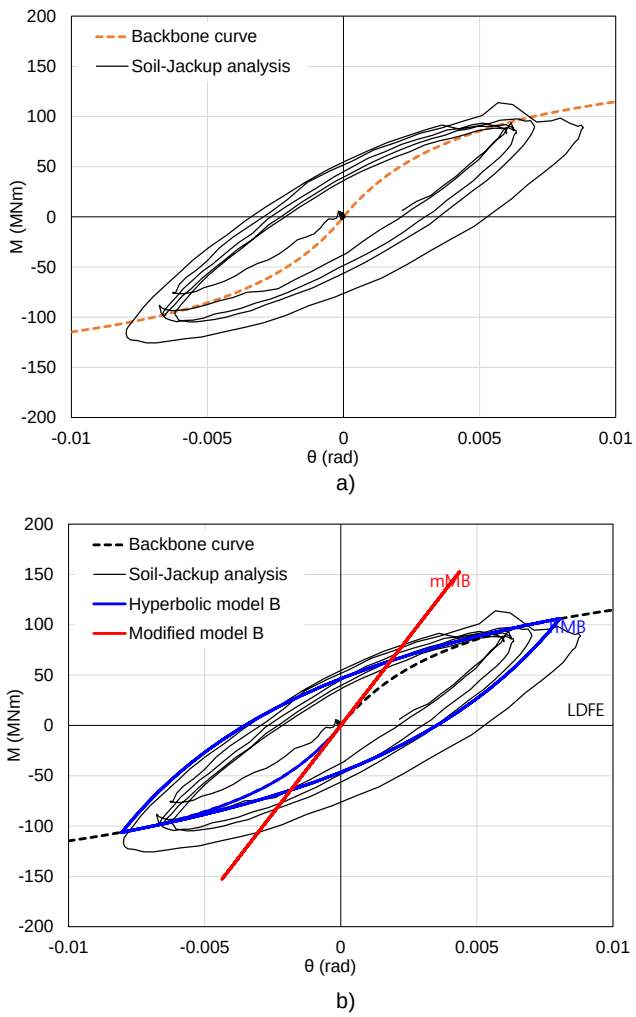

Fig. 110 Soil hysteresis curve; a) Comparison with proposed backbone curve; b) Comparison with yield interaction model

In case 2, the hysteresis curve in the soil continuum model also follows the backbone curve well. This means that verification of interpolated soil parameters has been performed. Corresponding hysteresis curve is implemented in Hyperbolic model B in this study. In the fatigue assessment of jack-up structure, Hyperbolic model B can be adopted as the simplified nonlinear foundation model because of consideration about hysteresis in the elastic region.

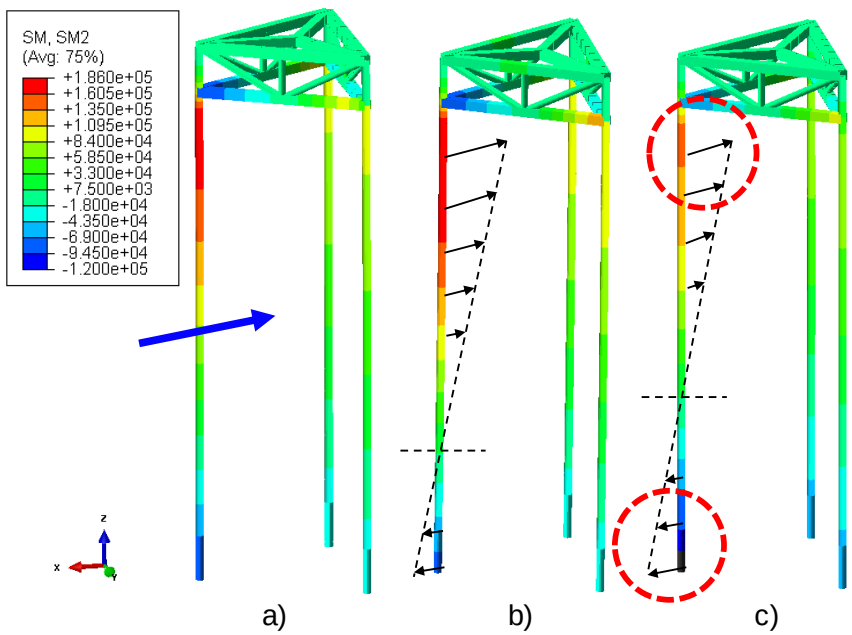

Fig. 111 Structure response : bending moment;

a) LDFE analysis; b) Hyperbolic model B; c) Modified model B

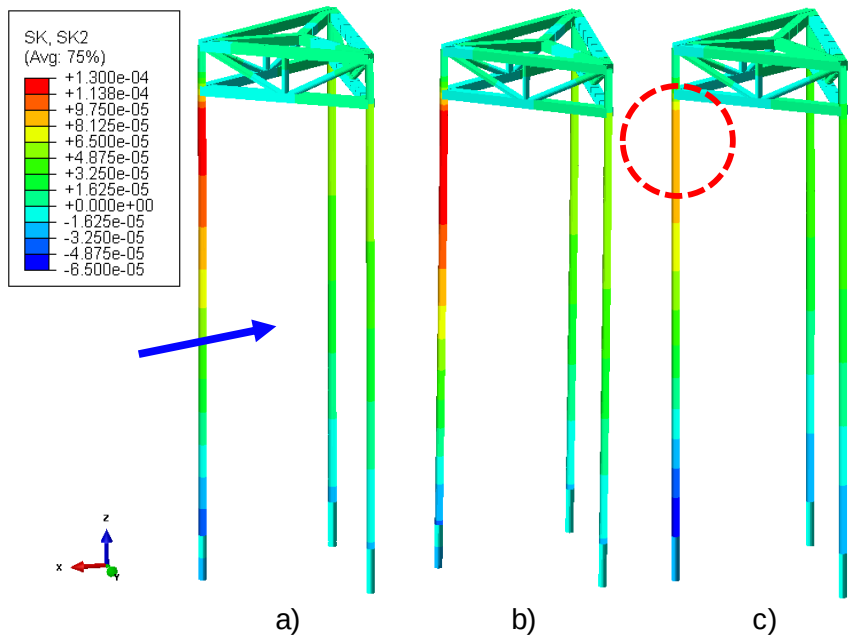

Fig. 112 Structure response : curvature;

a) LDFE analysis; b) Hyperbolic model B; c) Modified model B

Fig. 111 and Fig. 112 show the bending moment and curvature of the jack-up leg. Bending moment and curvature show the same trend, as in case 1. Because the windward leg is under the tension, a significant bending moment is applied. In case 2, where the wave period is far from the natural period, Modified model B also shows different moment distribution. Linear elastic relation results in the over-estimated moment acting on the soil in the elastic region. Moment distribution of leg has shifted value because of the large moment at the boundary condition, so the difference occurs at the hull-leg joint. Environmental loads are almost in the elastic region before reaching the yield envelope, and the underestimated bending moment at the hull-leg joint may have a great influence on the strength assessment in the corresponding structure.

Conclusion

Summary

This study aims to perform a jack-up structural analysis for dynamic loads using a foundation model considering structure-soil interaction. A nonlinear foundation model has been proposed using simplified soft over stiff clay as a target soil, and jack-up structural analysis has been performed with the proposed structure-soil interaction model.

The structure-soil interaction model refers to a two-way analysis model in which the plasticity of the soil and the response of the structure interact with each other. In ISO (2012), a secant model, a yield interaction model, and a soil continuum model have been proposed as the structure-soil interaction model. The secant model is the simplest model that considers structure-soil interaction. This model introduces the concept of secant stiffness in the rotational direction, which is only available at a specific design point. The model B was proposed as a yield interaction model to more accurately simulate the plastic behavior of the soil. The yield interaction model about clay has been improved from model B to the latest model, modified model B. The model B calculates the plastic displacement through an iterative calculation using the formulated equation of elasticity, yield envelope, flow rule, and hardening law. This model is known to calculate the plastic behavior of the soil well. In addition, Hyper-model B was proposed to simulate the strength

degradation in the rotational direction by introducing a nonlinear moment–rotation relationship into the model B framework.

Soft over stiff clay is a general case that can occur when the jack–up is operated in soft clay. Jack–up should penetrate until meeting the stiff clay to obtain sufficient bearing capacity in the soft soil. This case is stable in terms of installation. However, in the aspect of the operation, the foundation model and corresponding structural response can be changed because it is simultaneously affected by the upper soft clay and lower stiff clay. A study has been conducted on how the ground model and jack–up structures are affected by the lower stiff clay, assuming the spudcan in this transition zone. The foundation model has been studied using the LDFE technique, and disturbed soil properties by spudcan penetration are considered.

A study has been conducted on the yield envelope in soft over stiff clay. LDFE analysis is used to calculate the ultimate capacity through constant V test and yield envelope through a swipe test. Combined loads analysis for deep embedment is performed and confirmed to be consistent with the yield envelope of the existing single clay. The combined loads analysis on the soft over stiff clay has been performed with various embedments and lower clay stiffnesses. The lower stiff clay gives a large reaction force against the downward motion of the spudcan, so the compressive vertical capacity and rotational capacity have increased significantly. On the other hand, in the case of tensile vertical capacity, where the upward motion is involved, there is a negligible effect of lower stiff clay. In

consideration of these effects, the best-fit yield envelope expression of soft over stiff clay and the corresponding ultimate capacity are presented.

A study about the elasticity of model B, which determines the behavior inside the yield envelope, is performed. In the existing model, load-displacement has an almost linear relationship except for the horizontal-rotation interaction term. However, the actual soil shows the gradually degraded strength, and this study applies this nonlinear relationship to the horizontal and rotational directions. In the existing Hyper-model B, a nonlinear hyperbolic relationship was applied only to the rotational direction. Proposed model extends this nonlinear relationship in the horizontal direction and combines the state-of-art concept like the tensile capacity of modified model B. As a result, the material curve assumed to be linear can overestimate the soil response before the yield. In contrast, the nonlinear hyperbolic relationship shows degradation of strength before the yield effectively.

Incorporating yield envelope and elasticity inside the yield envelope about soft over stiff clay, Hyperbolic model B is proposed and implemented using Abaqus user elements. The proposed model is compared with the structure-soil interaction analysis using LDFE and the results are verified. Jack-up analysis with the yield interaction model and the soil continuum model analysis is performed on single clay and soft over stiff clay, and the results are compared and analyzed. As a result, the proposed Hyperbolic model B can simulate the response of the soil where gradually degraded

strength occurs similarly to LDFE, and the bending moment distribution of the leg is also well simulated due to the soil response.

A dynamic wave load analysis is performed using the structure–soil interaction model. Dynamic effects such as the Inertia effect and rate dependency are investigated. To validate the proposed soil parameters, application cases are selected and compared with the soil continuum model. As a result, the backbone curve of the proposed soil parameter is well–matched with the result of the soil continuum model. Hyperbolic model B also shows a similar hysteresis curve because this backbone curve is implemented.

Limitation and Future work

The nonlinear clay model used in this study only considers strain softening and rate hardening. In order to accurately simulate the tensile capacity, effects of suction force and consolidation should be considered. However, this phenomenon is difficult to consider using the current LDFE technique. In dynamic load analysis, several load cycles are generally simulated. However, due to computational cost, only a small number of cycles have been performed.

The dynamic effect is made up of a lot of factors, especially including soil damping. it is difficult to separate the each effect from the integrated dynamic response. For this, the effect of damping should be analyzed through experiments individually. Including the difficulties in calculation of the natural period, it is difficult to accurately calculate DAF, and only appropriate assumptions are made in this study. In addition, it is difficult to perform such dynamic analysis because the user element in which the yield interaction model is implemented is based on static analysis.

To achieve these limitations, the effect of time can be considered in LDFE analysis. Rani (2016) performed an LDFE analysis considering the effects of consolidation, by the implementation of additional nonlinear equations about time effect. In order to consider the dynamic effects of Jackup, it is necessary to use a macro element in which model B is implemented in a dynamic environment. This can be a model that replaces the time-consuming 3D soil

continuum model and is expected to be able to freely consider the equation for dynamic effects.

It is very important to use the proposed yield interaction model in structure design actually. For this, an external program, where the yield interaction model is implemented, can be used with the general code check program like SACS. This interface code for actual design is expected to have many uses. Also, this study has been omitted the lattice leg effect to clarify the structure-soil interaction. This effect can be necessary to accurately simulate the behavior of the jack-up within the soil.

Bibliography

[1] J. Wilson, F., Dynamics of Offshore Structures, 2nd ed, John Wiley & Sons Inc., 2002.

[2] B.-L. Zhang, Q.-L. Han, X.-M. Zhang, Recent advances in vibration control of offshore platforms, Nonlinear Dynamics 89 (2017) 755-771.

[3] V.P. Baglioni, G.S. Chow, S.N. Endley, Jack-Up Rig Foundation Stability in Stratified Soil Profiles, Offshore Technology Conference, Houston, Texas, Offshore Technology Conference, 1982, pp. 22.

[4] M.S. Williams, R.S.G. Thompson, G.T. Houlsby, Non-linear dynamic analysis of offshore jack-up units, Computers & Structures 69 (1998) 171-180.

[5] G.T. Houlsby, C.M. Martin, A.N. Schofield, Modelling of the behaviour of foundations of jack-up units on clay. Predictive soil mechanics (1992) 339-358.

[6] D. Mao, C. Zhong, L. Zhang, G. Chu, Dynamic response of offshore jacket platform including foundation degradation under cyclic loadings, Ocean Engineering 100 (2015) 35-45.

[7] W. Shi, H.C. Park, C.W. Chung, H.K. Shin, S.H. Kim, S.S. Lee, et al., Soil-structure interaction on the response of jacket-type offshore wind turbine, International Journal of Precision Engineering and Manufacturing-Green Technology 2 (2015) 139-148.

[8] API, Planning, designing and constructing fixed offshore platforms-working stress design, API-RP-2A-WSD, 21th ed, 2002.

[9] A.G. Young, B.D. Remmes, B.J. Meyer, Foundation Performance of Offshore Jack-Up Drilling Rigs, Journal of Geotechnical Engineering 110 (1984) 841-859.

[10] M.S. Williams, R.S.G. Thompson, G.T. Houlsby, A parametric study of the non-linear dynamic behaviour of an offshore jack-up unit, Engineering Structures 21 (1999) 383-394.

[11] P. Le Tirant, C. Pérol, Stability and operation of jackups, Editions Technip, 1993.

[12] M.S. Hossain, J. Zheng, A. Huston, Effect of spudcan geometry on penetration and extraction resistance in clay, Géotechnique 65 (2015) 147-154.

[13] R. Kee, B.W. Ims, Geotechnical Hazards Associated with Leg Penetration of Jack-up Rigs, Seabed Mechanics, Dordrecht, 1984

[14] S.N. Endley, P.J. Thompson, V.P. Baglioni, Prediction of Jack-up Rig Footing Penetration, Offshore Technology Conference, Houston, Texas, Offshore Technology Conference, 1981, pp. 12.

[15] G.T. Houlsby, C.M. Martin, Undrained bearing capacity factors for conical footings on clay, Géotechnique 53 (2003) 513-520.

[16] K.L. Teh, M.J. Cassidy, C.F. Leung, Y.K. Chow, M.F. Randolph, C.K. Quah, Revealing the bearing capacity mechanisms of a penetrating spudcan through sand overlying clay, Géotechnique 58 (2008) 793-804.

[17] M. Hossain, M. Randolph, Deep-penetrating spudcan foundations on layered clays: centrifuge tests, Géotechnique 60 (2010) 157-170.

[18] D. Menzies, R. Roper, Comparison of Jackup Rig Spudcan Penetration Methods in Clay, Offshore Technology Conference, 2008.

[19] D. Ahn, S.-c. Shin, S.-y. Kim, H. Kharoufi, H.-c. Kim, Comparative evaluation of different offshore wind turbine installation vessels for Korean west–south wind farm, International Journal of Naval Architecture and Ocean Engineering 9 (2017) 45-54.

[20] C. Nancy, M.J. B Rohani, R. Bt M Hazizy, A. B Abd Rahman, A.B.A. Jalil, Jack Up Suitability for South China Sea Sites, Offshore Technology Conference-Asia, Kuala Lumpur, Malaysia, Offshore Technology Conference, 2014, pp. 5.

[21] M. Randolph, S. Gourvenec, Offshore Geotechnical Engineering, CRC Press, 2017.

[22] K. Tho, C. Leung, Y. Chow, S. Swaddiwudhipong, Eulerian Finite-Element Technique for Analysis of Jack-Up Spudcan Penetration, International Journal of Geomechanics 12 (2010) 64-73.

[23] Y. Hu, M.F. Randolph, A practical numerical approach for large deformation problems in soil, International Journal for Numerical and Analytical Methods in Geomechanics 22 (1998) 327-350.

[24] G. Qiu, S. Henke, J. Grabe, Applications of Coupled Eulerian-Lagrangian Method to Geotechnical Problems with Large

Deformations Proceeding of SIMULIA Customer Conference, London, UK, 2009

[25] Y. Zhang, D. Wang, M. Cassidy, B. Bienen, Effect of Installation on the Bearing Capacity of a Spudcan under Combined Loading in Soft Clay, Journal of Geotechnical and Geoenvironmental Engineering 140 (2014) 04014029.

[26] G.J.M. Schotman, The Effects of Displacements on the Stability of Jackup Spud-Can Foundations, Offshore Technology Conference, Houston, Texas, Offshore Technology Conference, 1989, pp. 10.

[27] C.M. Martin, Physical and numerical modelling of offshore foundations under combined loads, Oxford University, UK, 1994.

[28] G. Vlahos, C.M. Martin, M.S. Prior, M.J. Cassidy, Development of a model jack-up unit for the study of soil-structure interaction on clay, International Journal of Physical Modelling in Geotechnics 5 (2005) 31-48.

[29] ISO, Petroleum and natural gas industries - Site specific assessment of mobile offshore units - Part 1 : Jack-ups, International Organization for Standardization ISO 19905-1 (2012).

[30] T. Aust, Accident to the mobile offshore drilling unit Maersk victory on November 16 1996, Mines and Energy Resources, South Australia, 1997.

[31] J.C. Simo, T.J. Hughes, Computational inelasticity, Springer Science & Business Media, 2006.

[32] N. Cheng, M.J. Cassidy, Development of a force–resultant model for spudcan footings on loose sand under combined loads, Canadian Geotechnical Journal 53 (2016) 2014–2029.

[33] O.A. Purwana, M.J. Perry, M. Quah, M.J. Cassidy, Comparison of ISO 19905–1 Framework and a Plasticity–based Spudcan Model for Jackup Foundation Assessments, Offshore Technology Conference, Houston, Texas, USA, Offshore Technology Conference, 2012.

[34] P.C. Wong, J. Templeton, III, O.A. Purwana, H. Hugo, M.J. Cassidy, M.S. Hossain, et al., Foundation Modeling and Assessment in the New ISO Standard 19905–1, Offshore Technology Conference, Houston, Texas, USA, Offshore Technology Conference, 2012.

[35] T. Sullivan, G. Calvi, M. Priestley, Initial stiffness versus secant stiffness in displacement based design, 13th World Conference of Earthquake Engineering (WCEE), 2004

[36] G. Vlahos, M.J. Cassidy, B.W. Byrne, The behaviour of spudcan footings on clay subjected to combined cyclic loading, Applied Ocean Research 28 (2006) 209–221.

[37] F. Pisanò, R. Schipper, G.–J. Schreppers, Input of fully 3D FE soil–structure modelling to the operational analysis of jack–up structures, Marine Structures 63 (2019) 269–288.

[38] ABS, Guidance notes on Dynamic Analysis Procedure For Self–Elevating Units, 2014.

[39] A. Abelev, P. Valent, Strain–rate dependency of strength of soft marine deposits of the Gulf of Mexico, OCEANS 2009, 2009

[40] S. Robinson, M. Brown, Rate effects at varying strain levels in fine grained soils, Proceedings of the 18th International Conference on Soil Mechanics and Geotechnical Engineering, 2013

[41] S. Nanda, V. Sivakumar, P. Hoyer, A. Bradshaw, K. Gavin, H. Gerkus, et al., Effects of strain rates on the undrained shear strength of kaolin, Geotechnical Testing Journal 40 (2017) 951-962.

[42] SNAME, Site specific assessment of mobile jack-up units, Society of Naval Architects and Marine Engineers SNAME T&R 5-5A (2008).

[43] M.S. Hossain, M.F. Randolph, Deep-penetrating spudcan foundations on layered clays: numerical analysis, Géotechnique 60 (2010) 171-184.

[44] P. Hu, D. Wang, S.A. Stanier, M.J. Cassidy, Assessing the punch-through hazard of a spudcan on sand overlying clay, Géotechnique 65 (2015) 883-896.

[45] J. Zheng, M.S. Hossain, D. Wang, Numerical investigation of spudcan penetration in multi-layer deposits with an interbedded sand layer, Géotechnique 67 (2017) 1050-1066.

[46] K.L. Teh, C.F. Leung, Y.K. Chow, y.M.J. Cassid, Centrifuge model study of spudcan penetration in sand overlying clay, Géotechnique 60 (2010) 825-842.

[47] P. Hu, M.J. Cassidy, Predicting jack-up spudcan installation in sand overlying stiff clay, Ocean Engineering 146 (2017) 246-256.

[48] D.S. Simulia, ABAQUS 6.13 User's manual, 2013.

[49] I. Einav, M.F. Randolph, Combining upper bound and strain path methods for evaluating penetration resistance, International Journal for Numerical Methods in Engineering 63 (2005) 1991-2016.

[50] M. Hossain, M. Randolph, Effect of Strain Rate and Strain Softening on the Penetration Resistance of Spudcan Foundations on Clay, International Journal of Geomechanics 9 (2009) 122-132.

[51] G. Qiu, J. Grabe, Numerical investigation of bearing capacity due to spudcan penetration in sand overlying clay, Canadian Geotechnical Journal 49 (2012) 1393-1407.

[52] D. Wang, D.J. White, M.F. Randolph, Large-deformation finite element analysis of pipe penetration and large-amplitude lateral displacement, Can Geotech J 47 (2010) 842.

[53] M.S. Hossain, M.F. Randolph, Y.N. Saunier, Spudcan deep penetration in multi-layered fine-grained soils, International Journal of Physical Modelling in Geotechnics 11 (2011) 100-115.

[54] J. Zheng, M.S. Hossain, D. Wang, Estimating Spudcan Penetration Resistance in Stiff-Soft-Stiff Clay, Journal of Geotechnical and Geoenvironmental Engineering 144 (2018) 04018001.

[55] N. Cheng, M.J. Cassidy, Combined loading capacity of spudcan footings on loose sand, International Journal of Physical Modelling in Geotechnics 16 (2016) 31-44.

[56] R. Butterfield, J. Ticof, Design parameters for granular soils

(discussion contribution), Proceedings of the 7th European Conference on Soil Mechanics and Foundation Engineering, Brighton, England, 1979

[57] K.H. Roscoe, A.N. Schofield, The stability of short pier foundations in sand, British Welding Journal 3 (1956) 343-354.

[58] M.J. Cassidy, Non-linear analysis of jack-up structures subjected to random waves, 1999.

[59] M.J. Cassidy, C.M. Martin, G.T. Houlsby, Development and application of force resultant models describing jack-up foundation behaviour, Marine Structures 17 (2004) 165-193.

[60] C.M. Martin, G.T. Houlsby, Combined loading of spudcan foundations on clay: numerical modelling, Géotechnique 51 (2001) 687-699.

[61] Y. Zhang, M.J. Cassidy, B. Bienen, A plasticity model for spudcan foundations in soft clay, Canadian Geotechnical Journal 51 (2014) 629-646.

[62] S. Gourvenec, M. Randolph, Effect of strength non-homogeneity on the shape of failure envelopes for combined loading of strip and circular foundations on clay, Géotechnique 53 (2003) 575-586.

[63] R. Ragni, B. Bienen, D. Wang, D. Mašín, M.J. Cassidy, Numerical modelling of the effects of consolidation on the undrained spudcan capacity under combined loading in silty clay, Computers and Geotechnics 86 (2017) 33-51.

[64] C. Vulpe, Design method for the undrained capacity of skirted circular foundations under combined loading: effect of

deformable soil plug, Géotechnique 65 (2015) 669-683.

[65] G. Vlahos, M.J. Cassidy, C.M. Martin, Experimental investigation of the system behaviour of a model three-legged jack-up on clay, Applied Ocean Research 30 (2008) 323-337.

[66] J.S. Templeton, Spudcan fixity in clay, further results from a study for IADC, 12th International Conference on the Jack-Up Platform Design, Construction & Operation, London, UK, 2009

[67] J.S. Templeton, J.N. Brekke, D.R. Lewis, Spud can fixity in clay, final findings of a study for IADC, 10th International Conference on the Jack-Up Platform Design, Construction & Operation, London, UK, 2005

[68] Y. Zhang, B. Bienen, M.J. Cassidy, S. Gourvenec, The undrained bearing capacity of a spudcan foundation under combined loading in soft clay, Marine Structures 24 (2011) 459-477.

[69] Y. Zhang, B. Bienen, M. Cassidy, S. Gourvenec, Undrained Bearing Capacity of Deeply Buried Flat Circular Footings under General Loading, Journal of Geotechnical and Geoenvironmental Engineering 138 (2011) 385-397.

[70] S. Abyaneh, J. Kennedy, A. Maconochie, J. Oliphant, Capacity of Strip Foundations on Sand Overlying Clay Soils Under Planar Combined Loading, The 28th International Ocean and Polar Engineering Conference, Sapporo, Japan, International Society of Offshore and Polar Engineers, 2018, pp. 5.

[71] J. Ko, J.K. Lee, H. Seo, Undrained Bearing Capacity of Circular Foundations on Two-Layered Clay Under Combined Loading, The 27th International Ocean and Polar Engineering Conference,

San Francisco, California, USA, International Society of Offshore and Polar Engineers, 2017, pp. 6.

[72] P. Rao, Y. Liu, J. Cui, Bearing capacity of strip footings on two-layered clay under combined loading, Computers and Geotechnics 69 (2015) 210-218.

[73] Q. Yin, S. Dong, Combined Bearing Capacity of Spudcans on a Double Layer Deposit of Strong-Over-Weak Clays, Journal of Ocean University of China 18 (2019) 133-143.

[74] Y. Wang, M.J. Cassidy, B. Bienen, Effect of Underlying Sand Layer on Undrained Capacity of Spudcan Foundations in Soft Clay Under Combined Loading, (2018) V009T010A031.

[75] H. Jin, K. Lee, J. Choi, B.-S. Jang, Study on Spudcan Soil-Structure Interaction of a Wind Turbine Installation Vessel, ISOPE-19-29-3-329 29 (2019) 329-338.

[76] M.S. Hossain, M.J. Cassidy, D. Daley, R. Hannan, Experimental investigation of perforation drilling in stiff-over-soft clay, Applied Ocean Research 32 (2010) 113-123.

[77] J. Zheng, M. Hossain, D. Wang, New Design Approach for Spudcan Penetration in Nonuniform Clay with an Interbedded Stiff Layer, Journal of Geotechnical and Geoenvironmental Engineering 141 (2015) 04015003.

[78] J. Zheng, M.S. Hossain, D. Wang, Prediction of spudcan penetration resistance profile in stiff-over-soft clays, Canadian Geotechnical Journal 53 (2016) 1978-1990.

[79] B. Bienen, C. Gaudin, M.J. Cassidy, L. Rausch, O.A. Purwana, H. Krisdani, Numerical modelling of a hybrid skirted foundation

under combined loading, Computers and Geotechnics 45 (2012) 127–139.

[80] F.S.C. Tan, Centrifuge and theoretical modelling of conical footings on sand, University of Cambridge, 1990.

[81] C.M. Martin, G.T. Houlsby, Combined loading of spudcan foundations on clay: laboratory tests, Géotechnique 50 (2000) 325–338.

[82] Y. Zhang, B. Bienen, M.J. Cassidy, Development of a combined VHM loading apparatus for a geotechnical drum centrifuge, International Journal of Physical Modelling in Geotechnics 13 (2013) 13–30.

[83] Y. Wang, M.J. Cassidy, B. Bienen, Evaluating the Penetration Resistance of Spudcan Foundations in Clay Overlying Sand, The 29th International Ocean and Polar Engineering Conference, Honolulu, Hawaii, USA, International Society of Offshore and Polar Engineers, 2019, pp. 8.

[84] J. Huang, J. Chen, Y. Lu, S. Yi, H. Cheng, L. Cui, Deformation Behaviors and Dynamic Backbone Curve Model of Saturated Soft Clay under Bidirectional Cyclic Loading, International Journal of Geomechanics 20 (2020) 04020016.

[85] C. Bolisetti, Site Response, Soil–Structure Interaction and Structure–Soil–Structure Interaction for Performance Assessment of Buildings and Nuclear Structures, 2014.

[86] G. Masing, Eigenspannumyen und verfeshungung beim messing, Proc. Inter. Congress for Applied Mechanics, 1926

[87] G. Vlahos, M.J. Cassidy, C.M. Martin, Implementation of a

Force-Resultant Model Describing Spudcan Load-Displacement Behaviour Using an Implicit Integration Scheme, The Eighteenth International Offshore and Polar Engineering Conference, Vancouver, Canada, International Society of Offshore and Polar Engineers, 2008, pp. 8.

[88] B. Bienen, M.J. Cassidy, Advances in the three-dimensional fluid–structure–soil interaction analysis of offshore jack-up structures, Marine Structures 19 (2006) 110-140.

[89] Y. Zhang, B. Bienen, M.J. Cassidy, Jack-up push-over analyses featuring a new force resultant model for spudcans in soft clay, Ocean Engineering 81 (2014) 139-149.

[90] Y. Zhang, M.J. Cassidy, B. Bienen, Elastic stiffness coefficients for an embedded spudcan in clay, Computers and Geotechnics 42 (2012) 89-97.

[91] H. Yu, X. Li, S. Yang, Dynamic analysis method of offshore jack-up platforms in regular and random waves, Journal of Marine Science and Application 11 (2012) 111-118.

[92] N. Spidsøe, D. Karunakaran, Nonlinear dynamic behaviour of jack-up platforms, Marine Structures 9 (1996) 71-100.

초록

잭업 해양 구조물은 수심 150m까지 설치되며, 시추 및 생산용 리그뿐 아니라 해상풍력발전기 전문설치선과 같은 설치 유닛에도 사용되어오고 있다. 잭업은 파도와 바람 등의 환경하중 하에서 작업이 수행되므로 설계 시 그에 따른 잭업의 거동 및 구조 반응을 명확히 이해해야 한다. 거동 및 구조 해석 시 해양구조물의 경계조건으로 작용하는 지반 모델은 구조물의 진동 모드에 영향을 주어 해석 결과에도 영향을 미치게 된다. 일반적인 지반 모델에는 단순 지지 조건이나 선형 스프링을 이용한 모델이 있으나, 이는 잭업의 구조-지반 상호작용을 반영하지 못한다. 그 대안으로 International Organization for Standardization (ISO) 에서는 가이드라인을 통해 구조-지반 상호작용을 고려하는 비선형 지반 모델들을 제시하고 있으며, 이는 가장 단순한 모델인 시컨트 모델 (secant model)부터 지반의 소성 변위를 고려하는 항복 상호작용 모델 (yield interaction model), 그리고 가장 정확하지만 시간이 걸리는 지반 연속체 모델 (soil continuum model)로 나뉘어진다. 이러한 비선형 지반 모델 중 이번 연구에서는 구조-지반 상호작용을 모사하기 위하여 항복 상호작용 모델과 지반 연속체 모델을 사용하였다. 동적 하중 하에서 구조-지반 상호작용을 고려한 지반 모델을 사용하여 잭업의 구조해석을 수행하였다. 상부 연약한 지반-하부 단단한 점토 조건에서 사용할 수 있는 적절한 항복 상호작용 모델을 제시하고 지반 연속체 모델을 통해 이를 검증 비교 하였다. 상부 연약한 지반-하부 단단한 점토 조건에서, 지반에 작용하는 복합 하중의 항복 여부를 결정하는 항복 곡면에 대한 연구를 수행하였다. 해당 지반 조건은 하부 단단한

점토 지반으로 인해 상부 지반이 압착되어 충분한 지지력이 확보되기 때문에 많은 연구가 수행되지 않았다. 그러나 잭업 운용 시 사용되는 지반 모델은 상부와 하부 지반의 영향을 모두 받으므로 상부 연약한 점토-하부 단단한 점토 지반에 대한 연구가 필요하다. 해당 지반에서 수직 압축 용량은 압착 효과로 인해 증가한 반면 수직 인장 용량은 하부 단단한 점토 지반의 영향을 받지 않았다. 해당 지반에 잘 맞는 항복 곡면 식과 이 때 사용되는 수직, 수평, 회전 방향의 극한 지지력(ultimate capacity)에 대하여 제안하였다. 점토 지반에서 모델 비(model B)로 불리는 항복 상호작용 모델은 소성 변위를 통해 지반의 비선형 거동을 고려하며, 구조-지반 상호작용을 단순화하여 고려할 수 있는 모델로 최근까지 연구되어 오고 있다. 기존 모델 비는 항복 곡면에 도달하기 이전의 탄성 영역에서 선형의 힘-변위 관계와 함께 수평-회전 방향의 상호작용을 고려한다. 그러나 실제 지반은 점진적으로 소성이 발생하며 그에 따라 선형의 힘-변위 관계를 갖지 않는다. 이번 연구에서는 비선형성이 큰 수평, 회전 방향에 대하여 비선형 쌍곡선 힘-변위 관계를 가정한 하이퍼볼릭 모델 비(hyperbolic model B)를 제안하고, 이 때 사용되는 초기 지반 강성에 대한 식을 제시하였다. 검증을 위하여 지반 연속체 모델을 이용한 잭업의 구조-지반 상호작용 해석을 수행하였다. 연약 점토에서의 깊은 관입 깊이로 인한 지반의 대변형을 잭업 구조 해석에 고려하였다. 제안된 항복 상호작용 모델인 하이퍼볼릭 모델 비는 상부 연약한 점토-하부 단단한 점토 조건에서 항복 곡면 이전과 이후 지반 연속체 모델과 해석 결과가 비슷한 경향을 보임을 확인하였다. 기존 모델 비는 항복 곡면 안에서 선형 힘-변위 관계로 인해 지반에 작용하는 모멘트를 과대평가하는 경향이 있고, 경계조건으로써 구조 해석에 영향을 미쳐 잭업 레그의 모멘트가 과소평가되는 경향이 발생하였다.

제안된 하이퍼볼릭 모델 비는 항복 곡면 이전의 비선형성을 고려함으로써 잭업 레그의 모멘트 분포를 잘 예측하였다. 이렇게 제안된 항복 상호작용 모델과 지반 연속체 모델을 이용하여 잭업의 동적 구조해석을 수행하였다. 동적 사인파 하중에 대한 지반 반응 및 잭업의 구조 반응을 계산하고 정적 하중 결과와 비교하였다. 일반적으로 사용되고 있는 동적증폭계수 뿐 아니라 지반의 동적 효과 및 관성력에 의한 효과가 존재하는 것을 확인하였으며, 이에 대하여 분석하였다. 항복 상호작용 모델 및 지반 연속체 모델을 통해 구조-지반 상호작용을 고려하여 동적 하중에 대한 잭업 구조해석을 수행하였고, 항복 곡면 이전과 이후 지반 반응 및 잭업 레그의 모멘트 분포를 잘 예측하는 것을 확인하였다.

Keyword : 잭업, 스퍼드캔, 항복 상호작용 모델, 지반 대변형 유한요소, 구조-지반 상호작용

Student Number : 2014-21827

Ph.D. Dissertation of Engineering

A Study on the Nonlinear Structure–Soil Interaction Model of Jack–up in Soft over Stiff clay

잭업의 비선형 구조–지반 연성 모델에 대한 연구 : 상부 연약한 점토–하부 단단한 점토 조건

August 2020

Graduate School of Engineering

Seoul National University

Naval Architecture & Ocean Engineering

Junhwan Choi

A Study on the Nonlinear Structure-Soil Interaction Model of Jack-up in Soft over Stiff clay

잭업의 비선형 구조-지반 연성 모델에 대한 연구 : 상부 연약한 점토-하부 단단한 점토 조건

지도교수 장 범 선

이 논문을 공학박사 학위논문으로 제출함

2020년 7월

서울대학교 대학원

조선해양공학과

최 준 환

최준환의 공학박사 학위논문을 인준함

2020년 7월

위 원 장 노 명일 (인)

부위원장 장 범선 (인)

위 원 추 연욱 (인)

위 원 원 종화 (인)

위 원 최 정인 (인)

Abstract

Offshore structures with jack-up systems can be operated at depths up to 150 meters and are used not only as drilling rigs and production rigs but also as support and accommodation units. The jack-up operation is carried out under environmental loads such as wind and wave, for which it is essential to understand jack-up behavior and structural response. As the boundary condition, the foundation model of offshore structures affects the vibration mode of the structure, and consequently, the behavioral and structural analysis results as well. Typical simple foundation models such as pinned and linear spring do not reflect a structure-soil interaction in the jack-up analysis. As an alternative, the International Organization for Standardization (ISO) guideline has suggested this structure-soil interaction model considering soil plasticity, from a simple secant model to a yield interaction model and a time-consuming but accurate soil continuum model. In this study, a structural analysis of jack-up has been conducted, focusing on the yield interaction model and the soil continuum model as a structure-soil interaction model. Jack-up structural analysis is performed for dynamic loads in consideration of the structure-soil interaction, and an appropriate interaction model for soft over stiff clay is presented in this study. A yield envelope study as yield criteria of the combined loads has been performed on soft over stiff clay. Studies on soft over stiff clay tend to be less studied because a squeezing effect ensures

sufficient vertical bearing capacity. Tensile vertical capacity is independent of the lower stiff clay, and a corresponding best-fit equation of yield envelope and the ultimate capacity ratio are presented about soft over stiff clay. The yield interaction model, the model B for clay, derived for consideration of the nonlinear behavior of soil, has been studied continuously improved until recently. The existing model generally assumes a linear load-displacement relationship in the elastic region. However, this linear relationship may overestimate the load as the plastic occurs gradually in soil behavior in practice. In this study, the Hyperbolic model B is proposed, and the horizontal and rotational load-displacement curves in the elastic region are assumed to have a hyperbolic relationship. The regression equation for the initial stiffness accompanying the model is presented. A fully coupled structure-soil interaction analysis with a soil continuum model has been performed to validate the yield interaction model. Large deformation of the soil accompanied by the deep penetration is considered simultaneously in the structural analysis of jack-up. The proposed yield interaction model uses yield envelope and ultimate capacities that are well suited to soft over stiff clay, and a hyperbolic nonlinear load-displacement relationship is assumed before the yield. As a result, inside the yield envelope, the existing model overestimates the moment acting on the soil, thereby underestimating the bending moment at the hull-leg joint. The model proposed in this study has predicted the soil response and bending moment distribution of the leg well, and these results are validated with the those of the soil continuum model. Wave

load analysis has been performed using the proposed yield interaction model and the soil continuum model. The dynamic effects that should be considered compared to the monotonic load analysis have been investigated, and it has been validated that the proposed yield interaction model can predict the response of the wave load analysis in the elastic region well.

Keyword : jack-up, spudcan, yield interaction model, soil LDFE, structure-soil interaction (SSI)

Student Number : 2014-21827

List of Contents

List of Figures

List of Tables

NOMENCLATURE

a : depth coefficient (yield envelope in ISO)

B : diameter of spudcan

e : eccentricity in yield envelope

D : diameter of spudcan (in Chapter 2)

E : elastic modulus of soil

E/s_u : rigidity index

f : yield envelope

$\boldsymbol{F}$: Combined loads vector $(V, H, M)^{\mathrm{T}}$

$\boldsymbol{F}_{trial}$: Trial load vector (in Chapter 5)

G : shear modulus of soil

G_H : shear modulus of soil at boundary $(w = H)$

H_{o} : horizontal capacity of soil

H : horizontal reaction force on spudcan

H_2 : horizontal reaction force component (x) in 3D

H_3 : horizontal reaction force component (y) in 3D

h_{o} : horizontal capacity ratio, H_{o}/V_{ult}

$H_{V=0}$: intercept value of horizontal axis

H_{nor} : normalized horizontal force, H/H_o

H_{trial} : horizontal component of trial load vector $\boldsymbol{F}_{trial}$

H_{env} : environmental load (in Chapter 5, 6)

H_{max} : design wave height (in Chapter 6)

$\boldsymbol{K}_{el}$: elastic stiffness matrix in yield interaction model

$\boldsymbol{K}_{tangent}$: tangent stiffness matrix

$\boldsymbol{K}_{ep}$: elasto-plastic stiffness matrix in model B

K_v : vertical stiffness

k_v : normalized vertical stiffness coefficient

K_h : horizontal stiffness

k_h : normalized horizontal stiffness coefficient

K_m : rotational stiffness

k_m : normalized rotational stiffness coefficient

$K_{m,r}$: reduced rotational stiffness in secant model (secant stiffness)

k : depth gradient of undrained shear strength

M : reaction moment on spudcan

M_2 : reaction moment component (y) in 3D

M_3 : reaction moment component (x) in 3D

M_{o} : rotational capacity of soil

m_{o} : rotational capacity ratio, M_{o}/V_{ult}

M_{nor} : normalized horizontal force, M/M_o

$M_{V=0}$: intercept value of rotational axis

M_{yield} : reaction moment at yield

M_{trial} : rotational component of trial load vector $\boldsymbol{F}_{trial}$

$M_{Jackup,\,wave}$: moment on spudcan of jack-up structural analysis with wave load (in Chapter 6)

$M_{Jackup,\,qs}$: moment on spudcan of jack-up structural analysis with quasi-static load (in Chapter 6)

$M_{spud.,\,dyn}$: moment on spudcan of single spudcan analysis with fast rotation motion equivalent to wave load (in Chapter 6)

$M_{spud.,\,qs}$: moment on spudcan of single spudcan analysis with slow rotation motion equivalent to quasi-static load (in Chapter 6)

R : radius of spudcan

s_u : undrained shear strength

s_{um} : undrained shear strength at seabed ($w = 0$)

$s_{u,H}$: undrained shear strength at boundary ($w = H$)

$s_{u,stiff}$: undrained shear strength of lower stiff clay

S_t : sensitivity of soil

T_n : natural period of jack-up

T_p : peak period of wave

u : horizontal displacement of spudcan

$\boldsymbol{u}$: displacement vector, $(w, u, \theta)^{\mathrm{T}}$

$\Delta\boldsymbol{u}$: displacement increment vector

V : vertical compressive reaction force on spudcan

V_{o} : vertical capacity of soil

V_{ult} : vertical capacity of soil ($=V_{\mathrm{o}}$)

V_{ten} : vertical tensile reaction force on spudcan

V_{nor} : normalized vertical force

w : vertical displacement of spudcan

z : coordinates in depth direction

$\alpha_{friction}$: friction coefficient of soil

γ' : effective unit weight of soil

δ_{rem} : strength ratio of the soil

θ : rotation of spudcan

θ_e : elastic component of rotation

θ_p : plastic component of rotation

μ : rate parameter

$\dot{\xi}$: maximum shear strain rate

$\dot{\xi}_{ref}$: reference strain rate

ξ : accumulated absolute plastic strain

ξ_{95} : accumulated absolute plastic strain required for 95% remolding

ν : Poisson's ratio of soil

χ : tensile capacity ratio, V_{ten}/V_{ult}

Chapter 1. Introduction

1.1. Research background

An offshore fixed platform is an offshore structure that installs structures on the seabed to withstand environmental loads such as waves and wind. Unlike floating platforms, it is relatively easy to install as it supports structures on the seabed. However, it is important to accurately consider this fixed state because the installed depth is limited and the behavior varies greatly depending on the seabed soil (Wilson, 2002). In the structural analysis of the fixed platform, these seabed soils act as boundary conditions. The boundary condition of the structure generally governs the global vibration mode and the local stress of the structure (Zhang et al., 2017). In the preliminary design of the fixed platform, a simple support model or a linear spring is used as a simplified foundation model (Baglioni et al., 1982; Williams et al., 1998). This simple foundation model is still limited in use to date and is known to exhibit high accuracy only when the deformation of the soil is very small. However, when designing offshore structures, it is required to calculate the response of structures under severe environmental conditions, and in this situation with large deformation of the soil, simple foundation models, such as simple support conditions and linear springs cannot accurately simulate the actual soil (Houlsby et al., 1992; Williams et al., 1998). Inaccurate boundary conditions

possibly misestimate not only the structural response at a specific site, but also the entire vibration mode of the structure. So how the accuracy of the foundation model is an essential factor in the structure design. Significant deformation of the soil occurs by the structure, which leads to a change in boundary conditions and affects the structure behavior again. It is known that it is more challenging to simulate the exact behavior and structural response of the structure due to structure–soil interaction (SSI).

A fixed platform generally refers to a jacket or a concrete caisson–structured platform supported by piles. In the case of piled structure, the pile–soil interaction (PSI) is considered and the soil is modeled through a linear spring for each depth of the pile penetrated deeply (API, 2002; Mao et al., 2015; Shi et al., 2015). A jack–up is a special platform that has both the characteristics of fixed and floating platforms. During operation, legs penetrated into soil behave like a fixed platform but can move like a floating platform before and after operation. Jack–up, called self–elevating unit, is equipped with a jacking system to lower and lift legs, and 3~6 legs are put on the seabed to support the hull from environmental loads (Young et al., 1984; Williams et al., 1999). The operation process of this jack–up is divided mainly into four stages: (1) transit, (2) installation, (3) operation, (4) retrieval (Le Tirant and Pérol, 1993). (1) The first stage is a transit process that moves to the target area while lifting the leg. In the case of a rig that does not have the self–movability, it moves through a tug boat. Second, after reaching the target area, through (2) the preloading process, the leg is penetrated

and the jack-up platform is installed. In this process, the leg is penetrated into the seabed through the hull weight, ballast water, and jacking power. It is easy to secure stability during this penetration process and subsequent work through the spudcan, an inverted conical steel structure under the leg. Legs must be penetrated deeply until sufficient resistance is obtained, and this process should involve a large deformation of the soil and changes in soil properties. (3) The third stage is an operation stage in which the work is carried out with the hull lifted after the installation is completed. This is the process in which the structure is affected by the environmental loads during the operation period. In this process, the jack-up behaves like a fixed platform, and an appropriate foundation model must be used for structural and global behavior analysis. (4) The last step is the retrieval process of lifting the leg after the work is done. Unlike jackets, repeated preloading and retrieval processes are essential for jack-up that require a relatively short-term operation and move to a different location. In this process, suction force due to adhesion of the clay soil must be considered.

In the preloading phase for the installation of the jack-up, the leg is penetrated into the seabed until their sufficient bearing capacity is obtained. A spudcan at the bottom of the leg has various shapes depending on applications but generally an inverted cone shape with a sharp spigot which help to facilitate penetration into the seabed, while allowing sufficient resistance through a large bearing area (Hossain et al., 2015). Leg penetration analysis calculates the

vertical bearing capacity curve of its corresponding spudcan shape through penetration and is necessary to determine the preloading load and leg penetration depth during design (Endley et al., 1981; Hossain and Randolph, 2010; Houlsby and Martin, 2003; Kee and Ims, 1984; Teh et al., 2008). The penetration process inevitably involves a large deformation of the ground, such as the backflow phenomenon where the spudcan is pushed directly under the ground and the surrounding ground moves. In particular, in the case of the North Sea, mainly consists of sand layer, sufficient resistance is secured even if the depth of penetration is not deep. However, in the case of the Gulf of Mexico (GoM), the South China Sea in the Southeast Asian region, and the southwest coast of Korea, the soft ground mainly composed of clay (Ahn et al., 2017; Menzies and Roper, 2008; Nancy et al., 2014). Spudcan must be deeply penetrated in this area, so the ground deformation behavior must be considered to perform the penetration analysis accurately. In order to calculate the bearing capacity of the spudcan by depth, analytical methods according to the existing bearing capacity theory have been verified and used, and the results of penetration analysis through the centrifugal model test have also been used in the design (Randolph and Gourvenec, 2017). In addition, recently, finite element analysis techniques using Arbitrary Lagrangian Eulerian (ALE) techniques or Coupled Eulerian–Lagrangian (CEL) techniques, which can simulate large deformation behavior, have been used for numerical simulation for this penetration behavior of a spudcan (Hu and Randolph, 1998; Qiu et al., 2009; Tho et al.,

2010). Large Deformation Finite Element (LDFE) analysis technique can simulate not only the penetration analysis of jack-up leg but also various situations in which large soil deformation can occur. It can be more useful when designing offshore structures considering the seabed soil.

In the operation stage, which is supported by the seabed soil and withstands environmental loads, the foundation model mentioned above affects the global behavior of the structure, and the structure-soil interaction in which boundary conditions change due to the soil is affected by the response (Martin, 1994; Schotman, 1989; Vlahos et al., 2005). In addition, the large deformation of the seabed soil that occurs during the preloading process before the operation phase also affects the properties and corresponding foundation model after spudcan penetration (Zhang et al., 2014). There are a number of failure modes that can occur during jack-up operation (Fig. 1). Representatively, the failure modes can be 'overturning' where the windward leg lifted up, sudden leeward leg penetration such as 'punch-through' (Fig. 2), and especially 'seabed slides' in which the leg is pushed without being able to penetrate stiff soil (Martin, 1994). In addition, a sudden collapse can be accompanied by structural failures at weak points such as spudcan-leg connections or leg-hull connections. In order to prevent risks, the failure should be predicted in the design phase through the calculation of the bearing capacity and the combined loads analysis, but few studies have been conducted to solve this problem.

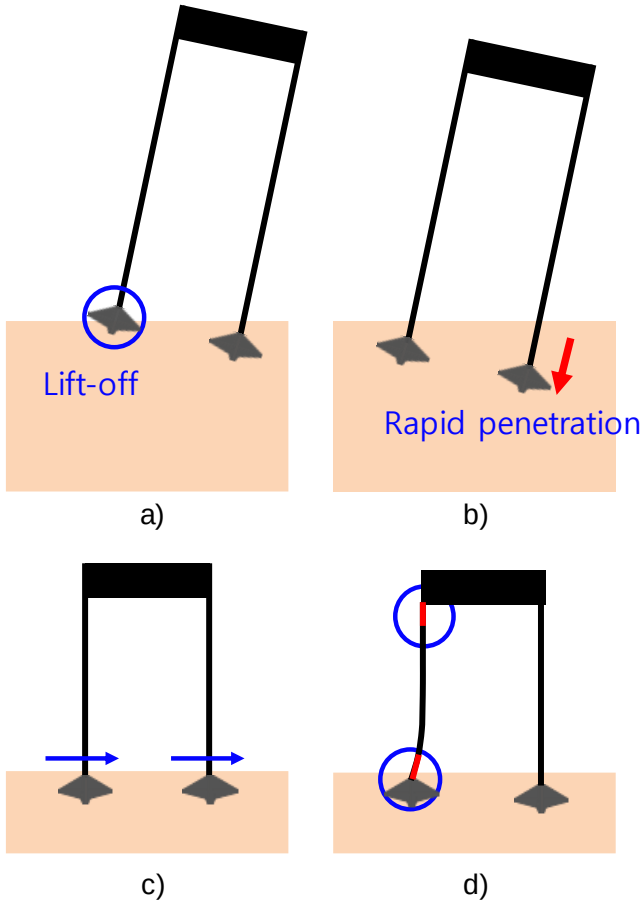

Fig. 1 Failure modes in jack-up operation; a) overturning; b) punch-through; c) seabed sliding; d) Critical point of leg

Fig. 2 Maersk Victory : punch-through failure (Aust, 1997)

In this way, the foundation model used in the operation of jack-up cannot be simplified as a simple boundary condition such as simple support or a linear spring because its complex behavior. Several foundation models have been proposed by ISO (2012). They are pinned model, linear spring, secant model, yield interaction model and soil continuum model as listed in Fig. 3. The secant model that uses arbitrarily reduced stiffness in the rotation direction. The yield interaction model that calculates plastic displacement using nonlinear stiffness. The secant model and yield interaction model are classified as simple foundation model. The soil continuum model that performs numerical analysis using soil continuum are representative foundation models that incorporate the interaction of structures and soil. From the pinned model to the soil continuum model, more accurate analysis is possible, and in the ISO, a more complicated model has been used when performing a high level of acceptance check (Table 1).

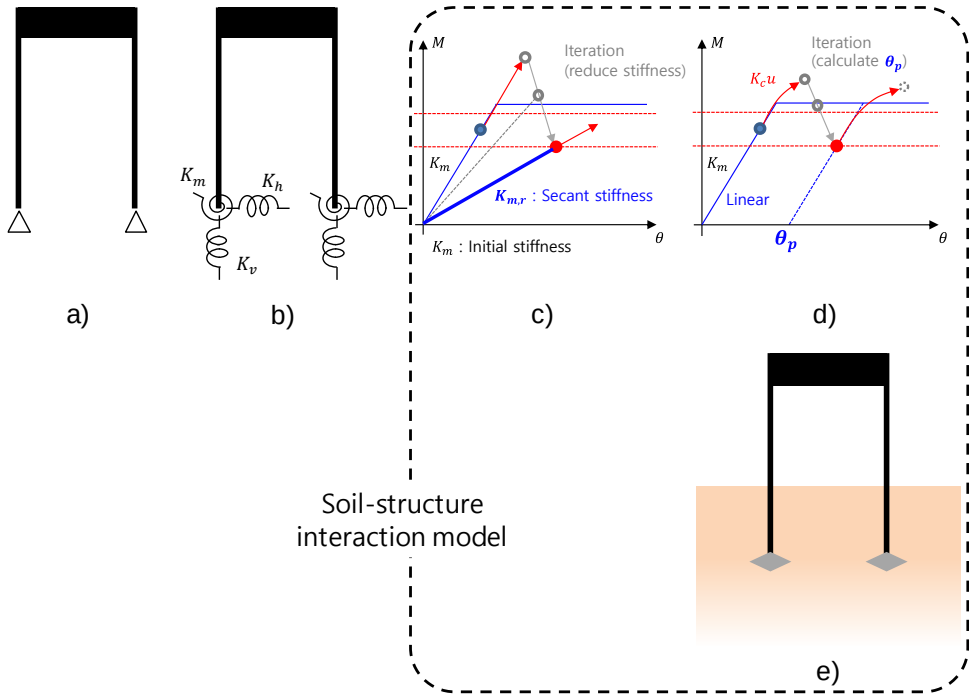

Fig. 3 Foundation models suggested in ISO (2012);
a) Pinned model; b) Linear spring model; c) Secant model;
d) Yield interaction model; e) Soil continuum model

Table 1 Acceptance check in ISO (2012)

Check level	**Step 1**		**Step 2**			**Step 3**	
	Step 1a	Step 1b	Step 2a	Step 2b	Step 2c	Step 3a	Step 3b
Foundation model	Pinned			Secant model	**Yield interaction model (Model B)**	Step 2 foundation model	**Continuum**
Check point	Preload (leeward leg)	Preload (windward leg)	Foundation capacity, Sliding (all leg)	Foundation capacity, Sliding (all leg)	Foundation capacity	Displacement (Additional penetration, sliding)	
Coverage	V	V	V, H	V, H	V, H, M	V, H (,M)	V, H, M

Before briefly explaining the existing foundation model, the load–displacement curve assumed for numerical analysis has been briefly described (Fig. 4). The elasto–perfectly plastic curve, which is assumed to be the simplest material property, has a linear relationship in the elastic section and the slope of the plastic section after yield is zero. Therefore, after yield, the element cannot have stiffness. Another commonly used model is elasto–plastic with strain hardening. It is the same as elasto–plastic in that it has a linear relationship in the elastic region, but differs in that hardening occurs in the plastic region after yield. Hardening relationships are modeled linearly, logarithmic, and hyperbolic, depending on the properties. And the model that best describes the behavior of the actual material is the nonlinear elastic–plastic model. Even in the elastic region before yield, a nonlinear relationship is shown, and accordingly, a hysteresis curve is drawn according to loading and unloading.

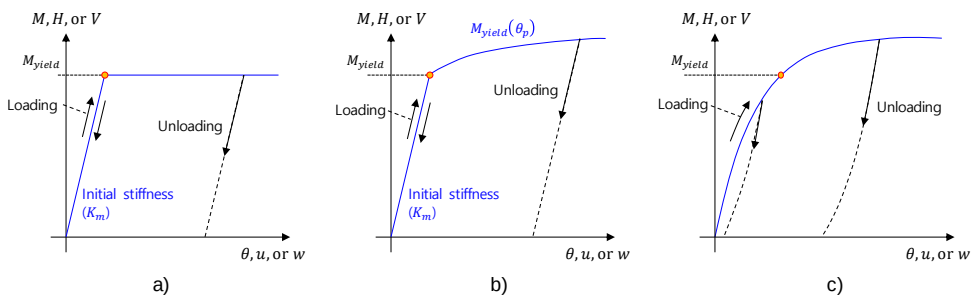

Fig. 4 Load–displacement curve in numerical analysis;
a) Elasto–perfectly plastic; b) Elasto–plastic;
c) Nonlinear elastic–plastic

The yield strength that determines yield is generally a material property. When a material is subjected to a 1-dof load, it appears as a single value, but when loads in multiple directions are applied, the combination of loads is a condition of yield. The yield envelope is a set of these yield points, and in general, the yield envelope in the n-dimensional load space is an n-1 dimensional figure (Simo and Hughes, 2006). In the spudcan study, the soil is assumed to follow a force-resultant yield envelope (Cheng and Cassidy, 2016b). It is mainly represented by a two-dimensional surface for vertical, horizontal, and rotational forces applied on the soil. In ISO(2012), the equations of yield surfaces for vertical, horizontal, and rotational loads are presented in Eq.(1), and cigar-shaped yield surfaces for clay and sand are also presented in Fig. 5 (Martin, 1994; Cassidy, 1999). If a combination of loads applied to the soil after the structure-soil analysis is inside the yield curve, it is considered to be in the elastic region. It is considered to be in the elasto-plastic if it is on the yield surface. If the combination of loads is outside the yield curve, it is assumed to plastic, and various foundation models try to explain their behavior in the plastic region.

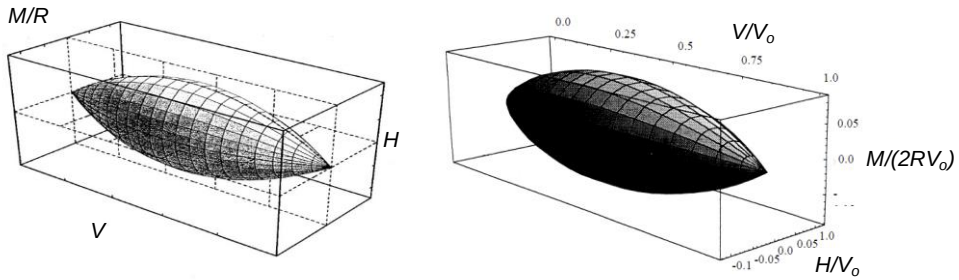

Fig. 5 Cigar-shaped yield surface in jack-up research;
a) Model B, clay (Martin, 1994); b) Model C, sand (Cassidy, 1999)

$$f = \left[\frac{H}{H_o}\right]^2 + \left[\frac{M}{M_o}\right]^2 - 16(1-a)\left[\frac{V}{V_o}\right]^2\left[1-\frac{V}{V_o}\right]^2 - 4a\left[\frac{V}{V_o}\right]\left[1-\frac{V}{V_o}\right] \quad (1)$$

where V_o, H_o, M_o is the maximum capacity of foundation in V, H, M direction, and V, H, M is the reaction forces applied on the spudcan in V, H, M direction. a is the coefficient about penetration depth.

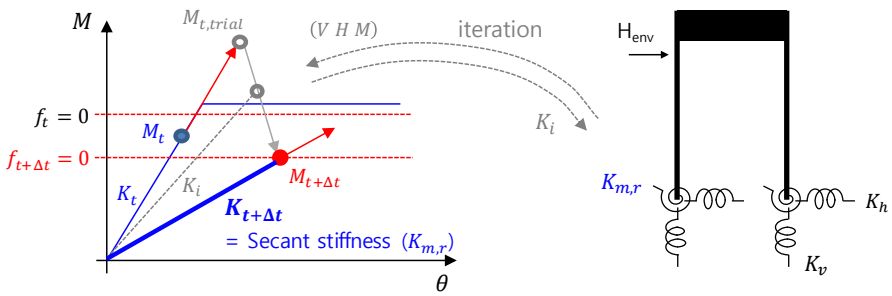

Fig. 6 Foundation model : Secant model in M- θ graph

ISO (2012) proposes a secant model as a simple foundation model that considers structure–soil interaction. The secant model in Fig. 6 uses secant stiffness in the rotational direction with linear vertical and horizontal stiffnesses (Purwana et al., 2012; Wong et al., 2012). In general, in numerical analysis, the behavior at the next increment is determined by considering the time increment (or load increment) and corresponding tangent stiffness of the load–displacement curve. However, secant stiffness refers to the stiffness that connects from the starting point to the design point when all of the load or displacement is applied (Sullivan et al., 2004). In this secant stiffness concept, the load–displacement at the design point coincides, but an incorrect load–displacement relation occurs at different locations. Although the secant stiffness that fits only at a certain point has limitations, it also has the advantage of being a foundation model that can be modeled simply in the form of a linear spring in the structure in consideration of the plasticity of the soil. In the ISO, when the load combination is in the plastic region, structural analysis is repeatedly performed by arbitrarily reducing the rotational stiffness, and the iterative calculation ends when the load combination is placed on the yield envelope. In this process, the rotational stiffness decreases, and this reduced stiffness is used for structural analysis as secant stiffness.

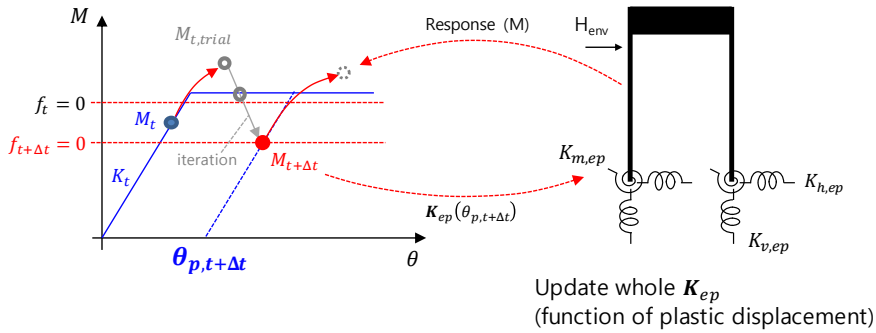

Fig. 7 Foundation model : modified model B in M− θ graph

The yield interaction model, which calculates moment failure through the calculation of plastic displacement, is called model B for clay soil. ISO has suggested this model as a more complex and accurate model than the secant model and recommends using it at a high acceptance check level. The model B was proposed by Martin in 1994 and introduced the Elasto−plasticity framework to predict the behavior when the load combination is in the plastic region. Elasticity, yield envelope, flow rule for plastic behavior, hardening law for additional vertical penetration are all formulated in an iterative procedure. As a result, plastic displacement corresponding to the time increment (or load increment) is calculated. When the plastic displacement converges, the tangent stiffness calculated together and the load state derived from the elastic displacement are updated and used for the calculation of the next increment. Such a framework is still in use today, and a modified model B of Zhang et al. (2014) has been presented an improved model (Fig. 7). In the model B, the effect of horizontal and rotational coupling behavior occurring in the actual soil is considered, and also in modified model

B, the tensile capacity due to spudcan extraction is implemented in yield envelope. This model has the advantage that it can express the elasto-plastic behavior of the soil relatively accurately and requires less time for analysis than the soil continuum model. Especially when the soil is in the plastic region and in a specific situation, there is an advantage that the accuracy of the model can be easily increased by improving the relational expression for it. However, by assuming a linear relationship other than the coupling in the horizontal-rotation direction in the elastic region, a vulnerability can be found in the case of repeated loads in the elastic area.

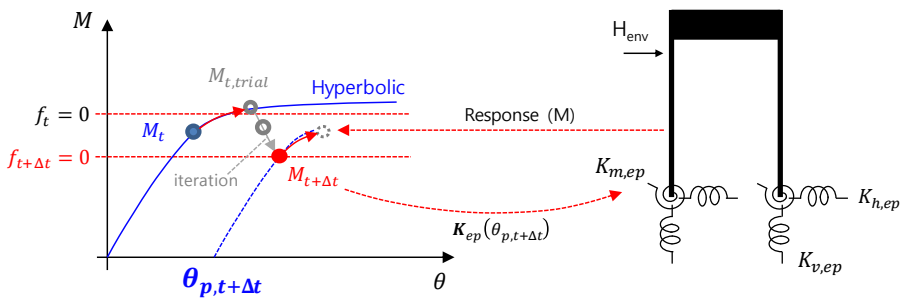

Fig. 8 Foundation model : Hyperbolic model B in M- θ graph

For this loading and unloading situation, Vlahos et al. (2006) has formulated the elasticity of the model B framework by introducing a hyperbolic backbone curve in the direction of rotation. In Vlahos et al. (2006), the hyperbolic backbone curve has been implemented through spring-slider element using hyperplasticity framework based on the thermomechanical energy potential. In this study, the hyperbolic relationship of load-displacement has been implemented

to follow in the elastic region, which was extended in the horizontal direction and introduced into the model B framework along with the coupling behavior in horizontal–rotational direction (Fig. 8). The behavior of the elastic region has been improved while maintaining the advantages of the model B plasticity framework for calculating the plastic displacement, and the hysteresis curve could be expressed in the elastic region.

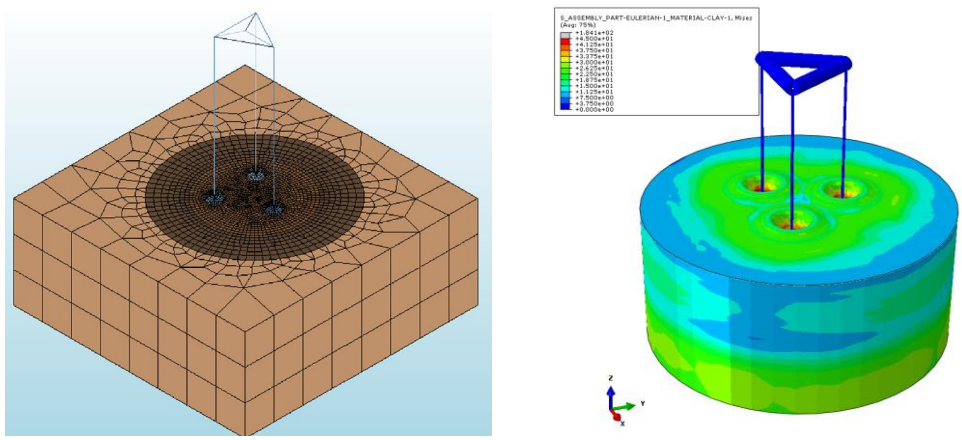

a) b)

Fig. 9 Foundation model : soil continuum model; a) Modified Mohr–Coulomb model for sand at shallow embedment (Pisanò et al., 2019); b) Jack–up structural analysis with soil LDFE technique

The soil continuum model is the most reliable and accurate method in the numerical method to consider the structure–soil interaction (Fig. 9). The load transferred from the structure is applied to the ground simultaneously, and the influence of the structure due to the corresponding behavior of the soil is considered as two–way. Even if this accuracy, the computational cost makes

the method difficult to use widely, especially for time series analysis. In the jack-up problem, the soil continuum model has been considered by using a basic mohr-coulomb model for sands with relatively small deformation (Pisanò et al., 2019). However, for clays accompanied by large deformations, the fully coupled structure-soil interaction analysis is not widely performed due to the excessively high cost to simulate the large deformations and the resulting changes in soil properties.

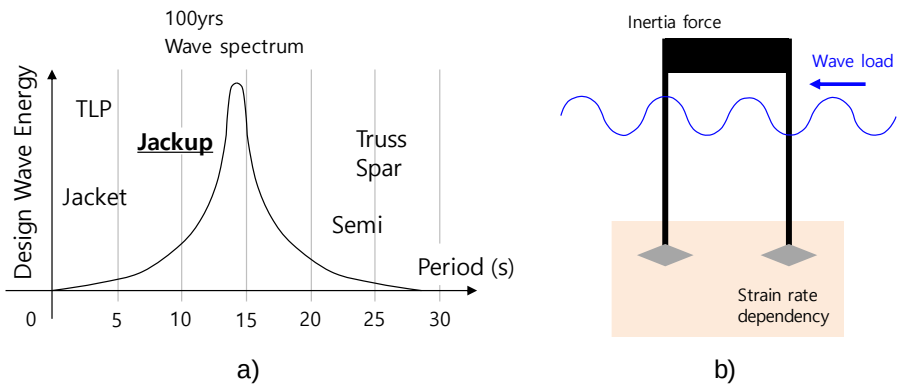

Fig. 10 Dynamic effects of wave load analysis in jack-up;
a) Natural period of offshore platform;
b) Jack-up structural analysis with dynamic load

In particular, when the structure-soil interaction analysis is performed using the above-described soil continuum model, dynamic effects occur in the results more (Fig. 10). The dynamic effects of structural aspects are 'phase shift' due to inertia force and 'Dynamic Amplification Factor (DAF)', which is a resonance effect according to the natural period of the structure. In a typical jack-up

structure, a natural period is in the range of 5 and 15 seconds, which makes dynamic effects in wave load analysis unavoidable (ABS, 2014). Meanwhile, wave load analysis in the soil continuum model also causes the dynamic effects of the soil. Clay is a representative rate-dependent material, and it is known that hardening occurs according to the strain rate (Abelev and Valent, 2009; Nanda et al., 2017; Robinson and Brown, 2013). In numerical analysis, quasi-static analysis is generally performed to remove dynamic effects. However, in the wave load analysis, in which a wave of about 10 seconds acts as environmental loads, quasi-static analysis can decrease the accuracy.

1.2. Research objective and scope

The objective of this study is to propose an accurate method of dynamic wave analysis for jack-up by improving the structure-soil interaction model. For this objective, the yield envelope for soft over stiff clay and hyperbolic model B is proposed and implemented as boundary condition of jack-up structural analysis. Fully coupled structure-soil interaction analysis using soil LDFE technique is performed and compared with proposed model. Accompanying dynamic effects of jack-up wave analysis has also been presented and investigated.

The southwest sea of South Korea is mainly deposited with clay, especially with a soil profile of stiff-soft-stiff clay. To operate a jack-up type "wind turbine installation vessel (WTIV)" to create an offshore wind farm, its legs should be penetrated until sitting on a stiff layer. In this case, penetrated spudcan are placed in transition zone that is affected by both the lower stiff and upper soft layers. To model this transition zone, the target soil has been simplified to soft over stiff clay. A nonlinear soil model for a general single clay soil has been studied by improving the accuracy of yield envelope and plastic potential from the model B, which considered the coupled effect of the combined loads. In addition, recently, studies on the nonlinear soil models for multi-layered soils, especially sand over clay, where punch-through can occur, have been conducted. On the other hand, studies have not been performed on soft over stiff clay where squeezing of the upper clay occurs. In the aspect of the

spudcan for installation, the squeezing phenomenon, in which the weak ground is squeezed due to the lower stiff soil and the bearing capacity increases, is very advantageous to secure sufficient bearing capacity. However, if a spudcan is placed between two clay soils during the operation phase of the jack-up, the spudcan is simultaneously affected by both upper soft clay and lower stiff clay, so the model on a single clay cannot be applied as it is.

In this study, a nonlinear foundation model that interacts with the structural response of jack-up in real time is presented. Combined loads, transferred to the soil through the jack-up structure from the environmental loads, change the foundation model and soil properties. The changed foundation model becomes a boundary condition and affects the structural behavior of jack-up in real time. This structure-soil interaction should be considered for simulating accurate jack-up behavior. This study has been conducted through numerical analysis considering the large deformation effect of the soil due to the spudcan penetration. For this, soil Large Deformation Finite Element (LDFE) analysis technique is implemented in Abaqus/Explicit commercial program, and validated (Chapter 2). Combined loads analyses on soft over stiff clay have been performed using the developed soil LDFE numerical model. Ultimate capacities in the vertical, horizontal, and rotational directions have been calculated and analyzed, and the effect of lower stiff clay on the capacities have been investigated. In addition, a best-fit yield envelope expression has been proposed (Chapter 3). The model B, the yield interaction model of clay, consists of elasticity, yield

envelope, flow rule, and hardening law. Unlike the actual soil in which gradual plasticity occurs, linear load-displacement relationship of the foundation model can overestimate the load acting on the soil. To improve this, a hyperbolic relationship has been applied to the elastic region, and a hysteresis curve in elasticity has been implemented. In addition, a regression model of initial stiffness is presented for the proposed hyperbolic model B (Chapter 4). The soil continuum model is the most accurate method to numerically simulate the structure-soil interaction. It was mainly used for small strain problems such as shallow embedment of sand due to computational cost. To validate the proposed hyperbolic model B, a fully coupled structure-soil interaction analysis using soil continuum has been performed. The interaction between the jack-up and the soil was considered simultaneously in this model. Using the LDFE technique in Chapter 2, large deformation of clay is simulated and reflected in combined loads analysis. It has been confirmed that the proposed model follows the LDFE results well before the yield, and it has also been shown that the moment distribution of the leg can be accurately predicted compared to the existing linear relationship model (Chapter 5). Wave load analysis of jack-up has been performed using the proposed yield interaction model in soft over stiff clay and the soil continuum model using the LDFE technique. Comparative analysis has been conducted on the involved dynamic effects of the structure and soil behavior. As a result of the analysis, it has been confirmed that the proposed model and the continuum model have similar results for the repetitive wave

load in the elastic region. This will allow the proposed model to be used when performing the fatigue strength assessment of jack-up (Chapter 6).

Chapter 2. Soil LDFE analysis technique

2.1. Introduction

The jack-up system uses a pinion and guide to raise and lower legs of the hull. This system is installed in a jack-up rig and a jack-up type Wind Turbine Installation Vessel (WTIV). When the jack-up system stands on legs, a spudcan directly touches the seabed underneath the leg to support the load of the entire structure of platform. Since the jack-up type offshore structure can be installed in various soil environment, precise assessment of the structure during installation and operation phase is required. Especially in the installation process of the jack-up, it is accompanied by large deformation of the soil due to penetration of spudcan. Therefore, it is necessary at the design stage to accurately predict the large deformation behavior and bearing capacity of the soil.

Table 2 Conventional researches of soil LDFE analysis

	Centrifuge	LDFE (RITSS)	LDFE (CEL)
Description	• Model test which simulate the realistic stress field through centrifugal force • Widely used in geotechnical problem	• Remeshing and Interpolation Technique with Small Strain (RITSS) • Based on Arbitrary Lagrangian and Eulerian (ALE)	• Coupled Eulerian-Lagrangian (CEL) method • Supported by Abaqus commercial program
First suggestion in geotechnical problem	• From 1960~1970 • Mikasa in Osaka univ. • Schofield in Cambridge univ.	• Hu (1998) – Large deformation problems in soil – Cavity Strip footing Spudcan	• Qiu (2009) – Large deformation problems in soil – Strip footing Pile jacking Ship grounding
Usage in Spudcan penetration issue	• Yu (2018), Lattice leg effect • Kim (2018), sloped seabed • Hossain (2017), Footprint	• Hossain (2009), Spudcan penetration prediction • Zhang (2018), Spudcan angle • Jun (2018), Spudcan shape	
Multi-layered soil	• Sand over clay – Hu (2014), Analytic expression of bearing capacity for sand over clay – Hu (2018), Post-peak behavior of spudcan in sand over clay – Li (2018), Bayesian approach of spudcan behavior in sand over clay • Multi-layered clay – Hossain (2010), Bearing capacity of spudcan in stiff-over-soft clay – Zheng (2018), Spudcan behavior in stiff-soft-stiff clay		

In general, three methods have been used to calculate the bearing capacity of the Spudcan. There are a method using a formula combining theoretical and empirical equations recommended by a guideline or rule (SNAME, 2008; ISO, 2012), a finite element method simulating the penetration behavior of the spudcan (Hossain and Randolph, 2010b; Hu et al., 2015; Zheng et al., 2017), and a centrifuge test method (Hossain and Randolph, 2010a; Hu and Cassidy, 2017; Teh et al., 2010). Various case studies have been conducted using numerical analysis methods. The remeshing and interpolation technique with small strain (RITSS) method developed by Hu and Randolph (1998) has been used for numerical analysis of large deformation problem based on ALE. In addition, Qiu (2009) has simulated the soil behavior using the CEL method provided in

the Abaqus/Explicit commercial program, and since then, the method has been used for the large deformation problem of soil.

In this paper, the large deformation behavior of the soil is simulated using the finite element method. Since the mesh distortion occurs due to the large deformation, the penetration behavior of the spudcan cannot be analyzed by general finite element method. Analysis technique for large deformation is adopted in the soil problem, and verification about the various case is performed. Simple structure is verified first, and then the spudcan penetration on clay and sand is verified, too. The soil model and the details of verification case is introduced. As a result, it is confirmed that the developed Large Deformation Finite Element (LDFE) method shows similar results to the centrifuge model test results and the existing LDFE analysis results.

2.2. Numerical methodology

Generally, the Lagrangian description is used for structural analysis problems, and the Eulerian description is used for fluid problems. In Lagrangian description, the detailed history of material deformation is represented by the movement of mesh. Lagrangian elements are always 100% full of single material, so it is easy to divide the material boundary. On the contrary, in Eulerian description, the mesh is fixed and the materials pass through the mesh. The material is allowed to move independently of the finite

elements, so the Eulerian elements may not always be 100% full of material. The CEL technique has been developed combining the Lagrangian description with advantages for boundary and contact problems and the Eulerian description, which are less affected by mesh distortion (Simulia, 2013). Remesh and advection process simulate large deformation of the soil.

Tresca model incorporating strain softening and rate dependency is used for the numerical modeling of clay soil. The undrained shear strength is determined using the following strain / strain rate dependent equation proposed by Einav and Randolph (2005) (Eq. (2)).

$$s_u = \left[1 + \mu \log\left(\frac{\mathrm{Max}\left(|\dot{\xi}|, \dot{\xi}_{ref}\right)}{\dot{\xi}_{ref}}\right)\right] \left[\delta_{rem} + (1 - \delta_{rem}) e^{-3\xi/\xi_{95}}\right][s_{um} + kz] \quad (2)$$

where, s_u is the undrained shear strength at the depth z considering strain softening and rate hardening. μ is a rate parameter and has a value of 0.05 to 0.2 in marine clay typically. $\dot{\xi}$ means the maximum shear strain rate. $\dot{\xi}_{ref}$ is the reference strain rate and is 1 to 4%/h in the triaxial test and 20%/h in the direct simple shear test. δ_{rem} is the inverse of the sensitivity as the strength ratio of the soil. In general, the sensitivity of marine clay is 2 ~ 5. ξ stands for accumulated absolute plastic strain and has the definition of the following equation. ξ_{95} is the value of ξ when 95% remolding is performed after the soil is disturbed. Generally, it has a value of 10

to 25 (Hossain and Randolph, 2009). s_{um} is the undrained shear strength at the top surface of the clay layer. The k value is a strength depth gradient. Using these two parameters, undrained shear strength at the corresponding depth, z, is obtained.

2.3. Analysis model

Using the CEL method provided by the Abaqus commercial program, the large deformation of soil caused by the penetration of the spudcan is simulated. As mentioned above, spudcan is modeled by using Lagrangian element, and soil by Eulerian element. Lagrangian element comprises both 6-noded linear triangular prism element(C3D6) and 8-noded linear brick element with reduced integration(C3D8R) is used for spudcan structure. Eulerian element comprises 8-noded linear brick element with reduced integration (EC3D8R) is used for the soil (Qiu and Grabe, 2012; Tho et al., 2010). Mesh size is determined by considering the diameter D of the spudcan, D, and mesh size of 0.025D ~ 0.05D is used. In the spudcan penetration simulation, the rate of penetration is also important. It should be slow enough to avoid the inertia effect. Penetration rate is also determined considering the D, and the speed of 0.005D ~ 0.01D/s is mainly used. This means a penetration rate of 0.05 ~ 0.1m/s assuming D of about 10m. The following figure is an example of the spudcan penetration model, which consists of spudcan structure and soil layer (Fig. 11).

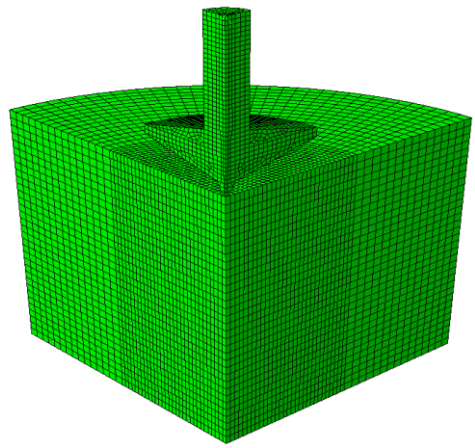

Fig. 11 Numerical analysis model about penetration of spudcan in clay

2.4. Verification results

2.4.1. Penetration of pipe in clay

Wang et al. (2010) is referred for the simulation about penetration of pipe in clay. In this referred paper, The LDFE approach has been verified by comparison with a centrifuge test of pipe-soil interaction in Kaolin clay, so the result of pipe penetration is used for this verification. Unit length (=1 m) is used to simulate 2D in 3D domain, and diameter of pipe, D, is 0.8m. Pipe structure is assumed to rigid body, because the deformation of pipe is too small to neglect.

Clay soil is modeled as the elasto-perfectly plastic material obeying a Tresca yield criterion. Effective unit weight of clay is 6.5kN/m^3. Undrained shear strength is 2.3 kPa at the top surface of

clay layer and increases to 3.6 kPa/m with depth. A rigidity index, the ratio between the Young's modulus to the undrained shear strength (E/s_u), is used as 500, the general value of marine clay. There are several factors that should be selected for nonlinear model of undrained shear strength. In the strain softening term, 0.3125 is used as strength ratio, δ_{rem}, and 10 of ξ_{95} is used for the value of ξ required for the soil to undergo 95% remolding. For the strain rate hardening term, 0.1 of rate parameter value μ is used, and 1.5%/h is used as reference shear strain rate, $\dot{\xi}_{ref}$.

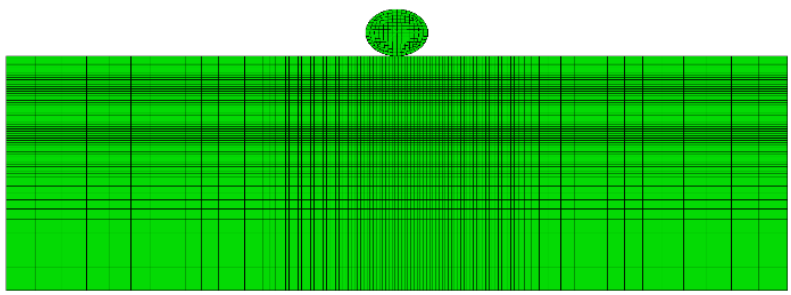

Fig. 12 Numerical analysis model about penetration of unit pipe

Numerical model of pipe penetration is introduced in Fig. 12. Pipe structure is modeled using Lagrangian element, and soil is modeled as Eulerian element. Mesh size is 0.04m, which is same with 0.05D, and penetration rate is 0.005m/s of 0.00625D.

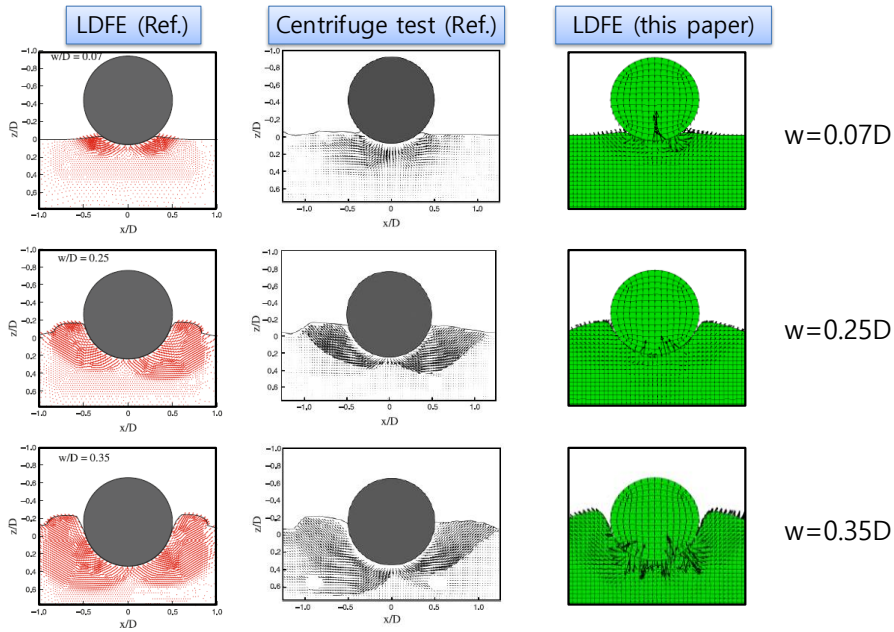

Fig. 13 Cross-sectional view of deformed shape of soil

(Ref. = Wang et al., 2010)

Fig. 13 shows the deformed shape of soil when the penetration depth is 0.07D, 0.25D, and 0.35D. At each depth, it can be seen that the deformed shape of soil is similar to the results of centrifuge tests and referred LDFE. The movement of the soil during penetration and the shape of soil berm could be compared and confirmed similar.

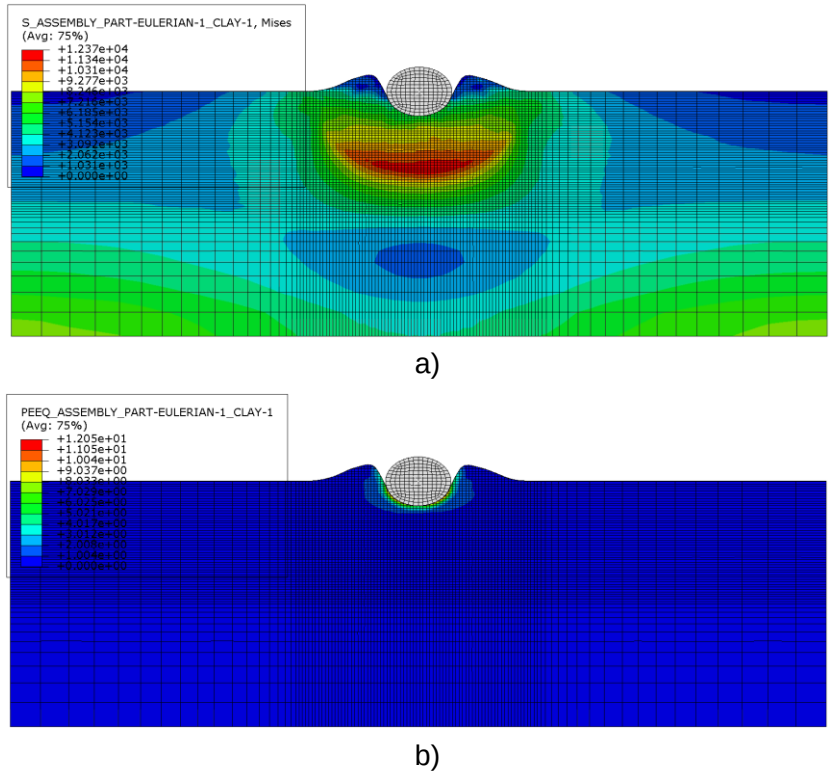

Fig. 14 Soil response in clay (unit pipe); a) Mises stress; b) Equivalent plastic strain

Soil stress and plastic strain after the penetration of pipe are presented at Fig. 14. High stress is observed under the pipe after the penetration. This high stress is dominantly affected by the elastic behavior of the soil, so the little plastic strain occurs in that region. Unlike elastic strain, plastic strain occurs right under the structure where force is applied directely.

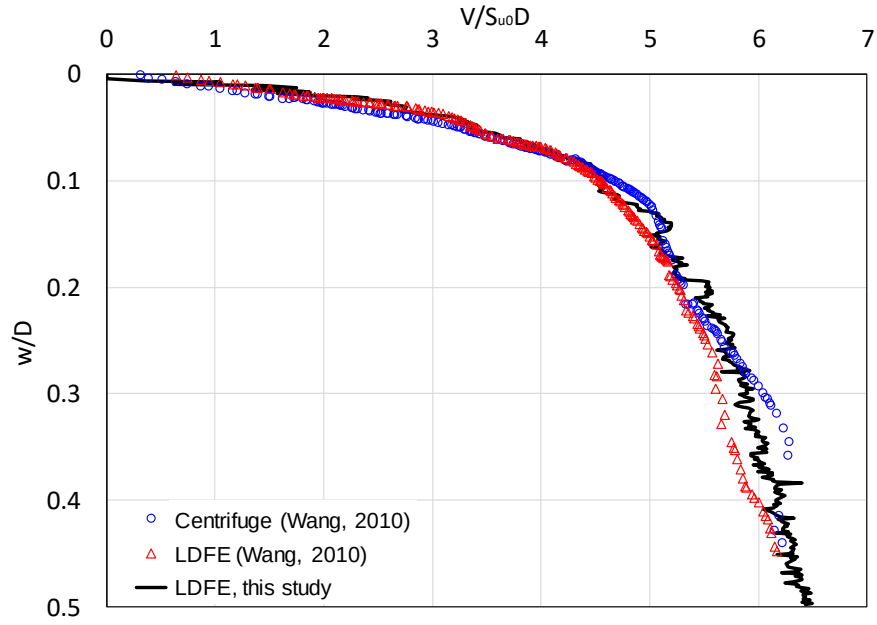

Fig. 15 Bearing capacity curve of unit pipe in clay

As a result of the penetration behavior simulation, the bearing capacity curve is shown in the Fig. 15. The penetration of 0.5D is simulated, and the non-dimensionlized results are compared with centrifuge model tests and LDFE results. Simulation results are similar to those of the two references.

2.4.2. Penetration of spudcan in single clay

In Hossain et al. (2015), the bearing capacity about penetration of various shape of spudcan in clay has been studied. Penetration and extraction resistance has been researched using a series of centrifuge tests and LDFE analyses. Three different base geometries used in the real field is treaed in this paper, so a

representative shape of spudcan is selected for this verification. The penetration behavior of the spudcan is simulated, and the maximum bearing area of the spudcan has 6m of diameter. Spudcan structure is assumed to rigid body, same as the case of pipe, because the deformation of pipe is small enough. Detailed configuration of spudcan is shown in Fig. 16.

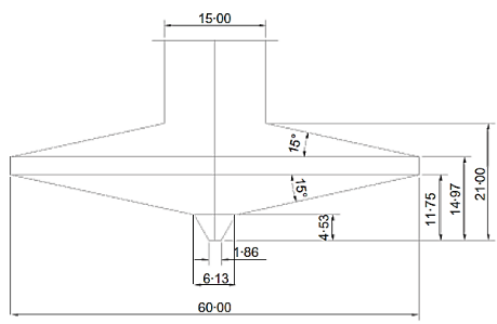

Fig. 16 Spudcan used in validation (Hossain et al., 2015)

Clay modeling is the same as the previous case of unit pipe. However, the properties are applied diffrenetly as used in Hossain et al. (2015). Soil layer is modeled as the elasto-perfectly plastic material obeying a Tresca yield criterion. Effective unit weight of clay is 7.5kN/m3. Undrained shear strength is 0.9kPa at the top surface of clay layer and increases to 1.95kPa/m as depth increases. The rigidity index is used as 500, the same as clay model used in unit pipe case. Several factors for nonlinear model of undrained shear strength is used in this clay model. In the strain softening term, 0.3436 is used as strength ratio, δ_{rem}, and 15 of ξ_{95} is used. For the strain rate hardening term, 0.1 of rate parameter value is used, and

1.5%/h is used as reference shear strain rate $\dot{\xi}_{ref}$. Numerical analysis model about this verification case is shown in Fig. 11. spudcan structure is modeled using Lagrangian element, and soil is modeled as Eulerian element. Mesh size is 0.3m, which is same with 0.025D, and penetration rate is 0.1m/s of 0.0083D, which is also used in the reference paper.

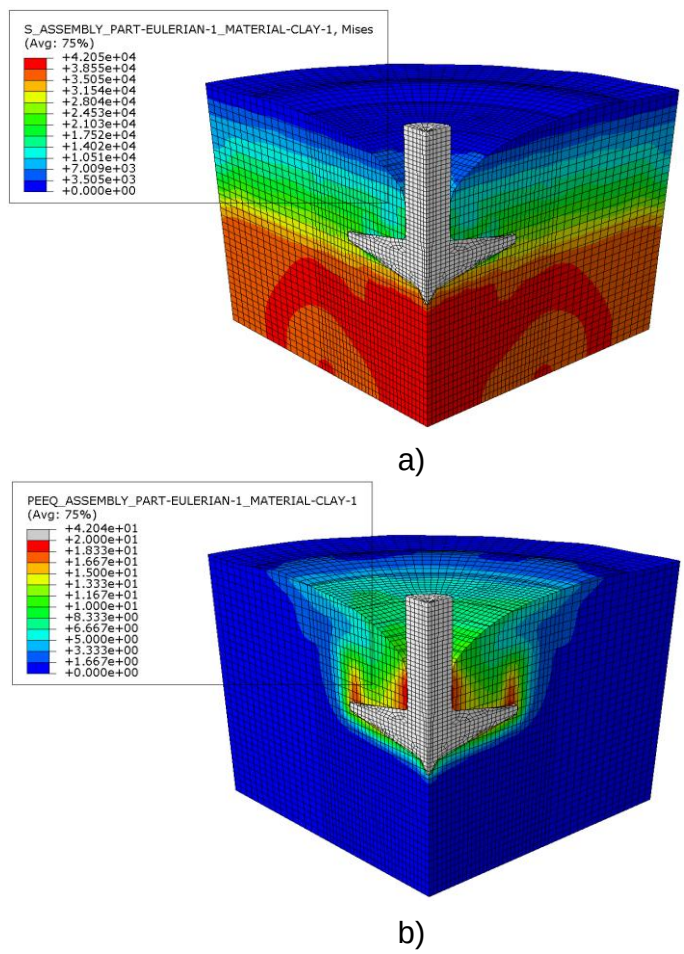

Fig. 17 Soil response at spudcan penetration; a) Mises stress; b) Equivalent plastic strain

Soil stress and plastic strain after penetration are presented at Figure. High stress is observed under the pipe after penetration. This high stress is caused by the elastic behavior of the soil, which can be confirmed from the plastic strain results. Unlike elastic strain, plastic strain usually occurs right under the structure where force is applied directely, shear deformed region by spudcan edge, and upper part of the spudcan where large deformation occurs due to backflow.

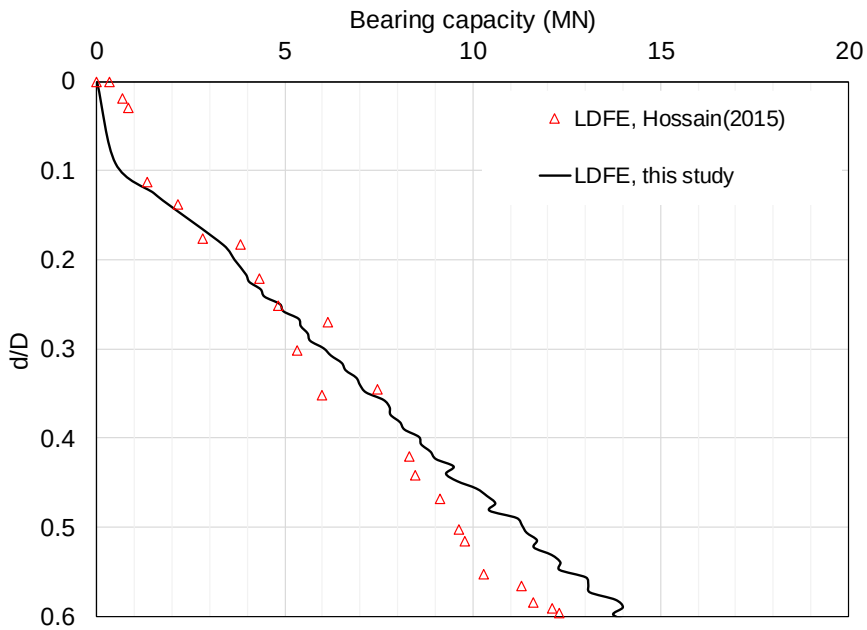

Fig. 18 Bearing capacity curve for numerical model validation

The bearing capacity curve of spudcan penetration is shown in Fig. 18. The penetration is simulated unitil 0.6D depth. Simulation results are similar to a reference, however, the value is larger as the penetration depth is deeper. Since the size of the domain is small

in the depth direction, it is considered that the boundary effect is generated. Therefore, the greater the depth, the greater the bearing capacity. These results are expected to improve when the size of domain is large enough.

2.4.3. Penetration of spudcan in multi-layered clay

Before carrying out the present numerical analysis, the soil LDFE analysis technique needs to be validated. The results of the penetration analysis of the multi-layered clay soils are compared with those of the centrifuge model test and the existing numerical LDFE analysis. Hossain et al. (2011) performed the centrifuge model test on multi-layered clay soils and analyzed the occurred punch-through and squeezing phenomena. Notably, squeezing was observed in their T8 test due to the lowest stiff layer, and this case was also simulated by LDFE analysis in Zheng et al. (2018).

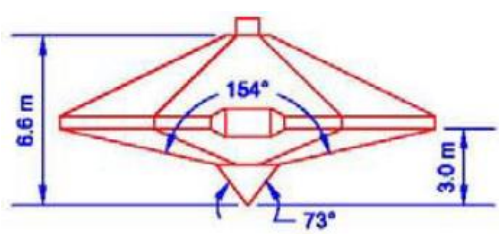

Fig. 19 Spudcan used in validation (Menzies and Roper, 2008)

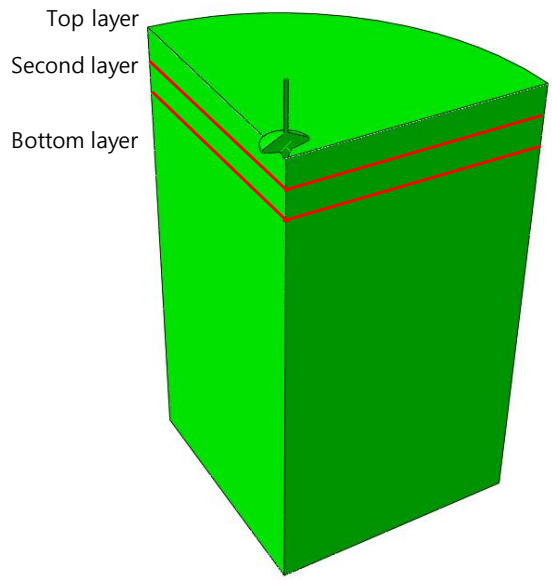

Fig. 20 FE model in multi-layered clay validation

Since squeezing is an important phenomenon in soft-over-stiff clay, which is the target soil of the present study, this case is selected for validation of this LDFE analysis. The T8 test covered three-layered clay with interbedded soft clay. The undrained shear strengths of each layer in Zheng et al. (2018) were, in order, 21 kPa, 8.5 kPa, and 35.5 kPa for the first, second, and third layers. With these undrained shear strengths, 200 rigidity index (E/s_u), rough condition of spudcan-soil interface, unit weights of 7.5 kN/m^3 (top layer) and 7.3 kN/m^3 (lower layers) in Zheng et al. (2014) are referred for the validation. The strain-softening and rate-hardening parameters in this validation also are the same values as in Zheng et al. (2018) (i.e., μ=0.1, $\dot{\xi}_{ref}$=1.5%/h, δ_{rem}=0.36, ξ_{95}=12).

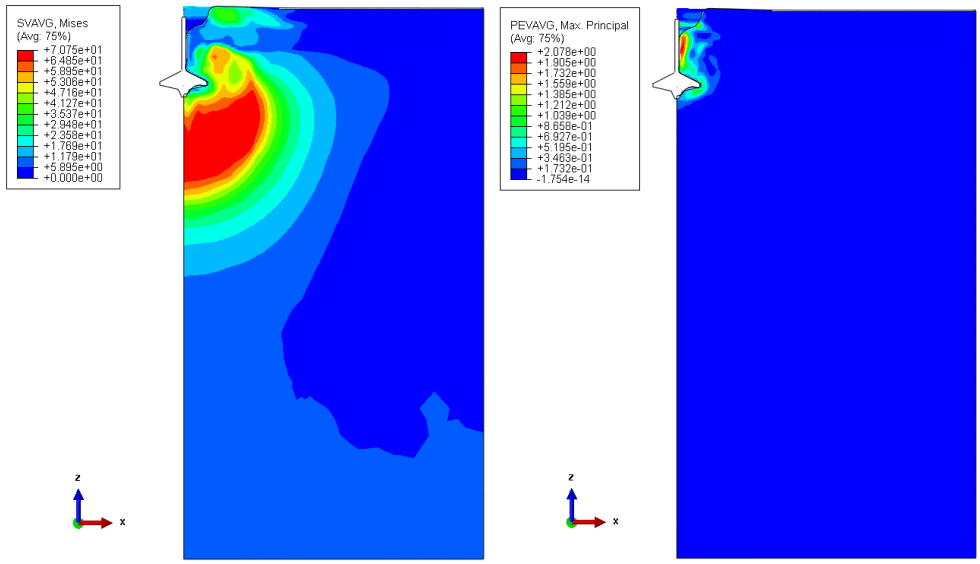

Fig. 21 Soil response in multi-layered clay validation;

a) Mises stress in penetration analysis;

b) Maximum principal plastic strain

Fig. 21 shows the total equivalent mises stress and plastic strain of the soil due to the spudcan penetration behavior in stiff-soft-stiff clay. In the strain rate dependent term in Eq. (2), total stress is used to calculate the total strain. Although not exactly the same, the range of mises stress plot is similar to the range affected by rate hardening. Likewise, although not exactly the same, the range that the maximum principal plastic strain plot affects is similar to that of strain-softening and has a large plastic strain around the disturbed soil.

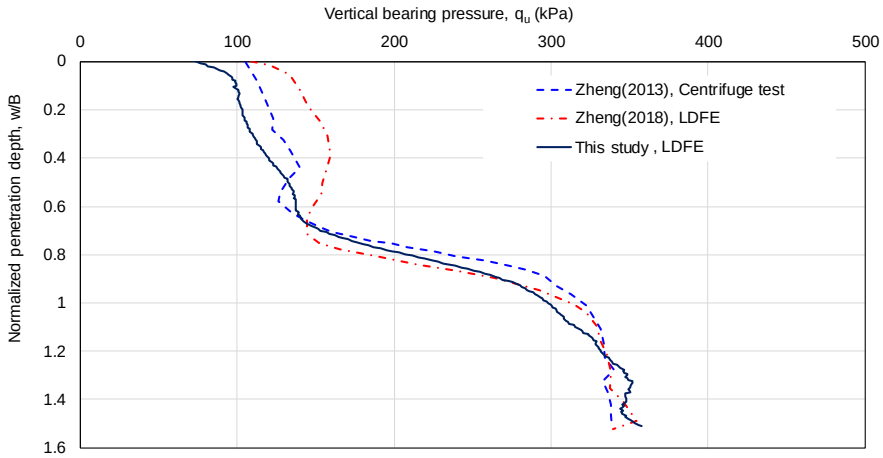

Fig. 22 Bearing capacity results of multi-layered clay

The centrifuge test data, existing LDFE analysis result, and numerical analysis results of the present study well shows the squeezing effect at the interface of the second soft layer and third stiff layer (w=0.92B). Although a small difference in bearing capacity curve can be caused by application of a different modeling technique in numerical analysis, it is thought that reasonable results have been obtained by using this LDFE analysis technique. Verification of the multi-layered clay soil has been performed, and it has been confirmed that the vertical capacity value obtained results similar to those of the existing results.

In this chapter, verification has been performed on the clay soil. For single clay and multi-layer clay soils, the results of the soil LDFE analysis developed in this study have been verified using the centrifugal model tests and LDFE results provided in the existing researches. As a result, it has been confirmed that the vertical

capacity value is well predicted according to the spudcan penetration behavior. This numerical analysis technique has been used to study the nonlinear soil model in the following chapters.

Chapter 3. Yield envelope in soft over stiff clay

3.1. Introduction

A fixed platform is an offshore structure that is fixed to the seabed in order to withstand wave, current, and wind loads. Whereas fixed platforms have long been used owing to their convenient installation, the operatable water depth is significantly limited. jack-up platforms, in-service mainly at depths within 150m, behave like fixed platforms by penetrating their legs into the seabed, but transport in float before and after operation. A jack-up platform consists of a superstructure, hull, and three-to-six independent lattice legs, each with an underlying footing called a spudcan. The Legs need to be embedded until achieving sufficient bearing capacity. Especially in clay seabed such as in the Southwest Sea of South Korea, spudcans can penetrate up to three times their diameter or until meeting stiff soil (Menzies and Roper, 2008). In the operation phase after penetration, a jack-up platform is subjected to environmental loads in addition to the load of its own weight, applying combined loads to the spudcan. Combined loads applied to the spudcan can be simplified in their classification as vertical (V), horizontal (H) loads, and rotational moment (M).

Strength assessment of a jack-up system subject to environmental loads is dynamically sensitive to the stiffness of the spudcan foundation due to the limited number of supporting

legs(Cheng and Cassidy, 2016a). Simple support and linear soil springs have been often used as the simplest stiffness models, and recently, a force–resultant model based on a plasticity framework has been formulated as an alternative foundation model. Models that described the combined foundation capacity and the empirical yield envelope expressed in terms of allowable combinations of V, H, M loads were pioneered and developed by Butterfield and Ticof (1979), Roscoe and Schofield (1956), and Schotman (1989). In the intervening years, significant improvements have been achieved in terms of clay and sand, as represented in the model B and model C, respectively (Cassidy, 1999; Cassidy et al., 2004; Martin, 1994; Martin and Houlsby, 2001). These models for both clay and sand have been the basis for plasticity framework models as well as modified models (Cheng and Cassidy, 2016b; Zhang et al., 2014a). In particular, for single clays, extensive research has been conducted into strength non–homogeneity, cyclic loading, soil plugs, and consolidation (Gourvenec and Randolph, 2003; Ragni et al., 2017; Vlahos et al., 2006; Vulpe, 2015). Vlahos et al. (2008a) demonstrated the concept of tensile capacity using a centrifuge model test, and Zhang et al. (2014b) formulated a modified model B by combining improvements such as tensile capacity, non–associated plastic potential, and others. Centrifuge model tests have mainly been used in the development of foundation models, while additionally, numerical studies have been performed by Templeton (2009); Templeton et al. (2005); Zhang et al. (2011b). However, most of the conventional studies in this vein have used numerical

analysis that has assumed an embedded position of spudcans as wished-in-space, with no consideration of soil disturbance caused by spudcan penetration (Zhang et al., 2014b). Meanwhile, studies on multi-layered soil considering actual soil profiles also have been carried out. The relevant previous studies have mainly investigated conditions wherein a strong layer overlies a soft layer with a possibility of punch-through failure (Abyaneh et al., 2018; Hu et al., 2017; Ko et al., 2017; Rao et al., 2015; Yin and Dong, 2019); that is to say, there has been no detailed investigation into a foundation model in soft-over-stiff layered soil such as clay-over-sand or soft-over-stiff clay, wherein the squeezing effect is operative (Wang et al., 2018).

The present study aims to derive yield envelope for soft-over-stiff clay, a condition that is mainly prevalent in the Southwest Sea of Korea. Large deformation finite element (LDFE) analysis using the Coupled Eulerian-Lagrangian (CEL) technique is adopted to simulate spudcan penetration and to perform a subsequent combined loads analysis to determine the disturbed soil properties owing to penetration and obtain, thereby, the yield envelope. Prior to the case of soft-over-stiff clay, the yield envelope data for single clay with a deep-embedded spudcan is accounted for. It is found that the conventional yield envelope equation is well matched for single clay, even at deep embedment more than 1.5 times the spudcan diameter. Subsequently, the effect of the lower stiff clay on the yield envelope is examined in two aspects: ultimate capacity and normalized shape. The underlying stiff clay enlarges the yield envelope directly in the

vertical direction due to the squeezing effect, which in turn affects the horizontal and rotational directions. As mentioned above, the squeezing effect refers to the phenomenon where the upper soft soil is squeezed due to the lower stiff soil. With this effect, the vertical bearing capacity of the foundation increases significantly, and the yield envelope changes accordingly. Furthermore, the shape of the resulting yield envelope cannot be represented by a simple quadratic surface. Consequently, it is found that the conventional equation for single clay has a limitation in its utility to express results for soft-over-stiff clay. Accordingly, based on the form of the conventional formulation of the yield envelope for single clay, this paper proposes a modified equation that is applicable to soft-over-stiff clay.

3.2. Numerical methodology

3.2.1. Soil conditions and spudcan specifications

Offshore wind farms have been established in the Southwest Sea of South Korea, in which location a common soil profile is soft-over-stiff clay (Ahn et al., 2017; Jin et al., 2019). A wind turbine installation vessel (WTIV) of the jack-up type that is operated in this region needs to penetrate its legs into the stiff soil layer to ensure sufficient bearing capacity.

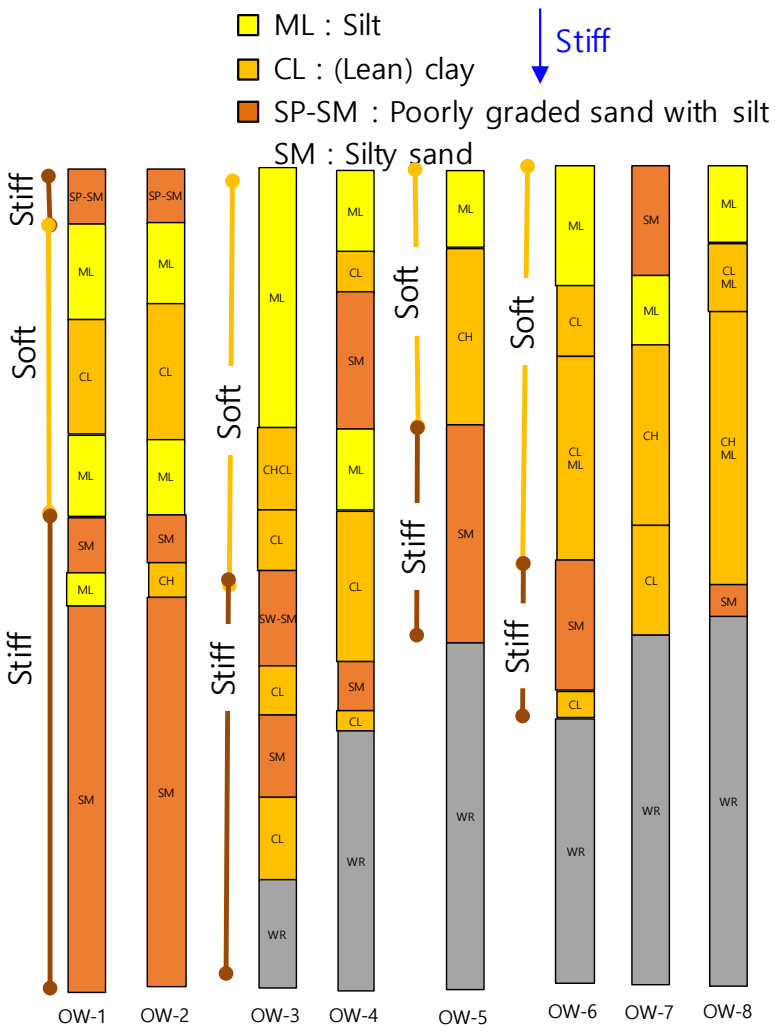

Fig. 23 Soil profiles of 8 boreholes in Southwest sea

Eight boreholes were drilled to investigate the soil properties of the southwest sea of South Korea (Fig. 23). The result is a soil profile consisting mainly of stiff−soft−stiff clay layer or soft over stiff clay layer. In the jack−up design, stiff clay near the seabed is not enough to obtain sufficient bearing capacity. That is why the jack−up leg should penetrate deeply until meeting the stiff soil.

When encountering such stiff soil, the spudcan is placed in the

transition area affected by both the upper soil clay and the lower stiff clay. However, the foundation model affected by both layers has not yet been established. In this study, soft over stiff clay is assumed as target soil of this study for simplicity.

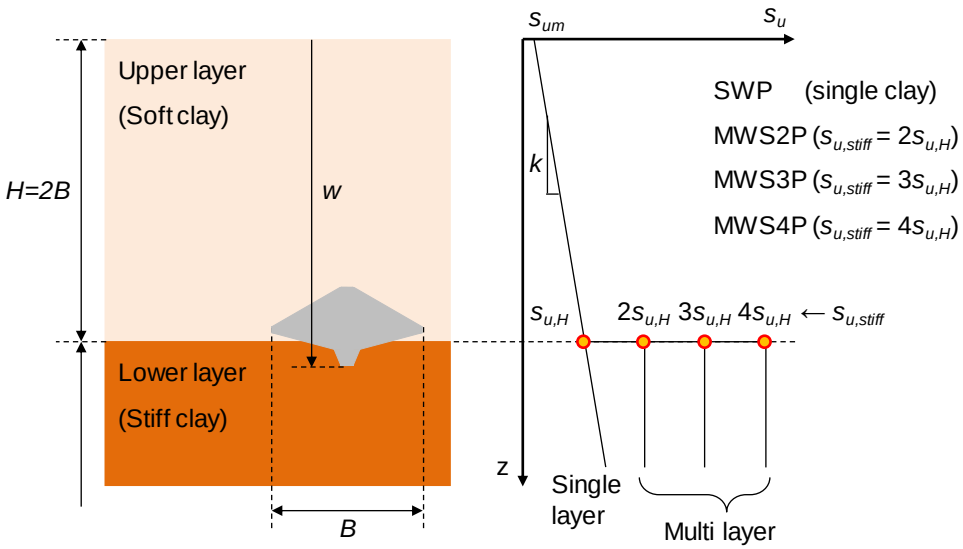

Fig. 24 Shear strength profiles of soft-over-stiff clay

Assuming this general soil condition of soft-over-stiff clay, the present study adopts representative soft marine clay properties for the upper layer. Menzies and Roper (2008) obtained Gulf of Mexico (GoM) jack-up data for spudcan specifications, soil properties and the corresponding observed vertical bearing capacity. Among these data sets, the spudcan specifications and clay properties for their site 1 are used in the present study to represent the upper soft clay layer. Also, an intact undrained shear strength of 2.4 kPa and an increasing slope of 1.35 kPa/m with depth are applied (s_u =

2.4+1.35z kPa). An averaged value of unit weight (γ = 5.36 kN/m^3) is assigned to the upper layer, and the general rigidity index and the Poisson ratio value of marine clay are used in the numerical analysis (E/s_u = 500, ν = 0.49). The height of the upper layer is modeled as 2.0B for the deep embedment necessary to achieve sufficient bearing capacity in soft clay.

In the case of the lower stiff clay layer, homogeneous undrained shear strength is assumed for the purposes of a simplified case study on soil stiffness. The stiff clay layer in multi-layered seabeds has often been assumed as homogeneous in literatures (Hossain and Randolph, 2010; Zheng et al., 2015; Zheng et al., 2016), and so accordingly, the lower stiff layer in the present study is also assumed to have uniform properties. The undrained shear strength is set as two, three, and four times the value at the interface of the upper layer, which cases are named MWS2P, MWS3P, and MWS4P, respectively. In fact, the realistic profile of soil has the continuous increase of s_u in the boundary of multi-layered soil. However, there is no exact information about soil profile in this transition zone. This detailed soil profile can affect the soil capacities like horizontal capacity, so the specific discontinuous soil profile has been used to clarify the lower clay effect. A comparative study on the effect of the lower stiff layer is performed using these three cases along with a single clay case (SWP). These cases and the corresponding shear strength profiles are illustrated in Fig. 24.

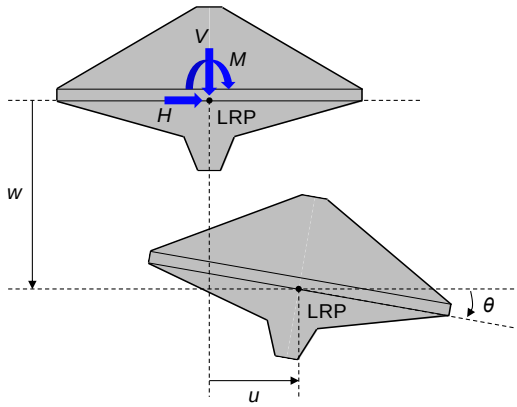

Fig. 25 Combined loads applied to spudcan (Zhang et al., 2014)

As noted earlier, a spudcan used in a real GoM field (Marathon LeTourneau Design, Class 166-C) is used as the basis for the simplified spudcan applied in the present study (Menzies and Roper, 2008). The simplified spudcan has a circular cross-sectional shape with same maximum bearing area. The slope of the lower conical geometry and the overall volume are maintained, but the sharp edge is smoothed out for numerical stability and cost efficiency. Therefore, the simplified spudcan has an equivalent diameter of 13.52m, a maximum bearing area of 143.6m^2, and a volume of 275m^3. Vertical, horizontal and rotational motions are loaded to the load reference point (LRP), the center of the lowest cross-section with the maximum bearing area. Displacements w, u, θ and reaction forces V, H, M in the vertical, horizontal, and rotational directions at the LRP, respectively, are given in Fig. 25.

3.2.2. Finite element model

A soil LDFE analysis based on the CEL technique and using the Abaqus/Explicit commercial program is performed to simulate soil behavior. Eulerian description is generally used to simulate the behavior of fluid, and so, in this description, the movement of the continuum is taken as a function of its instantaneous position and time. By comparison, Lagrangian description is mainly used for structural analysis with small deformation, and this description describes the movement of the continuum as a function of its initial coordinates and time (Qiu et al., 2009). Especially in large soil behavior problems such as spudcan penetration, Lagrangian description can incur mesh distortion. Eulerian description can solve this mesh distortion problem; however, it remains difficult to define an interface between structure and soil. Because the CEL technique overcomes each difficulty by taking advantage of both descriptions, spudcan penetration behavior has been simulated through this technique (Qiu and Grabe, 2012).

Soil properties change sensitively according to significant environmental disturbances. These clay properties are known to be dependent on both strain and strain rate (Einav and Randolph, 2005). In order to simulate the disturbed properties of clay, elasto-perfectly plastic material obeying a Tresca yield criterion incorporating strain softening and rate dependency is used. Einav and Randolph (2005) proposed the following equation of undrained shear strength as a function of strain softening and rate hardening

and this nonlinear model is presented in Eq.(2).

In the case of the upper soft layer, s_{um} is 2.4 kPa and k has the value of 1.35 kPa/m, as mentioned above. For general marine clay, the typical values of the parameters in Eq.(2) are provided below. The parameters in this study for the penetration and combined loads analysis (δ_{rem}=0.35, ξ_{95}=15, μ=0.1, $\dot{\xi}_{ref}$=1.0%/h) are adopted appropriately from within the following ranges:

- δ_{rem} (strength ratio) : 0.2 ~ 0.5
  (inverse of sensitivity S_t, 2 ~ 5)
- ξ_{95} (value of ξ for 95% remolding) : 10 ~ 25
- μ (rate parameter) : 0.05 ~ 0.20
- $\dot{\xi}_{ref}$ (reference strain rate) : 1 ~ 4%/h in triaxial sehar test, 20%/h in direct simple shear test.

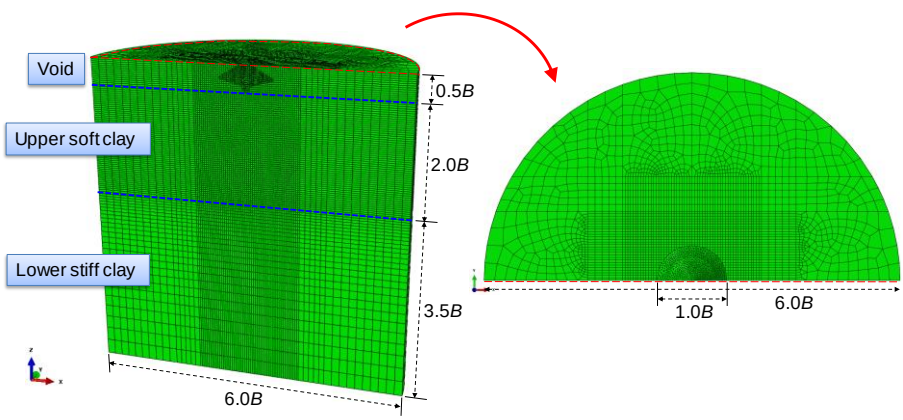

Fig. 26 Finite element model for constant V test and swipe test

The numerical analysis is performed using the CEL technique and the nonlinear undrained shear strength model. The geometry of the spudcan is face symmetric, and the vertical, horizontal, and

rotational motions also have symmetricity. Therefore, the half model and corresponding soil domain are modeled in this simulation (Fig. 26). The Eulerian element comprises 8-node linear brick elements with reduced integration (EC3D8R) for the soil domain, and the Lagrangian element comprises both a 6-node linear triangular prism element (C3D6) and an 8-node linear brick element with reduced integration (C3D8R) for the Spudcan structure. To avoid the boundary effect, a sufficiently large soil domain should be selected. Considering several previous numerical analyses such as penetration and combined loads analyses, 6.0B (=81.12m) of diameter and 6.0B of depth have been determined and validated through parametric study (Bienen et al., 2012; Ragni et al., 2017; Zhang et al., 2014b).

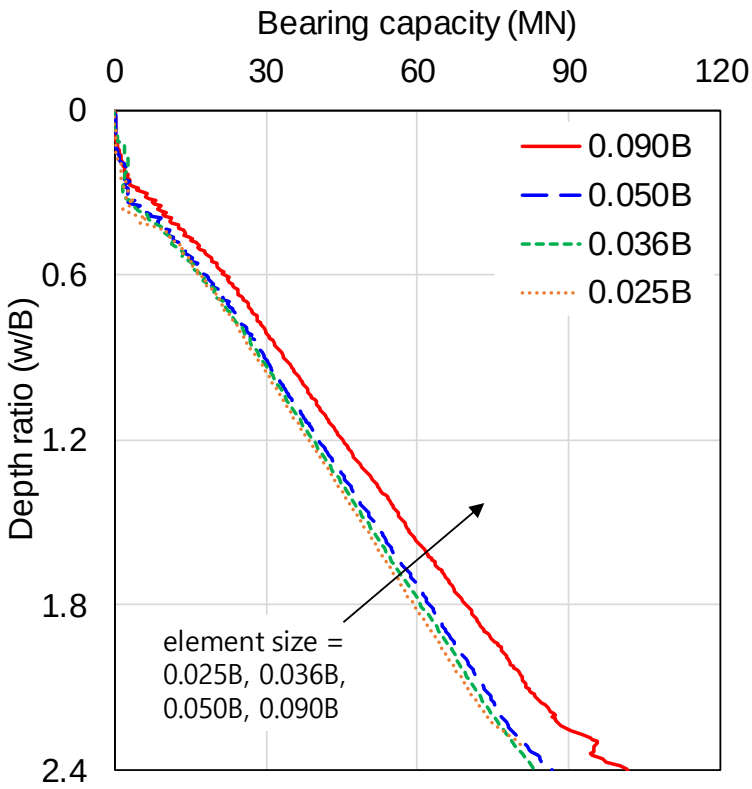

Fig. 27 Mesh convergence test in single spudcan analysis

A mesh convergence test has been carried out (Fig. 27), based on which, the spudcan and its surrounding mesh size used in this study are adopted as 0.05B (=0.676m). This fine mesh zone is modeled in the 3.0B range, with larger mesh sizes being used outside the region for computational efficiency. In the penetration analysis and subsequent combined loads analysis in this study, the coefficient of friction between the spudcan structure and the soil is assumed to be 0.1.

3.3. Penetration analysis to simulate soil disturbance

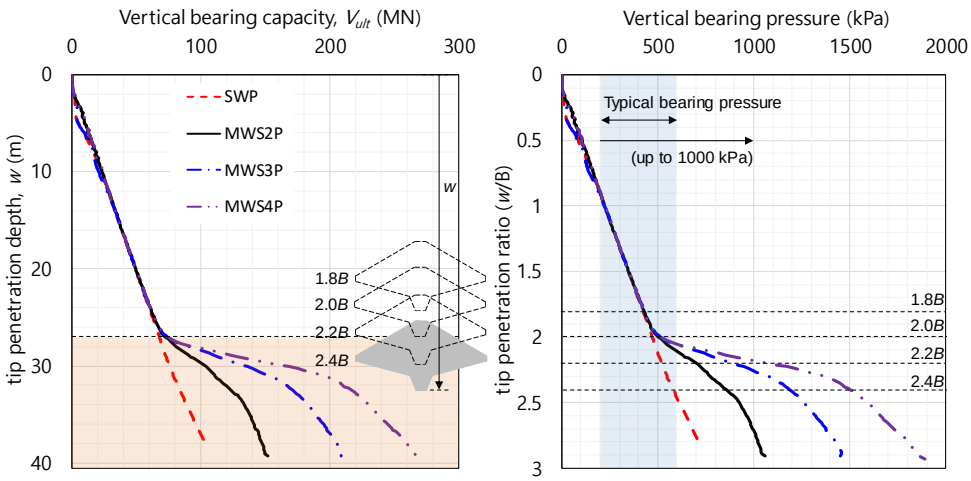

a) b)

Fig. 28 Penetration curve for soft-over-stiff clay;

a) Bearing capacity curve;

b) Bearing pressure curve and typical bearing pressure of jack-up

Penetration analysis, performed for consideration of disturbed soil properties due to large deformation, is completed prior to the combined loads analysis for the yield envelope calculation. The vertical bearing capacities for the soft-over-stiff clay cases (MWS2P, MWS3P, and MWS4P) as well as the single clay case (SWP) are shown in Fig. 28(b).

The effects of lower layer stiffness on the vertical bearing capacity can be checked in this penetration curve. As the spudcan tip passes to the boundary of the two layers, w = 27.04 m (= 2.0B), the squeezing effect starts to occur. The stiffer the clay is in place below, the larger the squeezing effect and the greater the increase

of vertical bearing capacity. On the basis of the depth at the boundary, 1.8B, 2.0B, 2.2B, and 2.4B are selected as the spudcan embedment for the yield envelope research. 1.8B shows a slight squeezing effect, which starts from the depth of 2.0B (the upper layer height). This squeezing effect becomes large at 2.2B, and the 2.4B embedment represents a situation wherein the maximum bearing area of the spudcan has passed to the boundary between the two layers. The calculated bearing capacity results for these penetration depths are shown in Table 3. There is little difference in these results according to the lower clay property at 1.8B, and the bearing capacity starts to vary at 2.0B. From the embedment of 2.2B, the bearing capacity has a larger value as the lower clay property becomes stiff. Typical spudcan bearing pressure is known to be in the range of 200 ~ 600 kPa, and a few cases have shown higher bearing pressures up to 1000 kPa (Hu & Cassidy, 2017). The penetration depths between 2.0B and 2.2B are calculated for the soft-over-stiff clay cases based on 600 kPa, which is generally the maximum bearing pressure. The stiffer cases, MWS3P and MWS4P, are also able to cover the specific case of 1000 kPa before 2.4B (Fig. 28(b)). Therefore, it can be thought that the selections of upper layer height and clay properties are appropriate in that the typical spudcan bearing pressure can be covered.

Table 3 Penetration results for single clay and several cases of soft-over-stiff clay

Bearing capacity (MN)				
w/B	SWP	MWS2P	MWS3P	MWS4P
1.8	60.70	61.86	61.83	61.97
2.0	68.15	72.56	74.41	74.82
2.2	75.00	99.53	127.44	153.64
2.4	83.25	123.27	170.84	216.44
Bearing pressure (kPa)				
w/B	SWP	MWS2P	MWS3P	MWS4P
1.8	422.78	430.87	430.71	431.64
2.0	474.70	505.45	518.29	521.16
2.2	522.41	693.29	887.71	1070.21
2.4	579.92	858.61	1190.01	1507.60

3.4. Combined loads analysis for single clay

3.4.1. Applied load sequence and load cases

Combined loads (V, H, M) analysis is conducted for the calculation of the yield envelope following the penetration analysis. This analysis is divided into two types of test, the swipe test and the constant V test. A commonly used swipe test has been

performed to outline the overall shape of the yield envelope. Both the compressive swipe test, which is the horizontal/rotational motion or combined motion after spudcan penetration, and the tensile swipe test, which is the motion after a small extent of extraction, are carried out. In addition, a constant V test is used to calculate the horizontal and rotational capacities at a specific constant vertical load. The obtainable results from the swipe test and constant V test are illustrated conceptually in Fig. 29. As shown in the figure, the overall shape of the yield envelope can be calculated through two swipe tests (blue line). Then, the maximum values of the horizontal/rotational directions are calculated through the constant V test (red line).

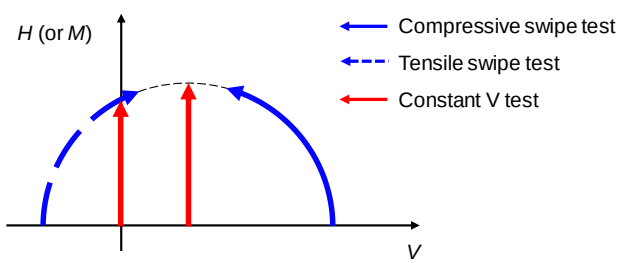

Fig. 29 Conceptualization of swipe test and constant V test

Through the swipe test, the combined critical state can be calculated from the load path after spudcan penetration and subsequent achievement of the critical state of the soil. Since it was adopted from the yield envelope studies by Tan (1990), the swipe test has often been used to calculate the yield envelope in conventional studies (Cassidy et al., 2004; Cheng and Cassidy, 2016;

Gourvenec and Randolph, 2003; Martin and Houlsby, 2000; Zhang et al., 2014a). The swipe test first moves the spudcan in a vertical direction by displacement control until the vertical capacity converges. The critical state is then maintained when the spudcan moves in the horizontal or rotational direction while fixing the vertical displacement. The critical load combination is calculated during the displacement controlled motion, and consequently, the load path tracks the yield envelope (Gourvenec and Randolph, 2003). The test is divided into the compressive and tensile swipe test, according to whether the vertical motion is penetration or extraction, respectively. In the present study, the approximate shape of the yield envelope is calculated using these swipe tests.

The constant V test has been used mainly in conventional studies to calculate the plastic behavior of soil. However, calculating the reaction force through the displacement-controlled motion occurring in a specific environment is the most common way to calculate the capacity. In this study, the specific point in the yield envelope is calculated by this test, especially a capacity at $V = 0$ and the maximum capacity in the horizontal or rotational direction (red line). Existing studies have indicated that the maximum value of horizontal/rotational capacity is reached at the median of the compressive and tensile vertical capacities (Vlahos et al., 2008; Zhang et al., 2013), and this is also shown in the numerical analysis of the present study. After calculating the compressive and tensile vertical capacities from the penetration and extraction motion, the median value is loaded vertically. While the vertical load is kept

constant, the horizontal/rotational movement is given. The converged reaction force in each direction is defined as the horizontal and rotational maximum capacity, respectively.

At the various spudcan embedments (1.8B, 2.0B, 2.2B, and 2.4B), capacity calculations and combined loads analyses for the yield envelope are carried out for both the single clay and soft-over-stiff clay cases. Prior to the multi-layered clay cases, a numerical analysis for single clay is conducted with the different embedments. The results for above the 1.4B embedment are recorded and validated against the existing theories suggested for single clay at a shallow depth. The capacities at 1.4B are additionally calculated for comparison. Then, the capacities in the three directions and the yield envelopes are calculated for the soft-over-stiff clay cases. Owing to the lower stiff clay, spudcan embedment and soil stiffness can affect the capacities and yield envelopes. The representative soft-over-stiff clay case (MWS2P) is selected for the case study with various embedments. Also, for the same penetration depth (w = 2.2B), the calculated yield envelope results are analyzed by changing the stiffness of the lower clay (MWS2P, MWS3P, MWS4P). The results from the softest case (SWP) to the stiffest case (MWS4P) for the effect of the lower stiff clay on the yield envelope are analyzed according to spudcan embedment and the soil properties.

3.4.2. Maximum capacity analysis for single clay

As mentioned earlier, the maximum capacities are calculated by constant V test. Fig. 30 shows the load−displacement ($H-u$) curve in the horizontal direction and the moment−rotation ($M-\theta$) curve in the rotational direction. The displacement−controlled motion is applied in the horizontal and rotational directions under the vertical median load between the compressive and tensile vertical capacities. Consequently, as in the experiments with plastic materials, the linear $H-u$ ($M-\theta$) relationship is shown until the yield point and then gradually converged in the plastic region. The converged values of H and M are defined as the horizontal and rotational maximum capacities (H_o and M_o), respectively. At this time, the location of the convergence point can have a significant effect on the calculation of the capacity. Based on the yield point, which is the end of the linear relationship, the convergence load becomes too small. If the displacement is applied until load convergence, it is difficult to determine the end, because the load and moment continue to increase little by little due to the characteristics of the nonlinear material. For this reason, a clear criterion is needed to determine the convergence. In previous research, the maximum capacity was defined based on a displacement of 0.5% diameter in the horizontal direction (Martin and Houlsby, 2000). Vlahos et al. (2008a) presented the horizontal load−displacement relationship until $0.035B$, and Cassidy et al. (2006) and Zhang et al. (2013) described the displacement up to $0.15B$ and $0.083B$ for clay and sand,

respectively. Taken together, it can be confirmed that the convergence is sufficiently satisfied if the horizontal displacement of $0.1B$ is considered as the criterion. In the present study, convergence loads corresponding to 4, 7, and 10% diameters (u = $0.04B$, $0.07B$, $0.1B$) are defined as the horizontal maximum capacity. The rotation multiplied by the diameter ($B\theta$) is also used on the same basis as the horizontal displacement (u), so the moment at the $B\theta$ of $0.04B$, $0.07B$ and $0.1B$ are calculated as the rotational maximum capacity. As such, since the convergence point can affect the capacity results, the equations of yield envelope are proposed with three different criteria. No matter which criterion is adopted, reasonable conclusions can be drawn if the capacity is calculated on a consistent basis for convergence.

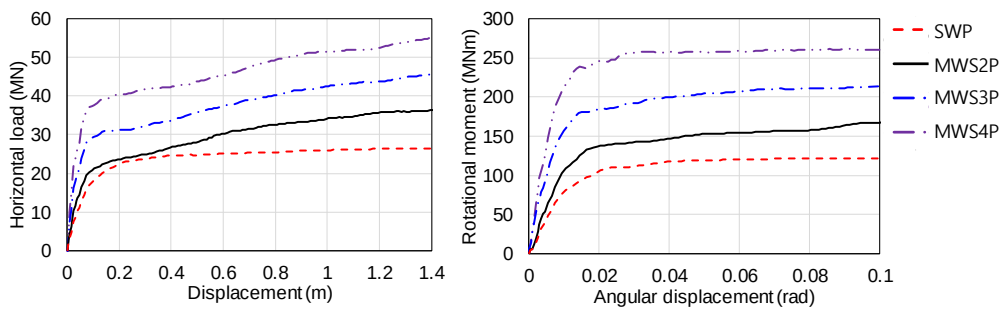

a) b)

Fig. 30 Load(Moment)−displacement(rotation) curve;
a) in horizontal direction; b) in rotational direction

$$h_o = \frac{H_o}{V_{ult}} \tag{3}$$

$$m_o = \frac{M_o}{V_{ult}} \tag{4}$$

The horizontal and rotational maximum capacities of single clay are calculated, and the results are shown in Fig. 31. h_o and m_o are the maximum capacity ratio and the mean of the horizontal maximum capacity and rotational maximum capacity divided by the vertical ultimate capacity, respectively (Eq. (3), (4)). These ratio values are used to compare the maximum capacities on the same basis as in the conventional studies. First, as mentioned above, the maximum capacities are calculated by using the constant V test. This test can calculate the horizontal/rotational capacity for the specific vertical load under which other factors are not taken into account. However, conventional studies such as that of Zhang et al. (2014c) have calculated the maximum capacities by regression of the peak from the swipe test results. Conventional studies suggested that the yield envelope from numerical analysis accords the ellipsoid, and that the yield envelope from the centrifuge test follows the paraboloid. In consideration of this, in the present study, both the elliptic and parabola shapes are fitted to the swipe test results of each VH, VM plane. The regressed peak values of the two shapes are illustrated with the results of conventional studies in Fig. 31.

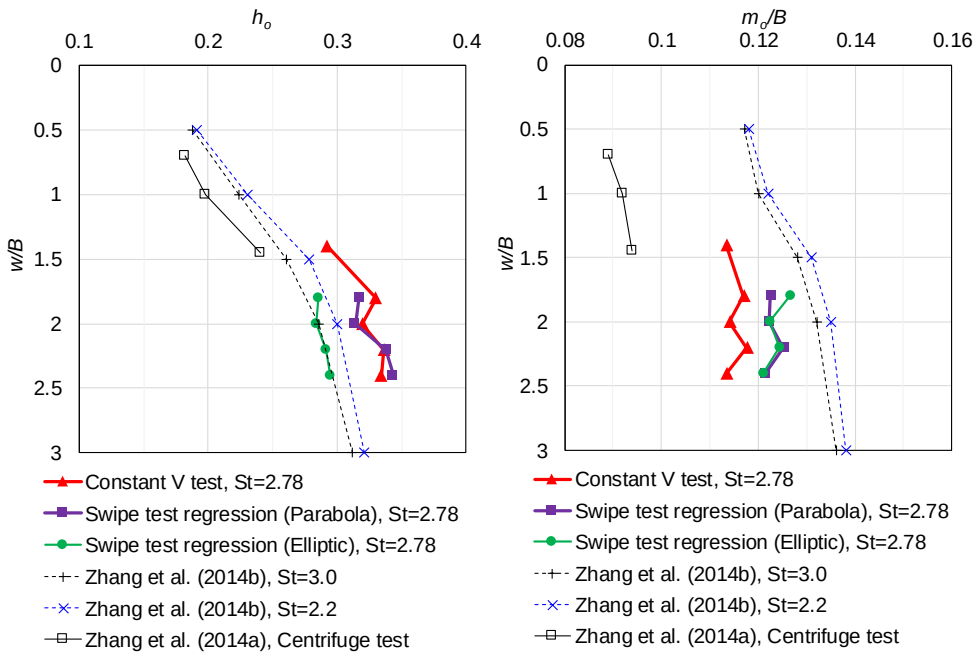

a) b)

Fig. 31 Comparison of maximum capacity ratio;
a) horizontal direction; b) rotational direction

In Fig. 31(a), the calculated horizontal maximum capacity ratio (h_o) is compared with the results from the centrifuge tests and numerical analyses of conventional studies (Zhang et al., 2013; Zhang et al., 2014b). The two numerical analysis cases that can cover the sensitivity of 2.78 used in the present study are presented (S_t = 2.0, 3.0), and the regression results for the elliptic shapes exist between those cases. The results of the constant V test and the regression with the parabola have a larger value of about 0.33. In the numerical results of the previous study, the slope of the h_o value decreased as the embedment increased, which is the same as the result of the present study. For 1.4B, the h_o value is smaller

than 0.3, but approaches to a larger value for $1.8B$ and above. The results of the centrifuge test exist only below $1.45B$ of embedment, and the ratio value also increases as the depth increases in that range. In summary, it is found that h_o increases linearly with embedment up to a specific depth (about $1.5B$). After that depth, the rate of increase decreases and h_o finally comes close to a certain value, about 0.33.

The ratio values of rotational maximum capacity (m_o/B) are shown in Fig. 31(b) in the same way as in the horizontal direction. The m_o/B values of this study are found to exist between the numerical analysis and the centrifuge test results of conventional studies. In the previous study, the slope in the rotational direction was smaller than that in the horizontal direction, and the same result is shown in this figure. The m_o/B values from the constant V test at embedments from $1.4B$ to $2.4B$ have a similar value of about 0.115, and the regression results also converge near 0.12. Unlike the horizontal direction, the maximum capacity in the rotational direction can be considered to show a relatively similar trend to that of the vertical ultimate capacity, due to the converged capacity ratio.

3.4.3. Yield envelope in single clay

Fig. 32(a) summarizes the calculated yield envelope results for the vertical–horizontal (VH) plane, vertical–rotational (VM) plane, and horizontal–rotational (HM) plane in the case of single clay. Combined loads analyses are carried out for the embedments of 1.8B, 2.0B, 2.2B and 2.4B, respectively. The size of the yield envelope increases regularly as the embedment deepens. The uniform spacing of the graphs means that the shapes of the yield envelope are similar, which phenomenon can also be seen in the normalized yield envelope (Fig. 32(b)). The graphs in Fig. 32(a) are normalized using the vertical ultimate capacity (V_{ult}) in the vertical direction, and the capacities at $V = 0$ in the horizontal/rotational directions ($H_{V=0}$, $M_{V=0}$), respectively. These values represent the vertical positive intercept, the horizontal intercept, and the rotation. In the single clay, the normalized yield envelopes all have a similar shape in the VH, VM, and HM plane, regardless of the embedment. Since the normalization process divides the influence of the two factors of the yield envelope, the size and shape are analyzed separately.

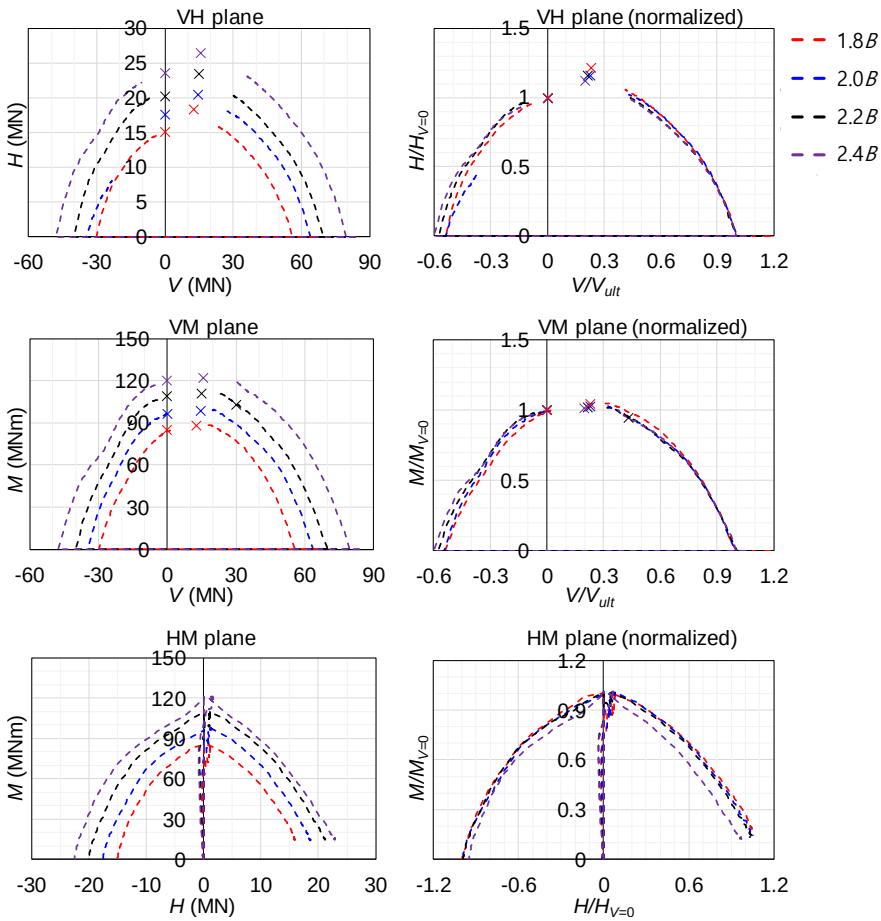

a) b)

Fig. 32 Numerical analysis results of SWP; a) Load path; b) Normalized shape with each intercept

In the VH, VM planes, the shape has a vertex defined as the maximum horizontal/rotational capacities at the median between the compressive and tensile vertical capacities. This load path is shaped like a quadratic curve, which is consistent with the results of Vlahos et al. (2008a) and Zhang et al. (2013) considering the tensile capacity. Backfill soil has a significant impact on the calculation of tensile capacity, which has already been considered in this study.

However, time effects such as consolidation and suction effects have not considered in this study. The calculated tensile capacity ratio is similar to the value in the existing centrifuge model test, and it is used as it is. However, it is considered that a more accurate yield envelope can be calculated by using the tensile capacity reflecting these effects.

The yield envelope at deep embedments above $1.5B$ through numerical analysis is calculated in the present study, unlike the existing studies which used relatively shallow embedment. The normalized yield envelope illustrates that the embedment does not affect the yield envelope shape, and so the conventional analytic equation for shallow depth can also be applied to the deeper case. This conventional equation is fitted to the single clay results at deep embedments in the present study, and the regression results are reported in Table 4.

Table 4 Parameters fitted with conventional equation of single clay

	W	h_o	m_o	e	χ
Centrifuge test (Zhang et al., 2014a)	0.7D	0.182	0.089	0.380	0.6
	1.0D	0.198	0.092	0.244	0.6
	1.45D	0.242	0.094	0.150	0.6
Numerical analysis (present study)	1.8B	0.317	0.123	0.140	0.54
	2.0B	0.314	0.122	0.118	0.54
	2.2B	0.338	0.125	0.079	0.58
	2.4B	0.344	0.122	0.053	0.60

The h_o and m_o values of Table 4 are also presented in Fig. 31 above, where the conventional centrifuge test data is the black line with empty square points, and the numerical analysis result is the purple line with filled square points. The trend in the centrifuge test that appears as the embedment increases is also continued in the numerical analysis. The eccentricity continues to decrease, so that the yield curve approaches symmetry, and the tensile capacity ratio (χ) has a similar value of 0.6. This slight eccentricity is presented in the HM plane. Zhang et al. (2011a), who performed a small-strain finite element (SSFE) analysis below the $1.4B$ depth, documented that the deeper the embedment, the more minor the eccentricity. The embedment covers in the present study ranged from $1.8B$ to $2.4B$, and the earlier study noted above also has determined that the eccentricity is not significantly revealed at these depths. The normalized shapes of the HM plane are grouped as one regardless of embedment, like those of the VH, VM planes. This shows that, in the formulation of the yield envelope, size and shape can be considered separately through the normalization process.

3.4.4. Soil flow mechanism in combined loads analysis

Combined loads analyses are subsequently performed on the soft-over-stiff clay, which is the target soil of the present study. Fig. 33 shows the soil behavior of each motion when the tip of the spudcan has touched the boundary. As can be seen in Fig. 33(a), when the spudcan penetrates vertically, the soil below is first

pressed. At the same time, the soil on both sides moves upward, and so the soil below flows round and rises up. This flow of soil is called backflow, and ISO (2012) suggests an analytic equation for this. As such, the lower soil has a great influence on the vertical behavior of the spudcan. On the other hand, the horizontal behavior of the spudcan causes movement of the lateral and upper soil (Fig. 33(b)). When the spudcan rotates, the around soil rotates in the same direction (Fig. 33(c)). The right-side soil of the spudcan moves downward and the left-side soil moves upward, and so both the soil below and above affect the rotational behavior of the spudcan. The main concern for soft-over-stiff clay is the existence of lower stiff clay. Penetration behavior is predicted to be strongly influenced by the underlying soil, whereas horizontal behavior is predicted to be relatively independent. Rotational behavior, meanwhile, is expected to be affected by both the upper and lower soils, depending on the side of the spudcan.

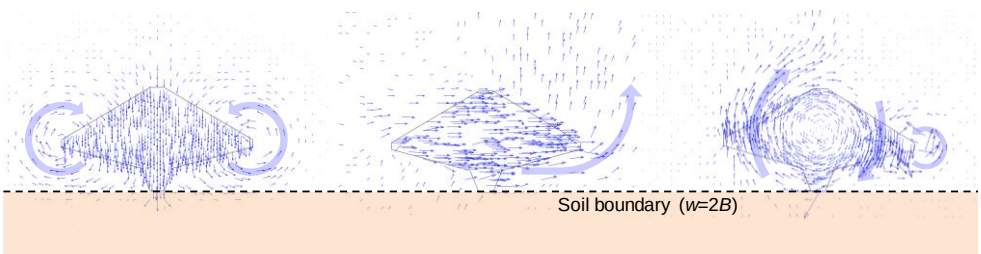

a) b) c)

Fig. 33 Soil flow in combined loads analysis; a) vertical direction; b) horizontal direction; c) rotational direction

3.5. Combined loads analysis for soft-over-stiff clay

3.5.1. Maximum capacity for soft-over-stiff clay respecting embedment

Fig. 34 shows the horizontal and rotational maximum capacities in a soft−over−stiff clay case (MWS2P), under the vertical median load between the compressive and tensile vertical capacities. The calculated results from the constant V test are plotted according to the embedment and the lower soil properties. The penetration results for soft−over−stiff clay and single clay show very little difference until the spudcan tip reaches 2.0B, the soil boundary (Fig. 34). The maximum capacity calculation of the embedment from 1.8B to 2.4B is performed to cover the range with and without influence from the lower stiff soil. The maximum capacity is greater with deeper embedment, due to stiffness, pressure, and so on. This tendency is presented not only in the vertical capacity, but also in the horizontal/rotational capacity in Fig. 34(a). The single clay results (the red dashed line) increase nearly linearly with increasing depth, whereas the soft−over−stiff clay shows a sharp increase in capacity values near 2.2B. When the spudcan tip penetrates more than 2.0B, the squeezing effect begins to occur, and 2.2B is the depth affected by the lower stiff clay, while 2.4B is the point where the maximum bearing area of the spudcan penetrates into the lower stiff clay, thus resulting in increased capacity.

Fig. 34(b) shows the ratio of the maximum capacity in the

horizontal/rotational directions to the vertical ultimate capacity. In the case of the horizontal direction, the ratio of the maximum capacity decreases at the depth of 2.2B. According to the soil flow mechanism and Wang et al. (2018) and Wang et al. (2019), the horizontal behavior of the spudcan is affected by the lateral soil. The laterally projected area of the spudcan is not overlapped with the lower stiff clay, and so the horizontal behavior is less affected by the lower stiff clay than is the vertical capacity. As the horizontal capacity increases less than the rapidly increasing vertical capacity, the ratio value starts to decrease at 2.2B. However, at 2.4B, where most of the spudcan has penetrated the soil, the laterally projected area overlaps much with the lower clay. This causes the horizontal capacity to be much larger, and the ratio value increases compared to the 2.2B depth. Regardless of the underlying soil stiffness and embedment, it is found that the ratio value in the stiff clay region becomes smaller than that of single clay, due to the squeezing effect.

The ratio value in the rotation direction shows a difference from the horizontal direction. The slightly reduced ratio value at 2.2B starts to decrease significantly at 2.4B. As shown in Fig. 33(c), the rotational behavior of the spudcan causes movement of the surrounding soil, and so both the soil below and above affects the capacity. Unlike the horizontal direction, a side of the maximum bearing area of the spudcan is pressed against the lower stiff layer at 2.2B (Fig. 33(c), right). As the squeezing effect occurs in that area, the rotational capacity also increases significantly. The capacity ratio decreases due to the left side, which is less affected

by the lower stiff clay, but the difference is small. However, as the spudcan penetrates, no further squeezing effect occurs, and the movement of the opposite side raises the upper soft clay. As a result, the rotational capacity does not increase much compared with the vertical capacity, which is affected directly by the lower stiff clay, and consequently, the capacity ratio decreases at 2.4B.

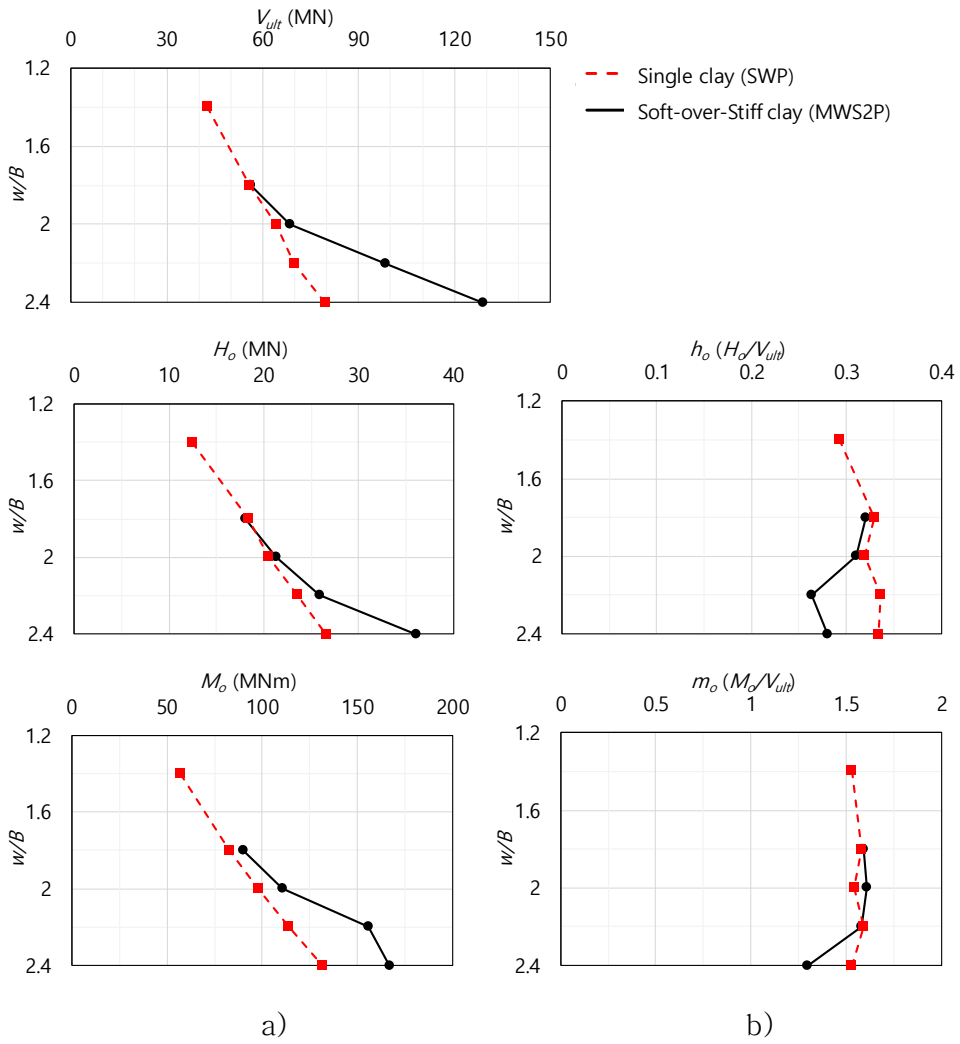

Fig. 34 Constant V test results for depth; a) maximum capacity; b) maximum capacity ratio

3.5.2. Maximum capacity in soft-over-stiff clay for lower clay properties

Fig. 35 shows the trend of the maximum capacity according to the stiffness of the lower clay. The results of the combined loads analysis in the $1.8B$ case, which show little difference between single clay and soft-over-stiff clay, are presented first. And then, the maximum capacities and the capacity ratios at the $2.2B$ and $2.4B$ depths represent the region affected by the lower stiff clay. At $1.8B$, where the spudcan tip does not reach the soil boundary, the soft-over-stiff clay has similar vertical, horizontal and rotational capacities to those of the single clay (Fig. 35(a)). This result is also consistent with the capacity results respecting embedment. In the regions where there is no effect from the lower stiff clay, the single clay and soft-over-stiff clay shows the same results.

At the graph about the maximum capacities of $2.2B$, the effects of the lower stiff clay are presented in Fig. 35(b). As the undrained shear strength of the lower clay becomes two, three, and four times stiffer than that of the upper soft clay, the maximum capacities in the horizontal/rotation direction all increase. Large capacities relative to single clay reflects a large effect of the lower layer, which has also been demonstrated by the tendency according to which stiffer lower clay properties mean greater maximum capacity values. In comparison, the maximum capacity ratio for the vertical ultimate capacity decreases as the lower clay properties become stiffer. The horizontal capacity is greatly reduced, and the rotational capacity is

small but also tends to decrease. As mentioned above, the horizontal behavior has been affected by the lateral soil, not the underlying soil, and so the horizontal capacity in the soft-over-stiff clay does not increase as much as the vertical capacity does. As a result, the horizontal maximum capacity ratio is greatly reduced. However, the rotational behavior is found to be related to the lower stiff soil, as it is influenced by both the soil below and above, and accordingly, the maximum capacity increases significantly according to the stiffness of the lower clay. Since this increase rate is smaller than that of the vertical capacity due to the squeezing effect, the capacity ratio decreases slightly as a result.

The maximum bearing area of the spudcan crosses the soil boundary at $2.4B$ of spudcan tip penetration, and so the squeezing effect is stronger and the trend mentioned in the previous paragraph becomes more pronounced (Fig. 35(c)). As shown in Fig. 34(a), the horizontal capacity starts to be affected by the lower clay at $2.4B$ because the spudcan laterally significantly overlaps the lower ground, and thus too, the capacity value is slightly increased. Nevertheless, the rate of increase in vertical capacity is the greatest, and the capacity rate decreases accordingly. The same phenomenon happens in the rotation direction. The value of maximum capacity increases due to the lower stiff clay; however, the capacity ratio for the vertical capacity decreases as the lower clay becomes stiffer.

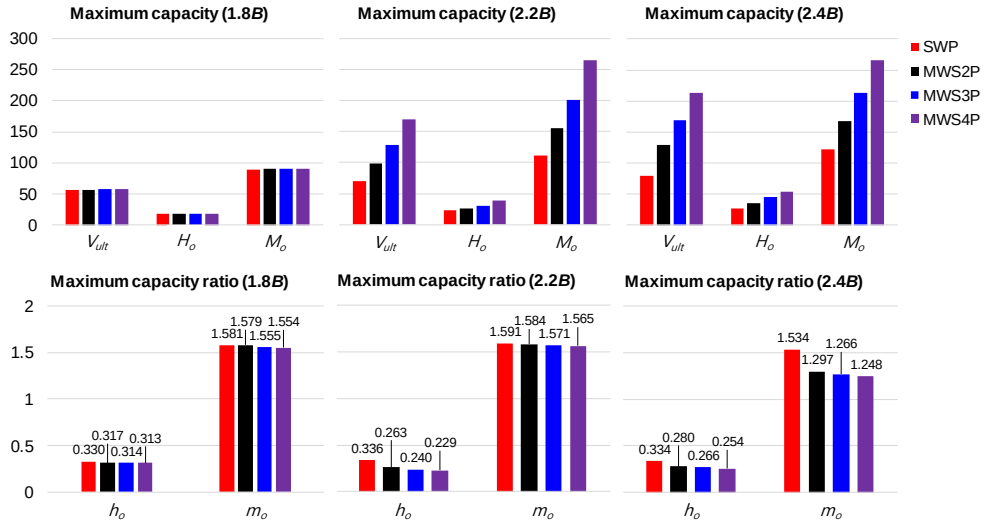

a) b) c)

Fig. 35 Constant V test results for lower clay properties;

a) w=1.8B; b) w=2.2B; c) w=2.4B

3.5.3. Yield envelope in soft-over-stiff clay respecting embedment

Fig. 36 shows the results of the yield envelope calculation for different depths of soft-over-stiff clay, the target soil of this study. The MWS2P case, where the undrained shear strength of the lower clay is twice the boundary value of the upper clay, is selected as the representative case. As with the case of single clay, the yield envelopes are shown for the VH, VM, and HM planes.

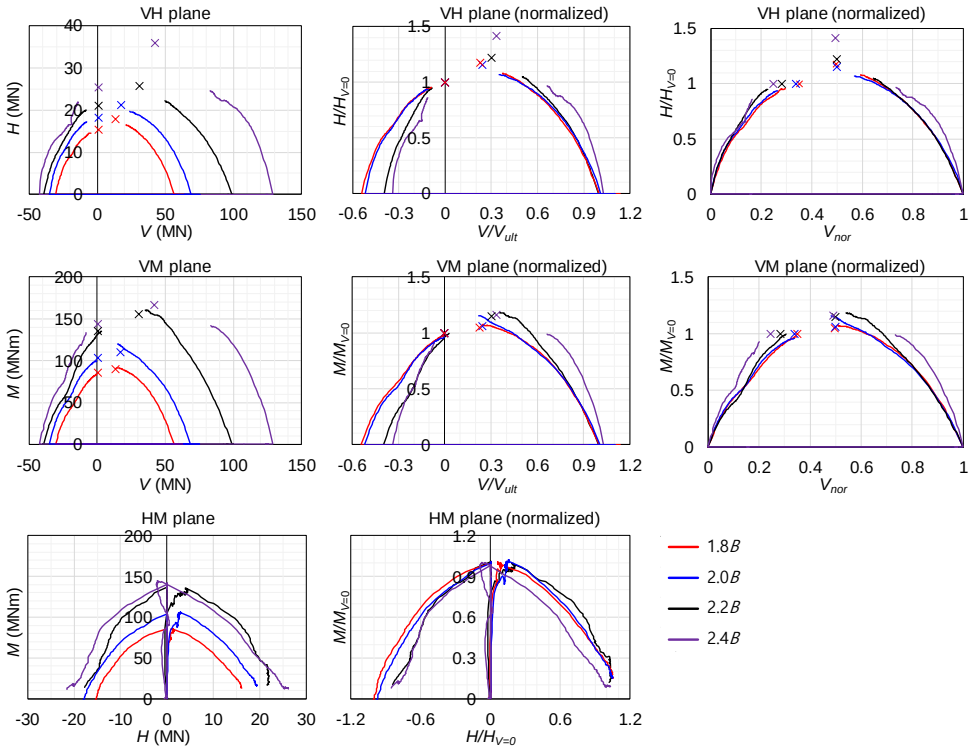

a) b) c)

Fig. 36 Numerical analysis results for MWS2P respecting depth; a) Load path; b) Normalized shape with each intercept; c) Normalized shape considering vertical tensile capacity

The increase in the compressive maximum vertical capacity can be seen in the yield envelopes of the VH, VM planes (Fig. 36(a)). This trend is also shown in the results for the penetration curve in Fig. 28. As the spudcan approaches the lower stiff clay, the deeper the depth, the greater the vertical capacity due to the squeezing effect becomes. In comparison, the tensile maximum vertical capacity does not increase significantly. The tensile capacity is calculated from the extraction of the spudcan, which is mainly influenced by the soft clay of the upper part. This change in vertical

capacity causes the center of the yield envelope to move to the right. The maximum capacity in the horizontal and rotational directions is calculated at this center point by moving along the vertical direction. As with the trend of maximum capacity, the yield envelope results from the swipe test consistently show increasing capacity. The deeper the embedment, the larger is the yield envelope in all directions.

Fig. 36(b) shows the yield envelope normalized to the compressive maximum vertical capacity, horizontal capacity at $V = 0$, and rotational capacity at $V = 0$, respectively. For the VH, VM planes, the yield envelope of $2.0B$ depth is similar to that of $1.8B$. There is little effect of the lower stiff clay at the embedment of $2.0B$, so that the shape is consistent as in the case for the single clays. However, the shape starts to change from $2.2B$, when the effect of the lower stiff clay begins to be not negligible. It is found that the tensile capacity does not increase relative to the compressive maximum vertical capacity, which increases due to the squeezing effect, and thus the normalized shape narrows in the tensile part. The tensile capacity is normalized as the tensile capacity ratio (χ), and it is found that χ gradually decreases from the typical value of single clay, about 0.6. This trend is further exacerbated at $2.4B$, where the effects of the lower stiff clay are greater.

Narrowed shape in the vertical direction makes the effect in the horizontal/rotational direction less obvious. The normalization method is changed in the vertical direction as depicted in Fig. 36(c),

so the maximum capacities at the different embedments gathers at a line. In Fig. 36(c), the yield envelope is normalized to have a value between 0 and 1 in the vertical direction. It is first horizontally shifted first by the tensile capacity and then is divided by the sum of the tensile and compressive capacities. The tensile capacity is defined as χV_o using the definition of the tensile capacity ratio used in the existing equation, and the equation summarized using this is shown in Eq. (5).

$$V \quad \rightarrow \quad V_{nor} = \frac{V + \chi V_o}{(1+\chi)V_o} \tag{5}$$

where V: Vertical reaction force in load path, V_o: Vertical ultimate capacity (compressive capacity), χ: Tensile capacity ratio.

Fig. 36(c) shows that deep embedment makes the ratio of the maximum capacity ratio large. As in the vertical direction, the shapes rise in the horizontal/rotational direction from the embedment of $2.2B$, and the maximum capacity ratio also increases. The ratios of the maximum capacity and intersection point at V=0 are constant in the case of single clay, so that the peak matches; however, lower stiff clay ensures that the horizontal/rotational capacities do not increase at a constant rate with respect to other vertical loads. This effect should be considered at the yield envelope of soft-over-stiff clay.

The yield envelope in the HM plane shows a different trend from the VH and VM planes. As indicated in Fig. 36(a), the deeper the

embedment, the larger the yield envelope. However, if the calculated yield envelope is normalized to the horizontal and rotational capacities at $V = 0$, the shape becomes similar regardless of the embedment. It is noted earlier that the tensile part is calculated from the extraction behavior of the spudcan and is affected by the upper soft soil. The point $V = 0$ is close to the tensile maximum vertical capacity, and so its cross-section, the yield envelope in the HM plane, is more affected by the upper soft soil. For this reason, it can be determined that the yield envelope in the HM plane is less affected by the lower stiff clay than in the VH and VM planes.

3.5.4. Yield envelope in soft-over-stiff clay for lower clay properties

In order to analyze the effect of lower stiff clay in detail, the yield envelope is plotted for varying undrained shear strengths of the lower layer (Fig. 37). It is noted above that the characteristics of single clay and soft-over-stiff clay diverge from $2.2B$ of embedment. Accordingly, with the $2.2B$ embedment fixed, the swipe test are performed when the undrained shear strength of the lower clay is two, three, and four times the boundary value of the upper clay, and those results are showed in Fig. 37. Those cases are named MWS2P, MWS3P, and MWS4P, and are plotted with the single clay case (SWP) for comparison.

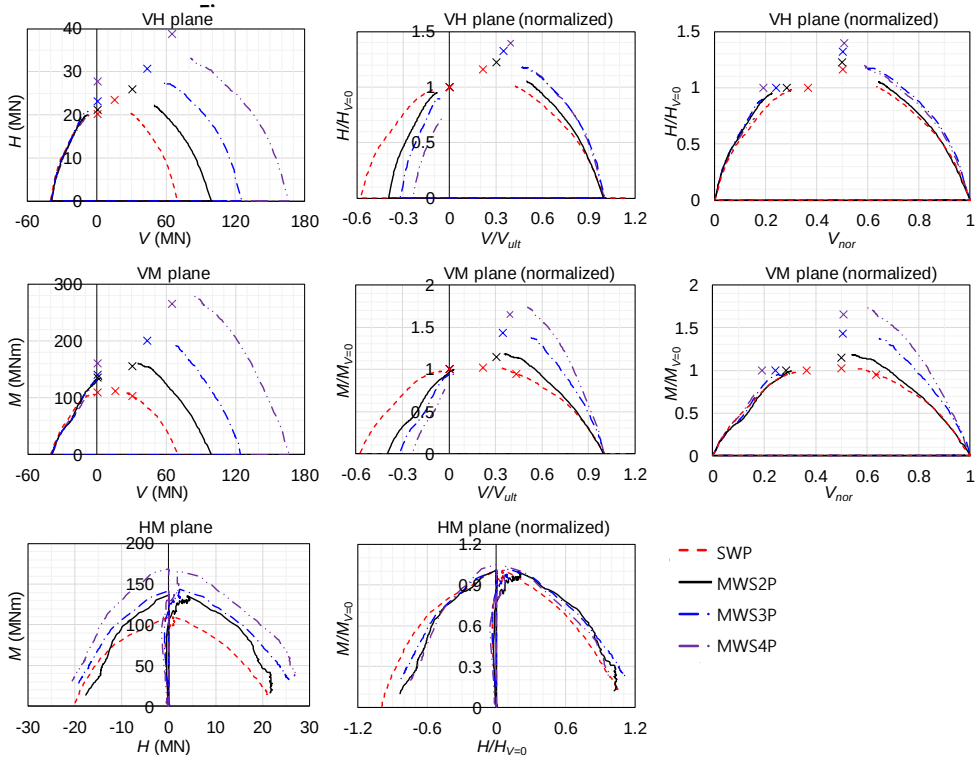

a) b) c)

Fig. 37 Numerical analysis results for lower clay properties at w=2.2B; a) Load path; b) Normalized shape with each intercept; c) Normalized shape considering vertical tensile capacity

Fig. 37(a) shows the calculated yield envelope according to the lower clay properties. There is a larger vertical capacity in the stiffer lower clay in the penetration curve, which is also presented in the compressive maximum vertical capacity of the yield envelope. On the other hand, it is apparent that the tensile capacity has a constant value regardless of the stiffness of the lower clay. From the results for embedment, it has already been concluded that the tensile capacity is less affected by the underlying soil. These results

according to the stiffness of the lower clay clearly indicate that the tensile capacity is little related to the lower stiff clay. These effects make the tensile part fixed and enlarge the yield envelope in the compressive direction. It can also be found that the maximum capacity increases in the horizontal and rotational directions as the lower clay stiffens. Just as the deeper embedment makes the effect of the lower clay increase, the stiffness of the lower clay also increases this effect.

The normalized shapes in Fig. 37(b) show the effect of the lower stiff clay, which increases with stiffness. As in the Fig. 36(b), the calculated yield envelopes are normalized using the intercept value of each axis. The width of the yield envelope is narrowed due to the decreasing tensile capacity ratio (χ). The ratio decreases due to the increasing compressive capacity relative to the constant tensile capacity. Fig. 37(c) shows the modified normalization in the vertical direction as in Eq. (5) considering the tensile capacity. According to the stiffness of the lower clay, the shape and the maximum capacity ratio are increased in the horizontal/rotational direction. All of these trends are identical to those observed at the embedments of $2.2B$ and $2.4B$, and so they can be considered to be characteristic of the shape of the yield envelope due to the lower stiff clay.

In the HM plane of Fig. 37, similar results are found between single clay and soft-over-stiff clay. The calculated yield envelopes are larger when the lower clay becomes stiffer, but similar when normalized. As with the results in Fig. 36, it is found that stiff clay affects the VH and VM plane sections of the yield envelope, but the

HM plane section less so. In this study, the effects of lower stiff clay in the VH and VM planes are quantified into an analytic expression. For the HM plane, since the soft-over-stiff clay has a shape similar to that of the single clay, the existing formula of the single clay is used as is.

3.6. Yield envelope equation proposed for soft-over-stiff clay

3.6.1. Derivation of the quadratic curve in the VH, VM plane

Keeping the form of the single clay equation suggested in the previous studies, an analytic equation that can express the yield envelope for soft-over-stiff clay is proposed. The equation for the yield envelope of single clay has been sought after in various studies. ISO (2012) has suggested a yield envelope equation with interpolating paraboloid and ellipsoid using a depth coefficient. In addition, spudcan-soil adhesion can be considered to provide additional horizontal and rotational capacity. Recently, a yield envelope in the form of a paraboloid in consideration of the tensile capacity was presented in Zhang et al. (2013) via a centrifuge model test. With reference to these equations, this paper intends to present an analytical equation that can represent soft-over-stiff clay in consideration of its tensile capacity.

Before presenting the analytic expression, the normalization

method is modified in order to express the result of the swipe test as a representative shape. In the vertical direction, the yield envelope is normalized to have a value between 0 and 1 (Eq. (5)). In the horizontal and rotational directions, the calculated load path is normalized using the maximum capacity in each direction (Eq. (6), (7)). The maximum capacity value is obtained using the constant V test at the specific vertical load, and the swipe test results are divided by this value. All normalized values should be between 0 and 1 in theory. However, in Fig. 38, there are some graphs that are expected to exceed 1 at the vertex. This is due to the fact that, because of the calculation procedure of the constant V test, a slight difference can exist between the calculated maximum capacity from the constant V test and that from the swipe test. In numerical analysis, instability occurs when horizontal or rotational motion has been given immediately after penetration behavior. In order to prevent this, a small downward displacement is applied along with the vertical load prior to loading of the horizontal or rotational motion. Especially in the cases of the $2.2B$ and $2.4B$ embedments, where squeezing occurs, the vertical capacity is sensitively increased even with a slight downward movement, which is considered to affect the maximum horizontal and rotational capacity. However, these effects are not significant, and so analysis stability is given priority in the present study.

$$H \quad \rightarrow \quad H_{nor} = \frac{H}{H_o} \tag{6}$$

$$M \quad \rightarrow \quad M_{nor} = \frac{M}{M_o} \tag{7}$$

where H, M: Horizontal reaction force and Rotational reaction moment in load path, H_o, M_o: Horizontal and Rotational maximum capacity

Through this normalization process, the load path becomes a curve that passes through (0,0), (1,0) and has vertices of (0.5, 1) in the VH and VM planes. Before presenting the new expression of this curve, a quadratic curve is derived. First, a parabola is assumed, one of the representative quadratic curves (blue dashed line). Assuming that the cross-section in VH (VM) plane is a parabola, the yield envelope becomes paraboloid. The parabola about the VH plane is summarized through the procedure of Eq. (8). Since the form of the equation is the same in the VM plane, it is omitted.

$$\begin{aligned} H_{nor} &= 4 \cdot V_{nor} \cdot (1 - V_{nor}) \\ &= 4 \cdot \frac{V + \chi V_o}{(1+\chi)V_o} \cdot \left(\frac{V_o + \chi V_o}{(1+\chi)V_o} - \frac{V + \chi V_o}{(1+\chi)V_o} \right) \\ &= \frac{4}{(1+\chi)} \cdot \left(\frac{V}{V_o} + \chi \right) \cdot \left(1 - \frac{V}{V_o} \right) \end{aligned} \tag{8}$$

As in Eq. (8), the exponent of V in three-dimensional paraboloid has two times that of H (or M). Regardless of the consideration of tensile capacity, this form of paraboloid has been used as the yield envelope by Martin (1994); Martin and Houlsby (2000); Vlahos et al. (2008a); Zhang et al. (2014b). ISO (2012) also has

recommended a paraboloid formula for shallow depths (w=0). If the tensile capacity is not taken into account, the ratio of V to V_o is used as the value of V_{nor} (V/V_o).

Second, the equation is derived by assuming the normalized shape as an elliptic, another form of quadratic curve (blue dotted line). The cross-section of the ellipsoid becomes an ellipse, and so this elliptic equation is derived as Eq. (9) by formulating it with respect to the VH plane. Also, the result for the VM plane is the same as that for the VH plane.

$$\frac{(V_{nor}-0.5)^2}{0.5^2}+ {H_{nor}}^2 = 1$$

$$\begin{aligned} {H_{nor}}^2 &= 4 \cdot V_{nor} \cdot (1 - V_{nor}) \\ &= \frac{4}{(1+\chi)^2} \cdot \left(\frac{V}{V_o}+\chi\right) \cdot \left(1-\frac{V}{V_o}\right) \end{aligned} \tag{9}$$

In the form of the last expression, the right side is the same as the parabolic equation in Eq. (8), but the exponent of H_{nor} on the left side is square. This type of equation has been used as the yield envelope for the case of deep penetration ($w > 2.5B$) in ISO (2012).

Through this derivation procedure, it is found that the existing equations of the yield envelope have used parabolic and elliptic quadratic equations. The expression of the normalized shape is adjusted in this study while maintaining the form of the existing equation.

3.6.2. Modified equation of soft-over-stiff clay

As noted above in the case of ISO (2012), linear interpolation between paraboloid and ellipsoid has been used in the equation for single clay. In the present study, the shape of the curve is controlled by exponent fitting rather than linear interpolation. A different form of expression from the quadratic curve can effectively represent the results of the swipe test, and this exponent-fitting process was carried out by Vulpe (2015). Fig. 38 shows the newly normalized shapes of all of the load paths calculated by the swipe test, along with the fitted curves to all of those results.

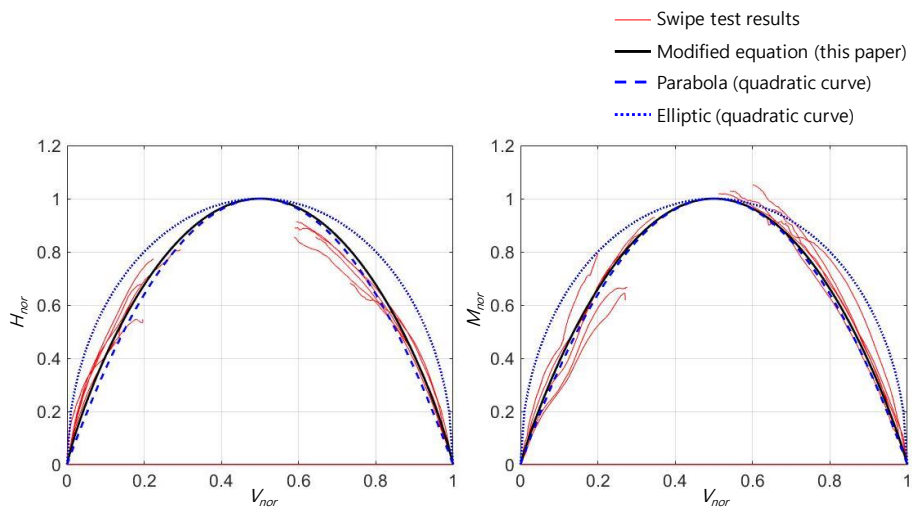

a) b)

Fig. 38 Fitted results to quadratic curves and modified equation; a) VH plane; b) VM plane

Fig. 38(a) shows the fitting results for the VH plane and Fig. 38(b) for the VM plane. The values of the exponent fitted in the two planes are applied to the equation of the yield envelope, respectively. The soft-over-stiff clay shows similar behavior to that of the single clay in the HM plane, and so the related terms are not changed. The fitted equations in the two planes and the final three-dimensional equation of the yield envelope are shown in Eq. (10) to Eq. (11). As formulated above, an exponent of 1 in H_{nor} and M_{nor} term represents the parabolic shape, so that the regressed result approaches to the parabolic. Although somewhat different, Eq. (11) has a similar form compared to that of single clay. This means that the lower stiff clay does not significantly affect the shape of the newly normalized yield envelope. The yield envelope in soft-over-stiff clay is found to be more sensitive to the capacity in each direction than the interaction of V, H, and M.

$$H_{nor}{}^{1.140} = 4 \cdot V_{nor} \cdot (1 - V_{nor}) \tag{10}$$

$$M_{nor}{}^{1.075} = 4 \cdot V_{nor} \cdot (1 - V_{nor}) \tag{11}$$

$$\left(\frac{H}{H_o}\right)^{2.28} + \left(\frac{M}{M_o}\right)^{2.15} - \frac{2HMe}{H_o M_o} - \left(\frac{4}{(1+\chi)^2}\right)^2 \left(\frac{V}{V_o} + \chi\right)^2 \left(1 - \frac{V}{V_o}\right)^2 = 0 \tag{12}$$

Yield envelope expressed as Eq. (11) is represented in three dimensions (Fig. 39). First, in the Fig. 39(a), the yield envelope is

shown along with all swipe test results about soft-over-stiff clay in the normalized space. The results in HM plane when V is zero are shown in several planes, with V_{nor} varying with the compressive and tensile maximum vertical capacities at each case. It is found that the yield envelope obtained from the swipe test results effectively is represented in three dimensions. Fig. 39(b) shows the non-normalized results of MWS2P case, for example. The yield envelope when the spudcan is subjected to upward force ($V < 0$) is revealed. Tensile swipe tests are performed through numerical analysis, and the yield envelope of soft-over-stiff clay including the negative region can be calculated.

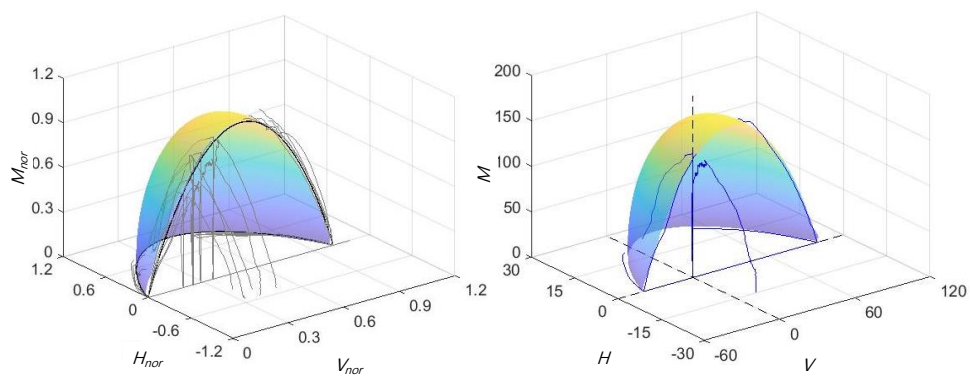

a) b)

Fig. 39 Three-dimensional yield envelope;

a) Yield envelope with the swipe test results in normalized space;

b) MWS2P case results and corresponding yield envelope

3.6.3. Effect of convergence criteria on the yield envelope

The maximum capacity is defined as the converged value of the load–displacement (moment–rotation) curve at the constant V test (Chapter 3.4.2). Convergence criterion is properly decided through the existing studies as $u = B\theta = 0.1B$, however, it is needed to find out how this criterion affects the yield envelope calculation. Maximum capacity is one of the main reasons why the yield envelope of soft–over–stiff clay differs from that of single clay, and convergence criterion can affect this value significantly. This study focuses on how the yield envelope is changed by the maximum capacity values obtained through three different criteria. Table 5 summarizes the estimation results. The maximum capacities increase with the displacement criteria, which results in reduced exponents. As mentioned above, the exponent close to 1 means a parabola, so this means that large convergence criterion makes the normalized shape narrower and closer to the parabola. This tendency is represented in Fig. 40. As the criteria for capacity calculation, small displacement criteria render the yield envelope closer to an ellipsoid, while large criteria to a paraboloid.

Table 5 Regression results for different maximum capacity criteria

Displacement criteria	$H_{nor}{}^{a}$	$M_{nor}{}^{b}$
0.04B	1.508	1.467
0.07B	1.239	1.216
0.10B	1.140	1.075

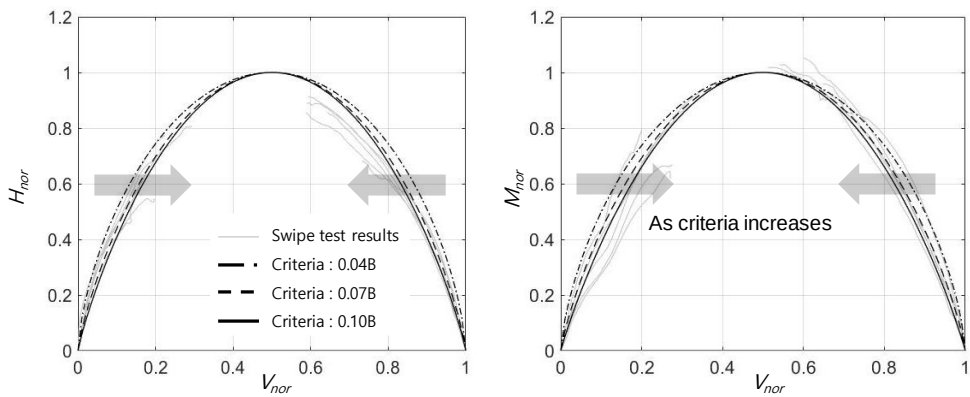

a) b)

Fig. 40 Fitted results according to the convergence criteria; a) VH plane; b) VM plane

Chapter 4. Yield envelope in soft over stiff clay

4.1. Introduction

During the operation phase where the jack-up is designed, the leg penetrates and receives environmental loads under sufficient bearing capacity. Due to the environmental loads, the soil experiences loads in the V, H, and M directions. The study on the yield envelope, which determines the yield for these acting loads, has been conducted in Chapter 3. How the force-resultant yield envelope for V, H, and M in soft over stiff clay is different has been figured out.

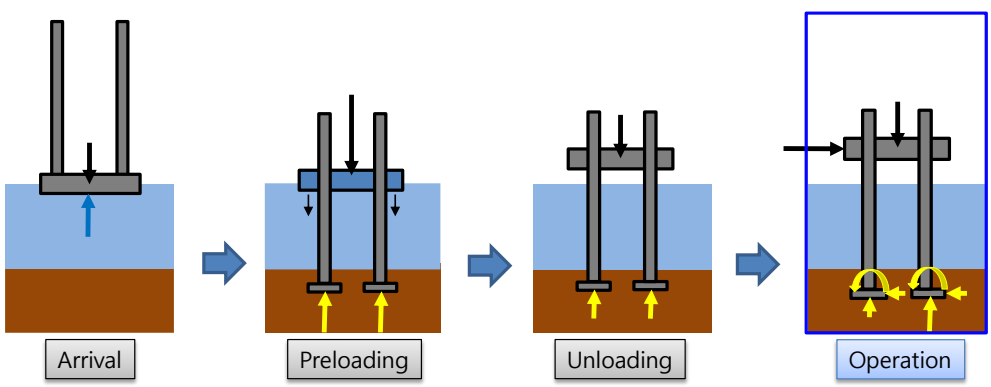

Fig. 41 Jack-up operation in overall procedure

The fitted parameter values and the expression of yield envelope for the soft over stiff clay within the possible range have been presented in Chapter 3. The foundation model, which is a boundary condition for structural analysis, is a ground model that performs

structural–soil interaction analysis through the process of determining the reaction force of the soil by receiving the reaction force in real–time. Model B framework, the foundation model of clay, formulates not only the yield envelope that determines yield, but also the elasticity that defines the behavior before yield, the flow rule that determines the behavior in plasticity, and the hardening law that establishes the additional penetration of spudcan. Plastic displacement is calculated through the formulation of those relations, and this is reflected to simulate the plastic behavior of the soil. In this chapter, a study on elasticity has been conducted to determine the behavior in the elastic range before yield. Hyperbolic relation is suggested as the more realistic elasticity relationship than that of the existing model. Through this, spudcan behavior in the elastic region along with the yield envelope of Chapter 3 has been described. Through the yield envelope that determines the elastic region and the elasticity within the elastic region, it has been intended to accurately represent the behavior within the elastic region in soft over stiff clay.

The existing model B is a work hardening plasticity–based numerical model for spudcan behavior on clay, as briefly described above. This concept of work hardening plasticity–based numerical model was first introduced in jack–up behavior by Schotman(1989) as model A. Afterward, elasticity, yield envelope, flow rule, and hardening law were improved overall by Martin(1994) and presented as model B. The model B presented an empirical yield envelope formula based on the results of the 1g experiment. After a

minor improvement, a yield envelope formula was proposed that included an eccentricity concept in a horizontal–rotation plane as a cigar–shaped shape.

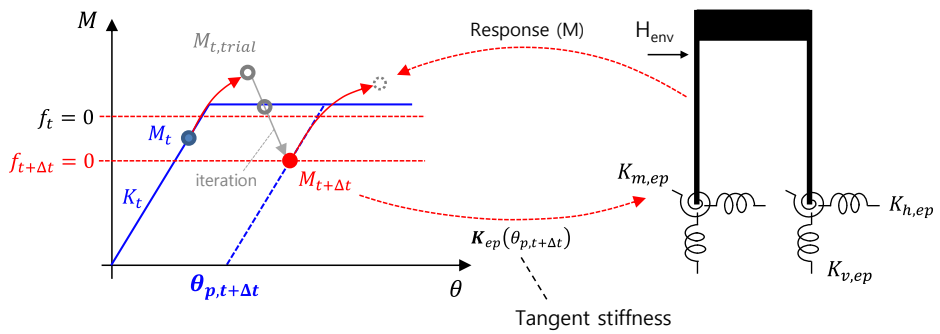

Fig. 42 Schematic diagram of model B in M–θ graph

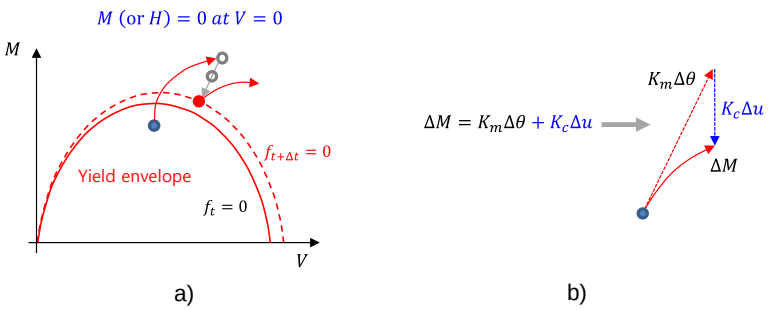

Fig. 43 Schematic diagram of model B; a) Load path in yield envelope; b) Horizontal–rotational interaction term in elasticity

In the elasticity relationship inside the yield envelope, Martin(1994) introduced terms related to interaction with horizontal and rotational directions (Eq. (13)). Through this, despite the linear diagonal term, it shows a characteristic that does not have a perfectly linear relationship in each material curve in the horizontal and rotational directions.

$$K_{el} = \begin{bmatrix} K_v & 0 & 0 \\ 0 & K_h & K_c \\ 0 & K_c & K_m \end{bmatrix} = \begin{bmatrix} k_v GR & 0 & 0 \\ 0 & k_h GR & k_c GR^2 \\ 0 & k_c GR^2 & k_m GR^3 \end{bmatrix} \quad (13)$$

The model B expresses plasticity by calculating the plastic displacement of the soil. First, if displacement is given through global jack-up analysis, it is assumed to be elastic, and response is calculated by using elasticity relation. If the calculated response is in the plastic region outside the yield envelope, an iterative calculation is performed. Elasticity, yield envelope, flow rule, and hardening law are all formulated and used for iterative calculation. Plastic displacement is calculated through iteration, and design point and tangent stiffness are calculated using this value. These calculated values are the result of this step and are used to calculate the next step in the global jack-up analysis. Through this process, model B proposed a plasticity framework reflecting each equation.

Modified model B is the state-of-art yield interaction model for clay that has improved model B. The plasticity framework of the model B was used as it was. Still, the model was improved, considering the backflow and surrounding soil in spudcan behavior. The modified model B is proposed by Zhang et al. (2014b) and is applied not only to single clay but also to various multi-layered soils containing clay in subsequent studies.

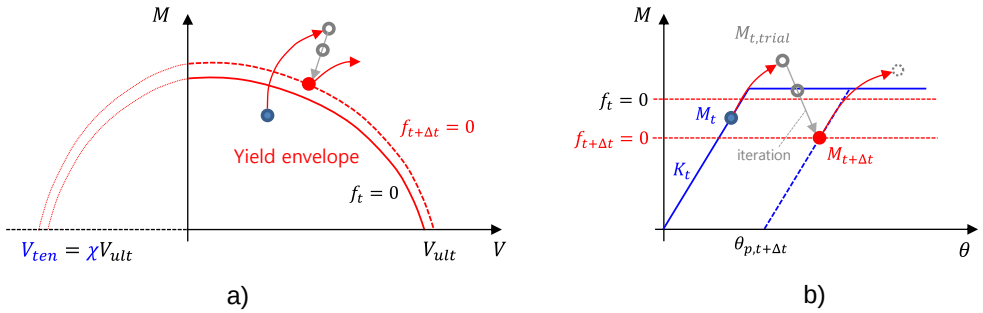

Fig. 44 Schematic diagram of modified model B;
a) Load path in yield envelope; b) Modified model B in M–θ graph

First, Zhang et al. (2014b) proposed a yield envelope equation considering tensile capacity through a centrifuge model test and suggested the coefficients for this expression. In the improved yield envelope, horizontal and rotational capacity remained even when the vertical load is zero due to tensile capacity. In actual single clay, capacity remains even when there is no vertical load due to backflow and adhesion after the penetration, and this phenomenon was reflected. The elastic relationship and plasticity are the same as that of the existing model B of Martin (1994), but the necessary coefficients for the elastic relation were presented for a single clay in various embedments and properties. Accordingly, improvements have been made to simulate the behavior of spudcan more accurately in a single clay.

Vlahos et al. (2006) simulated a non-linear relationship rather than a linear relationship as the elastic behavior within the yield envelope. In the rotational direction, the stiffness decreases as rotation occurs, and the hysteresis curve in the elastic region is

simulated through this (Eq. (14)). To simulate this strength degradation, Vlahos et al. (2006) introduced the hyperplasticity theory to simulate the rotational direction spring, which adopted the thermomechanical principle to formulate soil plasticity. The spring–slider element suggested in the hyperplasticity theory, the non–linear spring in the rotational direction is simulated (E_{N*}^{t}). In contrast, the horizontal and rotational interaction term of the elastic relation is removed for simplicity. Hyper–model B with this nonlinear rotational spring was introduced.

$$K_{el} = \begin{bmatrix} k_v GR & 0 & 0 \\ 0 & k_h GR & 0 \\ 0 & 0 & 8E_{N*}^{t} GR^3 \end{bmatrix} \tag{14}$$

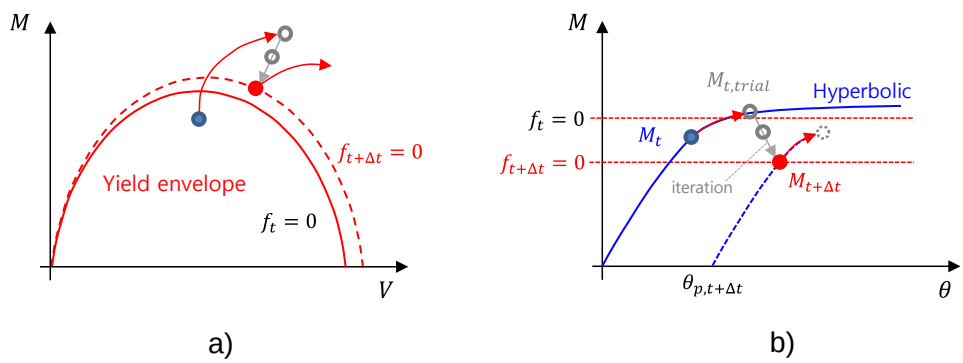

Fig. 45 Schematic diagram of Hyper–model B;
a) Load path in yield envelope; b) Hyper–model B in M–θ graph

Like the previous yield interaction model, Hyper–model B has the same plasticity framework because it is based on existing model B. First, the response is calculated according to elastic relation and

displacement. At this time, the moment of rotation is calculated according to the hyperbolic relationship. At this time, if the response is in the plastic region, iterative calculations are performed as well, and the plastic displacement is calculated. And the reaction force and moment also decrease accordingly. In this process, hyperbolic relations are used.

In this chapter, hyperbolic model B is proposed, which extends the nonlinear hyperbolic relation in the elastic region in the horizontal and rotational directions and presents the coefficients for this. The existing Hyper-model B applied a nonlinear relationship only to the direction of rotation; however, the proposed model has extended it in the horizontal direction and added the interaction terms of horizontal and rotational directions (Eq. (15)). In addition, the state-of-art model for single clay proposed by Zhang et al. (2014b) has been combined and applied.

$$K_{el} = \begin{bmatrix} k_v GR & 0 & 0 \\ 0 & \boldsymbol{f_{K_h}(u)} & f_{K_c}(\theta) \\ 0 & f_{K_c}(\theta) & \boldsymbol{f_{K_m}(\theta)} \end{bmatrix} \tag{15}$$

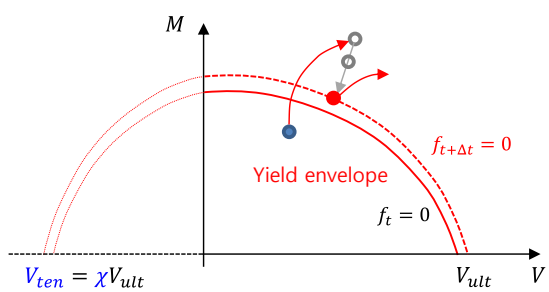

Fig. 46 Schematic load path in Yield envelope

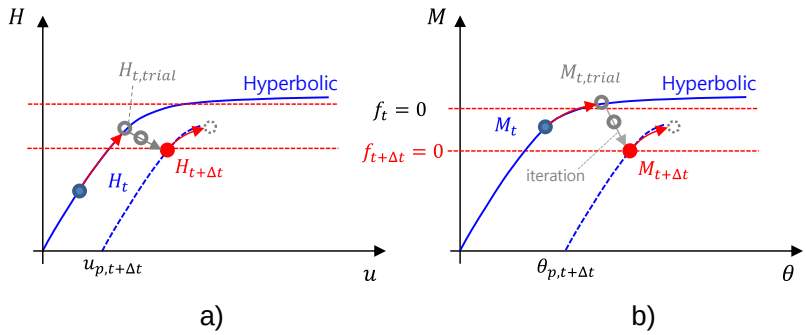

Fig. 47 Hyperbolic model B in a) H–u; b) M–θ graph

The yield envelope for the soft over stiff clay presented in Chapter 3 has been applied. Also, the nonlinear hyperbolic relation can be used not only to the moment–rotation but also to the horizontal force–displacement relation. The interaction terms of the horizontal and rotational direction of the elastic relation of the model B is considered as a function of rotation. In the plastic region, the existing model B plasticity framework is used as it is. So the response is calculated according to the given nonlinear elastic relation within the yield envelope, and the plastic displacement is calculated to simulate the behavior outside the yield envelope. At this time, the nonlinear hyperbolic relation is determined by the initial stiffness and capacity. In particular, the initial stiffness can vary significantly depending on the criteria. Accordingly, a regression model has been proposed to present the initial stiffness for the soft over stiff clay. When using the hyperbolic model B presented in this chapter, the regression model and fitting results are expected to be used for nonlinear hyperbolic relations.

4.2. Model B with hyperbolic elastic curve

Hyperbolic backbone curves have often been used to express ground hysteresis behavior (Vlahos et al., 2006; Huang, 2020). The equation of the hyperbolic curve is as follows in Eq. (16).

$$f_{hyper}(x) = \frac{x}{a + bx} \tag{16}$$

This hyperbolic curve equation has been used to express the strength degradation in the horizontal and rotational directions. In Chapter 3, the combined loads analysis of the single spudcan has been performed. Spudcan penetration has been simulated, and then reaction force and moment have been calculated through a horizontal and rotational motion under a specific vertical force with the maximum capacity. In this chapter, H−u and M− θ relationships are assumed to be hyperbolic, and this relation is fitted to those results of single spudcan analysis. The model B with hyperbolic elastic curve is proposed as Hyperbolic model B.

First, the hyperbolic expression has been formulated using physically meaningful parameters (Eq. (17), (18)).

$$H(u) = \frac{\mathrm{u}}{\left(\frac{1}{K_h} + \frac{1}{H_o} abs(u)\right)} \tag{17}$$

$$M(\theta) = \frac{\theta}{\left(\frac{1}{K_m} + \frac{1}{M_o} abs(\theta)\right)} \tag{18}$$

where, K_h and K_m are initial stiffness, respectively, and mean the slope at u= θ =0. H_o and M_o mean the capacity and converged value at u= θ =∞. Each soil parameter is presented in Fig. 48.

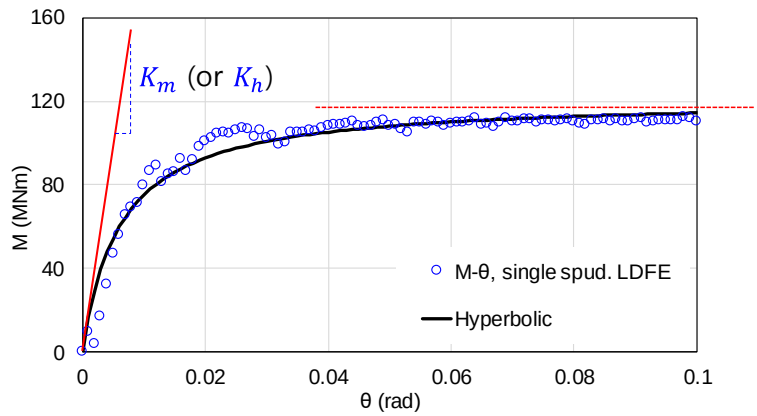

Fig. 48 load-displacement curve from single spud. LDFE

The results of fitting according to the proposed equation are shown in Fig. 49, Fig. 50 and Table 6. In one of several cases, the results of single clay and soft over stiff clay at w=2.2B has been selected.

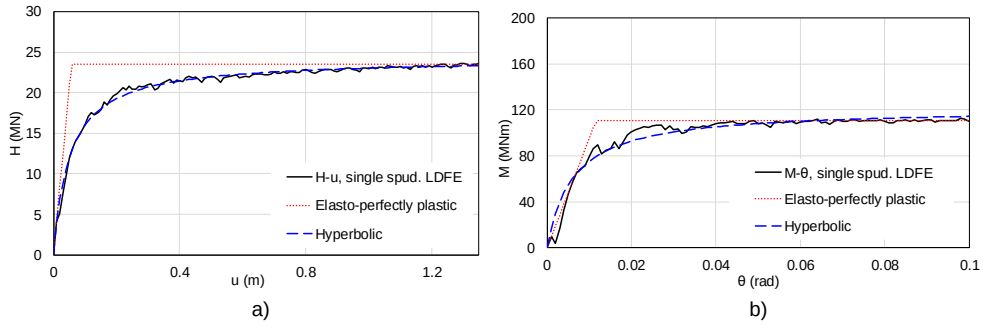

Fig. 49 Fitting results in single clay;

a) horizontal direction; b) rotational direction

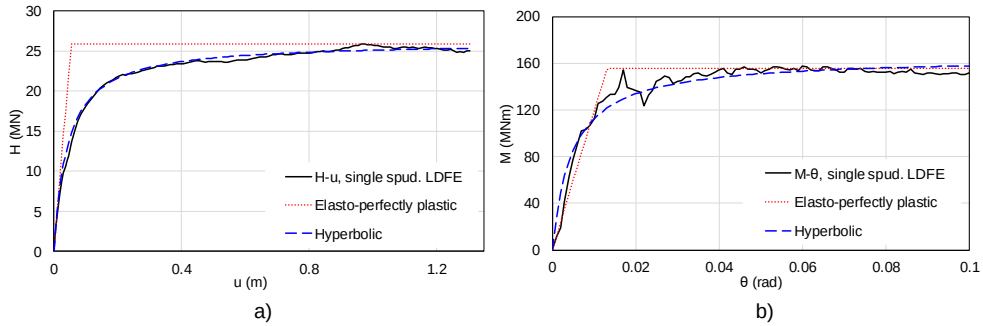

Fig. 50 Fitting results in soft over stiff clay;

a) horizontal direction; b) rotational direction

Table 6 soil parameter of single clay and soft over stiff clay (MWS2P)

	Single clay	Soft over stiff clay
K_h	473.90 MN/m	622.90 MN/m
H_o	24.20 MN	26.16 MN
K_m	19760 MNm/rad	35080 MNm/rad
M_o	121.40 MNm	165.20 MNm

As shown in the Fig. 49 and Fig. 50, the fitted hyperbolic curve (blue dashed line) fits the single spudcan analysis (black line) result. When it is assumed to be elastic−perfectly plastic (red dotted line), the strength degradation is poorly expressed. The effect of lower stiff clay on soil parameters obtained through fitting is well revealed. In Chapter 3, vertical and rotational capacity with downward motion have increased in soft over stiff clay due to squeezing effect. In the case of soil parameters obtained through the fitting, the horizontal capacity does not change much, while the moment capacity increases. Initial stiffness is a parameter that determines the initial part of the material curve. Both the horizontal and rotational stiffness increases due to the influence of the lower stiff clay. In particular, the rotational stiffness affected by the surrounding soil increases significantly. The fitting results for different embedments and properties of lower clay are as follows.

Table 7 Fitted result about horizontal initial stiffness (MN/m)

K_h	SWP	MWS2P	MWS3P	MWS4P
1.8B	415.73	478.01	505.89	522.12
2.0B	444.22	605.58	706.74	759.16
2.2B	455.64	646.88	918.74	1014.40
2.4B	524.81	806.74	1661.17	2502.79

Table 8 Fitted result about rotational initial stiffness (MNm/rad)

K_m	SWP	MWS2P	MWS3P	MWS4P
1.8B	12829	19214	22400	23646
2.0B	17366	27448	36762	41904
2.2B	17581	30432	41698	18796
2.4B	17711	35113	44346	75547

Table 9 Fitted result about horizontal capacity (MN)

H_o	SWP	MWS2P	MWS3P	MWS4P
1.8B	18.73	18.47	18.61	18.65
2.0B	21.32	21.67	21.54	21.50
2.2B	24.62	25.96	28.98	32.77
2.4B	28.03	28.62	35.42	44.42

Table 10 Fitted result about rotational capacity (MNm)

M_o	SWP	MWS2P	MWS3P	MWS4P
1.8B	99.44	97.99	97.28	96.62
2.0B	108.87	117.26	116.85	116.14
2.2B	127.63	174.68	183.34	299.08
2.4B	140.84	175.32	227.13	284.55

4.3. Regression model of initial stiffness

To define the horizontal and rotational hyperbolic relations in Hyperbolic model B, two parameters, initial stiffness and capacity, should be determined. It is not easy that the response reaches the capacity in the jack-up analysis, because combined loads are applied to the soil and the capacity is the yield condition of a single dof. Initial stiffness, dominant factor of the initial phase of the material curve, is very important in this respect. However, the initial stiffness is determined by the response at a small strain, and the value varies greatly depending on the criteria of the displacement causing the small strain.

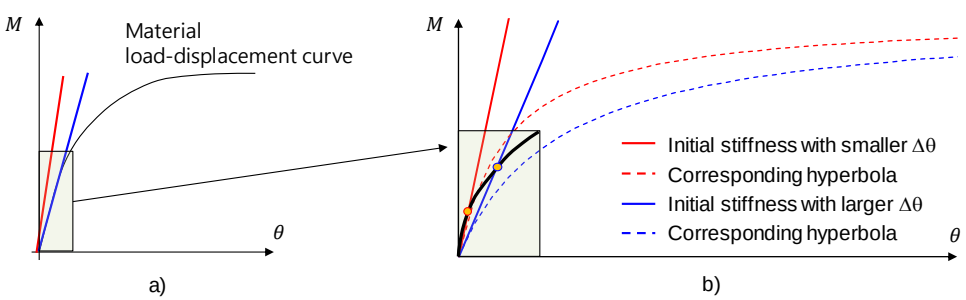

Fig. 51 Difficulties in determination of initial stiffness;
a) initial stiffness of two different criteria; b) enlarged graph

The Fig. 51 shows that the initial stiffness may vary depending on the criteria. The smaller the displacement interval yields the larger the stiffness. It seems that the blue slope at a larger reference reveals the overall shape better in overall shape. In contrast, when

it is enlarged(Fig. 51(b)), it can be confirmed that the red slope is the better representative of the slope at the beginning. This difference in the initial slope also causes a difference in the hyperbolic curve using the corresponding value. Even if the capacity is the same, the difference in the initial slope can cause a large difference in the early stage as shown in the Fig. 51(b). As the displacement increases, it converges to the same capacity, but differences occur in small displacements where jack-up analysis experiences actually, which means that hyperbolic relations can be greatly affected by soil parameters. Although the initial stiffness obtained through centrifuge model tests or other methods is the correct value, if used differently in the hyperbolic model according to the criteria, the results may not be validated. This study has presented a regression model for initial stiffness in soft over clay that can be used in hyperbolic model B. Equations are presented so that the corresponding parameters can be used in the range of the given embedments and the lower clay properties.

Before presenting the regression equation, two variables that can reveal spudcan in soft over stiff clay have been selected. In chapter 3, the impact of the lower stiff clay has been analyzed by dividing it into the properties of lower clay and embedment. In the regression model of this chapter, two variables have been selected, undrained shear strength ratio and depth ratio, for the purpose of clarifying the effects of normalization and lower stiff clay.

$$\text{undrained shear strength ratio} = \frac{s_{u,stiff}}{s_{u,H}} \tag{19}$$

$$\text{depth ratio} = \frac{w}{H} \tag{20}$$

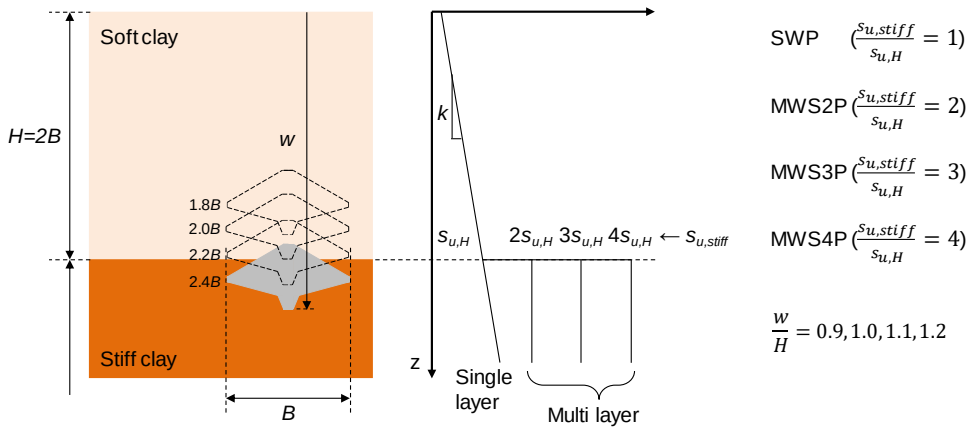

Fig. 52 Two variables in regression model

The undrained shear strength ratio refers to the ratio of the undrained shear strength of the upper soft clay and the lower stiff clay at the boundary (Eq. (19)). The effect of the lower clay can be normalized and expressed using the ratio of undrained strength. A regression model has been proposed for the lower stiff clay, which is 1 to 4 times harder than the upper clay. The depth ratio means the ratio of the depth of penetration to the height of the upper clay (Eq. (20)). Simple penetration depth cannot clearly present the relationship with the lower stiff soil, and for this purpose, the depth ratio has been selected by including the location of the lower stiff clay. A regression model has been proposed for depth ratios from 0.9 to 1.2, and in particular, when looking at the results of chapter 3, it is expected that the depth ratio of 0.9 or less will only affect

the upper soft clay and not the lower clay. This selected range can cover the bearing pressure of a typical jack-up.

For the selected undrained shear strength ratio and depth ratio, fitting has been performed for the combined loads analysis results in the horizontal and rotational directions. The soil parameters obtained through these fittings are listed in the Table 7 ~ Table 10.

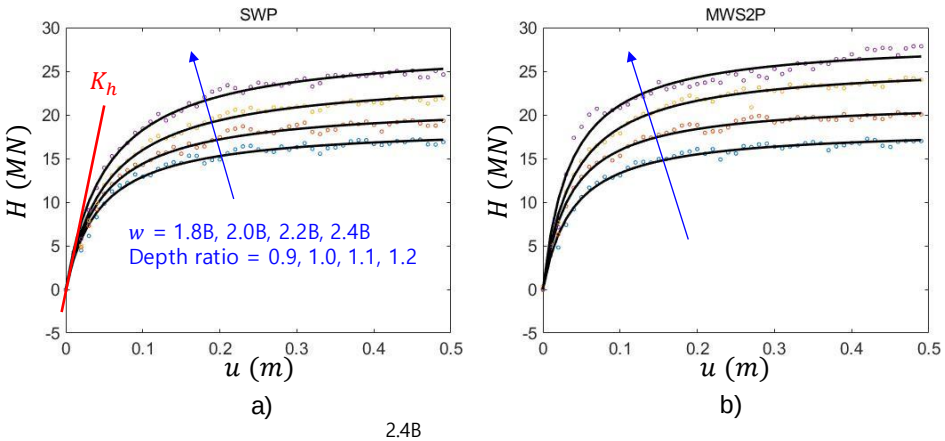

Fig. 53 Horizontal material curve obtained from single spudcan analysis and fitted results; a) SWP; b) MWS2P

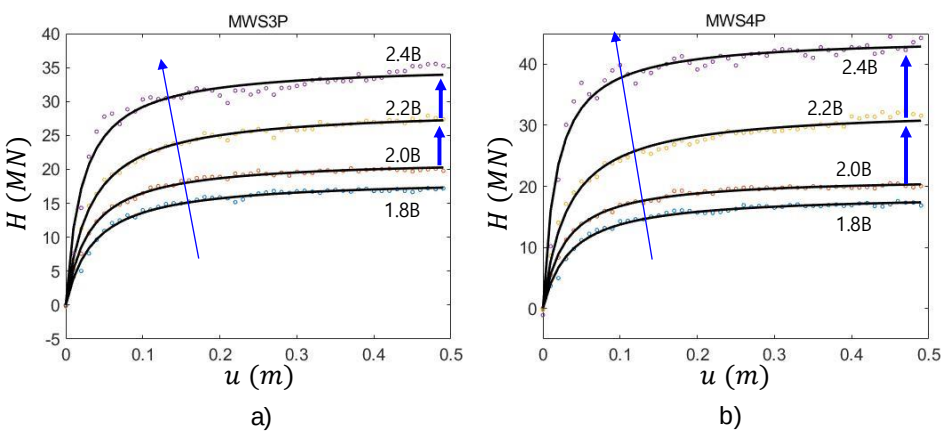

Fig. 54 Horizontal material curve obtained from single spudcan analysis and fitted results; a) MWS3P; b) MWS4P

The result of varying embedment according to the properties of the lower stiff clay has been shown for the H−u curve in the horizontal direction. The fitting result is shown as a solid black line. For all cases of SWP, MWS2P, MWS3P, and MWS4P, it has been confirmed that the deeper the penetration depth, the greater the initial stiffness and the capacity, which are the slope at the origin and the convergence value, respectively. This significant increase occurs in MWS3P and MWS4P, which have a large impact by the lower stiff clay. In addition, it is shown that the increase is large at w=2.2B and 2.4B.

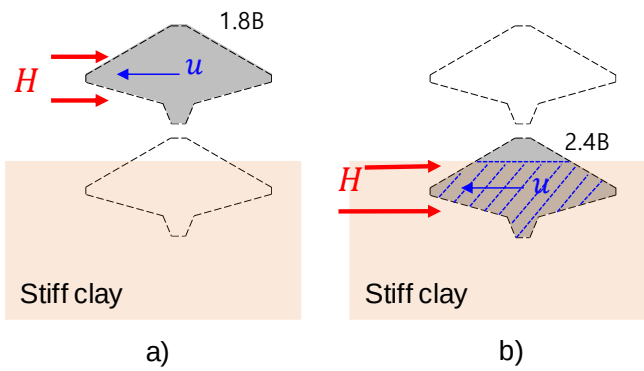

Fig. 55 Schematic diagram of horizontal reaction force acting on the spudcan at; a) w=1.8B; b) w=2.4B

As mentioned in Chapter 3, horizontal capacity is greatly influenced by the overlapped area with lower stiff clay. As shown in the figure, at w=1.8B, spudcan does not meet the lower stiff clay, so the soft clay applies the small reaction force. However, at w=2.4B, spudcan overlaps much with the lower stiff clay, and the

stiff clay applies a corresponding large reaction force. The horizontal capacity increases significantly in 2.2B and 2.4B, where overlapped areas are increased due to the large reaction force from the stiff clay.

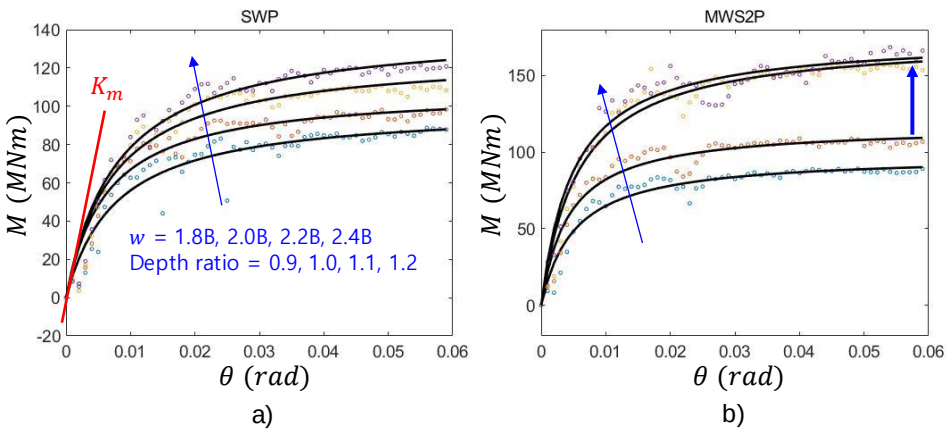

Fig. 56 Rotational material curve obtained from single spudcan analysis and fitted results; a) SWP; b) MWS2P

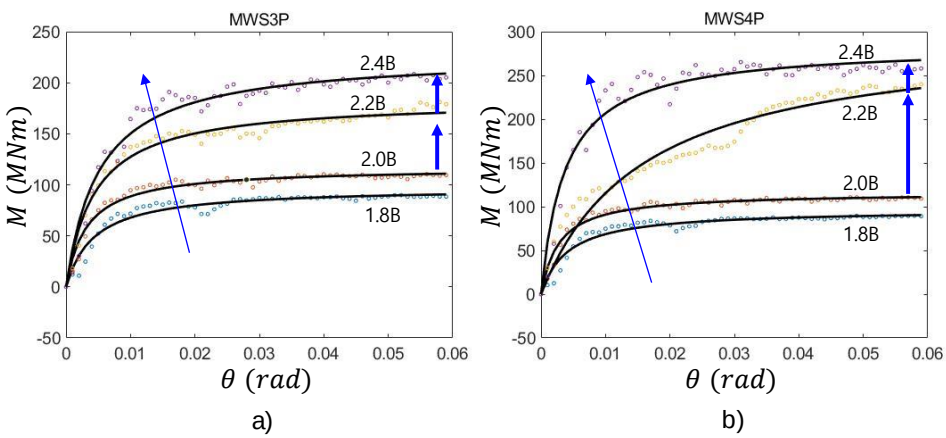

Fig. 57 Rotational material curve obtained from single spudcan analysis and fitted results; a) MWS3P; b) MWS4P

The result of varying the embedment according to each lower stiff soil is shown for the M− θ curve in the rotational direction in Fig. 56 and Fig. 57. The fitting result is shown as a solid black line. As in the horizontal direction, The initial stiffness, which is the slope at the origin, and the capacity, which is the convergence value, increases as the depth of penetration increases for all cases of SWP, MWS2P, MWS3P, and MWS4P.

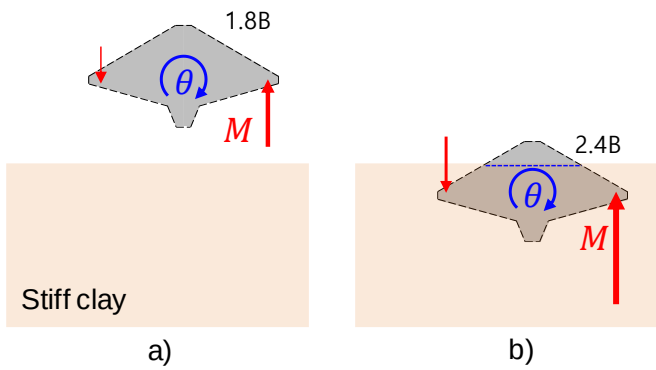

Fig. 58 Schematic diagram of rotational reaction moment acting on the spudcan at; a) w=1.8B; b) w=2.4B

The reaction moment increases more than the horizontal reaction force due to the downward motion of one side to the lower stiff clay. This increase is particularly pronounced in 2.2B and 2.4B, which also depends on the location of the spudcan. When the spudcan is located at 1.8B, the side with downward motion will be affected by squeezing. However, when the spudcan is located at 2.4B, the side with downward motion is only affected by the stiff clay, and the reaction force increases accordingly. On the other hand, the side

with upward motion is affected by soft clay and has little influence. Due to this effect, the stiffness and capacity in the rotational direction also have a more considerable value as the penetration depth increases and the lower clay is stiffer.

Initial stiffness and capacity for hyperbolic relations are calculated by the fitting from the results of single spudcan LDFE analysis. The following regression model is presented for the initial stiffness calculated as above.

$$k_h = 0.15\left(\frac{s_{u,stiff}}{s_{u,H}}\right)^{2.15}\left(\frac{w}{H}\right)^{14.78} + 1.04\left(\frac{s_{u,stiff}}{s_{u,H}}\right) + 9.03 \quad (21)$$

$$k_m = 13.89\left(\frac{s_{u,stiff}}{s_{u,H}}\right)\left(\frac{w}{H} - 0.85\right)^{0.53} + 1.01\left(\frac{s_{u,H}}{s_{u,stiff}} - 2.90\right) + 4.50 \quad (22)$$

The regression model is presented for the stiffness coefficient concept presented by ISO (Eq. (21), (22)). The actual fitting has been performed for K_h and K_m, but an equation for the normalized coefficient is provided to be applied to general properties and spudcan (Eq. (23), (24)). Shear modulus (G) and spudcan radius (R) have been used for normalization. G used at this time has been calculated by using the general relation with E and the relationship with s_u (Eq. (25)). G_H uses the upper soft clay properties at the boundary for the normalization (Eq. (26)). The properties of the lower clay have been considered in the regression model through the undrained shear strength ratio variable. Therefore, when

normalizing using the upper soft clay property, all the properties of soft over stiff clay can be considered.

$$K_h = k_h G_H R \tag{23}$$

$$K_m = k_m G_H R^3 \tag{24}$$

$$G = \frac{E}{2(1+\nu)} = \frac{500}{2(1+\nu)} s_u \tag{25}$$

$$G_H = \frac{500}{2(1+\nu)} s_{u,H} \tag{26}$$

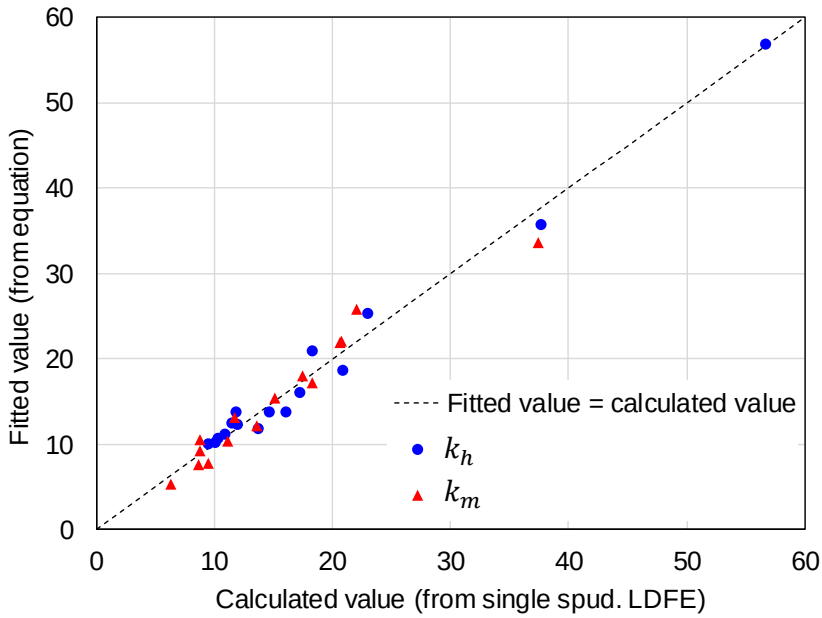

Fig. 59 Accuracy of regression model about initial stiffness

4.4. Hysteresis curve

The results from the LDFE analysis and that from the regression model are shown in the Fig. 59. In the Fig. 59, the x−axis represents the results from LDFE, and the y−axis represents the results from the regression model. The diagonal dotted line is a set of points where both results are the same, that is, the closer to this dotted line, the higher the accuracy of the regression model. Stiffness coefficients in both horizontal and rotational directions are shown. Both results are close to the linear dotted line. This means that the regression model expresses the initial stiffness well within the range (0.9~1.2 of depth ratio, 1~4 of undrained shear strength ratio).

The hyperbolic curve is introduced in the horizontal and rotational directions, and a backbone curve and hysteresis relation can be implemented in the elastic region. Bolisetti(2014) used hyperbolic backbone curves and implemented the hysteresis relation of the soil using the Masing rule (Masing, 1926). Masing rule is about material curves to be followed when loading and unloading and is divided into three rules.

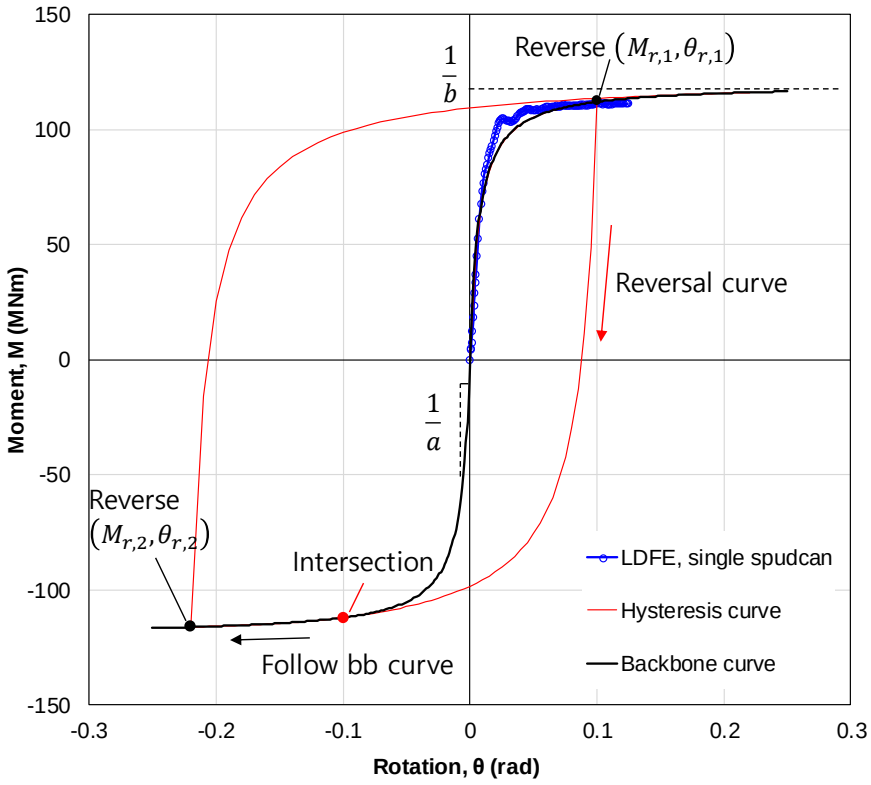

Fig. 60 Masing rule (Masing, 1926) for hysteresis curve

First, the initial loading follows the backbone curve. In this study, since the hyperbolic relation is adopted for the nonlinear material curve, the hyperbolic backbone curve has been used for implementation. The blue LDFE result(Fig. 60) can be seen as the initial loading, and it is shown to follow the hyperbolic backbone curve well. Second, after unloading occurs at a certain point, the material curve follows the reversal curve. The reversal curve is twice the enlarged backbone curve in the opposite direction (Eq. (27)).

$$\frac{M - M_r}{2} = F\left(\frac{\theta - \theta_r}{2}\right) \tag{27}$$

Finally, if unloading continues along this reversal curve, the backbone curve meets again at the origin symmetric point with the point where the unloading started. From this intersection point, the material curve follows the backbone curve again, not the reversal curve. Loading and unloading are repeated accordingly, and the hysteresis curve is made around the backbone curve.

This Masing rule is identical to the ideal hysteresis curve in general materials. The hyperbolic model B has been designed to express the hysteresis curve in the horizontal and rotational direction under repeated loads by implementing the hysteresis curve through the Masing rule. In the case of Modified model B, a linear relationship is used in the elastic region except for the interaction term, so the loading and unloading curves in the elastic region are almost the same. However, jack-up structure is frequently subjected to wave-like repetitive loads, and not only large loads that cause yield but also repetitive loads in the elastic region are important in terms of fatigue strength. In the hyperbolic model B, the nonlinear hyperbolic relationship and the hysteresis curve have been used to accurately simulate the response to repeated loads in the elastic region.

Chapter 5. Validation with structural analysis of jack-up using different foundation models

5.1. Introduction

The structure−ground interaction model among the foundation models of jack−up is the secant model, yield interaction model, and soil continuum model. Chapter 3 has studied the yield envelope of soft over stiff clay which can be used in the secant model and the yield interaction model. The characteristics of the yield envelope in soft over stiff clay have been analyzed and the yield envelope expression and corresponding coefficients have been presented. In Chapter 4, the elastic relationship that determines the behavior in the elastic region has been improved in the yield interaction model. Strength degradation in the elastic region has been implemented through hyperbolic relations, and soil parameters applicable to soft over stiff clay have been introduced in the form of regression model and tables.

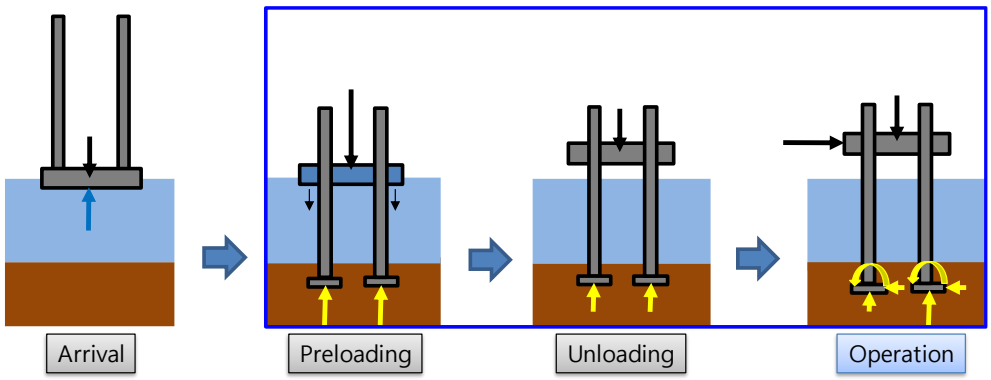

Fig. 61 Jack-up operating phase considered in Chapter 5

In Chapter 5, LDFE has been used to implement the soil continuum model. Structure-soil interaction analysis with soil continuum model has been performed. The yield interaction model in soft over stiff clay presented in Chapters 3 and 4 has been validated with the soil continuum model. The complicated structure-soil interaction model, yield interaction model and soil continuum model, have been presented that it can be applied to single clay and soft over stiff clay. In order to perform the jack-up structural analysis under the environmental loads during the operation phase, the penetration of the jack-up structure should be first simulated. Penetration procedure and corresponding disturbed soil properties are reflected in this chapter (Fig. 61).

5.2. User element (UEL)

5.2.1. Implementation of model B

The elasto-plastic framework of the model B, which is the basis of modified model B and hyperbolic model B, has been implemented first in order to perform structural analysis using the yield interaction model. For the explicit formulation of the model B, Vlahos et al. (2008b) is referred. The macro element reflecting the formulated expression has been implemented using the user element subroutine of Abaqus. UEL subroutine can directly define the constitutive equation of element, and thus the relationship between load and displacement for multiple dof. In particular, the model B, which is the yield interaction model of clay, is effectively implemented through the user element because it is necessary to perform repetitive calculations using displacement and reaction forces, and define elastic and plastic relations, respectively.

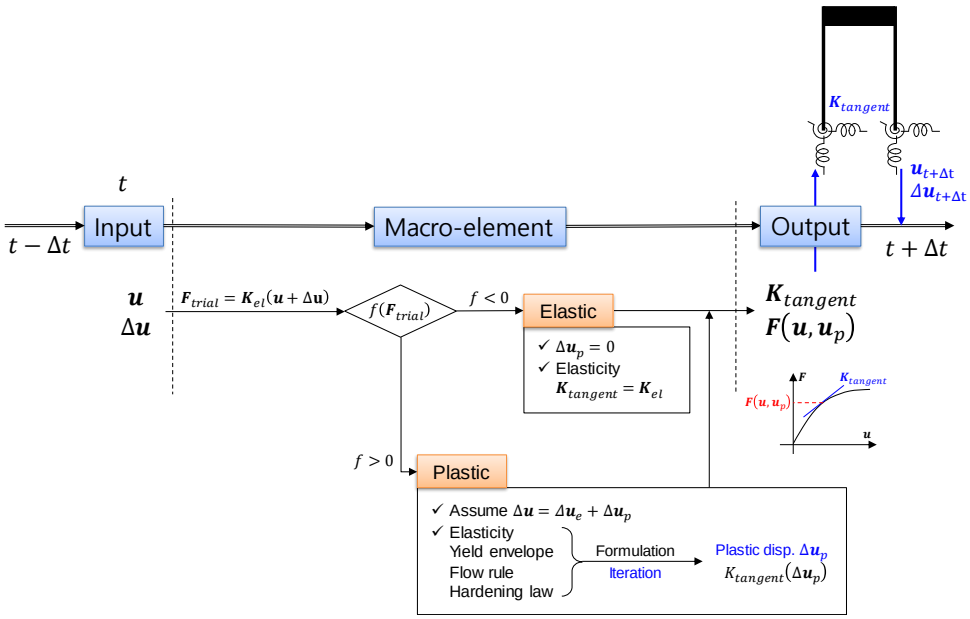

Fig. 62 Iterative procedure in macro element of the model B

First, the displacement of the increment from the global jack-up analysis of Abaqus is inputted. In the corresponding increment, the response is temporarily calculated according to the elastic relationship ($\boldsymbol{K_{el}}$) of the model B using the previously received displacement, and the value is defined as the trial load state ($\boldsymbol{F_{trial}}$). $\boldsymbol{F_{trial}}$ is substituted to the force-resultant yield envelope to determine whether the trial load state is in the elastic region or the plastic region. If the load state is in the yield envelope, it is elastic, so the elastic stiffness of the model B becomes tangent stiffness, and the trial load state becomes the final load state. However, if the trial load state is outside the yield envelope, iteration begins because it is plastic. The purpose of this iteration is to calculate the plastic displacement, so the elasticity, yield envelope, flow rule, and hardening law are considered in the interactive calculation. The

plastic displacement is finally calculated through the iterative calculation, and the total displacement is divided into elastic displacement and plastic displacement. The tangent stiffness is defined as a function of plastic displacement, and the load state is placed on the yield envelope through repeated calculations. This load state at this time is calculated from the elastic displacement. The calculated tangent stiffness and load state (response) become the load-displacement relationship in the corresponding increment. This information is transferred to the global jack-up analysis, where checks the analysis convergence and calculates the displacement of the next increment, and the same process is repeated.

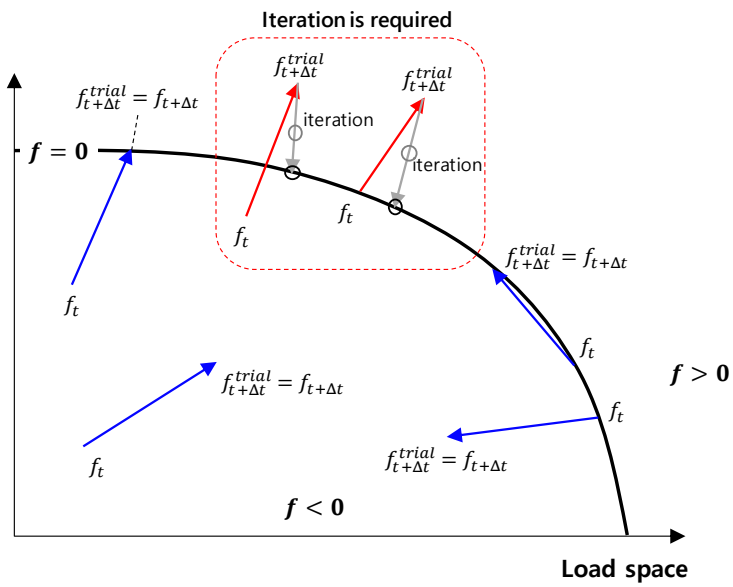

Fig. 63 Schematic diagram of yield envelope check using trial load state ($\boldsymbol{F}_{trial}$)

There are six cases where a trial load state can place on, among which two cases outside the yield envelope need the iteration(Fig. 63). After the plastic displacement is calculated through the iterative calculation, the final load state is placed on the yield envelope. In this procedure, the flow rule determines the direction and speed of approaching the yield envelope. If additional penetration in the vertical direction should be needed during this process, the vertical compression capacity is changed and the yield envelope and accompanying other equations are recalculated in consideration of this. Four plasticity equations, including elasticity which is the elastic relationship that determines the behavior within the elastic region, each play a role in the model B framework.

5.2.2. Validation of macro element

The model B implemented through the UEL in the Abaqus commercial program has been validated. First, the swipe test performed in Chapter 3 has been selected as a verification case as it has been to see if the result calculates well (Fig. 64).

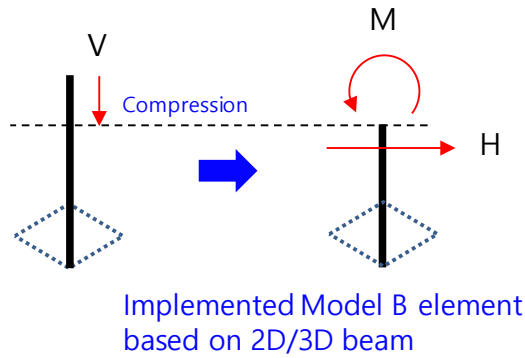

Fig. 64 Loading sequence of the swipe test

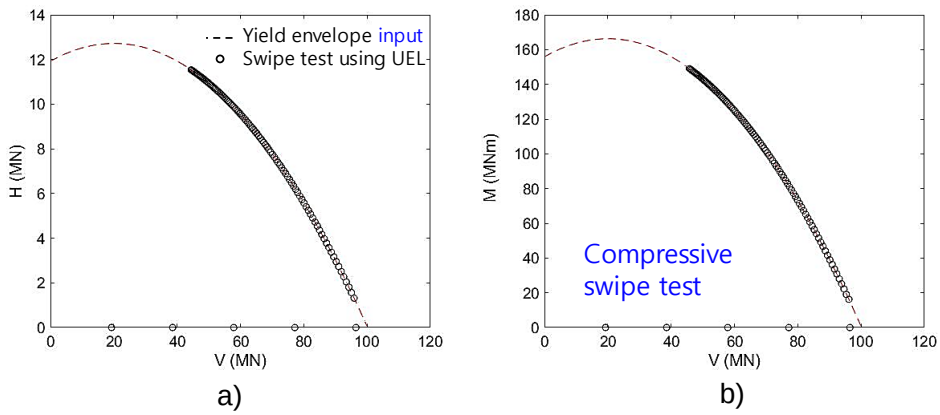

Fig. 65 Swipe test results in a) VH plane; b)VM plane

The vertical, horizontal, and rotational capacity and yield envelope entered in the subroutine are shown in dotted lines in the picture. As a result of the swipe test of the UEL, it has been confirmed that the results (circular point) follow the dotted line well. This well-matched result indicates that the input entered into the UEL is implemented as it is (Fig. 65).

Validation using jack-up structural analysis should be performed on whether the macro element is well implemented. 2D jack-up

analysis in Vlahos et al. (2008b) has been selected as a validation case. Validation on the simplified jack-up is conducted and then expanded into a 3D case to compare the results.

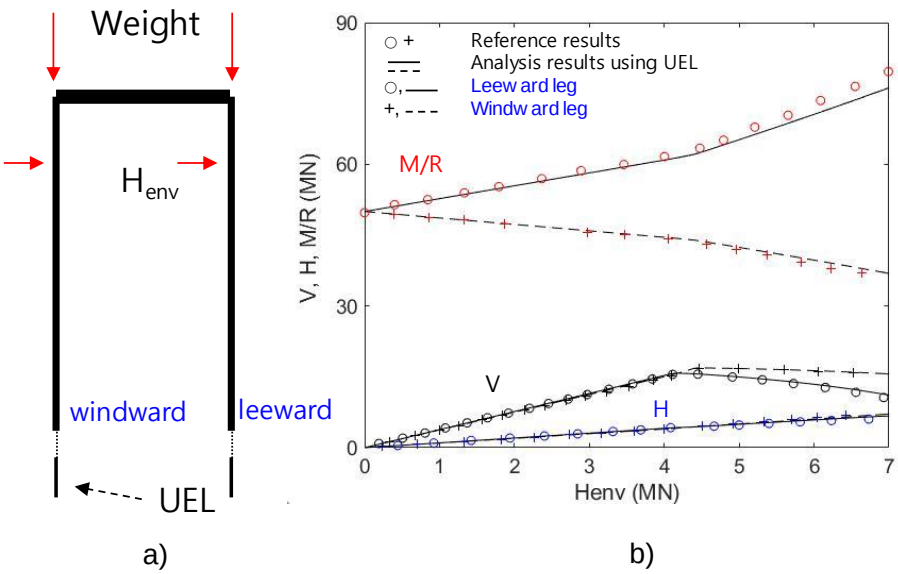

Fig. 66 2D Jack-up validation case;

a) Schematic diagram of validation case;

b) Soil responses of macro element and Vlahos(2008)

The environmental load is 7MN, and the applied vertical load is 50MN in the validation case. The capacity of each direction given in reference has been used as it is. The results of Vlahos et al. (2008b) are shown as a mark (o, +) in the Fig. 66. As a result, yielding at about H_{env}=4MN and moment failure of the leeward leg has been simulated well. In addition, the reaction force in the vertical and horizontal directions of the macro element follows the reference results well.

The same validation case has been used in expanded 3D UEL. 3D yield envelope equation (Eq. (28)) using symmetric conditions has been used (Bienen and Cassidy, 2006).

$$f = \left(\frac{H_2}{H_o}\right)^{\alpha} + \left(\frac{M_3}{M_o}\right)^{\beta} - 2e\frac{H_2}{H_o}\frac{M_3}{M_o} + \left(\frac{H_3}{H_o}\right)^{\alpha} + \left(\frac{M_2}{M_o}\right)^{\beta} + 2e\frac{H_3}{H_o}\frac{M_2}{M_o} + \left(\frac{Q}{Q_o}\right)^2 - \left(\frac{4}{(1+\chi)^2}\right)^2 \left(\frac{V}{V_o} + \chi\right)^2 \left(1 - \frac{V}{V_o}\right)^2 \quad (28)$$

The sign of horizontal and rotational direction is changed according to the sign convention, and a torsion term(Q) is added. As a result of performing the validation case analysis using this equation, the same result of the 2D UEL code result has been obtained. Through this validation process, it has been confirmed that the macro element using UEL subroutine can effectively implement the existing model B. Modified model B (state-of-art model) and hyperbolic model B presented in this study have been implemented based on the existing model B subroutine. These implemented yield interaction models are used in this chapter for the structure-soil interaction analysis.

5.3. Single clay at deep embedment

5.3.1. Jack-up structure

Jack-up, corresponding to the spudcan used in Chapter 3, has been selected for modeling of jack-up structure (Menzies and Roper, 2008). MLT 116C (Fig. 67) is a jack-up oil platform with leg length = 125.08m, leg spacing 39.32m, hull length 74.09m, and breadth 61.11m.

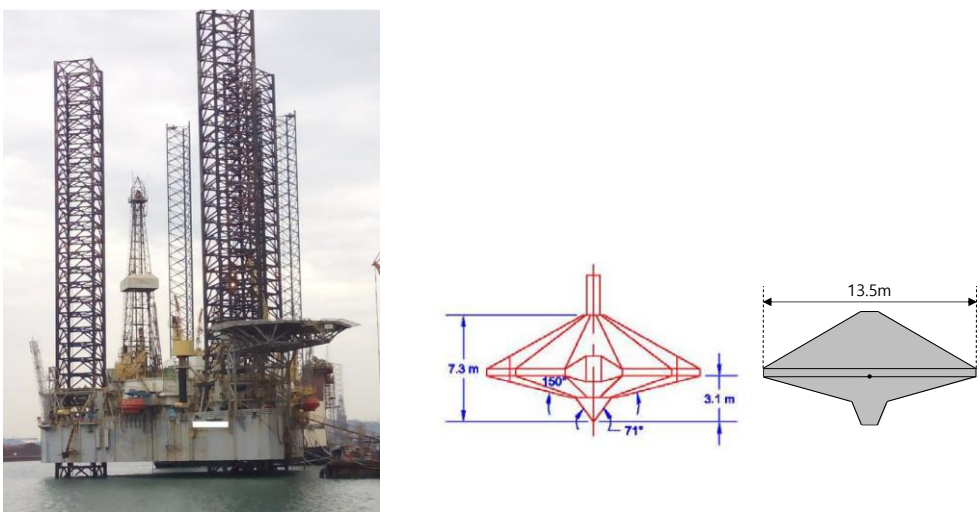

Fig. 67 Jack-up structure used in numerical analysis;
a) Jack-up oil platform (MLT-116C);
b) Simplified spudcan used in Chapter 3

However, it is challenging to know detailed information about this actual jack-up, so the similar-sized jack-up used in the other research has been selected. Zhang et al. (2014a) presented a

detailed specification of the jack-up structure used for verification of modified model B. Given detail has legs with 120m length and 37.87m spacing and spudcans with 14m equivalent diameter. This model closely resembles the leg and spudcan specification of MLT 116C, which is referred in this study. Therefore, corresponding leg section information and stiffness have been used in this study model. The second moment of area of the leg modeled by the equivalent 1D beam in the reference is $7.2m^4$, and this study assumes a rectangular-shaped section of 3.05 m with the same second section moment. In the case of Hull, the reference gives as a 1D beam with a second section moment of $72m^4$, and similarly, in this study, the hull structure is modeled with a rectangular-shaped section of 5.42 m with the same second moment of area. The elastic modulus and shear modulus of the leg use the value of 200 GPa and 80 GPa, respectively, which are common steel values.

5.3.2. FE model used in single clay analysis

The FE model used in structure-soil interaction analysis using the soil continuum model is shown in the figure.

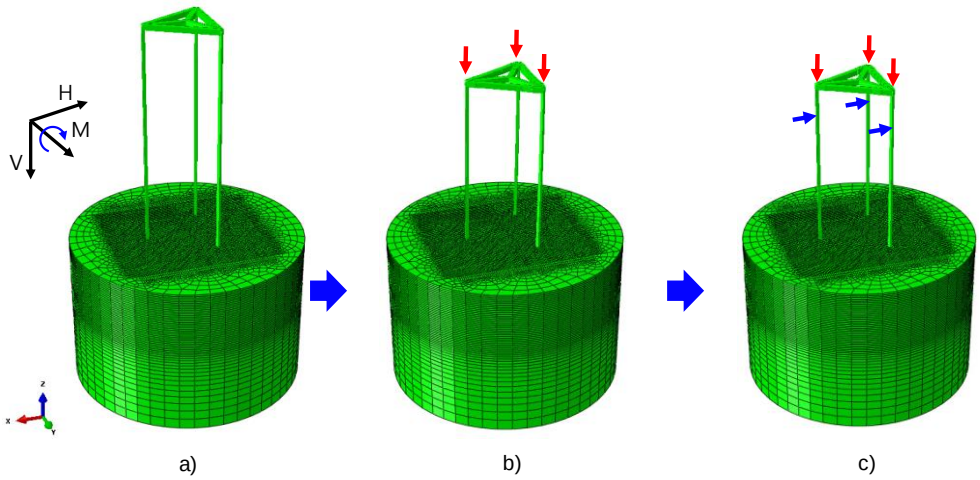

Fig. 68 FE model used in single clay analysis;
a) Starting position; b) Penetration; c) Environmental load analysis

First, jack-up penetrates from the seabed to the target location of 2.2B (Fig. 68(b)). The penetration process simulating the jack-up installation phase has been performed at a 0.2 m/s (=0.015 B/s) of penetration rate. After penetration and positioning at the target position, structure-soil interaction analysis has been performed by applying an environmental load (Fig. 68(c)). The weight of the jack-up structure has been applied to the hull-leg joint as a vertical point load. In the case of environmental loads, a load has been applied to the 105m position (airgap 15m) from the spudcan, assuming the water depth. The environmental load has been applied until the structure failure, so a total of 15MN has been applied by combining the three legs.

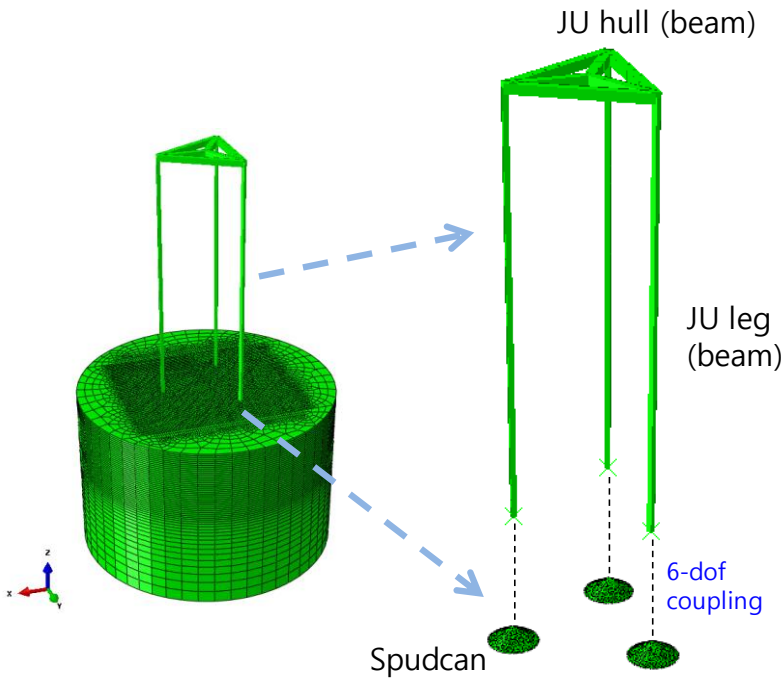

Fig. 69 FE model of jack-up structure

The details of the jack-up structure are as follows (Fig. 69). An equivalent beam model has been used for the jack-up model consisting of leg and hull. This model called stick model has been proposed as one of the leg model types, which can be used for structural analysis in ISO (2012). The stick model can calculate the global response of jack-up, such as base shear and overturning moment, and global leg force such as bending moment, and overturning check and foundation check are also possible because the overall soil reaction response and displacement are calculated. However, since detailed modeling of leg members has not been performed, it is impossible to calculate local response like member forces of legs, hulls, jacking unit, and fixation system. The beams

that make up the legs and hulls are modeled as Timoshenko beams that allow transverse shear deformation (Fig. 70(a)).

Model type	Applicability						
	I	II	III	IV	V	VI	VII
	Base shear and overturning moment	Overturning checks	Foundation checks	Global leg forces	Leg member forces	Jacking/fixation system reactions	Hull element forces
a) Fully detailed leg	Yes	Yes	Yes	Yes	Yes	Yes	See note
b) Equivalent leg (stick model)	Yes	Yes	Yes	Yes	—	—	—
c) Combined equivalent/detailed leg and hull	Yes	Yes	Yes	Yes	Yes	Yes	See note
d) Detailed single leg and leg-to-hull connection model	—	—	—	—	Yes	Yes	—
NOTE Hull stresses are only available from more complex hull models.							

Ref. ISO(2012), Table A.8.2-1

a)

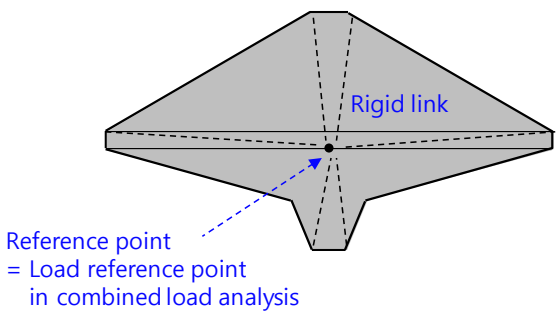

b)

Fig. 70 Analysis condition of jack-up structure;
a) Applicability of leg stick model suggested in ISO(2012);
b) spudcan assumed as rigid body

Spudcan is a steel structure that transfers reaction force and moment by directly performing interaction with the soil. For simulating the structure-soil interaction through the CEL technique, spudcan has been modeled using 3D solid elements. The lagrangian mesh comprises C3D6 and C3D8R elements. The local strength of the spudcan has a minimal effect in terms of overall structural

strength. Therefore, spudcan is assumed to be rigid to clarify the structure−soil interaction without compromising the accuracy of the global analysis. The load reference point(LRP) of spudcan becomes a rigid link (Fig. 70(b)), and this point has been connected to the lower part of the leg through 6−dof coupling.

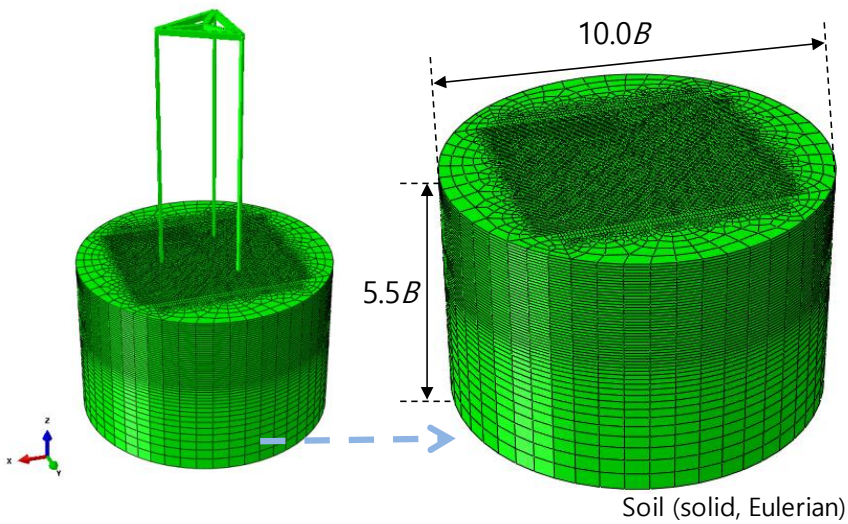

Fig. 71 FE model of soil continuum

The soil continuum has been modeled as 3D soild to perform LDFE analysis through CEL. The eulerian mesh comprises the EC3D8R element. Tresca model incorporating strain softening and rate dependency is used for modeling clay. This nonlinear clay model has been introduced in Chapters 2 and 3. Soil domain has been modeled large enough to avoid boundary effects, width 10 times the spudcan diameter, and height 5.5 times the spudcan diameter (Fig. 71).

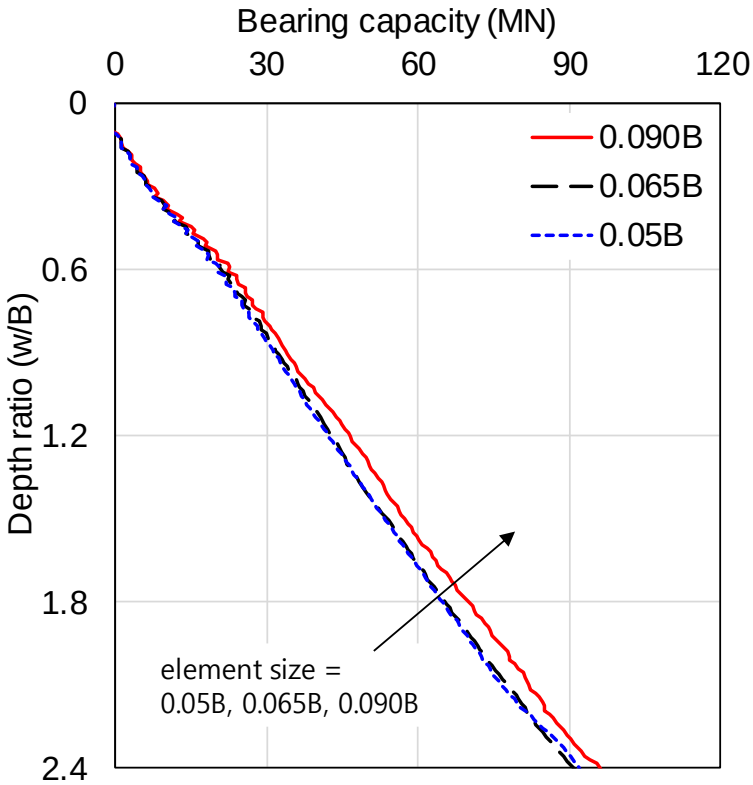

Fig. 72 Mesh convergence test in jack-up analysis

The element size has been determined to be 0.065B considering the computational cost and the accuracy of the analysis. As the element size increases, the analysis time decreases, but the accuracy of the analysis also decreases. Large-sized element typically shows that the bearing capacity value increases (Fig. 72). An element size of 0.065B, which shows similar results compared to 0.05B used in single spudcan analysis, has been adopted.

Table 11 Soil properties used in single clay analysis

	Value	Remarks
γ'	5.36 kN/m^3	Unit weight
s_{um}	2.4 kPa	s_u at mudline
k	1.35 kPa/m	s_u slope with depth
E/s_u	500	Rigidity index
ν	0.49	Poisson's ratio
$\alpha_{friction}$	0.35	Friction coefficient
$S_t\ (=1/\delta_{rem})$	2.86	$\left[\delta_{rem}+(1-\delta_{rem})e^{-3\xi/\xi_{95}}\right]$
ξ_{95}	15	
u	0.1	$\left[1+\mu\log\left(\frac{Max\left(\lvert\dot{\xi}\rvert,\dot{\xi}_{ref}\right)}{\dot{\xi}_{ref}}\right)\right]$
$\dot{\xi}_{ref}$	1%/h	

The soil properties used in single layer modeling are shown in the Table 11. The single clay used in Chapter 3 has been used in the same way. It has been attempted to compare under the same conditions as the yield interaction analysis using soil parameters obtained from the single clay analysis performed in Chapter 3.

5.3.3. Yield interaction model used in single clay analysis

jack-up structural analysis has been performed using the yield interaction model implemented in UEL and compared with the analysis results using the soil continuum model described above. The same model of jack-up structure with the soil continuum model in 5.3.2 has been used. This is for comparison of the differences according to the nonlinear foundation model in the same structure.

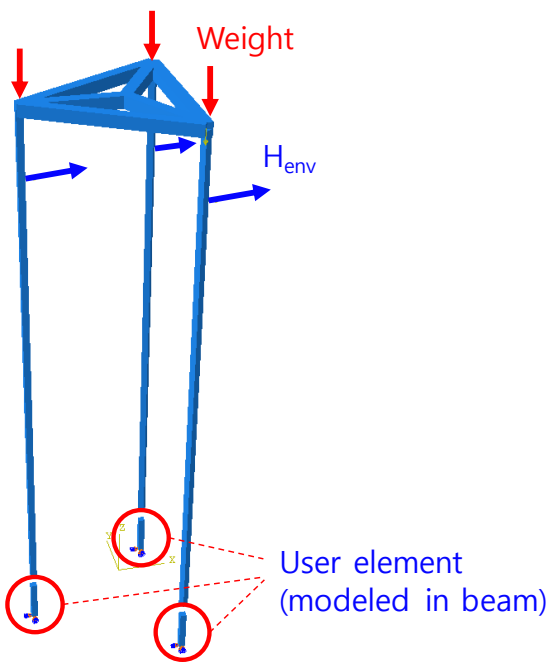

Fig. 73 FE model for structure-soil interaction analysis with yield interaction model (model B)

FE model of jack-up analysis using the yield interaction model is shown. The implemented user element is placed in the lower part of the jack-up leg as a 1D beam. Legs and user elements are

connected by 6-dof coupling like spudcan so that the reaction and displacement calculated from user elements can be transferred. The bottom of the user element is fixed so that only the user element reaction becomes the boundary condition of the jack-up structure.

Two types of yield interaction models have been used to compare each other. First, hyperbolic model B, a proposed model for soft over stiff clay, has been used in this study. Although it is a proposed model for soft over stiff clay, it is thought that the hyperbolic relation in the elastic region will be effective even for single clay. And for comparison, the modified model B (Zhang et al., 2014b), which is a state-of-art model on a single clay, has been used. The difference between the proposed model and the latest model is analyzed in this chapter.

Table 12 Soil parameter used in single clay analysis

Capacity	Value	Stiffness	Value
V_{ult}	69.79 MN	K_v	574.52 MN/m
H_o	24.20 MN	K_h	473.90 MN/m
M_o	121.40 MNm	K_m	19760 MNm/rad
		K_c	-120.27 MN/rad

For comparison in the same criteria, both models use the same soil parameters (stiffness, capacity). Zhang et al. (2012) has suggested stiffness and capacity for single clay. However, if two

models using different parameters are compared, the difference in methodology becomes unclear. To remove the effect of soil parameters on the results, the soil parameters obtained through single spudcan analysis (Table 12) have also been used in modified model B. It has been intended to show the difference of the methodologically proposed model and existing model.

5.3.4. Results

The results of the jack-up analysis considering structure-soil interaction by using a nonlinear foundation model for single clay were compared. The results of the reaction force, moment, and displacement acting on the soil are shown in the figure. The results of the soil continuum model and two yield interaction models, described in 5.3.2 and 5.3.3 respectively, are shown in the figure.

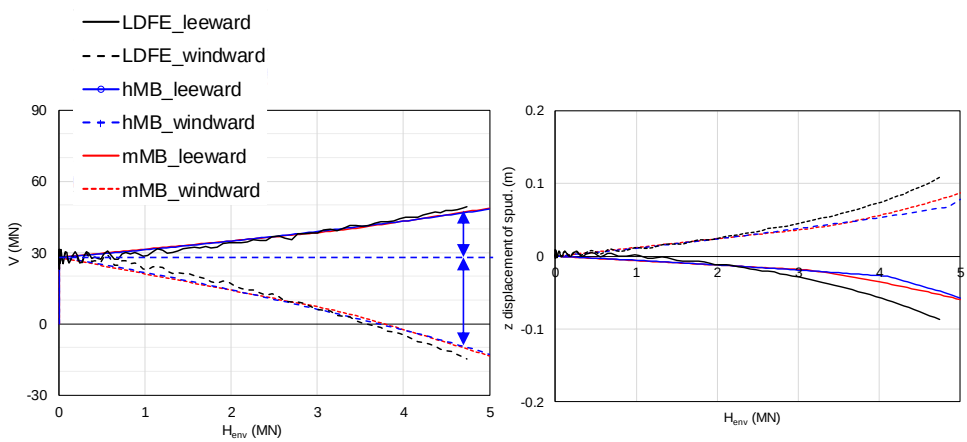

Fig. 74 Soil response in vertical direction of single clay analysis; a) Reaction force; b) Displacement

The Fig. 74 shows the vertical reaction force and displacement of the structure-soil interaction models. When an environmental load is applied, the whole structure rotates in the environmental load direction, so that the leeward leg shows the downward motion and the windward leg shows upward motion. This phenomenon is shown in the Fig. 74 about the vertical load and displacement. The reaction force of Leeward leg increases, and accordingly downward motion is shown in the vertical direction. The windward leg shows upward motion and the corresponding reaction force decreases accordingly. The load applied direction is the direction in which two of the three legs are leeward leg and one is the windward leg. Accordingly, it is shown that the displacement and reaction force of the windward leg are about twice as large as the leeward.

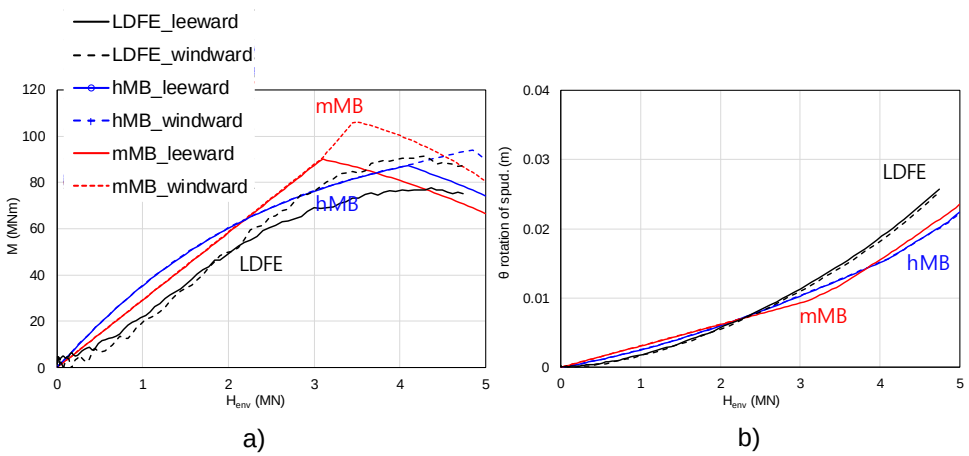

Fig. 75 Soil response in rotational direction of single clay analysis; a) Reaction moment; b) Rotation

The Fig. 75 shows the rotational reaction moment and rotation of the structure-soil interaction models. In general, the soil experiences moment failure first among the other directions during jack-up behavior. That is the reason why the secant model introduced the concept of secant stiffness for moment stiffness. Soil continuum model (LDFE) and yield interaction results have also confirmed that failure occurs first in the rotational direction. When looking at the LDFE results, the increased rate of moment gradually decreases as the environmental load increases and eventually starts to fall near 4 MN. This moment failure occurs gradually, and the displacement also shows increasing the slope progressively. In the case of the yield interaction models, both models well predicted the moment failure. In particular, plasticity occurs in the case of the environmental load 5MN, where the failure of the structure occurs. In the hyperbolic model, strength degradation in the elastic region has been simulated through hyperbolic relation before plasticity occurred. Accordingly, the reaction moment gradually decreased as the environmental load increased, such as LDFE. In contrast, the modified model B shows that the reaction moment increased relatively linearly as the environmental load increased before yield occurs. Thus it has been confirmed that the moment is slightly overestimated at the yield point. In the case of displacement, hyperbolic model B results are gradually increased, but the difference between foundation models is not significant.

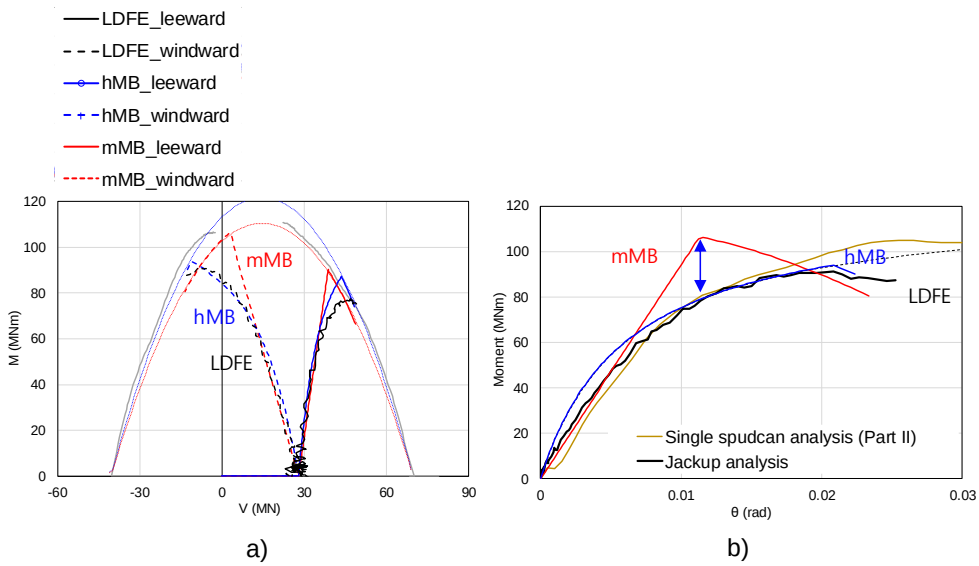

Fig. 76 Soil response of single clay analysis;

a) Load path in VM plane; b) M− θ relationship of analysis

The difference between the two yield interaction models is better shown in the Fig. 76(a). The load path for the vertical reaction force and the rotational reaction moment shows the difference between the two models before the yield point. In the case of Hyperbolic model B, the overall load path, including the gradual moment failure, follows the LDFE results relatively well, especially in the windward leg. In the case of modified model B, the behavior after the yield point is similar to that of the other two models. However, the behavior before yield is somewhat close to linear so that the difference is presented.

Fig. 76(b) shows the moment−rotation material curve in the rotational direction where yield occurs. By using the same soil properties, the material curve obtained from single spudcan analysis

and that from jack-up structural analysis are almost identical. Hyperbolic model B using hyperbolic relation fitted from singe spudcan analysis follows the strength degradation before yield and moment failure after yield. However, the modified model B accurately simulates the plastic behavior after yielding, while the elastic behavior shows a curve close to linearity. Gradual moment failure in LDFE results has not been simulated in modified model B.

5.4. Soft over stiff clay

5.4.1. FE model used in soft over stiff clay analysis

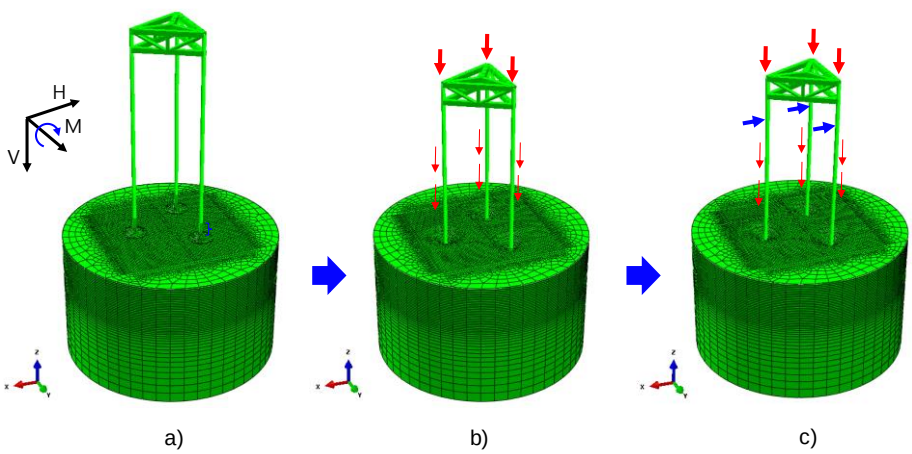

Fig. 77 FE model used in soft over stiff clay analysis; a) Starting position; b) Penetration; c) Environmental load analysis

The FE model used in structure-soil interaction analysis using the soil continuum model is shown in Fig. 77. As a typical soft over stiff clay, the MWS2P case is selected, in which the physical

properties of the lower clay is twice as hard as the upper soft clay. After the penetration of the jack-up structure, the same load sequence with the single clay case is performed to apply the environmental load. The penetrated location of 2.2B and the penetration rate of 0.015B/s have also been the same. In the soft over stiff clay case, the soil profile, which is the main point of the analysis, has been changed, as well as the jack-up structure and the applied load. jack-up structure has been damaged by the impact due to lower stiff clay. To prevent this, the hull leg joint and spudcan-leg joint have been reinforced. First, the hull-leg joint has been reinforced through additional brace structures to increase strength. In addition, the local spudcan-leg joint has been changed from the pipe section to the circular section to increase the strength without changing the outer diameter. Also, in the case of vertical load, the total load is the same, but the leg weight is applied as the distribution load. And as the soil properties changed, the environmental load reaching the failure of the structure has been changed. A total of 19.5MN of the load has been applied to the leg by combining the three legs.

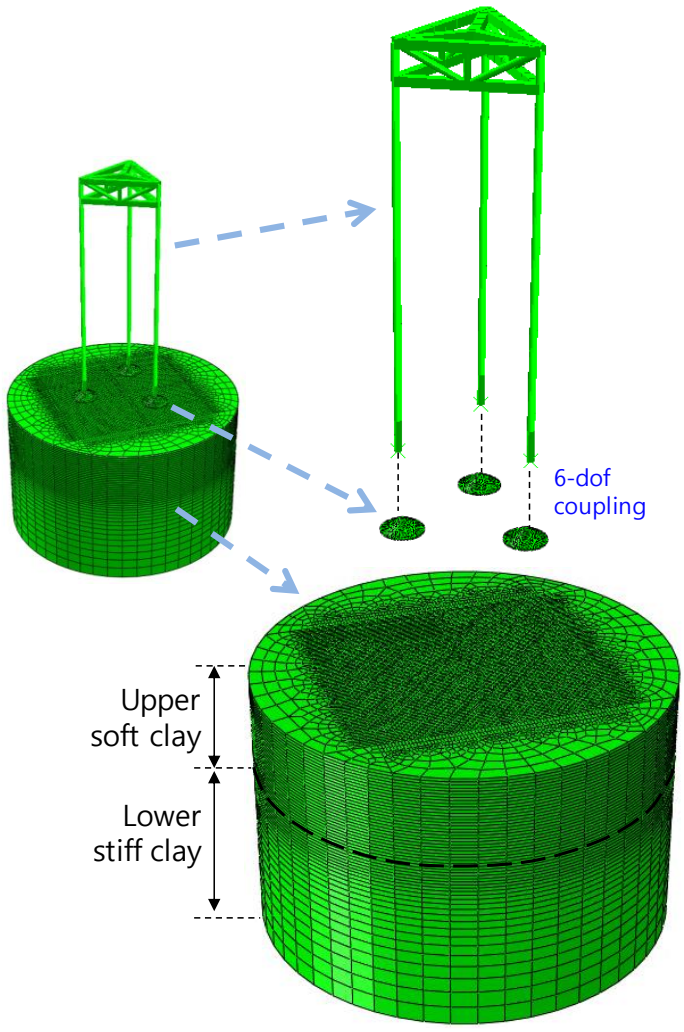

Fig. 78 Detailed FE model used in soft over stiff clay analysis

As described above, the same jack-up structure and spudcan as single clay case are used in soft over stiff clay case. Jack-up modeling has been performed with a stick model using a Timoshenko beam. To use the CEL technique, the spudcan has been modeled as a 3D solid lagrangian model and assumed to be a rigid body for analysis clarity. Jack-up structure and spudcan is connected using 6-dof coupling which transfers the reaction force, moment and

displacement. The whole soil domain has remained the same, and accordingly, the domain size and element size of the eulerian mesh is the same (Fig. 78). However, the soil domain has been divided into two layers to model the upper and lower clays. The upper layer is composed of the same soft clay as the existing single clay, and the lower layer is modeled by applying twice the undrained strength at the boundary of the upper soft clay. This is the same as the MWS2P case of Chapter 3, which is for comparison under conditions such as yield interaction analysis using soil parameters obtained from soft over stiff clay analysis performed in Chapter 3. Details are given in the Table 13.

Table 13 Soil properties used in soft over stiff clay analysis

	Value	Remarks
γ'	7.46 kN/m^3	Unit weight
s_{um}	77.81 kPa	$s_{u,stiff} = s_{u,H}$ Twice the upper clay strength
k	–	Homogeneous soil (assumed)
E/s_u	500	Rigidity index
ν	0.49	Poisson’s ratio
$\alpha_{friction}$	0.35	Friction coefficient

5.4.2. Yield interaction model used in soft over stiff clay analysis

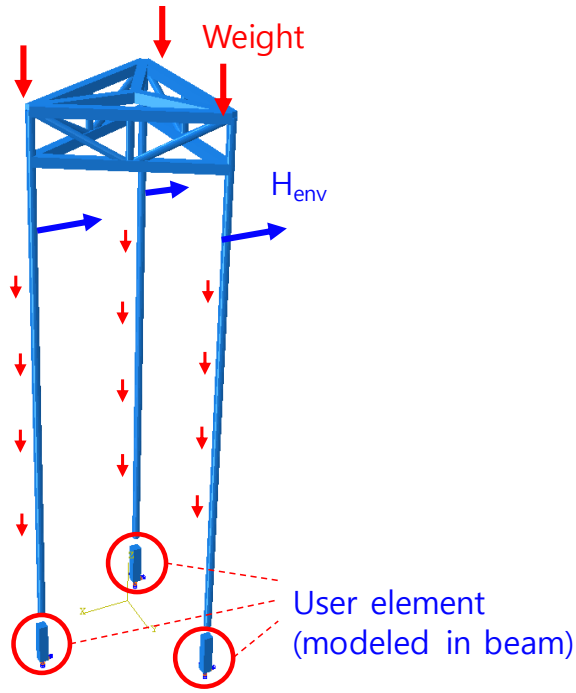

Fig. 79 FE model used in soft over stiff clay cas for structure-soil interaction analysis with yield interaction model (model B)

The jack-up structure changed in 5.4.1 has been used in the yield interaction model for consistency (Fig. 79). The soil continuum model described in 5.4.1 and the jack-up analysis with yield interaction model with the same structure are compared. Like a single clay case, the user element with the yield interaction model is implemented as a 1D beam and placed at the bottom of the leg. UEL and leg is connected by using 6-dof coupling. In the soft over stiff clay case, the hyperbolic model B proposed in this study and the latest modified model B have been used (Zhang, 2014). Modified model B is a model for a single clay, but soil parameters obtained

from soft over stiff clay have been applied for analysis.

Table 14 Soil properties used in soft over stiff clay analysis

Capacity	Value	Stiffness	Value
V_{ult}	110.95 MN	K_v	654.94 MN/m
H_o	26.16 MN	K_h	622.90 MN/m
M_o	165.20 MNm	K_m	35080 MNm/rad
		K_c	−62.62 MN/rad

There is no suggested soil parameter of modified model B for soft over stiff clay. Accordingly, the soil parameter obtained in this study has been applied equally to both models for consistency. The comparison between two yield interaction models in soft over stiff clay is intended to be analyzed by methodology.

5.4.3. Results of soft over stiff clay analysis

Fig. 80 shows the vertical reaction force and displacement of the structure–soil interaction models.

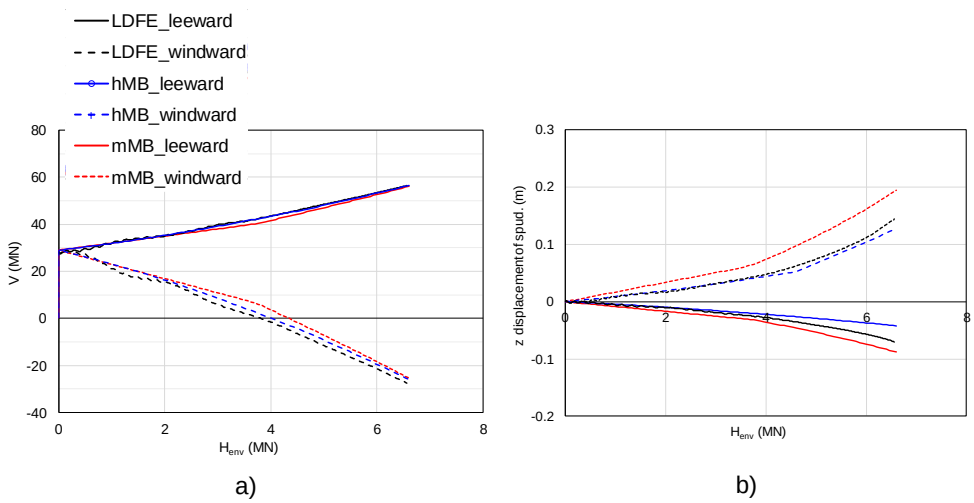

Fig. 80 Soil response in vertical direction of soft over stiff clay analysis; a) Reaction force; b) Displacement

As mentioned in 5.3.4, when an environmental load is applied, the jack–up rotates as a whole in the direction in which the environmental load is applied, so that the leeward leg is downward and the windward leg is subjected to upward forces. This phenomenon also occurs in the soft over stiff clay case. Leeward leg shows downward motion, and at the same time, vertical reaction force increases. In contrast, the windward leg shows upward movement, and the vertical reaction force decreases.

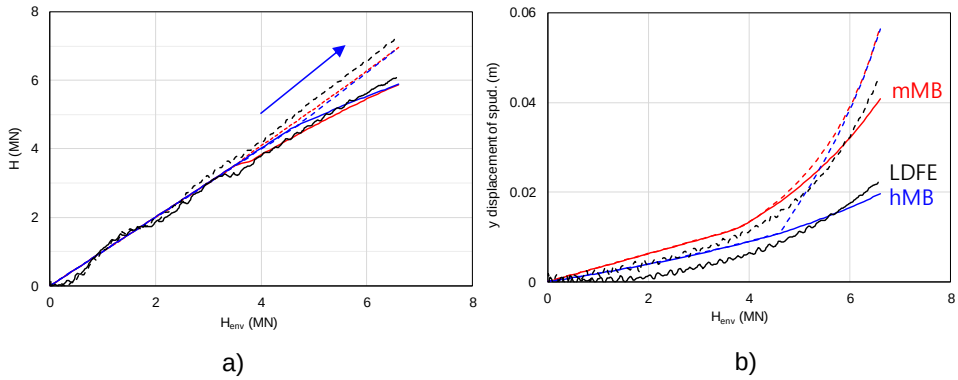

Fig. 81 Soil response in horizontal direction of soft over stiff clay analysis; a) Reaction force; b) Displacement

Fig. 81 shows the horizontal reaction force and displacement. As the environmental load is applied in the horizontal direction, in the elastic region, the horizontal reaction force acting in the opposite direction should be the same value by the principle of action-reaction. Before the yield occurs near H_{env}=4MN, it has been confirmed that the horizontal reaction force of the same magnitude as the environmental load occurs in both the soil continuum model and the two yield interaction models. When yield occurs, moment failure occurs first, and redistribution of force occurs accordingly. The horizontal response of the leeward and windward legs is changed because of their different vertical forces. Typical pushover test using centrifuge also shows an increased H of windward leg. As a result of the structure-soil interaction analysis of this study, it is shown that the response of the two legs becomes different due to the redistribution of the force after yield, and the response of the windward leg is greater.

Displacement results show a difference between the hyperbolic model B and the existing modified model B, in which the hyperbolic relation is implemented in the horizontal direction in the hyperbolic model B (Fig. 81(b)). The soil continuum model by using LDFE analysis results in a gradual increase in displacement, which is also simulated in hyperbolic model B. However, modified model B shows a relatively linear relationship, and accordingly, the yield occurs more quickly. As a result, there is a difference in displacement between two yield interaction models. Hyperbolic model B shows similar results to the soil continuum model, especially in the leeward leg.

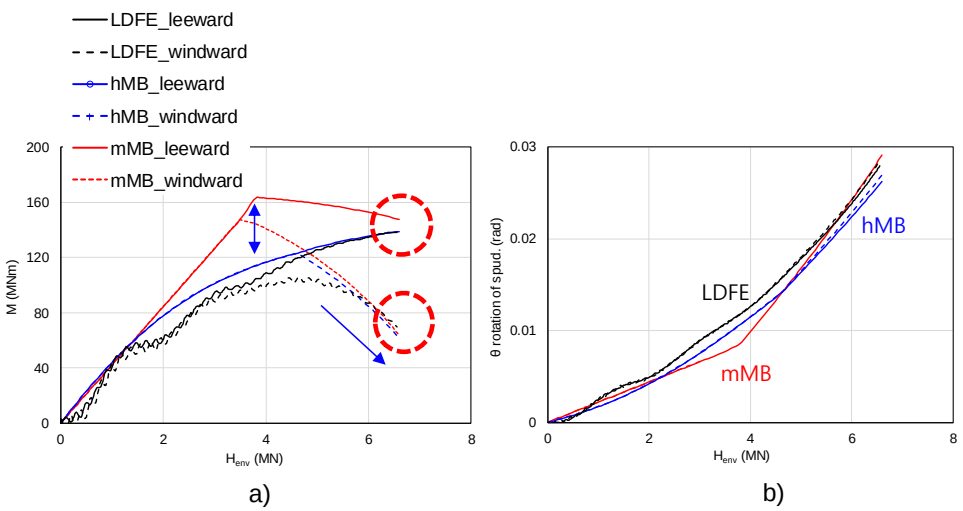

Fig. 82 Soil response in rotational direction of soft over stiff clay analysis; a) Reaction moment; b) Rotation

Fig. 82 shows the rotational reaction moment and rotation according to the environmental load. Soil failure usually occurs first

in the rotational direction, and in this respect, it is important to simulate the reaction moment precisely. In soft over stiff clay cases subjected to larger environmental loads, the gradual moment failure appears well. The moment increases slowly as the environmental load increases in the results of the soil continuum model, and it is shown that the moment values of the windward leg become different due to yield near the environmental load of 4MN. Modified model B predicted the yield point of 4MN well, and it is shown that the moment in the plastic region is close to the LDFE result. In Hyperbolic model B, the yield point is somewhat slower (Henv=4.5MN), but the strength of degradation at the moment is well simulated. With this nonlinear hyperbolic relation in the rotational direction, the moment results about the environmental load approach close to the LDFE result. In the case of modified model B, despite the similar results after yield, the moment is overestimated due to the near-linear moment increase in the elastic region. In the case of rotation of the spudcan(Fig. 82(b)), hyperbolic model B expresses a gradual increase due to hyperbolic relation, but modified model B also shows a good fit with LDFE results due to the changed slope after yield.

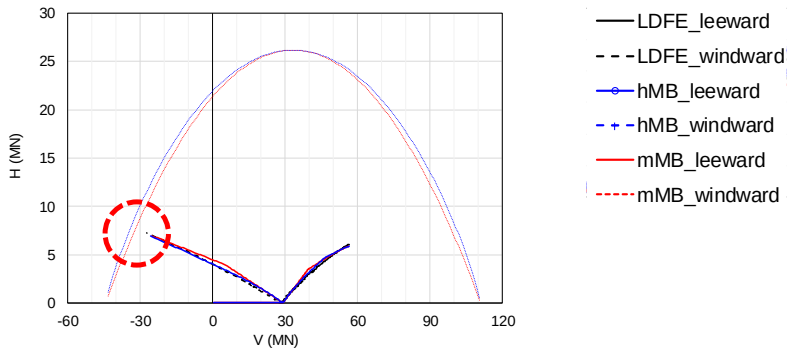

Fig. 83 Load path of soft over stiff clay analysis in VH plane

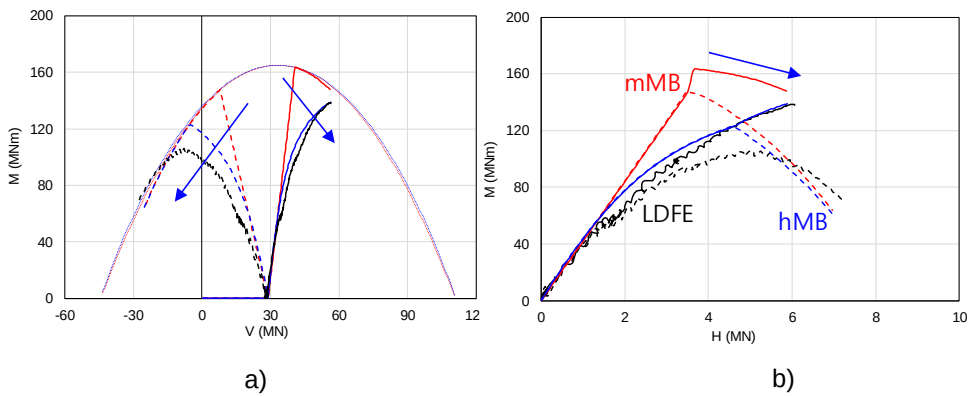

Fig. 84 Load path of soft over stiff clay analysis;

a) in VM plane; b) in HM plane

For the vertical reaction force, horizontal reaction force and rotation reaction moment shown above, the load path is plotted on the plane with each force as the axis (Fig. 83, Fig. 84). First, in the case of the load path in the VH plane (Fig. 83), LDFE, hyperbolic model B, and modified model B results are similar. Compared with the yield envelope used in the yield interaction model, the load path has not yet been reached the yield envelope in a horizontal direction. Therefore, the horizontal reaction force reduction did not occur

because of yield, such as the moment.

The load path in the VM plane and HM plane shows the effect of moment failure (Fig. 84). The load path in the VM plane shows that the results of hyperbolic model B follow the results of LDFE better. Unlike modified model B, which approaches the yield envelope in a direction close to linear at initial stiffness, the slope of hyperbolic model B gradually decreases in the increment of the moment and thus becomes similar to the result of the soil continuum model, where the gradual moment failure occurs. In addition, the modified model B rapidly approaches the yield envelope, and yield occurs in the leeward leg. In contrast, the hyperbolic model B does not reach the yield envelope, and yield does not occur. This indicates that, like the load path in the HM plane, the linear elastic relationship of modified model B can overestimate the moment before yield. On the other hand, hyperbolic model B similarly simulates gradual moment failure due to the implemented nonlinear hyperbolic relations.

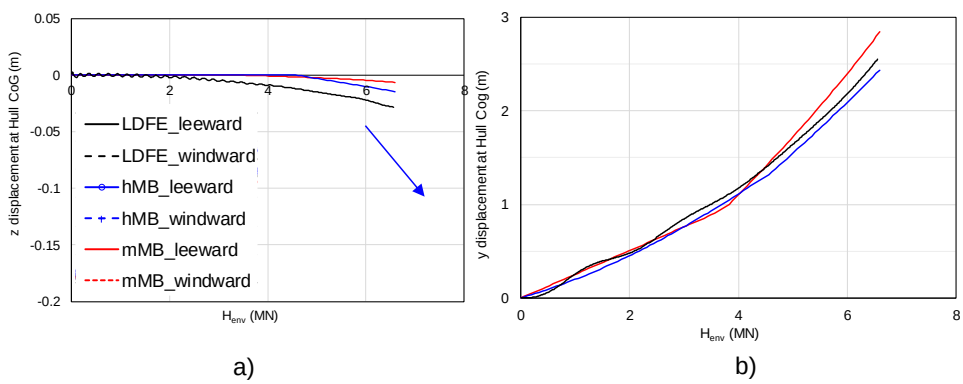

Fig. 85 Hull displacement of soft over stiff clay analysis;
a) Vertical displacement; b) Horizontal displacement

The vertical and horizontal hull displacements are shown in the Fig. 85. As the soil continuum model simulates the gradual plasticity of the soil, the hull gradually moves down and shifts in the horizontal direction. In the yield interaction model, these plastic deformations can be simulated, but due to the characteristics of the elasto-plasticity framework, plastic deformation is not calculated before yield occurs. Accordingly, both yield interaction models have a vertical displacement of 0 in the elastic region, and then plastic deformation increases after yield. The plastic displacement of the hull calculated in the hyperbolic model B approaches the LDFE result faster (Fig. 85(a)). In general, horizontal behavior in the hull is affected by rotation at the spudcan due to the long leg length. Spudcan rotation is similar in the three models, so the horizontal displacement of the hull is also similar (Fig. 85(b)).

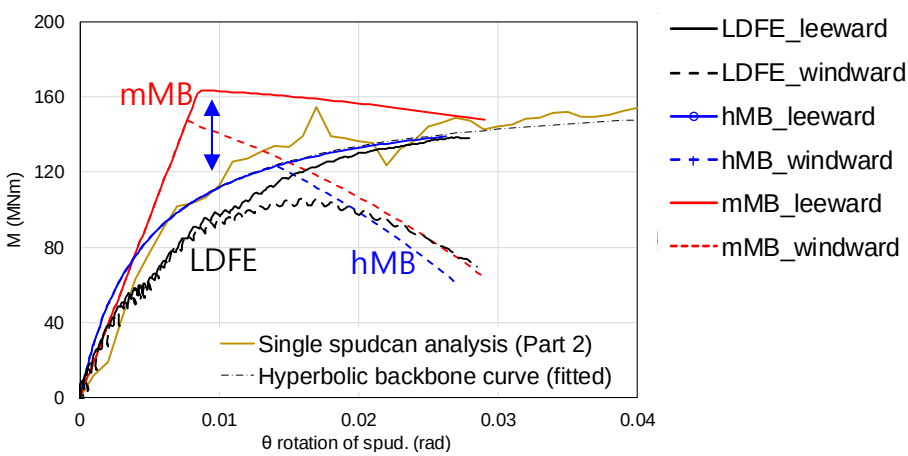

Fig. 86 M-θ material curve of soft over stiff clay analysis

To present the moment failure, the M− θ material curve in single spudcan analysis, jack−up analysis using a soil continuum model, and those of two yield interaction models are shown in Fig. 86. Hyperbolic model B uses a fitted hyperbolic curve from the results of single spudcan analysis and follows the entered curve well. The decreasing moment has also been simulated in the windward leg where yield occurs due to the vertical and horizontal forces. A smaller moment is available under vertical and horizontal reaction force than that under no vertical and horizontal forces in the concept of force−resultant yield envelope. In contrast, in the case of modified model B, the moment overestimates in the elastic region before yield. However, the results approach the LDFE results fast after yield.

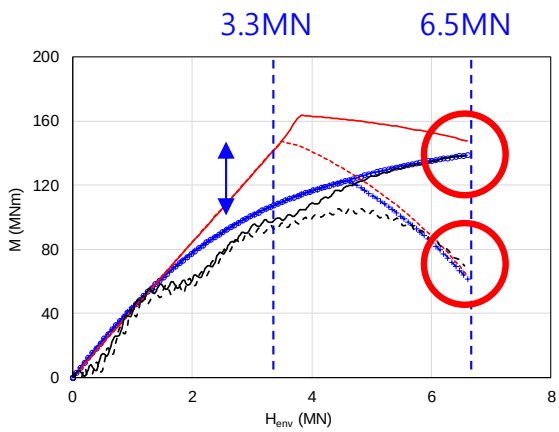

Fig. 87 Two moments for structural response of jack−up (H_{env}=3.3MN for elastic, 6.5MN for plastic)

Two moments are selected to compare the structural response of jack−up. First, the point within the elastic region, where the

moments of the two yield interaction models are different (H_{env}=3.3MN in Fig. 87), and the point within the plastic region, where ground failure and structure failure occur (H_{env}=6.5MN in Fig. 87), are selected.

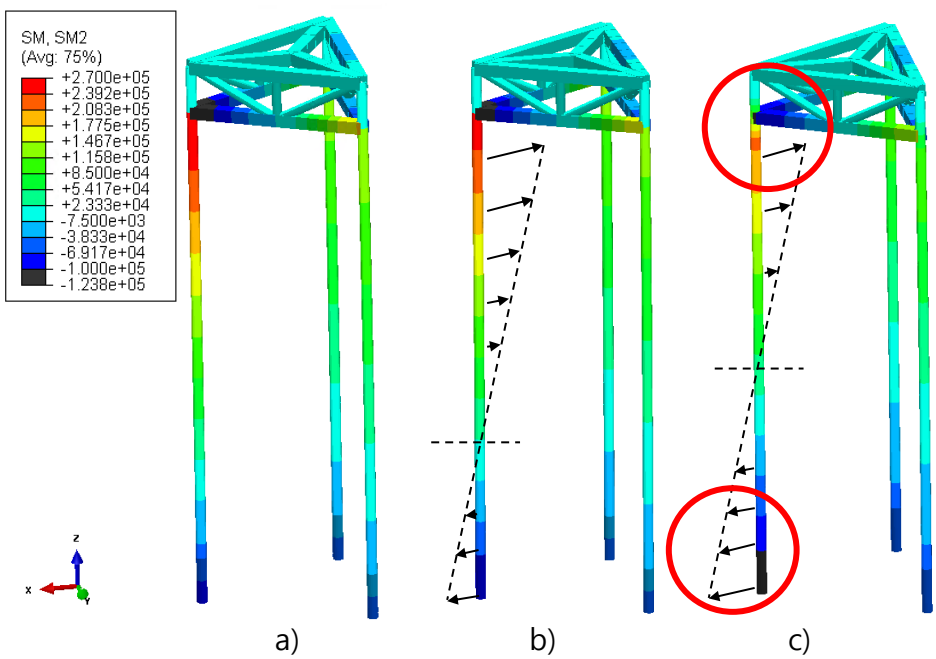

Fig. 88 Bending moment at H_{env}=3.3MN; a) LDFE analysis; b) Hyperbolic model B; c) modified model B

The structural response at the H_{env}=3.3MN, where a difference in soil reaction moment between modified model B and hyperbolic model B occurs, is shown in Fig. 88. The stick model is suitable for viewing the global jack-up response, not local member forces, and thus the distribution of the bending moment of the leg is presented. Hyperbolic model B shows a similar distribution to soil continuum model results using LDFE. On the other hand, modified model B

shows that the reaction moment on the soil is larger than the other two models, and the bending moment of the leg is also different accordingly. The moment acting on the spudcan–leg joint is larger than the other two models like soil response, so the distribution of the moment of the entire leg is shifted. As a result, the bending moment at the hull–leg joint is underestimated due to the shifted distribution. This joint is the critical point of jack–up structural analysis, and the hyperbolic model B shows a more accurate bending moment distribution of leg.

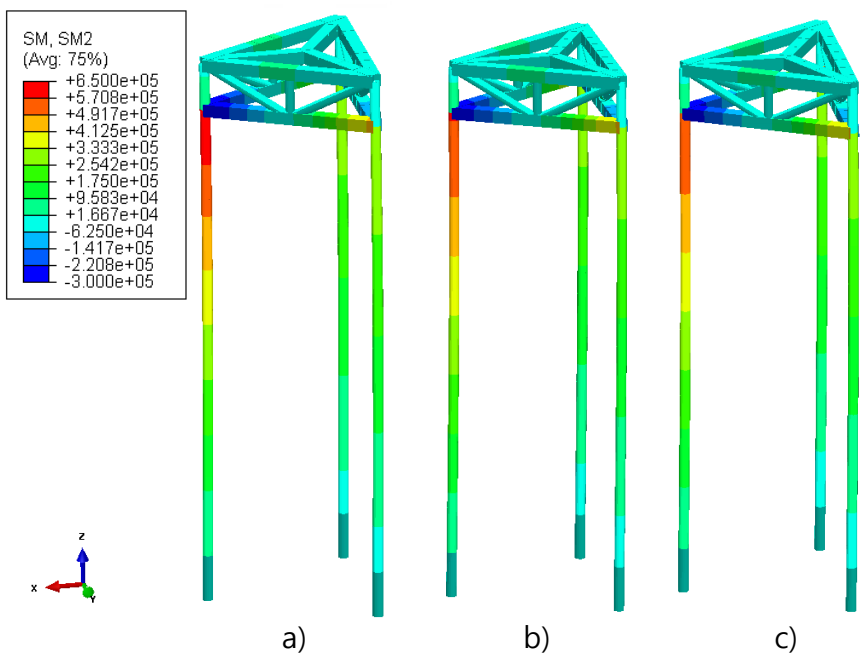

Fig. 89 Bending moment at H_{env}=6.5MN; a) LDFE analysis; b) Hyperbolic model B; c) modified model B

The structure response at H_{env} = 6.5MN, where the plasticity of the soil and the failure of the structure occurs, is shown in Fig. 89.

In this plastic region, the three models show similar values. This is because modified model B simulates a moment in the plastic region well through the plasticity framework after yield. As a result, all three models showed a similar distribution in terms of the bending moment of the leg.

Through the bending moment results, it has been confirmed that the magnitude of the reaction moment acting on the spudcan, which is the same with the applied moment on soil, affects the distribution of the bending moment of the leg. The distribution of bending moments is similar if they show similar soil reaction moments (Fig. 89). However, it is important that the large reaction force on the soil may lead to an underestimation of the bending moment in the hull–leg joint (Fig. 88).

Chapter 6. Dynamic effects of jack-up structural analysis

6.1. Introduction

Jack-up is an offshore structure that is subjected to environmental loads such as wave, current, and wind during operation. Random wave is generally expressed as the sum of regular waves of different periods and heights, and have a great influence on the dynamic response of structures.

Offshore platforms are always designed for the specific field, so the natural period varies depending on the design and characteristics of the individual structures. However, in general, fixed offshore structures have a small natural period (T_n < 5s). In comparison, floating offshore structures typically have a comparatively long natural period (T_n > 20s). Jack-ups typically have a natural period between 5 ~ 15 seconds, depending on their size, which overlaps the maximum wave energy spectrum (ABS, 2014). This means that jack-up is the dynamically sensitive offshore platform in wave analysis (Fig. 90(a)).

To consider these dynamic characteristics, jack-up structural analysis of dynamic loads has been performed using a soil continuum model. In this chapter, the dynamic effects that accompany jack-up dynamic analysis are investigated. These include the effects due to inertia force, resonance with wave, and dynamic characteristics of

the soil (Fig. 90(b)). These effects were investigated and reflected in the yield interaction model and compared with the results of the soil continuum model.

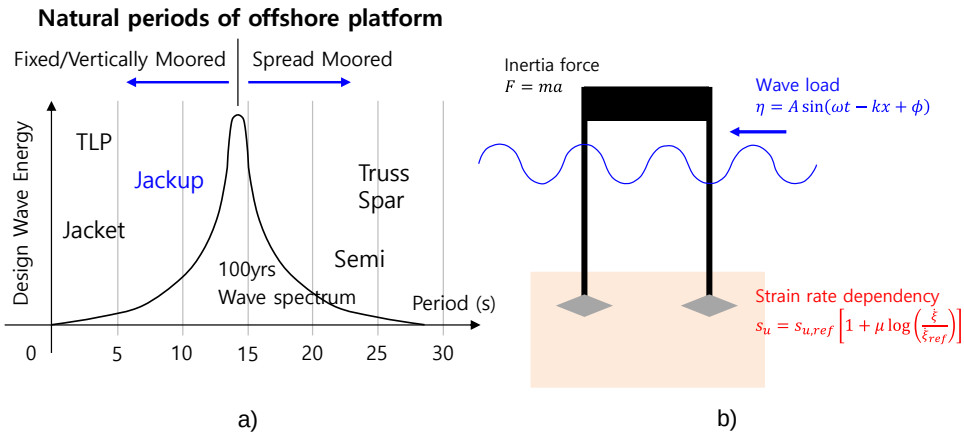

Fig. 90 Dynamic effects of jack-up;

a) Typical natural period of offshore platform;

b) Jackup structural analysis with dynamic load

6.2. Dynamic effects in jack-up structural analysis

6.2.1. Categorization of dynamic effects

Dynamic effects are caused by several factors about time. It has been divided into two categories in this chapter, structural aspect, and geotechnical aspect.

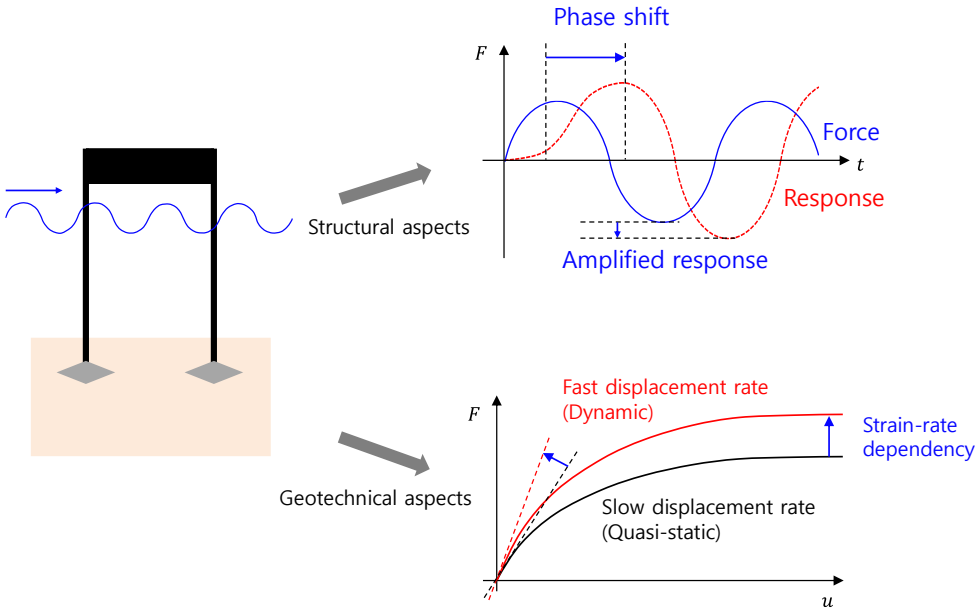

Fig. 91 Schematic figure of dynamic effects

Dynamic effects about clay can be a strain rate dependency of properties, energy dissipated damping, material damping, and so on. Damping is generally considered by observation and calculation of coefficient through experiments, and the material damping has been usually simulated using a viscous material model. Among these dynamic effects, the strain rate dependency has been described in this chapter. In general, as the strain rate increases, the strength increases, and the stiffness and capacity increase accordingly. This effect has been reflected in the numerical analysis with the soil continuum model. Soil parameters considering the rate hardening are entered into the yield interaction model, and the results are compared with those of LDFE analysis.

Structural dynamic effects include amplified response and phase shift, due to inertia force. The amplified response is caused by

several factors, such as resonance with a wave, wave damping, and the effect of soil damping on the boundary condition. In general, when determining the dynamic response of a structure, these various factors are collectively considered as DAF (Spidsøe and Karunakaran, 1996; Yu et al., 2012). Although it is difficult to calculate the exact DAF, this study has assumed the DAF carefully and applied to the yield interaction model. The analysis results are compared with those of the soil continuum model.

6.2.2. Strain rate dependency of clay on jack-up wave analysis

In general, as the strain rate increases, s_u increases in logarithmic scale. This relationship is also introduced in Abelev and Valent (2009) and Nanda et al. (2017). Rate hardening with logarithmic relation is also implemented in nonlinear clay model (Eq. (29)) used in this study.

$$s_{ui} = \left[1 + \mu \log\left(\frac{\mathrm{Max}\left(\left|\dot{\xi}\right|, \dot{\xi}_{ref}\right)}{\dot{\xi}_{ref}}\right)\right] \left[\delta_{rem} + (1 - \delta_{rem}) e^{-3\xi/\xi_{95}}\right] [s_{\mathrm{umi}} + kz_i] \tag{29}$$

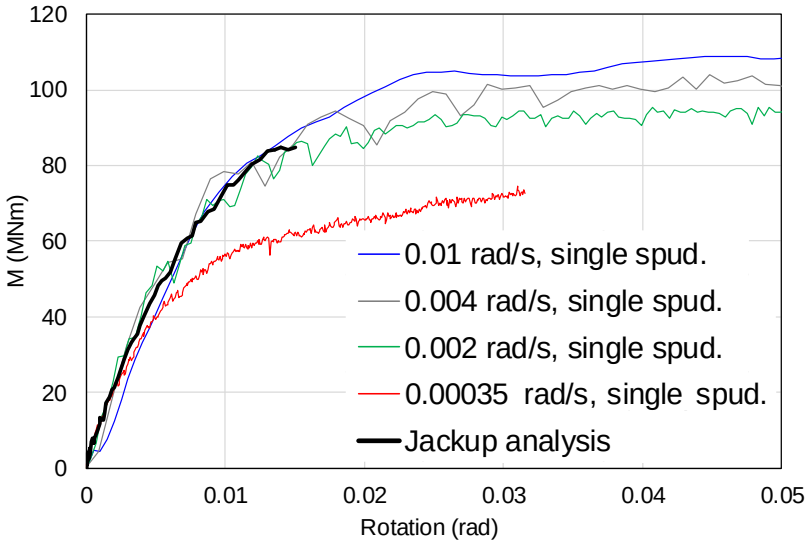

Fig. 92 M− θ curve according to the rotation rate

Fig. 92 shows the effect of rotation rate on material curve (M–θ) in single spudcan analysis. Wave load analysis results of Jackup is also plotted together (black line). Quasi static case has both small stiffness and small capacities (red line), but the rate is far from dynamic wave analysis. M–θ curve in this study (Chapter 3) based on 0.01 rad/s is rather close to wave analysis. When typically calculating soil parameters, the analysis has been performed at a sufficiently slow rate to eliminate the inertia effect. However, quasi−static analysis cannot accurately consider soil properties due to rate dependency. This rate dependency is considered in this study through soil parameter calculation, both stiffness and capacity, and these calculated soil parameters are used in static yield interaction model.

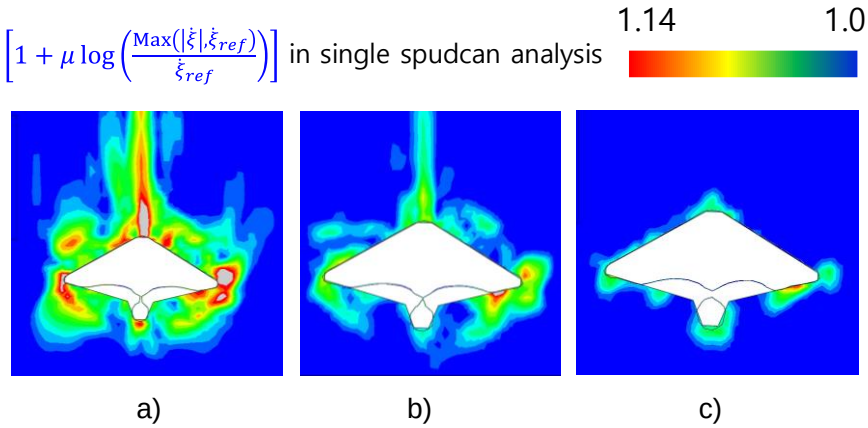

Fig. 93 Contour about rate hardening value in nonlinear clay model; a) 0.01 rad/s; b) 0.002 rad/s; c) 0.00035 rad/s

6.2.3. Phase shift effect

Phase shift is typically caused by inertia force in dynamic analysis. To identify the phase shift in jack-up analysis, mass scaling technique in Abaqus is used. Mass scaling technique increase the mass of the model artificially in numerical simulation. Mass scaling is a technique that forcibly increases the time increment by artificially increasing the mass term because this mass term is proportional to the time step in the explicit analysis. With this increased time increment, explicit analysis that takes longer can be performed more cost-efficiently. In this scaled-mass analysis, inertia effect is amplified through mass scaling, but the rate dependency of material is maintained (Simulia, 2013). This study has focused these features of the technique. In a situation where the response due to the rate dependency did not change, how the

amplified inertia effect by artificially increasing the mass affects the response is examined.

In Fig. 94, phase shift occurs in the case of amplified inertia effect (mass scaling = 4). Immediately after the load is applied, the response is delayed due to the high value of initial acceleration. However, inertia effect is reduced and responses converge as the analysis progresses. Under monotonic load analysis, phase shift due to inertia effect occurs at initial phase but does not affect the response after stabilization. When designing offshore structures, the magnitude of the response is more important than the phase. After sufficient stabilization, it is assumed that the inertia effect does not exist in the response, and the phase shift effect after stabilization is not considered in this study.

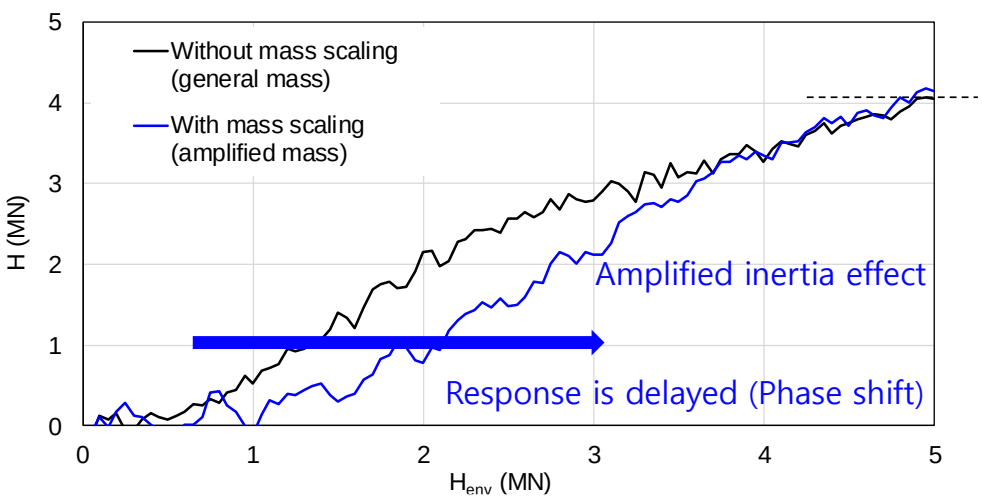

Fig. 94 Inertia effect on Jackup analysis under monotonic load analysis

6.2.4. Dynamic Amplification Factor (DAF)

Natural period is very important factor for calculating DAF in offshore platform. Typical natural period of jack-up is between 5~15s (ABS, 2014). Soil stiffness, as the boundary condition, has great influence on natural period. In the soil continuum model where the strength degradation occurs, it is impossible to accurately calculate the natural period. As an alternative, Fig. 95 shows the result of calculating the natural period using the initial stiffness. Calculated natural period is 7.76s, and 12.03s for pinned condition. Corresponding motion of 1st and 2nd mode are translated motion, which is surge, sway.

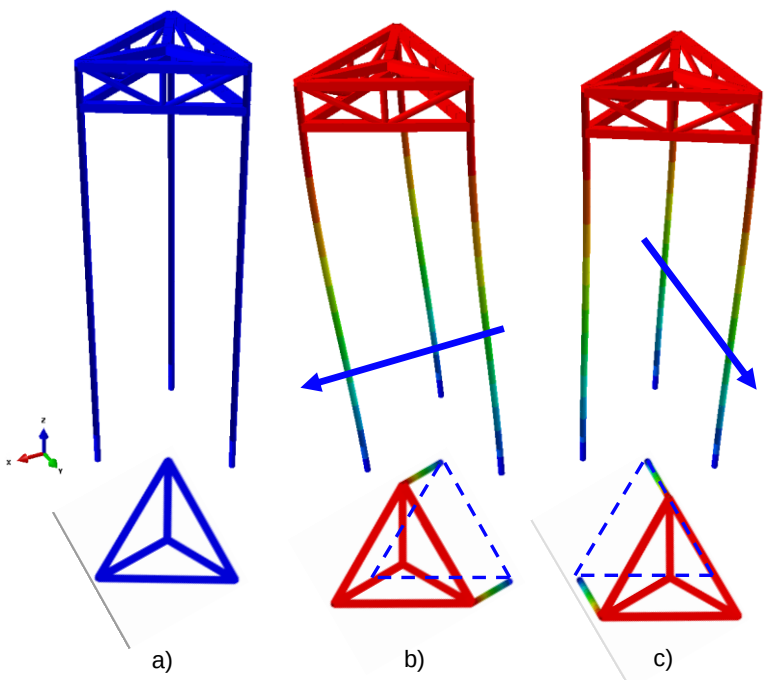

Fig. 95 Mode shape of jack-up; a) original structure; b) 1st mode (surge); c) 2nd mode (sway)

Definition of DAF is the structural response ratio between static and dynamic analysis. Conservative DAF is generally calculated using this definition, and then used in the platform design.

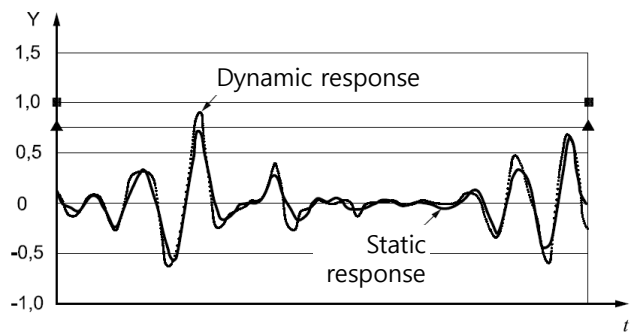

Fig. 96 Example of DAF (ISO, 2012)

For comparison of wave load analysis between static analysis with yield interaction model and dynamic analysis with soil continuum model, DAF should be considered. However, calculating DAF accurately is challenging. DAF calculation using classical single degree of freedom (SDOF) analogy is suggested in guideline (Eq. (30)).

$$DAF = \frac{1}{\sqrt{(1-\Omega^2)^2 + (2\zeta\Omega)^2}} \tag{30}$$

Where Ω is Natural period divided by the wave excitation period (T_n/T), and ζ is damping ratio. Natural period of structure, wave excitation period, wave damping, soil damping should be considered

in this DAF calculation using SDOF analogy, and this is the reason difficult to calculate DAF exactly. And also, this suggestion is conservative equation for design, not proper in calculation of realistic response. In this study, DAF is assumed excluding strain-rate dependency from amplified response (Fig. 97).

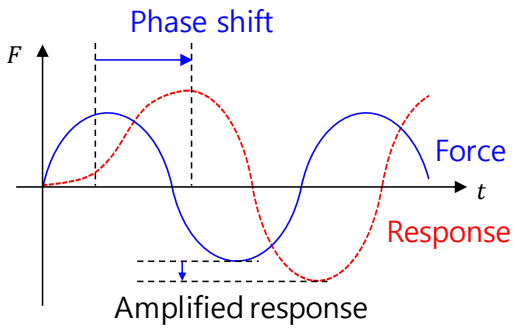

Fig. 97 Effect of DAF on the amplified response

6.3. Application : Jack-up structural analysis under dynamic wave load

6.3.1. Selection of soft over stiff clay

One of the purposes of the application is to validate the soil parameters, including regression model about initial stiffness, presented in Chapter 4. Soft over stiff clay soil has been presented for both depth ratio (w/H) and undrained shear strength ratio ($s_{u,stiff}/s_{u,H}$) variables. Soil parameters have been presented in the range of depth ratio from 0.9 to 1.2 and undrained shear strength ratio from 1 to 4. It is believed that this range can cover typical soft over stiff

clay properties. In this chapter, a middle point, 2.5 times stiffer lower clay and 2.1B of embedment case, has been selected to validate the interpolative capability of the regression model (Fig. 98). This is equivalent to a depth ratio of 1.05 and a undrained shear strength ratio of 2.5. Proposed regression model for initial stiffness and interpolated values of other soil parameters are used for validation.

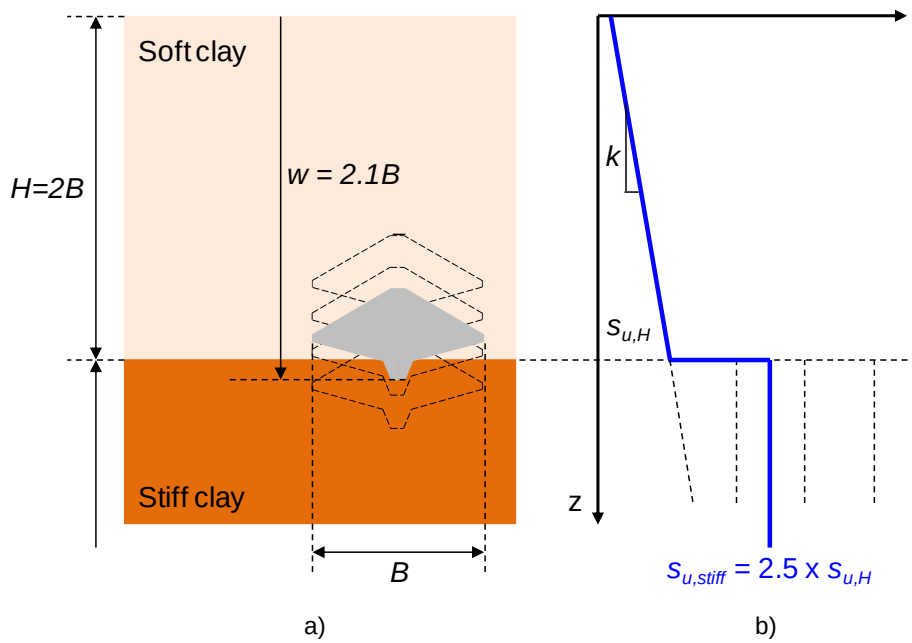

Fig. 98 Soft over stiff clay case used in application;
a) Depth ratio of 1.05; b) Strength ratio of 2.5

6.3.2. Wave environmental load

Wave environmental load is assumed as similar value with field data of reference jack-up (MLT-116C). Detailed information is shown in Table 15.

Table 15 Environmental condition for wave load

	Water depth	Airgap	Height (H)	Period (T)
reference	64~ 80m	15~ 20m	H_s=6.4~ 9.0m	T_p=11.1~ 13.1s
Case 1	65m	25m	H_{max}=8.0m	T_p=8.0s
Case 2	65m	25m	H_{max}=12.0m	T_p=13.0s

Load cases are selected for validation about hyperbolic relation of material in elastic region. Case 1, regular wave with H_{max} = 8m, T = 8s, is selected because the wave period is close to natural period with initial stiffness (7.76s). It has been selected to investigate the dynamic characteristics of the jack-up near the natural period, and the height suitable for wave steepness (0.08) has been calculated. Case 2, regular wave with H_{max} = 12m, T = 13s, is selected according to the concept of design wave selection. Design wave height is decided from the referenced significant wave

height is selected (H_s =6.4m). Corresponding wave period is calculated using proper wave steepness (0.046).

The wave load is calculated using the morison equation (Eq. (31)) depending on the location. This calculated load is especially key load in the cylinder structure like jacket or jack-up.

$$F = \rho C_m V\dot{u} + \frac{1}{2}\rho C_d A u|u| \tag{31}$$

Wave load applied at leg cannot be calculated using stick model, so the drag coefficient and inertia coefficient is modified according to leg design. For computational cost, Abaqus/Aqua analysis is performed in initial stiffness. Drag force and inertia force, including buoyancy, have been calculated and acted on the jack-up leg (Fig. 99). Corresponding nodal force is scanned and applied in 3D soil-jack-up interaction analysis (Fig. 100).

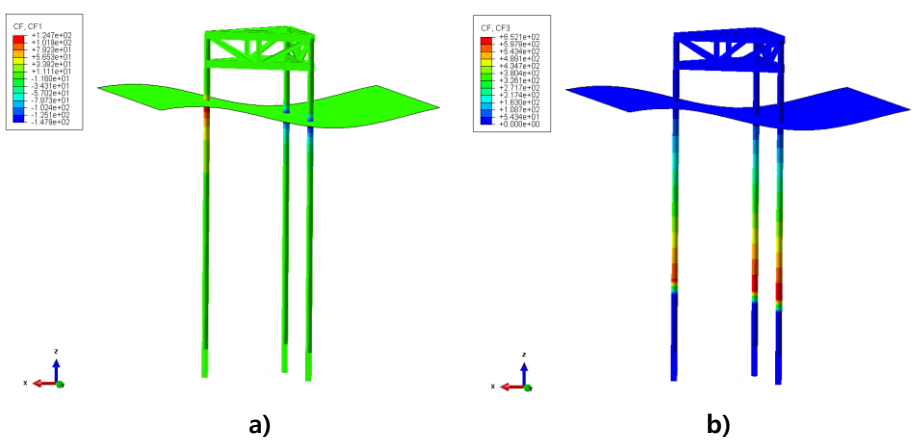

Fig. 99 Abaqus/Aqua analysis results;

a) Vertical force; b) Horizontal force

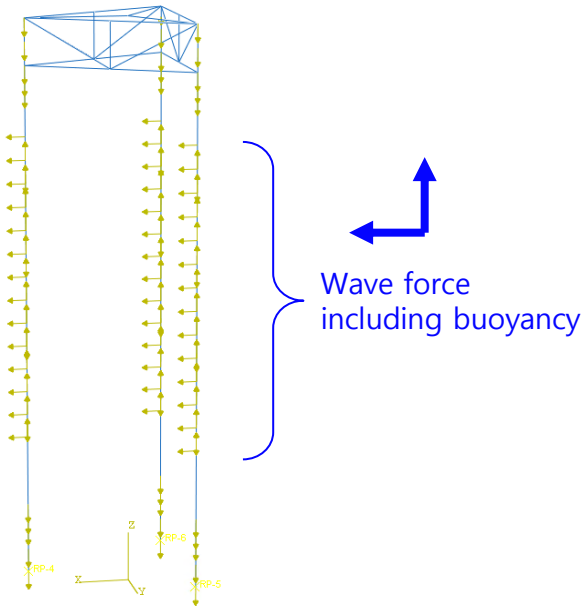

Fig. 100 Applied nodal force in jack-up

6.3.3. FE model for application

Same FE model with soft over stiff clay case, including reinforced jack-up structure, is used for application. Hull-leg joint and spudcan-leg joint have been reinforced so that the structure can withstand the impact due to the stiff soil below. Assuming a different payload, a vertical load of 33MN has been applied, and a repeated regular wave has been applied as an environmental load (Fig. 101(a)).

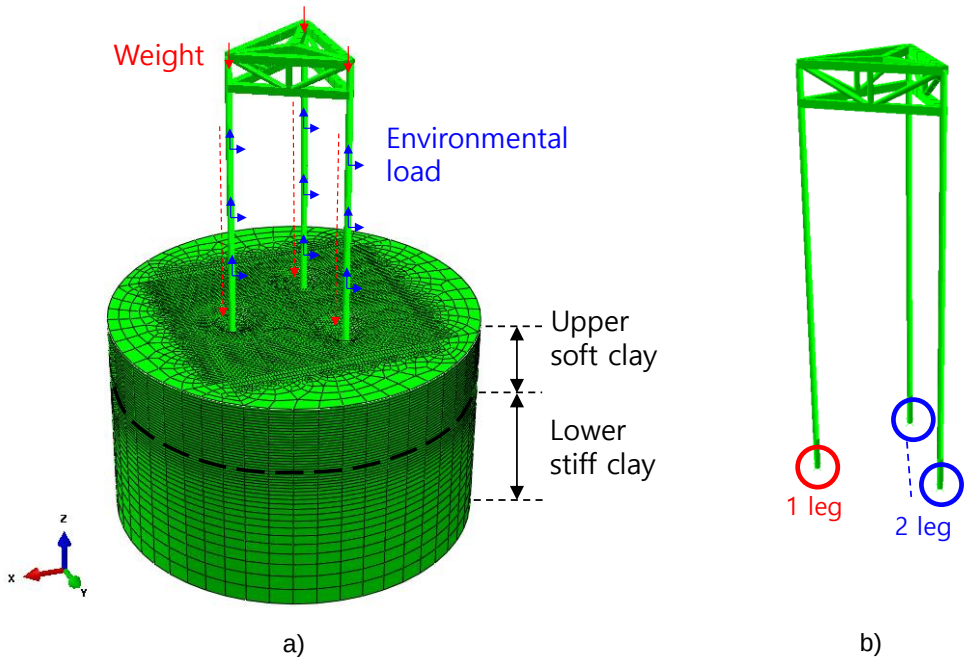

Fig. 101 a) FE model for application; b) Notation of legs

Since the direction of load is changed in regular wave, a specific leg cannot be defined as a leeward or windward leg in the application case. For the purpose of classification, the legs has named as "1-leg" and "2-leg" and the results have been shown accordingly (Fig. 101(b)).

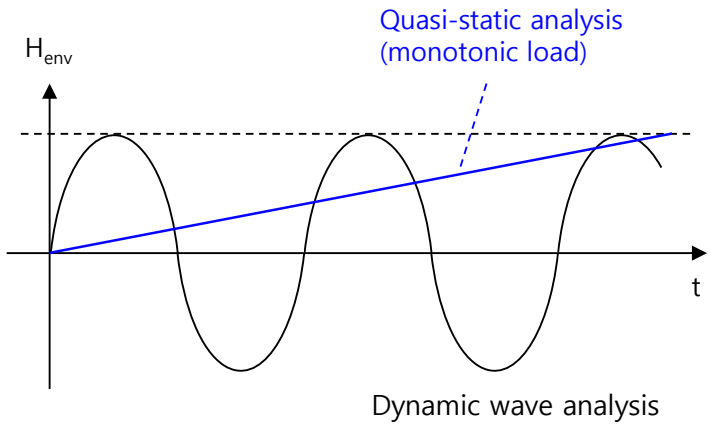

Fig. 102 Schematic figure of applied load

As an environmental load, a sinusoidal load has been assumed and applied using the peak load obtained through scanning like Fig. 100. To calculate DAF, the quasi-static analysis has also been performed in which the peak load of the wave is applied monotonically and slowly (blue line in Fig. 102). This is for using the definition of DAF, the ratio of dynamic response and quasi-static response.

The dynamic analysis has used the environmental load of the two cases mentioned above. Case 1, which is close to the natural period, has been used to investigate the dynamic effect, and case 2 has been used according to the design wave decision.

6.3.4. DAF calculation

As mentioned earlier, it is difficult to calculate the DAF. In the DAF calculation process using SDOF, the natural period of Jack-up, wave excitation period, wave damping, and soil damping should be considered. It is impossible to accurately calculate the natural period of Jack-up because the boundary condition is changed due to the change of the soil properties. Wave damping terms that vary depending on the structure are applied indirectly through the model tests. The soil damping term is divided into material damping and energy dissipation damping, and each influence must be accurately considered. It is not easy to accurately calculate and compare DAF under the influence of many factors.

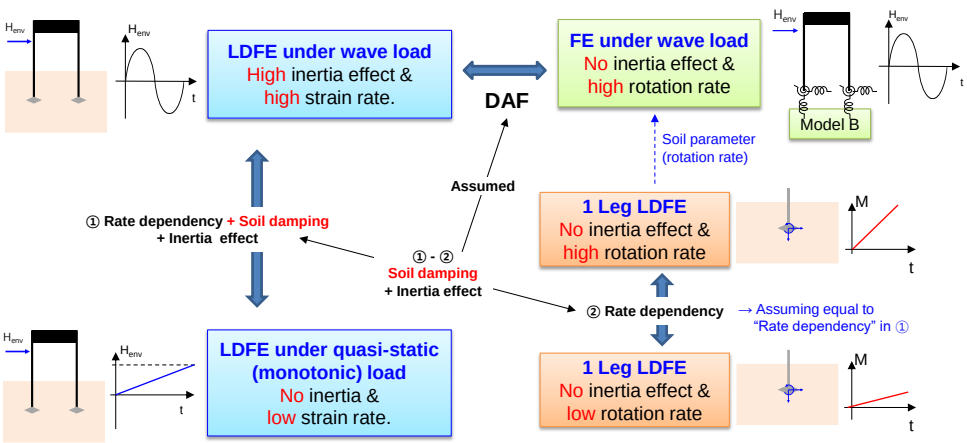

Fig. 103 Simplified diagram of DAF calculation procedure

In this study, since it is difficult to calculate all factors accurately, DAF has been assumed through an appropriate procedure. Using the

definition of DAF, the ratio between the time series analysis result and the quasi-static analysis result has been used, and the rate dependency of the soil strength has been considered separately. Rate dependency term has been calculated using a single spudcan analysis in which amplification of the reaction due to the inertia effect does not occur (Fig. 103).

First, in the Jack-up analysis using the soil continuum model, wave load analysis and quasi-static analysis have been performed (Fig. 102). Wave load analysis has a high inertia effect and a high strain rate, as a time series sinusoidal load has been applied. On the other hand, quasi-static analysis of slowly applying the load corresponding to the peak load has no inertia effect, and the strain rate is also sufficiently low. Therefore, the difference in response between the two analyzes can be divided into the effects of rate dependency, soil damping, and inertia effect. The difference in response between the two calculated analyzes is shown in the Table 16.

Second, the difference in soil strength due to rate dependency is considered. A single spudcan analysis has been used, reflecting only the effects of soil properties according to the rotation rate. The difference between the two responses is defined as a response that is different due to the rate-dependent soil strength by applying rotational motion at high speed and slow speed. The calculated results are also shown in the Table 16.

Table 16 Assumed DAF

	Case 1	Case 2	Remarks
$\frac{M_{Jackup,\,wave}}{M_{Jackup,\,qs}}$	5.50	2.66	① in Fig. 103 DAF + Rate dep.
$\frac{M_{spud.,\,dyn}}{M_{spud.,\,qs}}$	1.35	1.31	② in Fig. 103 Rate dependency
DAF	4.07	2.03	(① − ②) DAF

It has been assumed that the effect of soil strength obtained through single spudcan analysis is the same as the rate dependency term in Jack-up analysis. Finally, DAF to be applied to static analysis has been assumed using the difference in response from Jack-up analysis and the response from single spudcan analysis. The assumed DAF is applied to the static analysis result using the yield interaction model, and this has been compared with the Jackup analysis result using the soil continuum model analyzed in the time domain.

6.3.5. Analysis condition

Jack-up structural analysis with yield interaction model is performed in static analysis. Two yield interaction models are used; Hyperbolic model B, proposed in this study, and modified model B, state-of-art model of clay (Zhang et al., 2014b). According to the corresponding depth ratio of 1.05 and undrained shear strength ratio of 2.5, soil parameter from regression model proposed in Chapter 4 and interpolation with fitting results are used in application case.

Table 17 Soil parameters used in application case

Capacity	Value	Stiffness	Value
V_{ult}	106.32 MN	K_v	613.88 MN/m
H_o	29.34 MN	K_h	610.46 MN/m
M_o	173.65 MNm	K_m	33798 MNm/rad
→ From regression model		K_c	73.68 MN/rad

V_{ult} is obtained from the penetration analysis, and it is thought that this approach can use the V_{ult} in a nonlinear soil model using the bearing capacity obtained in the penetration process in the actual jack-up design. K_h and K_m is calculated from the proposed regression model in Chapter 4. Since the initial stiffness is sensitive to the criteria, the regression equation has been presented. Verification about this equation is attempted through this application.

Other soil parameters is interpolated from fitted results in Chapter 3 and 4 (Table 9, Table 10).

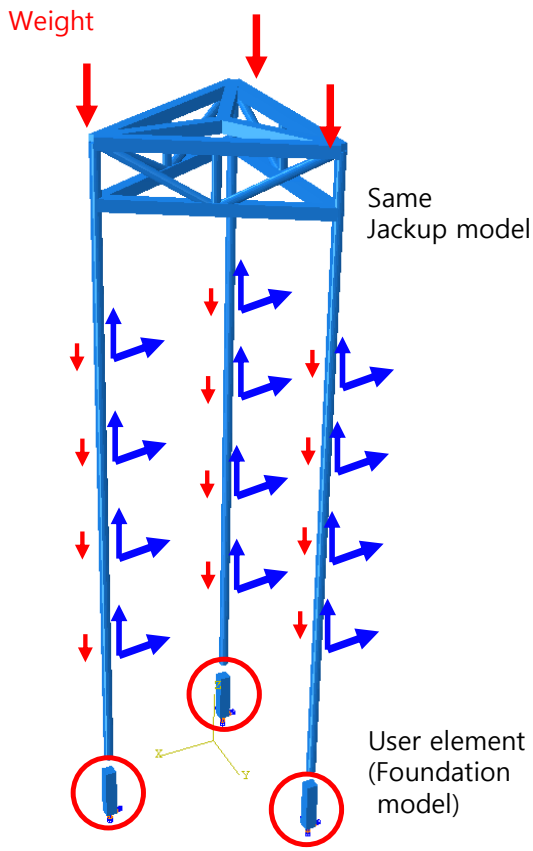

Fig. 104 FE model of jack-up analysis with yield interaction model

Nodal force equivalent to wave load is applied. Assumed DAF is multiplied to static nodal force for considering the dynamic effect on response (Fig. 104). In general, the DAF is multiplied by the response and used to compensate for the difference in response between static and dynamic analysis. However, in this study, since it is a linear analysis in the elastic region, it is an attempt to obtain

the corresponding material curve by multiplying the load by DAF rather than response. Vertical load is applied to reflect the weight and payload of the structure. The load corresponding to the weight has been applied to the leg through the distributed load, and the load corresponding to the hull weight and payload has been applied through the hull-leg joint. User elements which implements the yield interaction model are placed below the leg as the boundary condition of the jack-up analysis. The lower part of the UEL is fixed so that the behavior of UEL can be completely the boundary condition of the entire structure.

6.3.6. Case 1 : Analysis results

DAF is calculated based on the moment and rotation, so the soil response in rotational direction is shown in Fig. 105. DAF in case 1 is 4.07, which is close to the natural period and has a high value. DAF based on moment is applied in static analysis with two yield interaction models.

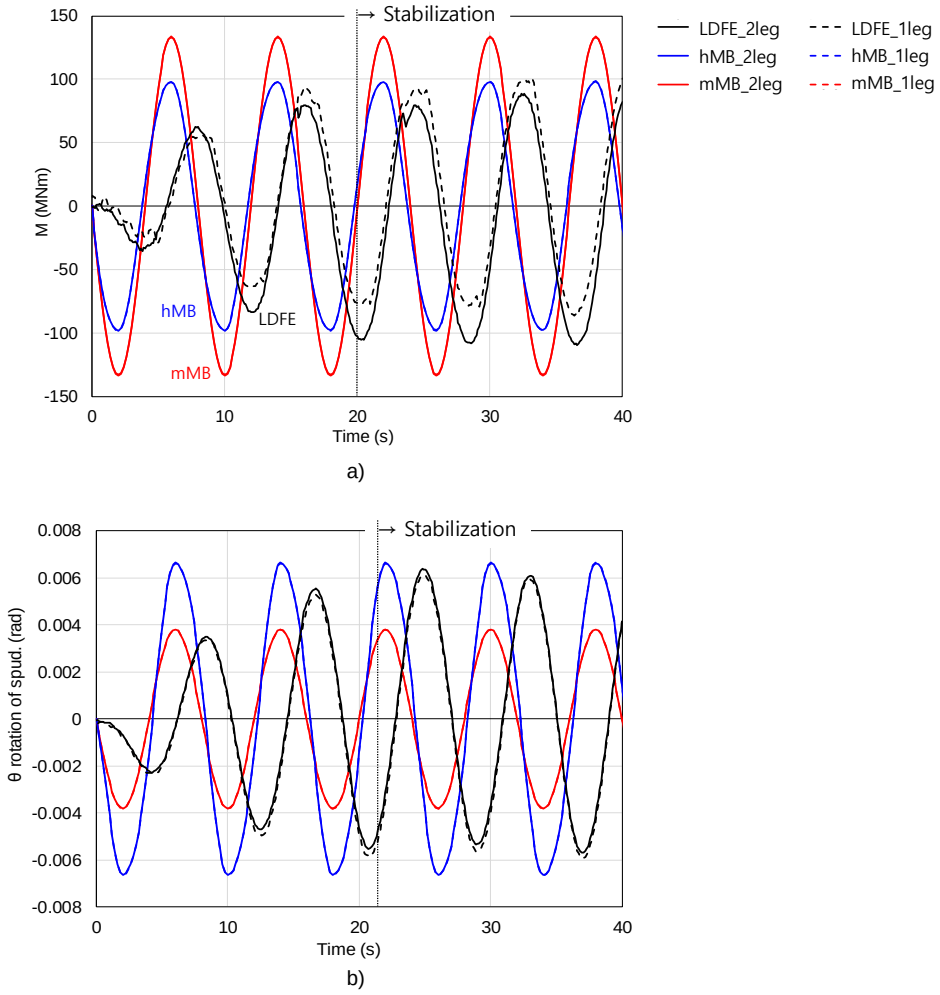

Fig. 105 Soil response in rotational direction;

a) Moment about time; b) Rotation about time

After stabilization, responses of Hyperbolic model B and those of soil continuum model shows similar results. In contrast, the rotation is small while the moment shows a large value in modified model B.

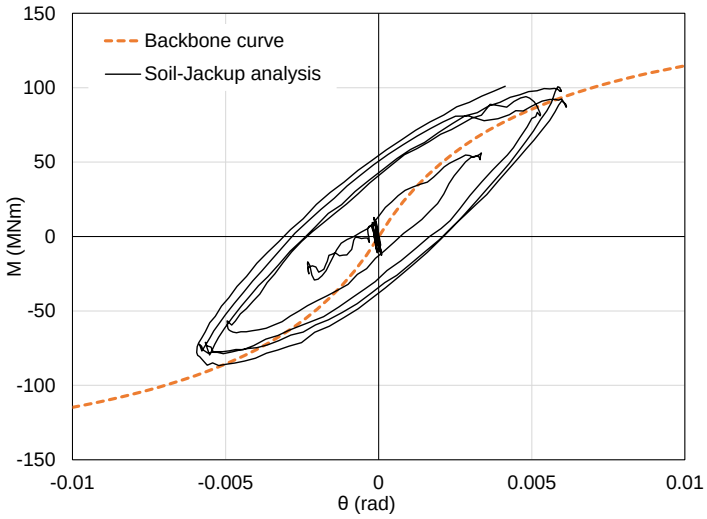

a)

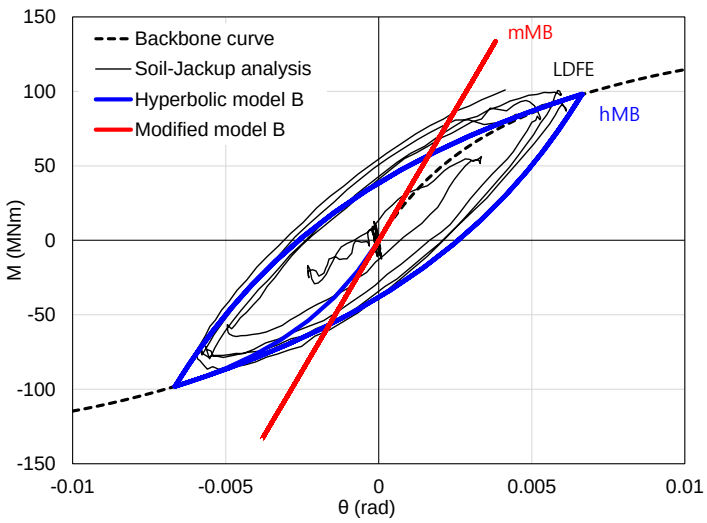

b)

Fig. 106 Soil hysteresis curve; a) Comparison with proposed backbone curve; b) Comparison with yield interaction model

Moment – rotation hysteresis curve occurs in results of soil continuum model (Fig. 106(a)). This hysteresis curve follows the backbone curve of soil parameters from regression model. Through this, regression model proposed in Chapter 4 shows good agreement

with LDFE analysis with dynamic load.

This well-matched backbone curve and hysteresis curve according to Masing rule are implemented in Hyperbolic model B. As a result, hysteresis curve simulated in Hyperbolic model B shows the similar shape with that of soil continuum model. Modified model B uses the almost linear relationship as elasticity relation, so the loading curve and unloading curve is the same as a line.

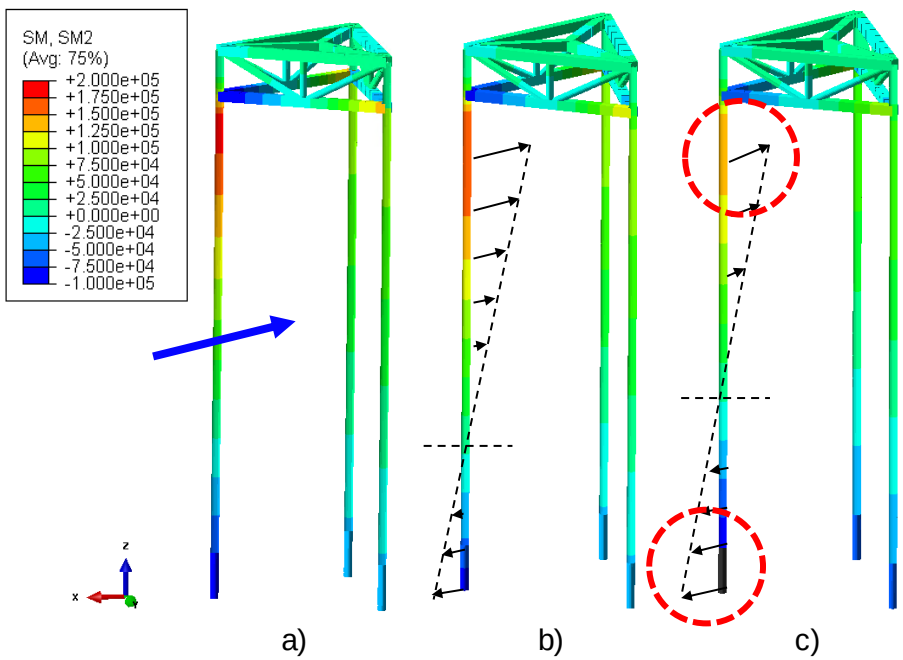

Fig. 107 Structure response : bending moment;

a) LDFE analysis; b) Hyperbolic model B; c) Modified model B

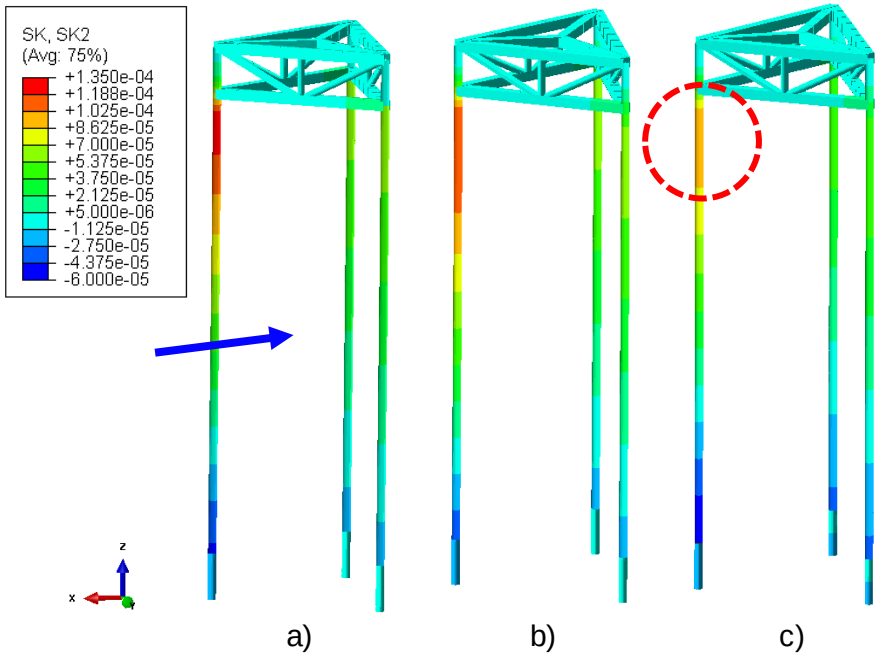

Fig. 108 Structure response : curvature;

a) LDFE analysis; b) Hyperbolic model B; c) Modified model B

Fig. 107 and Fig. 108 show the bending moment and curvature of jack-up leg. Bending moment and curvature show same trend. Because the windward leg is under the tension, large bending moment is applied. Among three structure-soil interaction model, Modified model m shows different moment distribution. Because of the over-estimated moment response of soil, hull-leg joint is under-estimated in bending moment and curvature. Different soil response can result in the different structural response.

6.3.7. Case 2 : Analysis results

DAF is calculated based on the moment and rotation, so the soil response in rotational direction is shown in Fig. 109. DAF in case 2 is 2.03, which is smaller than that of case 1. 13s of period is far from the natural period of jack-up, so the DAF is small value in case 2. Assumed DAF is applied in static analysis with two yield interaction models.

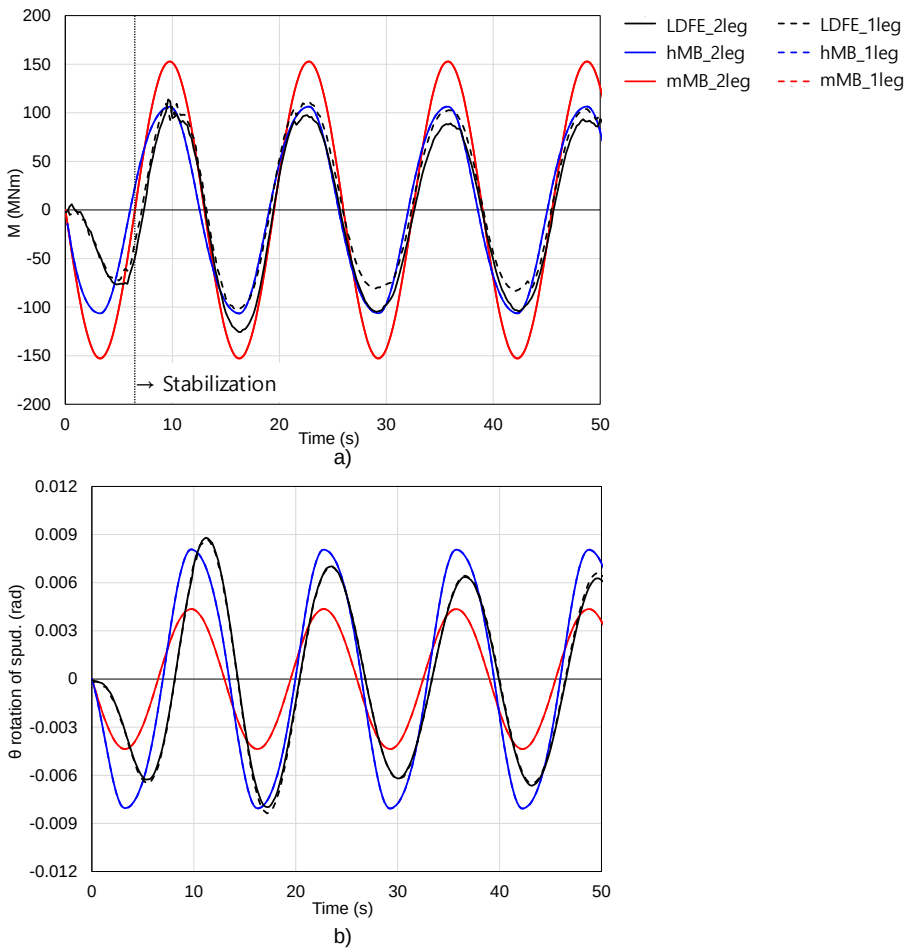

Fig. 109 Soil response in rotational direction;

a) Moment about time; b) rotation about time

After first peak, phase shift rarely occurs because the wave excitation period is far from natural period of jack-up. Compared to the case 1 of the 8s period, the dynamic characteristics are less when far from the natural period. Also in case 2, responses of Hyperbolic model B and structure-soil interaction analysis with soil continuum model are similar and the rotation is small while the moment has large value in modified model B.

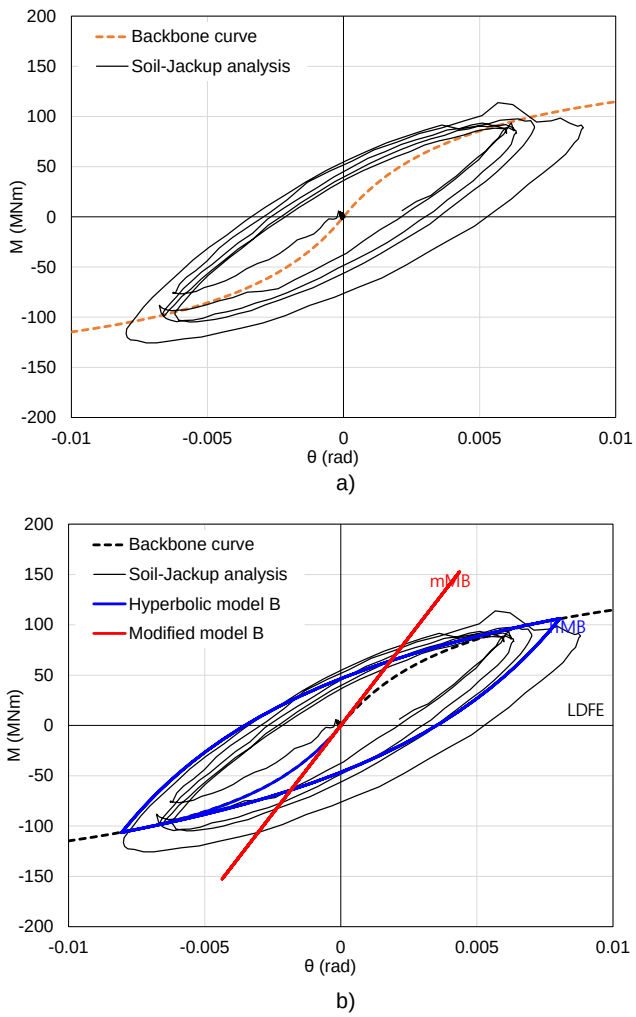

Fig. 110 Soil hysteresis curve; a) Comparison with proposed backbone curve; b) Comparison with yield interaction model

In case 2, the hysteresis curve in the soil continuum model also follows the backbone curve well. This means that verification of interpolated soil parameters has been performed. Corresponding hysteresis curve is implemented in Hyperbolic model B in this study. In the fatigue assessment of jack-up structure, Hyperbolic model B can be adopted as the simplified nonlinear foundation model because of consideration about hysteresis in the elastic region.

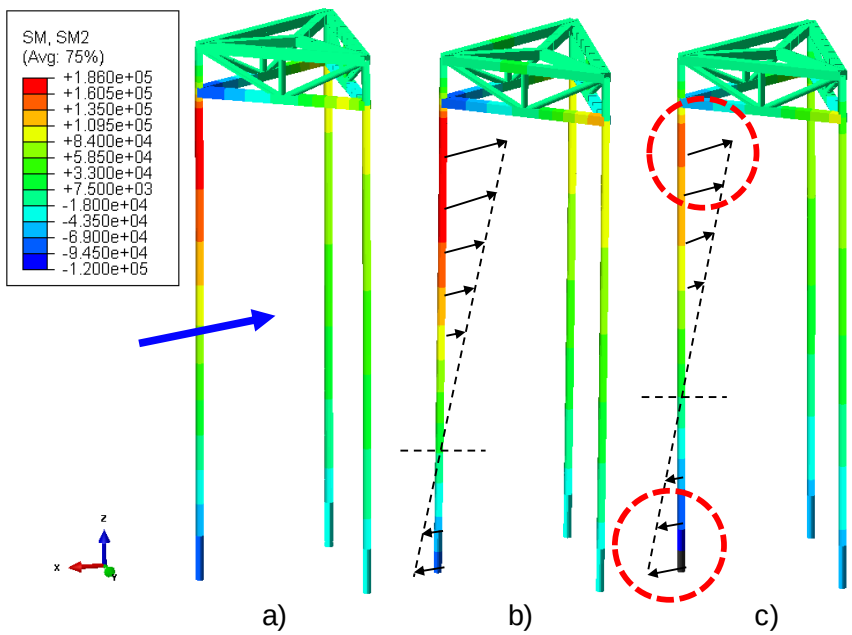

Fig. 111 Structure response : bending moment;

a) LDFE analysis; b) Hyperbolic model B; c) Modified model B

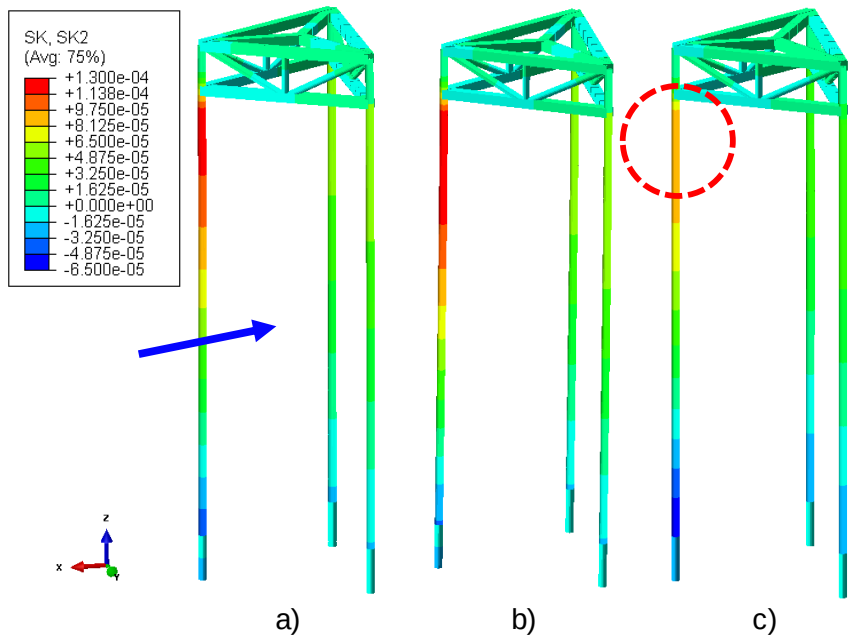

Fig. 112 Structure response : curvature;

a) LDFE analysis; b) Hyperbolic model B; c) Modified model B

Fig. 111 and Fig. 112 show the bending moment and curvature of the jack-up leg. Bending moment and curvature show the same trend, as in case 1. Because the windward leg is under the tension, a significant bending moment is applied. In case 2, where the wave period is far from the natural period, Modified model B also shows different moment distribution. Linear elastic relation results in the over-estimated moment acting on the soil in the elastic region. Moment distribution of leg has shifted value because of the large moment at the boundary condition, so the difference occurs at the hull-leg joint. Environmental loads are almost in the elastic region before reaching the yield envelope, and the underestimated bending moment at the hull-leg joint may have a great influence on the strength assessment in the corresponding structure.

Conclusion

Summary

This study aims to perform a jack-up structural analysis for dynamic loads using a foundation model considering structure-soil interaction. A nonlinear foundation model has been proposed using simplified soft over stiff clay as a target soil, and jack-up structural analysis has been performed with the proposed structure-soil interaction model.

The structure-soil interaction model refers to a two-way analysis model in which the plasticity of the soil and the response of the structure interact with each other. In ISO (2012), a secant model, a yield interaction model, and a soil continuum model have been proposed as the structure-soil interaction model. The secant model is the simplest model that considers structure-soil interaction. This model introduces the concept of secant stiffness in the rotational direction, which is only available at a specific design point. The model B was proposed as a yield interaction model to more accurately simulate the plastic behavior of the soil. The yield interaction model about clay has been improved from model B to the latest model, modified model B. The model B calculates the plastic displacement through an iterative calculation using the formulated equation of elasticity, yield envelope, flow rule, and hardening law. This model is known to calculate the plastic behavior of the soil well. In addition, Hyper-model B was proposed to simulate the strength

degradation in the rotational direction by introducing a nonlinear moment–rotation relationship into the model B framework.

Soft over stiff clay is a general case that can occur when the jack–up is operated in soft clay. Jack–up should penetrate until meeting the stiff clay to obtain sufficient bearing capacity in the soft soil. This case is stable in terms of installation. However, in the aspect of the operation, the foundation model and corresponding structural response can be changed because it is simultaneously affected by the upper soft clay and lower stiff clay. A study has been conducted on how the ground model and jack–up structures are affected by the lower stiff clay, assuming the spudcan in this transition zone. The foundation model has been studied using the LDFE technique, and disturbed soil properties by spudcan penetration are considered.

A study has been conducted on the yield envelope in soft over stiff clay. LDFE analysis is used to calculate the ultimate capacity through constant V test and yield envelope through a swipe test. Combined loads analysis for deep embedment is performed and confirmed to be consistent with the yield envelope of the existing single clay. The combined loads analysis on the soft over stiff clay has been performed with various embedments and lower clay stiffnesses. The lower stiff clay gives a large reaction force against the downward motion of the spudcan, so the compressive vertical capacity and rotational capacity have increased significantly. On the other hand, in the case of tensile vertical capacity, where the upward motion is involved, there is a negligible effect of lower stiff clay. In

consideration of these effects, the best-fit yield envelope expression of soft over stiff clay and the corresponding ultimate capacity are presented.

A study about the elasticity of model B, which determines the behavior inside the yield envelope, is performed. In the existing model, load-displacement has an almost linear relationship except for the horizontal-rotation interaction term. However, the actual soil shows the gradually degraded strength, and this study applies this nonlinear relationship to the horizontal and rotational directions. In the existing Hyper-model B, a nonlinear hyperbolic relationship was applied only to the rotational direction. Proposed model extends this nonlinear relationship in the horizontal direction and combines the state-of-art concept like the tensile capacity of modified model B. As a result, the material curve assumed to be linear can overestimate the soil response before the yield. In contrast, the nonlinear hyperbolic relationship shows degradation of strength before the yield effectively.

Incorporating yield envelope and elasticity inside the yield envelope about soft over stiff clay, Hyperbolic model B is proposed and implemented using Abaqus user elements. The proposed model is compared with the structure-soil interaction analysis using LDFE and the results are verified. Jack-up analysis with the yield interaction model and the soil continuum model analysis is performed on single clay and soft over stiff clay, and the results are compared and analyzed. As a result, the proposed Hyperbolic model B can simulate the response of the soil where gradually degraded

strength occurs similarly to LDFE, and the bending moment distribution of the leg is also well simulated due to the soil response.

A dynamic wave load analysis is performed using the structure–soil interaction model. Dynamic effects such as the Inertia effect and rate dependency are investigated. To validate the proposed soil parameters, application cases are selected and compared with the soil continuum model. As a result, the backbone curve of the proposed soil parameter is well–matched with the result of the soil continuum model. Hyperbolic model B also shows a similar hysteresis curve because this backbone curve is implemented.

Limitation and Future work

The nonlinear clay model used in this study only considers strain softening and rate hardening. In order to accurately simulate the tensile capacity, effects of suction force and consolidation should be considered. However, this phenomenon is difficult to consider using the current LDFE technique. In dynamic load analysis, several load cycles are generally simulated. However, due to computational cost, only a small number of cycles have been performed.

The dynamic effect is made up of a lot of factors, especially including soil damping. it is difficult to separate the each effect from the integrated dynamic response. For this, the effect of damping should be analyzed through experiments individually. Including the difficulties in calculation of the natural period, it is difficult to accurately calculate DAF, and only appropriate assumptions are made in this study. In addition, it is difficult to perform such dynamic analysis because the user element in which the yield interaction model is implemented is based on static analysis.

To achieve these limitations, the effect of time can be considered in LDFE analysis. Rani (2016) performed an LDFE analysis considering the effects of consolidation, by the implementation of additional nonlinear equations about time effect. In order to consider the dynamic effects of Jackup, it is necessary to use a macro element in which model B is implemented in a dynamic environment. This can be a model that replaces the time-consuming 3D soil

continuum model and is expected to be able to freely consider the equation for dynamic effects.

It is very important to use the proposed yield interaction model in structure design actually. For this, an external program, where the yield interaction model is implemented, can be used with the general code check program like SACS. This interface code for actual design is expected to have many uses. Also, this study has been omitted the lattice leg effect to clarify the structure-soil interaction. This effect can be necessary to accurately simulate the behavior of the jack-up within the soil.

Bibliography

[1] J. Wilson, F., Dynamics of Offshore Structures, 2nd ed, John Wiley & Sons Inc., 2002.

[2] B.-L. Zhang, Q.-L. Han, X.-M. Zhang, Recent advances in vibration control of offshore platforms, Nonlinear Dynamics 89 (2017) 755-771.

[3] V.P. Baglioni, G.S. Chow, S.N. Endley, Jack-Up Rig Foundation Stability in Stratified Soil Profiles, Offshore Technology Conference, Houston, Texas, Offshore Technology Conference, 1982, pp. 22.

[4] M.S. Williams, R.S.G. Thompson, G.T. Houlsby, Non-linear dynamic analysis of offshore jack-up units, Computers & Structures 69 (1998) 171-180.

[5] G.T. Houlsby, C.M. Martin, A.N. Schofield, Modelling of the behaviour of foundations of jack-up units on clay. Predictive soil mechanics (1992) 339-358.

[6] D. Mao, C. Zhong, L. Zhang, G. Chu, Dynamic response of offshore jacket platform including foundation degradation under cyclic loadings, Ocean Engineering 100 (2015) 35-45.

[7] W. Shi, H.C. Park, C.W. Chung, H.K. Shin, S.H. Kim, S.S. Lee, et al., Soil-structure interaction on the response of jacket-type offshore wind turbine, International Journal of Precision Engineering and Manufacturing-Green Technology 2 (2015) 139-148.

[8] API, Planning, designing and constructing fixed offshore platforms-working stress design, API-RP-2A-WSD, 21th ed, 2002.

[9] A.G. Young, B.D. Remmes, B.J. Meyer, Foundation Performance of Offshore Jack-Up Drilling Rigs, Journal of Geotechnical Engineering 110 (1984) 841-859.

[10] M.S. Williams, R.S.G. Thompson, G.T. Houlsby, A parametric study of the non-linear dynamic behaviour of an offshore jack-up unit, Engineering Structures 21 (1999) 383-394.

[11] P. Le Tirant, C. Pérol, Stability and operation of jackups, Editions Technip, 1993.

[12] M.S. Hossain, J. Zheng, A. Huston, Effect of spudcan geometry on penetration and extraction resistance in clay, Géotechnique 65 (2015) 147-154.

[13] R. Kee, B.W. Ims, Geotechnical Hazards Associated with Leg Penetration of Jack-up Rigs, Seabed Mechanics, Dordrecht, 1984

[14] S.N. Endley, P.J. Thompson, V.P. Baglioni, Prediction of Jack-up Rig Footing Penetration, Offshore Technology Conference, Houston, Texas, Offshore Technology Conference, 1981, pp. 12.

[15] G.T. Houlsby, C.M. Martin, Undrained bearing capacity factors for conical footings on clay, Géotechnique 53 (2003) 513-520.

[16] K.L. Teh, M.J. Cassidy, C.F. Leung, Y.K. Chow, M.F. Randolph, C.K. Quah, Revealing the bearing capacity mechanisms of a penetrating spudcan through sand overlying clay, Géotechnique 58 (2008) 793-804.

[17] M. Hossain, M. Randolph, Deep-penetrating spudcan foundations on layered clays: centrifuge tests, Géotechnique 60 (2010) 157-170.

[18] D. Menzies, R. Roper, Comparison of Jackup Rig Spudcan Penetration Methods in Clay, Offshore Technology Conference, 2008.

[19] D. Ahn, S.-c. Shin, S.-y. Kim, H. Kharoufi, H.-c. Kim, Comparative evaluation of different offshore wind turbine installation vessels for Korean west–south wind farm, International Journal of Naval Architecture and Ocean Engineering 9 (2017) 45-54.

[20] C. Nancy, M.J. B Rohani, R. Bt M Hazizy, A. B Abd Rahman, A.B.A. Jalil, Jack Up Suitability for South China Sea Sites, Offshore Technology Conference-Asia, Kuala Lumpur, Malaysia, Offshore Technology Conference, 2014, pp. 5.

[21] M. Randolph, S. Gourvenec, Offshore Geotechnical Engineering, CRC Press, 2017.

[22] K. Tho, C. Leung, Y. Chow, S. Swaddiwudhipong, Eulerian Finite-Element Technique for Analysis of Jack-Up Spudcan Penetration, International Journal of Geomechanics 12 (2010) 64-73.

[23] Y. Hu, M.F. Randolph, A practical numerical approach for large deformation problems in soil, International Journal for Numerical and Analytical Methods in Geomechanics 22 (1998) 327-350.

[24] G. Qiu, S. Henke, J. Grabe, Applications of Coupled Eulerian-Lagrangian Method to Geotechnical Problems with Large

Deformations Proceeding of SIMULIA Customer Conference, London, UK, 2009

[25] Y. Zhang, D. Wang, M. Cassidy, B. Bienen, Effect of Installation on the Bearing Capacity of a Spudcan under Combined Loading in Soft Clay, Journal of Geotechnical and Geoenvironmental Engineering 140 (2014) 04014029.

[26] G.J.M. Schotman, The Effects of Displacements on the Stability of Jackup Spud-Can Foundations, Offshore Technology Conference, Houston, Texas, Offshore Technology Conference, 1989, pp. 10.

[27] C.M. Martin, Physical and numerical modelling of offshore foundations under combined loads, Oxford University, UK, 1994.

[28] G. Vlahos, C.M. Martin, M.S. Prior, M.J. Cassidy, Development of a model jack-up unit for the study of soil-structure interaction on clay, International Journal of Physical Modelling in Geotechnics 5 (2005) 31-48.

[29] ISO, Petroleum and natural gas industries - Site specific assessment of mobile offshore units - Part 1 : Jack-ups, International Organization for Standardization ISO 19905-1 (2012).

[30] T. Aust, Accident to the mobile offshore drilling unit Maersk victory on November 16 1996, Mines and Energy Resources, South Australia, 1997.

[31] J.C. Simo, T.J. Hughes, Computational inelasticity, Springer Science & Business Media, 2006.

[32] N. Cheng, M.J. Cassidy, Development of a force–resultant model for spudcan footings on loose sand under combined loads, Canadian Geotechnical Journal 53 (2016) 2014–2029.

[33] O.A. Purwana, M.J. Perry, M. Quah, M.J. Cassidy, Comparison of ISO 19905–1 Framework and a Plasticity–based Spudcan Model for Jackup Foundation Assessments, Offshore Technology Conference, Houston, Texas, USA, Offshore Technology Conference, 2012.

[34] P.C. Wong, J. Templeton, III, O.A. Purwana, H. Hugo, M.J. Cassidy, M.S. Hossain, et al., Foundation Modeling and Assessment in the New ISO Standard 19905–1, Offshore Technology Conference, Houston, Texas, USA, Offshore Technology Conference, 2012.

[35] T. Sullivan, G. Calvi, M. Priestley, Initial stiffness versus secant stiffness in displacement based design, 13th World Conference of Earthquake Engineering (WCEE), 2004

[36] G. Vlahos, M.J. Cassidy, B.W. Byrne, The behaviour of spudcan footings on clay subjected to combined cyclic loading, Applied Ocean Research 28 (2006) 209–221.

[37] F. Pisanò, R. Schipper, G.–J. Schreppers, Input of fully 3D FE soil–structure modelling to the operational analysis of jack–up structures, Marine Structures 63 (2019) 269–288.

[38] ABS, Guidance notes on Dynamic Analysis Procedure For Self–Elevating Units, 2014.

[39] A. Abelev, P. Valent, Strain–rate dependency of strength of soft marine deposits of the Gulf of Mexico, OCEANS 2009, 2009

[40] S. Robinson, M. Brown, Rate effects at varying strain levels in fine grained soils, Proceedings of the 18th International Conference on Soil Mechanics and Geotechnical Engineering, 2013

[41] S. Nanda, V. Sivakumar, P. Hoyer, A. Bradshaw, K. Gavin, H. Gerkus, et al., Effects of strain rates on the undrained shear strength of kaolin, Geotechnical Testing Journal 40 (2017) 951-962.

[42] SNAME, Site specific assessment of mobile jack-up units, Society of Naval Architects and Marine Engineers SNAME T&R 5-5A (2008).

[43] M.S. Hossain, M.F. Randolph, Deep-penetrating spudcan foundations on layered clays: numerical analysis, Géotechnique 60 (2010) 171-184.

[44] P. Hu, D. Wang, S.A. Stanier, M.J. Cassidy, Assessing the punch-through hazard of a spudcan on sand overlying clay, Géotechnique 65 (2015) 883-896.

[45] J. Zheng, M.S. Hossain, D. Wang, Numerical investigation of spudcan penetration in multi-layer deposits with an interbedded sand layer, Géotechnique 67 (2017) 1050-1066.

[46] K.L. Teh, C.F. Leung, Y.K. Chow, y.M.J. Cassid, Centrifuge model study of spudcan penetration in sand overlying clay, Géotechnique 60 (2010) 825-842.

[47] P. Hu, M.J. Cassidy, Predicting jack-up spudcan installation in sand overlying stiff clay, Ocean Engineering 146 (2017) 246-256.

[48] D.S. Simulia, ABAQUS 6.13 User's manual, 2013.

[49] I. Einav, M.F. Randolph, Combining upper bound and strain path methods for evaluating penetration resistance, International Journal for Numerical Methods in Engineering 63 (2005) 1991-2016.

[50] M. Hossain, M. Randolph, Effect of Strain Rate and Strain Softening on the Penetration Resistance of Spudcan Foundations on Clay, International Journal of Geomechanics 9 (2009) 122-132.

[51] G. Qiu, J. Grabe, Numerical investigation of bearing capacity due to spudcan penetration in sand overlying clay, Canadian Geotechnical Journal 49 (2012) 1393-1407.

[52] D. Wang, D.J. White, M.F. Randolph, Large-deformation finite element analysis of pipe penetration and large-amplitude lateral displacement, Can Geotech J 47 (2010) 842.

[53] M.S. Hossain, M.F. Randolph, Y.N. Saunier, Spudcan deep penetration in multi-layered fine-grained soils, International Journal of Physical Modelling in Geotechnics 11 (2011) 100-115.

[54] J. Zheng, M.S. Hossain, D. Wang, Estimating Spudcan Penetration Resistance in Stiff-Soft-Stiff Clay, Journal of Geotechnical and Geoenvironmental Engineering 144 (2018) 04018001.

[55] N. Cheng, M.J. Cassidy, Combined loading capacity of spudcan footings on loose sand, International Journal of Physical Modelling in Geotechnics 16 (2016) 31-44.

[56] R. Butterfield, J. Ticof, Design parameters for granular soils

(discussion contribution), Proceedings of the 7th European Conference on Soil Mechanics and Foundation Engineering, Brighton, England, 1979

[57] K.H. Roscoe, A.N. Schofield, The stability of short pier foundations in sand, British Welding Journal 3 (1956) 343-354.

[58] M.J. Cassidy, Non-linear analysis of jack-up structures subjected to random waves, 1999.

[59] M.J. Cassidy, C.M. Martin, G.T. Houlsby, Development and application of force resultant models describing jack-up foundation behaviour, Marine Structures 17 (2004) 165-193.

[60] C.M. Martin, G.T. Houlsby, Combined loading of spudcan foundations on clay: numerical modelling, Géotechnique 51 (2001) 687-699.

[61] Y. Zhang, M.J. Cassidy, B. Bienen, A plasticity model for spudcan foundations in soft clay, Canadian Geotechnical Journal 51 (2014) 629-646.

[62] S. Gourvenec, M. Randolph, Effect of strength non-homogeneity on the shape of failure envelopes for combined loading of strip and circular foundations on clay, Géotechnique 53 (2003) 575-586.

[63] R. Ragni, B. Bienen, D. Wang, D. Mašín, M.J. Cassidy, Numerical modelling of the effects of consolidation on the undrained spudcan capacity under combined loading in silty clay, Computers and Geotechnics 86 (2017) 33-51.

[64] C. Vulpe, Design method for the undrained capacity of skirted circular foundations under combined loading: effect of

deformable soil plug, Géotechnique 65 (2015) 669-683.

[65] G. Vlahos, M.J. Cassidy, C.M. Martin, Experimental investigation of the system behaviour of a model three-legged jack-up on clay, Applied Ocean Research 30 (2008) 323-337.

[66] J.S. Templeton, Spudcan fixity in clay, further results from a study for IADC, 12th International Conference on the Jack-Up Platform Design, Construction & Operation, London, UK, 2009

[67] J.S. Templeton, J.N. Brekke, D.R. Lewis, Spud can fixity in clay, final findings of a study for IADC, 10th International Conference on the Jack-Up Platform Design, Construction & Operation, London, UK, 2005

[68] Y. Zhang, B. Bienen, M.J. Cassidy, S. Gourvenec, The undrained bearing capacity of a spudcan foundation under combined loading in soft clay, Marine Structures 24 (2011) 459-477.

[69] Y. Zhang, B. Bienen, M. Cassidy, S. Gourvenec, Undrained Bearing Capacity of Deeply Buried Flat Circular Footings under General Loading, Journal of Geotechnical and Geoenvironmental Engineering 138 (2011) 385-397.

[70] S. Abyaneh, J. Kennedy, A. Maconochie, J. Oliphant, Capacity of Strip Foundations on Sand Overlying Clay Soils Under Planar Combined Loading, The 28th International Ocean and Polar Engineering Conference, Sapporo, Japan, International Society of Offshore and Polar Engineers, 2018, pp. 5.

[71] J. Ko, J.K. Lee, H. Seo, Undrained Bearing Capacity of Circular Foundations on Two-Layered Clay Under Combined Loading, The 27th International Ocean and Polar Engineering Conference,

San Francisco, California, USA, International Society of Offshore and Polar Engineers, 2017, pp. 6.

[72] P. Rao, Y. Liu, J. Cui, Bearing capacity of strip footings on two-layered clay under combined loading, Computers and Geotechnics 69 (2015) 210-218.

[73] Q. Yin, S. Dong, Combined Bearing Capacity of Spudcans on a Double Layer Deposit of Strong-Over-Weak Clays, Journal of Ocean University of China 18 (2019) 133-143.

[74] Y. Wang, M.J. Cassidy, B. Bienen, Effect of Underlying Sand Layer on Undrained Capacity of Spudcan Foundations in Soft Clay Under Combined Loading, (2018) V009T010A031.

[75] H. Jin, K. Lee, J. Choi, B.-S. Jang, Study on Spudcan Soil-Structure Interaction of a Wind Turbine Installation Vessel, ISOPE-19-29-3-329 29 (2019) 329-338.

[76] M.S. Hossain, M.J. Cassidy, D. Daley, R. Hannan, Experimental investigation of perforation drilling in stiff-over-soft clay, Applied Ocean Research 32 (2010) 113-123.

[77] J. Zheng, M. Hossain, D. Wang, New Design Approach for Spudcan Penetration in Nonuniform Clay with an Interbedded Stiff Layer, Journal of Geotechnical and Geoenvironmental Engineering 141 (2015) 04015003.

[78] J. Zheng, M.S. Hossain, D. Wang, Prediction of spudcan penetration resistance profile in stiff-over-soft clays, Canadian Geotechnical Journal 53 (2016) 1978-1990.

[79] B. Bienen, C. Gaudin, M.J. Cassidy, L. Rausch, O.A. Purwana, H. Krisdani, Numerical modelling of a hybrid skirted foundation

under combined loading, Computers and Geotechnics 45 (2012) 127–139.

[80] F.S.C. Tan, Centrifuge and theoretical modelling of conical footings on sand, University of Cambridge, 1990.

[81] C.M. Martin, G.T. Houlsby, Combined loading of spudcan foundations on clay: laboratory tests, Géotechnique 50 (2000) 325–338.

[82] Y. Zhang, B. Bienen, M.J. Cassidy, Development of a combined VHM loading apparatus for a geotechnical drum centrifuge, International Journal of Physical Modelling in Geotechnics 13 (2013) 13–30.

[83] Y. Wang, M.J. Cassidy, B. Bienen, Evaluating the Penetration Resistance of Spudcan Foundations in Clay Overlying Sand, The 29th International Ocean and Polar Engineering Conference, Honolulu, Hawaii, USA, International Society of Offshore and Polar Engineers, 2019, pp. 8.

[84] J. Huang, J. Chen, Y. Lu, S. Yi, H. Cheng, L. Cui, Deformation Behaviors and Dynamic Backbone Curve Model of Saturated Soft Clay under Bidirectional Cyclic Loading, International Journal of Geomechanics 20 (2020) 04020016.

[85] C. Bolisetti, Site Response, Soil–Structure Interaction and Structure–Soil–Structure Interaction for Performance Assessment of Buildings and Nuclear Structures, 2014.

[86] G. Masing, Eigenspannumyen und verfeshungung beim messing, Proc. Inter. Congress for Applied Mechanics, 1926

[87] G. Vlahos, M.J. Cassidy, C.M. Martin, Implementation of a

Force-Resultant Model Describing Spudcan Load-Displacement Behaviour Using an Implicit Integration Scheme, The Eighteenth International Offshore and Polar Engineering Conference, Vancouver, Canada, International Society of Offshore and Polar Engineers, 2008, pp. 8.

[88] B. Bienen, M.J. Cassidy, Advances in the three-dimensional fluid–structure–soil interaction analysis of offshore jack-up structures, Marine Structures 19 (2006) 110-140.

[89] Y. Zhang, B. Bienen, M.J. Cassidy, Jack-up push-over analyses featuring a new force resultant model for spudcans in soft clay, Ocean Engineering 81 (2014) 139-149.

[90] Y. Zhang, M.J. Cassidy, B. Bienen, Elastic stiffness coefficients for an embedded spudcan in clay, Computers and Geotechnics 42 (2012) 89-97.

[91] H. Yu, X. Li, S. Yang, Dynamic analysis method of offshore jack-up platforms in regular and random waves, Journal of Marine Science and Application 11 (2012) 111-118.

[92] N. Spidsøe, D. Karunakaran, Nonlinear dynamic behaviour of jack-up platforms, Marine Structures 9 (1996) 71-100.

초록

잭업 해양 구조물은 수심 150m까지 설치되며, 시추 및 생산용 리그뿐 아니라 해상풍력발전기 전문설치선과 같은 설치 유닛에도 사용되어오고 있다. 잭업은 파도와 바람 등의 환경하중 하에서 작업이 수행되므로 설계 시 그에 따른 잭업의 거동 및 구조 반응을 명확히 이해해야 한다. 거동 및 구조 해석 시 해양구조물의 경계조건으로 작용하는 지반 모델은 구조물의 진동 모드에 영향을 주어 해석 결과에도 영향을 미치게 된다. 일반적인 지반 모델에는 단순 지지 조건이나 선형 스프링을 이용한 모델이 있으나, 이는 잭업의 구조-지반 상호작용을 반영하지 못한다. 그 대안으로 International Organization for Standardization (ISO) 에서는 가이드라인을 통해 구조-지반 상호작용을 고려하는 비선형 지반 모델들을 제시하고 있으며, 이는 가장 단순한 모델인 시컨트 모델 (secant model)부터 지반의 소성 변위를 고려하는 항복 상호작용 모델 (yield interaction model), 그리고 가장 정확하지만 시간이 걸리는 지반 연속체 모델 (soil continuum model)로 나뉘어진다. 이러한 비선형 지반 모델 중 이번 연구에서는 구조-지반 상호작용을 모사하기 위하여 항복 상호작용 모델과 지반 연속체 모델을 사용하였다. 동적 하중 하에서 구조-지반 상호작용을 고려한 지반 모델을 사용하여 잭업의 구조해석을 수행하였다. 상부 연약한 지반-하부 단단한 점토 조건에서 사용할 수 있는 적절한 항복 상호작용 모델을 제시하고 지반 연속체 모델을 통해 이를 검증 비교 하였다. 상부 연약한 지반-하부 단단한 점토 조건에서, 지반에 작용하는 복합 하중의 항복 여부를 결정하는 항복 곡면에 대한 연구를 수행하였다. 해당 지반 조건은 하부 단단한

점토 지반으로 인해 상부 지반이 압착되어 충분한 지지력이 확보되기 때문에 많은 연구가 수행되지 않았다. 그러나 잭업 운용 시 사용되는 지반 모델은 상부와 하부 지반의 영향을 모두 받으므로 상부 연약한 점토-하부 단단한 점토 지반에 대한 연구가 필요하다. 해당 지반에서 수직 압축 용량은 압착 효과로 인해 증가한 반면 수직 인장 용량은 하부 단단한 점토 지반의 영향을 받지 않았다. 해당 지반에 잘 맞는 항복 곡면 식과 이 때 사용되는 수직, 수평, 회전 방향의 극한 지지력(ultimate capacity)에 대하여 제안하였다. 점토 지반에서 모델 비(model B)로 불리는 항복 상호작용 모델은 소성 변위를 통해 지반의 비선형 거동을 고려하며, 구조-지반 상호작용을 단순화하여 고려할 수 있는 모델로 최근까지 연구되어 오고 있다. 기존 모델 비는 항복 곡면에 도달하기 이전의 탄성 영역에서 선형의 힘-변위 관계와 함께 수평-회전 방향의 상호작용을 고려한다. 그러나 실제 지반은 점진적으로 소성이 발생하며 그에 따라 선형의 힘-변위 관계를 갖지 않는다. 이번 연구에서는 비선형성이 큰 수평, 회전 방향에 대하여 비선형 쌍곡선 힘-변위 관계를 가정한 하이퍼볼릭 모델 비(hyperbolic model B)를 제안하고, 이 때 사용되는 초기 지반 강성에 대한 식을 제시하였다. 검증을 위하여 지반 연속체 모델을 이용한 잭업의 구조-지반 상호작용 해석을 수행하였다. 연약 점토에서의 깊은 관입 깊이로 인한 지반의 대변형을 잭업 구조 해석에 고려하였다. 제안된 항복 상호작용 모델인 하이퍼볼릭 모델 비는 상부 연약한 점토-하부 단단한 점토 조건에서 항복 곡면 이전과 이후 지반 연속체 모델과 해석 결과가 비슷한 경향을 보임을 확인하였다. 기존 모델 비는 항복 곡면 안에서 선형 힘-변위 관계로 인해 지반에 작용하는 모멘트를 과대평가하는 경향이 있고, 경계조건으로써 구조 해석에 영향을 미쳐 잭업 레그의 모멘트가 과소평가되는 경향이 발생하였다.

제안된 하이퍼볼릭 모델 비는 항복 곡면 이전의 비선형성을 고려함으로써 잭업 레그의 모멘트 분포를 잘 예측하였다. 이렇게 제안된 항복 상호작용 모델과 지반 연속체 모델을 이용하여 잭업의 동적 구조해석을 수행하였다. 동적 사인파 하중에 대한 지반 반응 및 잭업의 구조 반응을 계산하고 정적 하중 결과와 비교하였다. 일반적으로 사용되고 있는 동적증폭계수 뿐 아니라 지반의 동적 효과 및 관성력에 의한 효과가 존재하는 것을 확인하였으며, 이에 대하여 분석하였다. 항복 상호작용 모델 및 지반 연속체 모델을 통해 구조-지반 상호작용을 고려하여 동적 하중에 대한 잭업 구조해석을 수행하였고, 항복 곡면 이전과 이후 지반 반응 및 잭업 레그의 모멘트 분포를 잘 예측하는 것을 확인하였다.

Keyword : 잭업, 스퍼드캔, 항복 상호작용 모델, 지반 대변형 유한요소, 구조-지반 상호작용

Student Number : 2014-21827